Development of Gene Therapy for the Treatment of Inherited Retinal Degeneration

Clare Jean Stephens

A thesis submitted for the degree of
Doctor of Philosophy

2001

Department of Molecular Genetics
Institute of Ophthalmology
University College
University of London

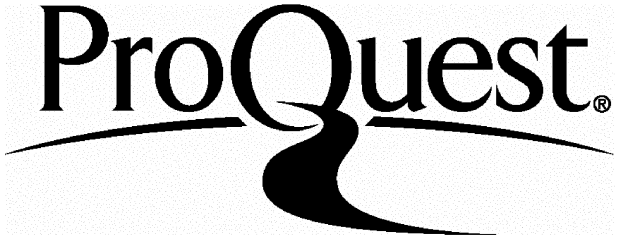

Abstract

Retinitis pigmentosa (RP) is the name given to a group of inherited retinal diseases that cause atrophy of the retina and retinal pigment epithelium (RPE), and frequently lead to a progressive loss of vision. Molecular techniques have implicated a large number of gene defects as causes of RP. In general the genes in which these occur are expressed in the photoreceptor and RPE cells of the retina. Currently there is no available treatment that can alter the primary defect of these diseases.

This thesis describes a programme of work that examines the potential of gene therapy in the treatment for RP. It centres on the use of recombinant adeno-associated virus (rAAV) for the transfer of a therapeutic gene to photoreceptor cells. Vector plasmids containing a photoreceptor cell-specific promoter and a reporter gene were cloned. These were used to produce high titre rAAV using a novel method involving replicating herpes simplex amplicons. In subsequent *in vivo* studies these viruses and others were injected sub-retinally into normal mouse eyes. The resulting expression of the reporter gene in photoreceptor cells demonstrated the potential of rAAV in the efficient transduction of this cell type. Expression of the reporter gene did not decrease before the final time point of 1 year.

The information gained from these studies was then utilised in the treatment of the *Prph2*$^{Rd2/Rd2}$ mouse, an animal model of RP that results from a null mutation in a photoreceptor cell-specific gene. A vector plasmid encoding a wild type copy of this gene was cloned and used to produce rAAV. Sub-retinal injection of this virus into *Prph2*$^{Rd2/Rd2}$ mice resulted in partial rescue of the disease phenotype by re-establishing the structural integrity of the photoreceptor cell layer. Functional tests performed on treated animals showed this was accompanied by a partial correction of electrophysiological responses.

Table of Contents

Figures

Tables

Abbreviations

AAV	adeno-associated virus
Ad	adenovirus
ANOVA	analysis of variance
ANS	adult neural stem cell
AP	alkaline phosphatase
BFGF	basic fibroblast growth factor
BHK	baby hamster kidney (cell line)
BNTF	brain-derived neurotrophic factor
bp	base pair
cGMP	cyclic guanosine monophosphate
cLSO	confocal laser scanning ophthalmoscope
CMV	immediate early promoter of cytomegalovirus
CNTF	ciliary neurotrophic factor
CTL	cytotoxic T lymphocyte
DISC-HSV	disabled single-cycle herpes simplex virus
dNTP	deoxynucleotide triphosphates
E	early region (of the wild type adenoviral genome)
EGFP	enhanced green fluorescent protein
ERG	electroretinography, electroretinographic or electroretinogram
FCS	foetal calf serum
FGF	fibroblast growth factor
FISH	fluorescent *in situ* hybridisation
GCL	ganglion cell layer
GFP	green fluorescent protein
GTP	guanosine triphosphate
Hd	hammerhead (ribozyme)
HIV	human immunodeficiency virus
Hp	hairpin (ribozyme)
HRP	horseradish peroxidase
IL	interleukin (cytokine)
INL	inner nuclear layer
IS	inner segments
ITR	inverted terminal repeat
iu/ml	infectious units per ml
LacZ	β-galactosidase
LB	Luria-Bertani bacterial growth medium
LID	lipofectin/integrin targeting peptide/DNA complexes
LTR	long terminal repeat
mcd/m^2	millicadellas per metre^2
MoMLV	Moloney murine leukaemia virus
NGS	normal goat serum
NK	natural killer (cell)

ONH	optic nerve head
ONL	outer nuclear layer
P20	postnatal day 20
PCR	polymerase chain reaction
PDE	phosphodiesterase
PR	photoreceptor (cell)
PRPH2	peripherin-2
rAAV	recombinant adeno-associated virus
rAd	recombinant adenovirus
RCR	replication competent recombinants
RCS	Royal College of Surgeon's (rat)
ROM-1	rod outer segment protein-1
RP	retinitis pigmentosa
RPE	retinal pigment epithelium
RT-PCR	reverse transcription PCR
SAC	small animal camera
SCID-X1	severe combined immunodeficiency X1
SEM	scanning electron microscope or microscopy
SIN	self-inactivating
TEM	transmission electron microscope or microscopy
TH	helper T cell
UTR	untranslated region
VSVG	vesicular stomatitis virus G protein
WRPE	woodchuck hepatitis virus post-transcription regulatory element

Publications

The work presented in this thesis has contributed to the following publication, and submitted articles.

R. R. Ali, G-M. Sarra, **C. Stephens**, M. de Alwis, J. W. B. Bainbridge, P. M. Munro, S. Fauser, M. B. Reichel, C. Kinnon, D. M. Hunt, S. S. Bhattacharya, A. J. Thrasher (2000) Restoration of photoreceptor ultrastructure and function in retinal degeneration slow mice by gene therapy. *Nature Genetics* **25,** 306-310.

G-M. Sarra, **C. Stephens**, M. de Alwis, J. W. B. Bainbridge, A. J. Smith, A. J. Thrasher, R. R. Ali (2001) Gene replacement therapy in the retinal degeneration slow (*rds*) mouse: the effect on retinal degeneration following partial transduction of the retina. *Human Molecular Genetics*. In press.

G-M. Sarra, **C. Stephens**, F. Schlichtenbrede, J. W. B. Bainbridge, A. J. Thrasher, P. J. Luthert, R. R. Ali (2001) Kinetics of transgene expression in the mouse retina following sub-retinal injection of recombinant adeno-associated virus. *Vision Research*. In press.

Acknowledgements

My thanks go to – Robin Ali, my supervisor, for his help and support over the past four years; Sander Smith for answering all my questions and reading drafts of this thesis; Geno Sarra for lots of help and guidance; Mahesh de Alwis for producing rAAV; Sascha Fauser for his help with cloning; Jim Bainbridge for all those injections; Peter Munro for his assistance with microscopy; Lyndon da Cruz for his help with ERGs; Adrian Thrasher for his advice; Alison Hardcastle for her help with writing up; Martin Reichel and Naheed Kanuga for their help early on in the project; and Caroline and Ross Graham for their comments on the results chapters. I am also grateful to everyone else in the group, Frank Schlichtenbrede, Jim McAlister, Ajay Mistry and Angus MacNeil, for their help.

In addition, I would like to thank Kate, Miranda, and my parents for their support.

1

Introduction

The human eye is often regarded as one of the most evolved organs in the body. It is a complex, finely balanced and highly developed photosensitive structure that permits an accurate analysis of the form, light intensity and colour reflected from objects. As such it provides us with the ability to interact with our environment. Its complexity and sensitivity makes it susceptible to disease and it is therefore not surprising that it is one of the commonest sites of genetic disorders, with diseases of the retina making up a significant proportion of these. The end result of many of these diseases is blindness, which, although not life threatening, places severe restrictions on the patient. In 1990 Dryja *et al.* [1] were the first to link a mutation in the gene encoding rhodopsin to a family suffering from inherited retinal dystrophy. Since then rapid progress has been made in determining the genes and mutations behind many of these diseases [2]. This information however has not yet brought much in the way of clinical benefit.

1.1 Eye structure and function

The eye is composed of three concentric layers: (1) the outer layer that consists of the sclera and the cornea; (2) the middle, vascular layer consisting of the choroid, ciliary bodies and iris; and (3) the inner layer of nerve tissue, the retina (Fig. 1.1).

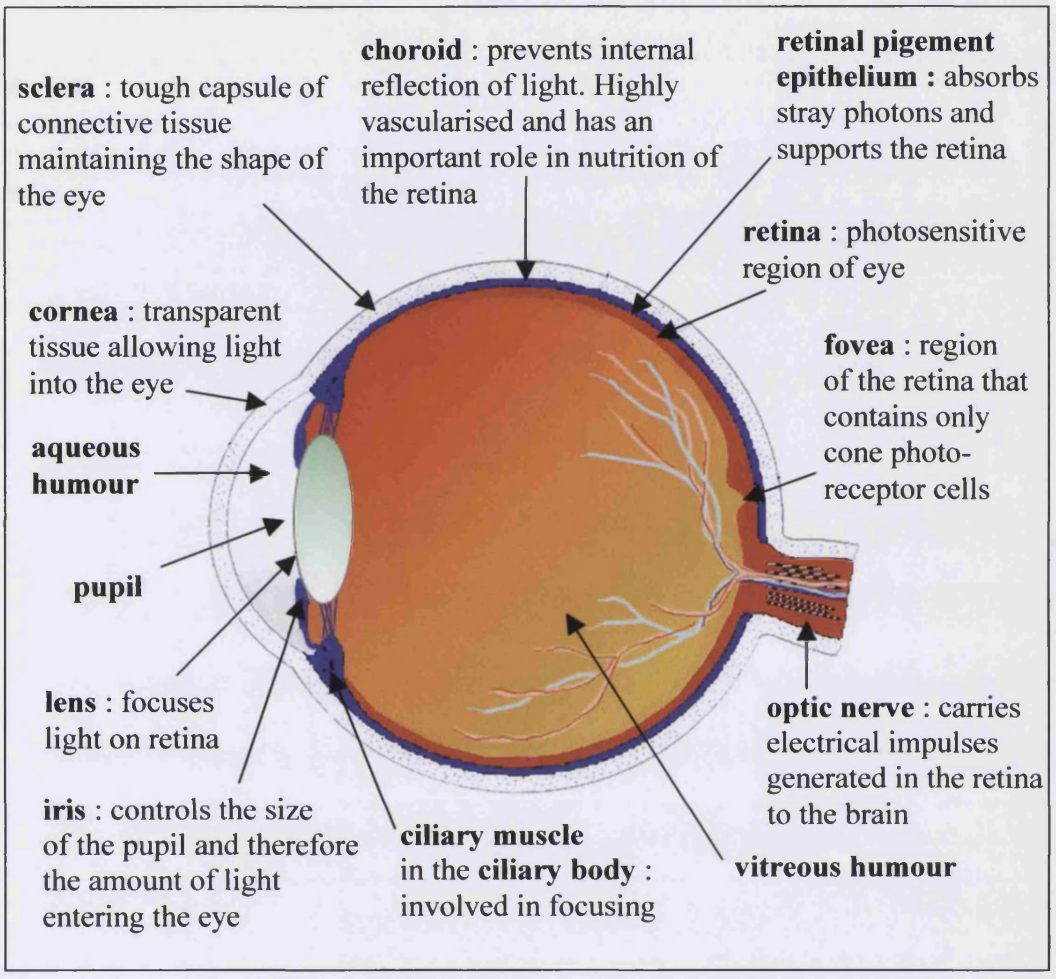

Figure 1.1 A vertical section through the human eye. Figure based on one found at http://retina.umh.es/Webvision.

1.1.1 The retina

The retina is part of the central nervous system, derived from the neural tube, and lines the inside of the eyecup. The neural retina of all vertebrates is made up of three layers of cell bodies and two layers of synapses that connect them (Fig. 1.2). The retina is separated from the choroid by a single layer of cells known as the retinal pigment epithelium (RPE). This layer of cells is also derived from the neural tube and contains melanin granules that absorb stray light in the eye.

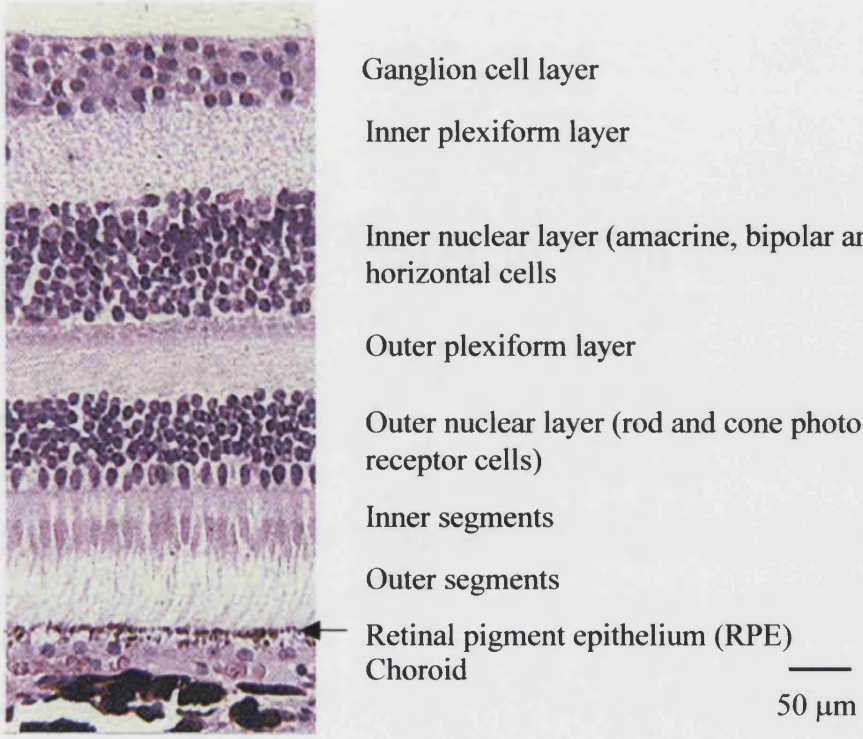

Figure 1.2 A semithin section showing the layers of the retina, and the retinal pigment epithelium. Figure based on one found at http://retina.umh.es/Webvision.

The outer nuclear layer contains the photoreceptor (PR) cells, responsible for converting light stimulus into first a biochemical and then an electrical signal by a process known as phototransduction. There are two types of PR cell, rods and cones, which differ in the types of visual pigment that they contain. While cones operate under conditions of bright light and are responsible for colour vision, rods function in dim light and do not discern colour. In the human retina there is a centrally located cone-rich region called the fovea, which is found in the centre of a yellowish spot within the retina named the macula. The fovea is the area of highest visual acuity and daytime living dictates that the majority of human vision relies heavily upon cones despite the fact that they make up only 5% of the PR cells [3]. In contrast, rodents, such as mice and rats, rely almost entirely on rod-mediated vision and these animals do not have a fovea or macula.

Each PR cell can be divided into outer and inner segments, a nuclear region, and a synaptic region. While the synaptic region provides the connection with the cells of the inner nuclear layer, the nuclear region and the inner segments are the metabolic hub of the cell where proteins and phospholipids are synthesised. The energy required for the visual process and protein synthesis is also produced here in the accumulation of

mitochondria at one end of the inner segment. Beyond this area there is a constriction in the inner segment that forms a cilia connecting the rest of the cell to the outer segment. The outer segments are cylindrical structures and are made up of hundreds of stacked discs where the visual pigments reside. This is where the process of phototransduction occurs. The outer segments interlace with apical processes from the RPE. Photoreceptor cells do not divide but the pigments and discs are not permanent. They are constantly turned over with the oldest discs being phagocytosed by the RPE cells while new discs are formed at the top of the outer segment. New discs are formed at a rate of 3 or 4 per hour in most mammals, and a newly formed disc will spend approximately 10 days as part of the outer segment before it is removed by phagocytosis [4]. The retina is one of the most metabolically active tissues in the body but it is poorly vascularized and it is thought that the PR cells derive their metabolites from the capillaries in the choriod through the RPE. In humans each RPE cell contacts approximately 45 outer segments and plays a role not only in the removal of old discs and nutrition but also in the process of phototransduction.

1.1.2 Phototransduction

Light passes through the layers of the retina to the rods and cones where it is absorbed by the visual pigments. In vertebrates these pigments consist of an apoprotein, opsin, which is covalently linked to a chromophore, 11-*cis* retinal, an aldehyde-derivative of vitamin A. Photons of light reaching the outer segments cause the isomerisation of the 11-*cis* retinal to all-*trans* retinol [247] which then dissociates from the opsin. This dissociation is also known as bleaching. The all-*trans* retinol is transported to the RPE where it is converted back into 11-*cis* retinal for re-association with the opsin. The activated opsin species with the all-*trans* retinol attached undergoes a conformational change and initiates the phototransduction cascade. It activates transducin [244], a photoreceptor-specific G protein. Transducin in its active state, bound to GTP (guanosine triphosphate), displaces the inhibitory sub-unit (γ) of a cyclic GMP phosphodiesterase (cGMP-PDE) then allowing it to catalyse the hydrolysis of cGMP to GMP. The resultant lowering of intra-cellular cGMP concentrations causes the closure of a cGMP-gated cation channel in the outer segment plasma membrane [245]. This has the effect of lowering the influx of sodium and calcium ions and causes membrane hyperpolarisation [246]. In turn this leads to the release of neurotransmitter at the photoreceptor synapse and the initiation of an electrical stimulus to the inner nuclear

layer and beyond. Within the outer segment there is initiated a recovery phase in which the components of the cascade are recycled to their inactive states.

1.1.3 Human retinal disease

The retina exists in a fine balance and it is therefore not surprising that it is a common site for inherited Mendelian disease. These diseases have been extensively studied and, in general, are divided into central dystrophies and peripheral dystrophies, according to the area of retina that they initially affect. Central dystrophies can be further divided into those that are confined to the macular and those that eventually involve the loss of the peripheral retina as well. The most widely recognised form of peripheral dystrophy is retinitis pigmentosa (RP).

1.2 Retinitis pigmentosa

First identified over 140 years ago [248], RP is perhaps the most extensively studied of the retinal dystrophies. Today the term encompasses a large heterogeneous group of diseases that are believed to have a combined incidence rate of between 1 in 3000-4000 worldwide, making it the most common form of inherited blindness [5, 6]. RP is primarily non-syndromic but like other retinal dystrophies it may also be a part of a multi-system disorder, such as Usher syndrome and Bardet-Biedl syndrome. It can be inherited as an X-linked, autosomal dominant or an autosomal recessive trait. Patients with RP are classified according to their clinical phenotype, electroretinographic responses, and the characterisation of the causative genes.

1.2.1 Clinical phenotype

Typical cases of RP are described as rod-cone RP since the rods are the predominantly affected PR cell type [239]. This results in the early characteristic clinical symptoms of night blindness and an impaired ability to adapt to changing light levels. There is bilateral symmetrical loss of the mid-peripheral visual fields. This gradually extends both peripherally and centrally so that the cone photoreceptors are also involved, resulting in a later reduction in central acuity and day vision. Another variant of RP is cone-rod dystrophy that is characterised by the simultaneous involvement of rods and cones [240]. In these cases there is a greater loss of the central area of vision much

earlier in the development of the disease in addition to night blindness and the restriction of the peripheral visual field. The rate of vision loss is variable, some patients becoming blind at an age of 30, while others retain some sight, albeit with a much-reduced visual field. The progression of the disease is accompanied by the release of pigment by degenerating RPE cells. Initially this gives the fundus a mottled, granular appearance. However, the pigment commonly accumulates in perivascular clusters called "bone-spicule formations" around the mid-periphery (Fig. 1.3) where the rod photoreceptors are at their highest concentration [241]. The presence of these retinal pigment deposits is a distinctive feature of advanced RP but earlier diagnosis can be made with an electroretinogram (ERG).

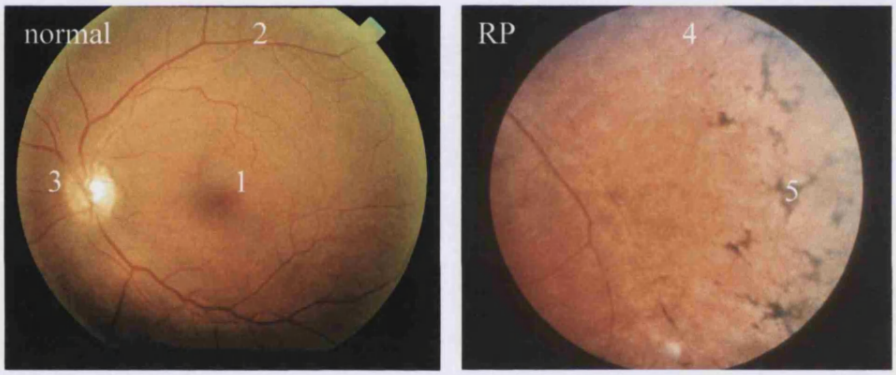

Figure 1.3 Retinal photographs illustrating the clinical appearance of the fundus in a normal individual and a RP patient. (a) Normal retina, (1) macula, (2) peripheral retina, (3) optic nerve head. **(b)** the periphery of an RP retina, (4) retinal atrophy , (5) bone-spicule formations. **(a)** figure was a kind gift from L. Da Cruz and **(b)** figure taken from Chong *et al.* [7]

1.2.2 Electroretinography

Electroretinography is a tool that is central to the diagnosis and classification of retinal disorders [242]. Electrodes placed on the cornea of the patient record the summed electrical response of the retina over a brief period after its stimulation with flashes of light. The ERG is affected by changes in the stimulus and recording parameters and by the adaptive state of the eye. Measurements are made after the subjects are either dark-adapted (scotopic ERG) or light adapted (photopic ERG). In essence, a dark-adapted subject stimulated with a dim light flash produces a rod specific response giving an indication of rod function. In contrast, a light adapted patient stimulated with a white flickering light will give a cone specific ERG response. The result of the recording is a trace of the electrical response over time that can be separated in to different parts. A recording of the maximal ERG from a normal dark-adapted individual (Fig. 1.4a) is

often used as a standard. This response has a cone component but is primarily driven by rod activity. It begins with the a-wave, whose polarity is negative relative to the cornea, but is interrupted by a large corneal-positive potential, the b-wave. The c-wave is a second corneal-positive response, but is much slower and therefore seen towards the end of the trace.

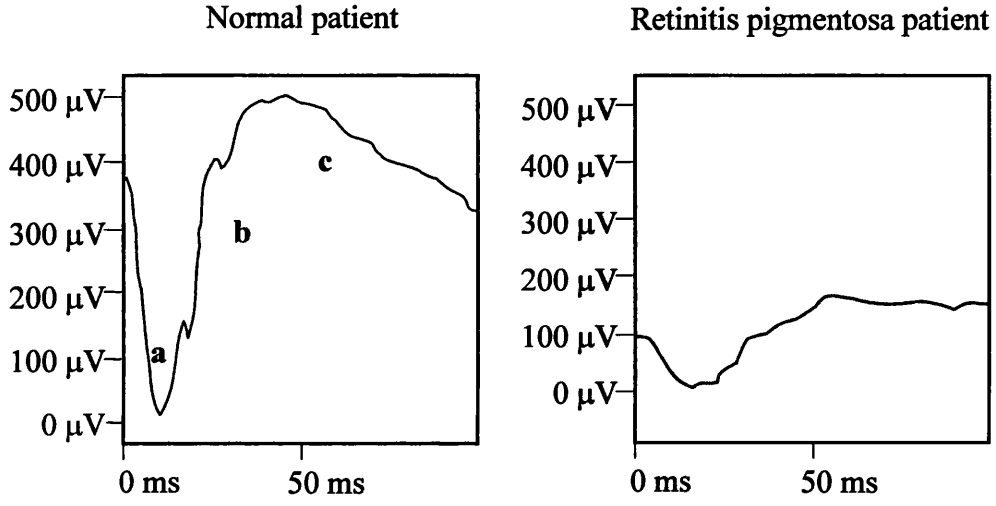

Figure 1.4 Maximal ERG responses from a normal individual and a retinitis pigmentosa patient. The response from a normal individual is characterised by an initial corneal-negative potential (the a-wave), followed by larger corneal-positive potentials (the b- and c-waves). In a patient suffering from retinitis pigmentosa all potentials are reduced in amplitude and delayed. Figure taken from Chong *et al.* [8].

The negative potential of the a-wave has its origins in the closure of cyclic nucleotide gated cation channels in the photoreceptor outer segments in response to the capture of photons (section 1.1.2). The b-wave is thought to be generated in the Muller and bipolar cells of the inner nuclear layer. The small oscillatory potentials on its ascending edge are also generated here, although their exact origins are not clear. It is though that individual oscillatory peaks have different origins with earlier potentials arising more proximally within the retina than later ones [9]. Understanding the components of the traces and their origins is critical to the use of the ERG as a diagnostic tool. Its value is that it allows the detection of patients with early stages of the disease before any other ocular features are present. Typically the ERG responses of patients with RP are delayed and have reduced amplitudes (Fig. 1.4b), reflecting the loss of photoreceptor function. These tests also distinguish between rod and cone responses indicating which type of photoreceptor cells are degenerating or functioning abnormally.

1.2.3 Genetics of retinitis pigmentosa

The relatively recent advances in the field of genetics have revealed that behind the range of clinical phenotypes lies an equally heterogeneous array of genetic defects. At present there are approximately 40 known RP loci (http://www.sph.uth.tmc.edu/Retnet /disease.htm) and genes have been cloned for approximately half of these regions. The majority of these encode proteins that are specifically transcribed in the PR cells or RPE and code for proteins involved in the phototransduction cascade [10-13], the structure of PR cells [14, 15] and retinol metabolism [16] as well as PR cell transcription factors [17, 18]. It is common for different types of mutations in the same gene to cause a variety of different diseases. Mutations within the gene for the PR cell specific protein, peripherin-2, have been shown to cause dominant RP [14] as well as several macular dystrophies [19, 20]. The protein is located in the rims of rod and cone outer segment discs and in rods it has been shown to be associated with a homologous protein, rod outer-segment protein-1 (ROM-1) [21]. Mutations within *ROM-1* have been implicated in digenic RP, where they occur in combination with mutations within *peripherin-2* (*Prph2*) [15]. Together these proteins are thought to have a role in the stabilisation of the disc.

In retinal degeneration the link between the mutation and the degeneration of PR cells is not clear. There are also other factors beyond the nature of the defect to consider since some mutations are known to result in different clinical presentations even between members of the same family [20]. While the factors involved are still uncharacterised it is difficult to go further and establish the route between the defect and the triggers involved in cell death. Apoptosis has been shown to be the mechanism of cell death in several animal models of retinal dystrophy [22, 23] as well as in cases of RP [24]. Therefore it is thought that all photoreceptor degeneration occurs via this pathway. Apoptosis affects isolated cells rather than patches of tissue and occurs in the absence of an inflammatory response. However, in mosaic mouse models of RP diseased or dying PR cells can induce cell death in adjacent genetically normal PR cells [25, 26]. The mechanisms involved in triggering cell death in these cases (to be discussed further in section 5.1.2) may also be the cause of the loss of cones in those RP patients that carry rod-specific gene defects.

1.2.4 Treatments for retinitis pigmentosa

With the exception of a few rare metabolic disorders, such as Refsum disease and gyrate atrophy [27], there are no treatments that target the primary cause of RP and current therapy is limited to the relief of symptoms, such as cataract removal. A variety of new treatments are currently being developed in experimental animal models. Survival factors, such as neurotrophic factors, growth factors and cytokines, have been shown to slow the rate of degeneration in mouse models of retinal degenerations after intra-vitreal injection [28] (see section 1.5.3.2). However, survival factors act over a short distance and it is not known how effective they would be in a larger eye. Moreover, they have a short half-life and a persistent effect would require repeat injections that are impractical. Transplantation is an alternative option that, unlike other therapies, presents the opportunity to replace lost PR cells. However, this form of treatment will have to overcome several barriers to be successful. The transplantation of PR cells requires not only long-term survival of the graft but also the re-establishment of the appropriate synaptic connections and the maintenance of delicate outer segment structures. Transplantation of mature photoreceptors into a mouse model of retinal degeneration has been attempted [29]. This study showed partial integration of the transplant into the host retina. However, at 30 days post operation only 10% of the retinal grafts had survived. Work is now moving towards the use of stem cells, multipotent cells that have the capacity to divide and differentiate. Adult neural stem cells (ANS) derived from the rat hippocampus and injected into the intra-vitreal space have the ability to migrate into the dystrophic retina, where they respect the local laminar organisation and differentiate into neurons [30]. However, they do not produce photoreceptor cells. Tropepe *et al.* [31] have described the isolation of mouse retinal stem cells from early post-natal and adult eyes. These cells can proliferate *in vitro* and differentiate into rod photoreceptor cells, but this capacity has yet to be shown *in vivo*. Transplantation may prove to be more successful with the RPE. Transplantation of healthy RPE cells has been shown to slow the loss of PR cells in this in the Royal College of Surgeon's (RCS) rat [32]. The retinal degeneration phenotype in this animal is the result of a failure of the RPE to phagocytose the shed outer segments from the PR cells. Mutations within the causative gene have also been shown to be responsible for some cases of autosomal recessive RP [33].

The absence of an effective treatment has heightened interest in other possible approaches. An alternative is to try to prevent the loss of photoreceptor cells by gene therapy and this is the subject of this thesis.

1.3 Gene therapy

Rapid advances in molecular genetics and molecular biology over the past two decades have provided a much greater understanding of the genetic basis of disease and have led to the development of many of the tools required for therapeutic intervention via gene therapy. The concept of gene transfer for correction or amelioration of genetic defects has been widely appreciated and as a result gene therapy is the focus of much research. Since the start of the first clinical trial in September 1990 [34] it has taken until April 2000 [35] for the publication of what is widely regarded as the first successful treatment of an inherited disorder via gene therapy. This trial treated two infants suffering from inherited severe combined immunodeficiency (SCID-X1), which is characterised by an early block in the T and natural killer (NK) lymphocyte differentiation as a result of a mutation in the gene for the γc subunit of certain cytokine receptors [243]. In this trial haematopoietic stem cells were taken from the bone marrow of the infants and incubated *ex vivo* with a retroviral vector carrying a normal copy of the γc cDNA. The transduced stem cells were then transfused back into the patients. The authors report follow-up data over 10 months on T and NK cell counts and antigen-specific responses of these cell types that were essentially comparable to those of age-matched controls.

That the first account of successful gene therapy is in a clinical trial that uses *ex vivo* transduction is telling. This approach involves the removal of the target cells from the body and gene transfer *in vitro*. The engineered cells are then re-implanted back into the body. The advantage of this is that transduced cells can be selectively propagated before re-implantation resulting in a higher efficiency of transduction. However, for many target cell types within the liver, kidney and brain, as well as the eye, removal and re-implantation is not possible. These cell types must be transduced *in vivo* by the direct administration of the gene-transfer vector into the vicinity of the affected tissue. Therefore initial efforts in gene therapy have been in the development of vectors, which will transport these transgenes efficiently to the appropriate cell type.

Selective and efficient gene transfer is hard to achieve as the human body has evolved to protect itself from the incorporation of foreign DNA into its genome. Viruses were therefore a natural choice from which to manufacture vectors since they have also evolved, with some success, to overcome the body's defences. They possess the ability to infect mammalian cells and to avoid endocytosis and lysosomal degradation, while the viral proteins help with import into and persistence of the viral genome within the infected cell. Non-viral vectors, such as those made by complexing DNA with liposomes, have also been developed. While progress is being made in this field current non-viral systems achieve relatively inefficient transfection in comparison to viral systems [36]. As a result vectors made from adapted viruses are receiving the most attention for *in vivo* delivery.

1.4 Vectors for *in vivo* gene delivery

1.4.1 Creating viral vectors

Successfully manipulating a virus and its life cycle to meet the requirements of gene transfer is not an easy task [38]. The viral genome must be replaced with a recombinant genome carrying the therapeutic gene and possible promoter regions to ensure its appropriate expression. Viral elements necessary for the packaging of the recombinant genome into a viral particle must be retained. Recombinant viral particles are manufactured *in vitro* in cell lines in which the viral genes can be expressed from other plasmids or even incorporated into the genome of the producer cell (Fig. 1.5).

Ideally all viral genes should be deleted, since transcription of the viral genes within infected cells may attract the attention of the immune system and result in the removal of transduced cell. In practice the minimum requirement is the deletion of viral genes so that the vector does not retain its ability to replicate *in vivo*. Deleting every viral gene, however, may not always be advantageous. For example a gene in the E3 region of the adenoviral genome encodes a protein that protects the virus from host immune surveillance [37]. Its deletion may result in an increased immune response against the adenovirally transduced cells. Moreover in a wild type life cycle the viral genome ensures an appropriate balance of viral protein production through interaction between regulatory regions and its genes. Deleting regions of the genome may often unbalance

the production of viral proteins and result in the production of defective viral particles or inefficient packaging of the recombinant genomes.

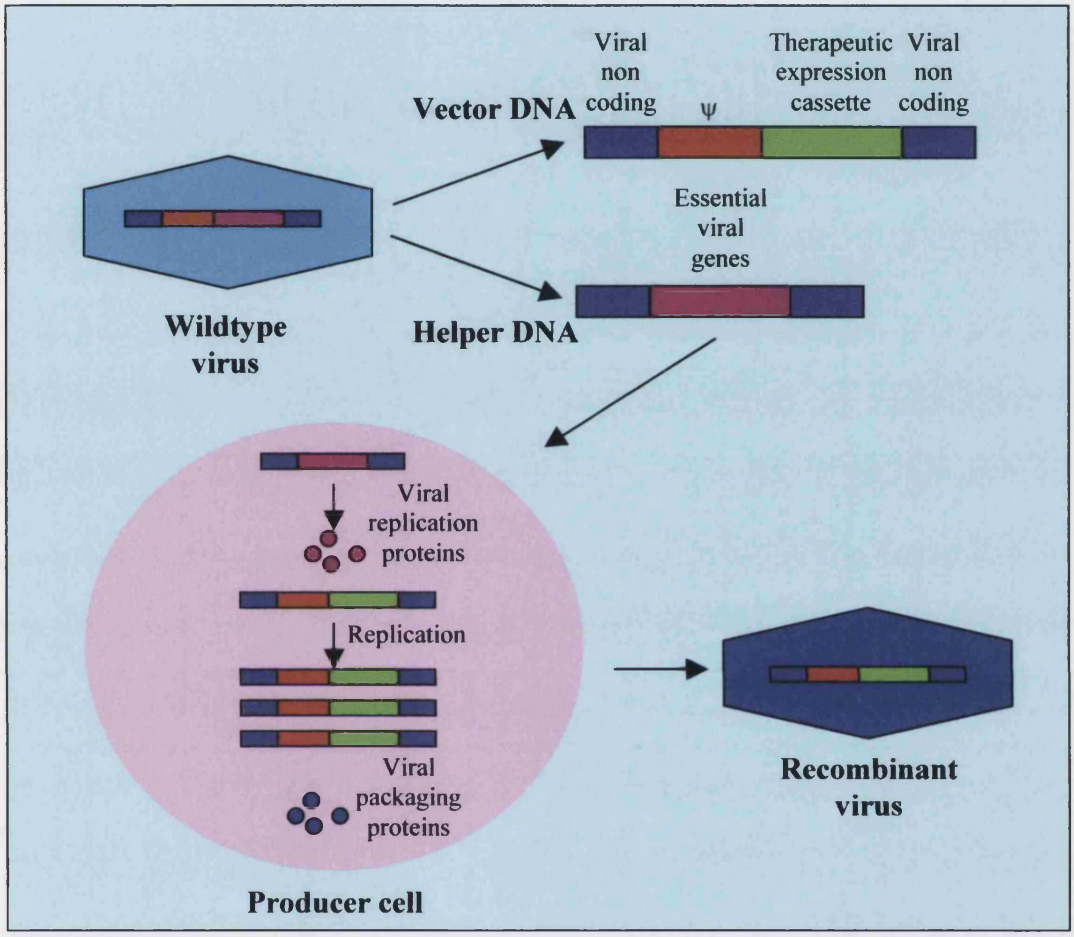

Figure 1.5 Generic strategy for engineering a virus into a vector. The helper DNA contains the genes essential for viral replication placed in a heterologous/unrelated DNA context that can be delivered as a plasmid, helper virus or inserted into the chromosomal DNA of the packaging cell. The helper DNA lacks the packaging domain (ψ) so it or its RNA cannot be packaged into a viral particle. The vector DNA contains the therapeutic expression cassette and the non-coding viral *cis*-acting elements that include the packaging domain. Inside the packaging cell the viral proteins required for the replication of the vector DNA are produced. Such production leads to the synthesis of many copies of the vector genome. Viral structural proteins recognise the vector sequence but not the helper sequence resulting in the packaging of the vector genomes into recombinant viral particles. Figure and adapted legend are taken from Kay *et al.* [38].

Since recombinant viruses are produced in biological systems there are also problems related to safety and post-production purification. Care must be taken to ensure that there is minimal risk of the creation of replication competent viral particles through recombination events with the producer cell line. The recombinant particles must also

be extensively purified to minimise toxicity, particularly in respect to clinical trials, requiring time and possibly reducing viral titre.

1.4.2 Properties of viral vectors

The key features of an ideal gene therapy vector are:

a) Easy production - The vector should be easy to produce to consistently high titre and purity without contaminating proteins and replication competent particles. Methods must have the capacity to be scaled-up for commercial production.

b) An ability to transduce only the target cell type - The transduction of only specific cell types is a highly desirable property, preventing not only expression of the therapeutic gene in inappropriate cell types but also the transduction of dendritic cells. These specialised antigen-presenting cells might trigger an immune response to transduced cells. The ultimate targeting vector would be systemically injected and transduce target cell types around the body.

c) Immunologically inert - The vector components should not elicit an immune response after delivery. A humoral antibody response will make a second injection of the vector ineffective, and a cellular response will remove the transduced cells.

d) Non-toxic - The vector components should be non-toxic even when multiple particles have transduced the same cell.

e) No size limitation - The therapeutic gene may be large or require large amounts of regulatory sequences and therefore the vector should have no limit to its capacity.

f) Have the ability to stably maintain itself within the transduced cell - In many diseases sustained expression of the therapeutic gene is required. The vector can ensure that the recombinant genome is maintained within the transduced cell by integrating it with that of the host genome. Site-specific integration is preferable since it prevents damaging effects of insertion into an important region, or insertion into an area where endogenous elements may interfere with expression of the therapeutic gene. Vectors that maintain the recombinant genome as an episome within the host nucleus are not so favourable since the episome may be lost - particularly in dividing cells.

None of the currently available vectors have all of these properties. A review of the three major viral vectors that have been used to deliver genes to the retina highlights the problems associated with developing these delivery systems to meet the requirements.

1.4.3 Retroviral vectors

Retroviruses have been considered good candidates for successful vectors since the beginning of viral vector development [249]. They have a large cloning capacity of approximately 8 kb but most importantly they have the ability to integrate efficiently into the host cell without the transfer of any viral genes. This creates the potential for stable long-term expression from the transgene without the immunological consequences of expression of viral genes.

Many of the original vectors were derived from the oncoretrovirus Moloney murine leukaemia virus (MoMLV) [249]. The major drawback with this type of virus, however, is that it is unable to transfer genes into non-dividing cells [39]. The pre-integration complex, containing the newly reverse transcribed viral DNA, is unable to penetrate the host cell's nucleus unless the nuclear membrane is fragmented as it is during cell division. For a large area of gene therapy this is a major drawback. Many cell targets such as neurons, hepatocytes and myocytes rarely, if ever, proliferate. Interest in retroviruses for transfer to non-dividing cells has been revived by the development of lentiviral vectors. Lentiviruses are retroviruses that can infect macrophages and lymphocytes, the most notorious of which is human immunodeficiency virus (HIV). As most tissue macrophages do not proliferate lentiviruses have evolved the ability to infect these cells in the absence of cell division. In contrast to viruses like MoMLV the pre-integration complex of lentiviruses contains nuclear localisation signals allowing it to cross the nuclear membrane by active transport through the nuclear pores when the cell is in interphase [40]. Since HIV type 1 (HIV-1) is the best characterised of all the lentiviruses it became the obvious choice as a vector. However, the major challenge was to design a production method that would minimise the risk of emergence of replication competent recombinants (RCR). The HIV genome is more complex than that of simple retroviruses and the first generation of lentiviral vectors retained much of these sequences. The viral sequence for the Env protein was substituted for the protein for vesicular stomatitis virus G protein (VSVG) resulted in HIV-1 vectors that were no longer dependent on the T-cell receptor protein, CD4, for entry into cells. These vectors were shown to successfully transduce terminally differentiated neurons [41], however, there were many concerns over the generation of RCRs. Subsequent work has therefore focused around the systematic deletion of the genes for the accessory proteins while attempting to retain the features of efficient recombinant vector production and

infection of non-dividing cells [42, 43]. Current third generation lentiviruses retain only three of the nine original genes and *trans*-acting elements are distributed over as many independent units as possible [44]. This maximises the number of recombination crossover events that would be required to produce a RCR. Self-inactivating (SIN) vectors have also been developed through engineering of the viral long terminal repeats (LTRs). Deletion of several viral regulatory elements results in the loss of LTR transcriptional activity once transferred to the target cells [45]. These vectors should reduce the risk of insertional activation after random integration of the genome and have the added advantage that the inactivated LTRs do not interfere with the transgene promoter.

Lentiviruses are now the vector of choice for transducing neurons and have been shown to mediate stable and long-term transgene expression for up to 6 to 8 months in this cell type [46, 47]. It may be possible to extend their range to other cell type by pseudotyping with other viral envelope proteins. They have shown promise in the transduction of certain cell types within the eye (to be discussed later) and certain cell types within the lympho-haematopoietic system, such as CD34+ haematopoietic stem cells [48]. However, they seem comparatively poor at transducing myocytes and hepatocytes. The reason for this is not yet clear. Recent work by Parks *et al.* [49] has shown that liver cells cannot be transduced *in vivo* unless they are induced to proliferate and it has been suggested that partial activation of some cell types in G_0 phase of the cell cycle may be necessary for successful transduction to occur.

1.4.4 Adenoviral (Ad) vectors

Adenoviruses are a family of human DNA viruses that cause benign infections in the respiratory tract. Viral particles are 80-90 nm in diameter and the genome, approximately 36 kb in length, is divided into several early (E) and late transcriptional regions according to involvement in the viral life cycle. Adenoviral particles have the ability to infect both dividing cells and those that are quiescent or terminally differentiated. First generation vectors were deleted for the E1 region, making them replication defective, and were easily produced to a high titre (10^{11} infectious units (iu)/ml) in 293 cells, a cell line that constitutively expressed the E1 proteins. These vectors were also deleted in the E3 region to make space for the insertion of the transgene, and could accommodate 7.5 kb of DNA. As one of the first viral vectors for

in situ transfer it was used for gene transfer to many tissues and found to have a widespread tropism. However, these first generation vectors provoked neutralising antibody responses against the proteins of the viral particle and expression of the residual viral genes led to cytotoxic-T-lymphocyte (CTL) responses directed against the transduced cells [50, 51]. As a result expression of the transgene was limited, often to within a few weeks of vector delivery. The complex nature of the adenoviral genome has made the deletion of further viral genes difficult and unlike lentiviruses the production of a packaging cell line has not been possible. Helper-dependent systems have now been developed by many groups which are capable of producing gutless adenoviral vectors that contain only the viral inverted terminal repeats and the packaging signal, and allow the incorporation of 28-32 kb of foreign DNA [52]. The viral genes required for production are provided in a second vector that has a conditional defect in its packaging signal and therefore is less efficiently packaged. Recombinant vector particles must be purified away from helper virus by labour intensive processes, such as ultracentrifugation, and low levels of contamination remain (less than 1%). Despite these drawbacks these vectors are less immunogenic and have been shown to prolong transgene expression [52, 53], with expression of up to 10 months demonstrated in hepatocytes [54].

The host immune responses, however, remain a challenge for adenoviral vectors. Kafri *et al.* have shown that even biologically inactive E1 deleted Ad from which there is no *de novo* synthesis of either viral or transgene proteins induced a strong cellular response [55]. This result was thought to be due to the ability of the viral particles to enter the MHC (major histocompatibility complex)-class I processing pathway, and demonstrates that even gutless vectors will not completely avoid the host immune response. In addition, the humoral immune response may also act to neutralise adenoviral particles, preventing efficient transduction. Although there are over 50 different human adenoviral serotypes the majority of current adenoviral vectors are derived from types 2 and 5. These are the most common serotypes to which many adults have been exposed, with over 55% of the adult population carrying pre-existing antibodies to Ad5 capable of neutralising infection *in vitro* [56]. Clinical studies in which adenoviral vectors have been used have confirmed that the extent of the antibody response appears to be dictated by pre-existing antibody titres and varies according to the route to injection [57]. It should also be considered that adenovirus does not integrate its genome into that of the

hosts and its episome may be lost in dividing cells. Long-term expression of a transgene may therefore require repeat injections.

While in the long-term immune suppression is not an ideal option attempts are being made to control the immune response in this way at the time of adenoviral injection. Available options for suppressing the humoral response are macrophage depletion [58], and blockade of co-stimulatory molecules [51, 59] or inflammatory cytokines [60]. These avenues of research may be worthwhile since for many cell types adenoviral vectors provide more efficient gene transfer compared to other systems. Additionally its relative ease of manufacture, in comparison to lentiviral and adeno-associated viral vectors, allows large-scale production. This is an advantage when the vector is to be used in large animal models and ultimately in clinical trials. As with lentiviral vectors work is underway to genetically engineer the viral capsid proteins to further extend virus tropism [61, 62].

1.4.5 Adeno-associated viral (AAV) vectors

Adeno-associated virus is a small (20-25 nm) non-pathogenic human virus that has the ability to infect both dividing and non-dividing cells. There are six known human viral serotypes, each of which appear to have different tropic properties [63, 64]. To date most studies have focused on AAV-2. The viral genome is single stranded DNA and consists of two separate open reading frames between two inverted terminal repeats (ITRs). One open reading frame encodes the viral capsid proteins (Cap) while the other gene encodes the Rep proteins that are required for its replication. After infection the single-stranded DNA genome is converted into its transcriptionally active double stranded form by the host's DNA repair machinery. The virus then shows preferential integration of its genome into the human genome at a particular locus on chromosome 19q13.3qter, AAVS1 [65]. This property appears to be unique among mammalian viruses because of its site-specific nature.

The ITRs, that are located at each end of the genome, are the only *cis*-acting elements required for production of infective recombinant AAV (rAAV) [66]. Therefore rAAV incorporates no viral genes but has a relatively small carrying capacity of just over 4.6 kb. Following transduction with a rAAV vector many tissues demonstrate long-term expression of a reporter transgene, particularly skeletal muscle [67-69] and the central

nervous system [70]. The ITRs, which are retained in the recombinant virus, are known to be involved with targeted integration [71], but Rep proteins, the genes for which are deleted from rAAV, are also required [72, 73]. The recombinant virus retains the ability to integrate although much less efficiently and into heterogeneous sites around the host genome [74, 75]. In a proportion of transduced cells *in vivo* the recombinant genome persists as high molecular weight concatamers, double stranded tandem arrays [67, 76]. At present it is not clear, when long-term expression is obtained *in vivo,* whether this originates from the integrated or extra-chromosomal DNA. However, work involving the FISH (fluorescent *in situ* hybridisation) analysis of metaphase chromosomes from transduced hepatocytes [77] and the isolation of rAAV vector-host DNA junctions from mouse liver [78] suggests the importance of integration in long-term expression from this tissue. It has recently been shown that by incorporating sections of the *rep* gene into rAAV it is possible to achieve site-specific integration of the transgene in human cells *in vitro* [79]. The utility of this must be weighed against the possibility of stimulating an immune response against the transduced cells as a result of the presence of Rep proteins.

Long-term AAV-mediated transgene expression has been demonstrated routinely in mice but also in dogs [80, 81] and primates [82] suggesting that rAAV is much less immunogenic than rAd. After intra-muscular injection AAV-transduced myocytes showed reporter gene expression for up to a year and a half, displaying only transient lymphocyte infiltration and without eliciting a cell-mediated immune response [67]. Further studies showed only a trace CD4+ TH2 IL-10 responses against the neoantigenic transgene product, *E.coli* β-galactosidase, with humoral responses generated primarily against the rAAV capsids [69]. The lack of strong CTL responses has been attributed to inefficient transduction of antigen presenting (AP) cells in this tissue [83]. This could potentially be a very useful property of AAV. However, this finding does not appear to be consistent. Brockstedt *et al.* [84] have demonstrated that CTL responses to rAAV, carrying the transgene encoding ovalbumin, vary according to the route of administration. Intra-muscular injection of the virus was the only route that did not show CTL responses, while intra-peritoneal, intra-venous and sub-cutaneous delivery all resulted in ovalbumin specific responses. All of these routes also resulted in the stimulation of humoral responses against the rAAV capsid proteins. As with adenovirus, in humans there is pre-existing immunity to AAV capsid proteins. Up to

80% of the population are seropositive for AAV, with antibodies against AAV-2 being the most prevalent [85]. This may be significant clinically particularly if re-administration of the vector is required.

AAV appears to suffer from three major drawbacks. Firstly it is a dependovirus and therefore requires helper virus, such as adenovirus, for its manufacture. Increasing production is also made difficult by the fact that the Rep proteins and some of the adenoviral helper genes are cytostatic and cytotoxic to the packaging cell line. The developments in production of rAAV will be discussed in greater detail in Chapter 3. The second drawback of AAV is its small capacity, limiting the size of the transgene and the amount of regulatory sequences that can be incorporated into particles. Recent research aimed at overcoming this problem utilises the knowledge that within the transduced cell nucleus the AAV genome forms concatamers. Systems that involve the use of two rAAV vectors, each coding for different halves of the same protein, have shown expression of a reporter gene *in vivo* at levels 60-85% of traditional AAV vectors [86, 87]. Finally the onset of expression of the transgene after transduction is slow in many cell types due to the time taken for the conversion of the single-stranded DNA to double-stranded DNA [88, 89].

Currently there are many challenges to be overcome before any of the vectors described above meet the standards of an ideal vector. Therefore the choice of vector becomes an important consideration in the application of gene therapy for the treatment of a specific disease, and the advantages and disadvantages of each type of vector must be evaluated. The choice will focus around the performance of the vector on a number of criteria but, in the first instance, it is likely to be governed by the efficiency of transduction of target cell.

1.5 Ocular gene therapy

The eye has a number of advantages as a target organ for gene therapy. It is accessible and its function and health can be monitored relatively easily. Non-invasive observations can reveal signs of disease progression and inflammation *in vivo*. Since the majority of diseases progress symmetrically in both eyes gene therapy protocols can

utilise the untreated eye as an internal control. Additionally the eye has long been seen as an immune-privileged site proved by the clinical success in corneal transplantation and experimental delivery of tissue grafts to the eye [90]. This may result in a decrease in responses to viral and transgene antigens for some vectors in comparison to other areas of the body, although this does not appear to be the case for adenoviral vectors (section 1.5.2.1). Systemic administration of the recombinant vector is unlikely to be effective at targeting tissues within the eye, particularly with the presence of the blood-retinal barrier, and would require an impractical volume of virus. Therefore local administration is required. The eye is separated into discrete departments and delivery must be through the relatively invasive approach of direct injection in the vicinity of the target cell type.

1.5.1 Gene therapy for retinitis pigmentosa

As previously discussed the two major cell types that are involved in RP are the PR cells and the RPE (see section 1.1.3). Most protocols targeting this cell type use the procedure of sub-retinal injection that mechanically delivers the virus between the RPE and PR cells. This procedure is commonly performed in vitreoretinal surgery and causes a transient detachment of the PR cell layer from the RPE. While this has the theoretical advantage in limiting cell types exposed to the virus there are concerns over the surgical damage resulting from this type of injection particularly in small mouse eyes where the procedure is more difficult.

Testing of procedures and treatment with gene therapy requires the use of animal models of the diseases. It is fortunate that there are two well-characterised naturally occurring mouse models of RP, the *Prph2*$^{Rd2/Rd2}$ mouse [91] and the *rd* mouse [92] that have formed the basis of many studies. The Irish setter *rcd1* dog also has a mutation within the same gene as the *rd* mouse and is a larger animal model for recessive RP [93]. The range of models has been extended with transgenic technology. Transgenic mice [94], rats [95] and pigs [96, 97] have been made with mutations in the *rhodopsin* gene providing models of autosomal dominant or autosomal recessive forms of RP. In addition the Tulp1 knockout mouse [98] and the RPGR knockout mouse [99] provide models for autosomal recessive RP and X-linked RP respectively. The RCS rat provides an example of an RPE cell defect, with a mutation within a receptor *tyrosine kinase*

gene (*MERTK*) providing a phenotype that is similar to autosomal recessive RP [100, 101].

While the smaller animal models have the advantage of short generation times, large litters and low cost, the small size of the mouse eye and the relatively large size of the lens make precise surgical procedures very difficult. Larger animals such as dogs provide the opportunity for more advanced testing of surgical techniques. In addition tests of visual acuity and behavioural assessment can more easily be performed. The PR cell loss in these larger animals is slower giving rise to a phenotype that is closer to human retinal degeneration, although the effect of therapy on degeneration takes longer to assess. However, there are differences between the retina in these animals and that of humans. Mice and rats have a lower cone-rod ratio than humans and lack a cone-rich central retina. Dog retinas have a larger number of cones, but only the primate retinas have a fovea and macula similar to humans. As yet there are no primate models of retinal degeneration.

1.5.2 Gene transfer to photoreceptor cells and RPE

Both the RPE and PR cells are terminally differentiated cell types and do not, under normal circumstances, divide. As a result vectors that can transduce only dividing cells are of limited use. Gene transfer to these cell types has been investigated in both normal animals and animal models of RP by the sub-retinal injection of vectors carrying reporter genes encoding bacterial β-galactosidase (lacZ) and green fluorescent protein (GFP). The viruses that have been most closely examined as potential vectors for the retina are adenovirus, lentivirus and adeno-associated virus.

1.5.2.1 Adenoviral vectors

The success of adenoviral mediated gene transfer to the brain [102] encouraged the use of adenoviral vectors in the eye. Therefore these were one of the first vectors to be injected into the sub-retinal space by Bennett *et al.* [103] and Li *et al.* [104]. Taken together these studies demonstrated that 1-2 μl of rAd carrying a *lacZ* gene driven by the immediate-early promoter of cytomegalovirus (CMV) at a titre of 10^{11} iu/ml (infectious units per ml) could transduce RPE cells with high efficiency (approximately 90%) in the area of detachment in normal adult mice. Positive staining of RPE cells was detected as early as 48 hours after injection and increased over the next two weeks. As

predicted an increase in the titre of the injected virus caused an increase in lacZ staining, with titres as low as 10^5 iu/ml producing obvious staining of the eyecup. Bennett *et al.* saw no staining in the neural retina after injections of less than 10^9 iu/ml of virus, while Li *et al.* saw no gene transfer to photoreceptors even with titres of 10^{11} iu/ml except in areas where retinal structures were damaged by the injection needle. These results indicate that adenoviral vectors are more efficient at transducing RPE than PR cells. However, an increased transduction efficiency of both rod and cone photoreceptor cells, to approximately 30 %, was observed after injection into 5 to 7-day old *rd* pups, whose photoreceptor cells were in the early stages of degeneration, and 5 to 7-day old normal pups, where the retina is still developing [104]. The common feature of these retinas is that the PR outer segments are shorter or absent. It was proposed that this allowed greater access of the rAd particles to the PR cells in contrast to the long, densely packed, outer segments of normal mice that could act as a physical barrier.

As with other tissues transgene expression in normal adult mice was of limited duration and this was largely attributed to leaky expression of late viral genes. In some studies expression was seen for approximately 3 weeks, while in T cell deficient Balb/c mice expression was detected for at least 15 weeks [105]. Further evidence for the CTL-mediated destruction of the transduced cells was gained when it was shown that blocking of activation of T-cells at the time of injection also extended transgene expression [106]. In contrast Bennett *et al.* described experiments in which there was no difference in the duration of expression between normal and immunodeficient mice (*nu/nu*) [107]. The differing reports might be explained by the differences in viral preparation, titres injected, mouse strain, and sub-retinal injection technique. For these reasons it is also not possible to make detailed comparisons between these sets of results and those gained in similar experiments in different tissues. Therefore it is difficult to assess whether the sub-retinal space retains some of its characteristics as an immune-privileged site in respect to rAd vectors and transduced cells. However, it is unlikely that the blood-retinal barrier in the mouse eye remains completely intact through the sub-retinal injection procedure and it is likely that the immune response has a part to play in loss of rAd transduced cells. Neither of these experiments demonstrated expression much beyond 100 days in both immunocompetent and immunodeficient mice. This may be due to loss of activity of the transgene promoter or loss of the adenoviral episome. Sub-retinal injections with gutless adenoviral vectors have been

performed by one group who reported transgene expression for up to 18 weeks in immunocompetent mice [108]. However, transgene expression was not localised to PR or RPE cells but assessed through RT-PCR (reverse transcription-polymerase chain reaction) and western analysis of retinal samples. Moreover, there was no data on the level of immune responses in treated animals.

1.5.2.2 Adeno-associated viral vectors

The first experiments in mice using rAAV revealed its potential in transduction of PR cells and it was shown to be 2000 fold more efficient at transducing this cell type than rAd [109]. All procedured animals showed an increase in reporter gene expression from the first detection of expression at 1-2 weeks post injection to strong expression at 6-8 weeks. The use of *egfp* (enhanced *gfp*) as a reporter gene allowed the study of expression *in vivo* by direct observation of fluorescence using an ophthalmoscope, with appropriate excitation-barrier filters [110]. The results from this experiment demonstrated the stability of expression of *egfp* over a 3-month post injection period in 7 mice during which there were no signs of an inflammatory response or toxicity to the vector. There is a systemic humoral response to rAAV capsid proteins injected into the sub-retinal space, but these have been shown not to prevent additional transduction events after re-administration of rAAV [111]. The success of these studies prompted the extension of these studies into larger animal such as non-human primates. Recombinant AAV constructs carrying the *egfp* gene driven by a CMV promoter were sub-retinally injected into these animals and expression of *egfp* followed *in vivo* over 1 year. The start of *egfp* expression was shown to vary from between 8-18 weeks, but expression appeared to be stable between 4 months and when the experiment ended at 11 months [112]. There was no electroretinographic or histological evidence of photoreceptor toxicity and the only local pathological effect that was observed was occasional pigment loss in RPE cells. Transgene expression was limited exclusively to rod photoreceptors.

1.5.2.3 Lentiviral vectors

Vectors based on HIV have also been evaluated in the eye. These vectors have been shown to transduce RPE cells efficiently after sub-retinal injection in normal adult rats and rat pups [113]. However, the distribution of positive RPE cells was more restricted in the adults than in the pups, and in the adults expression was only seen from PR cells around the injection site. In the pups a larger number of PR cells (16%) were transduced

and on injection of a vector containing a PR cell specific *rhodopsin* promoter this number was increased by 2.5 times. The authors attribute this to the difference in the relative efficiencies of each promoter in this cell type. The percentage of transduced cells remained constant between 2 weeks post-injection to 12 weeks when the studies were finished. Some inflammatory cells were observed in the area surrounding the injection site 2 weeks post injection, but were gone by 6-12 weeks post injection. These were likely to be due to surgical damage during injections since similar cells were seen in control animals that had had saline injections. The authors suggest that in adult rats expression of transgene was restricted around the injection site in comparison to pups because the interstitial space in between PR cells is tighter in adults than in pups making it difficult for HIV vector particles to diffuse away from the site of injection.

1.6 Gene therapy approaches in animal models of disease

While retinal gene therapy has lagged behind some areas of gene therapy in that it has not yet progresses to clinical trials there have been some successes in the treatment of animal models of RP that have been encouraging. Since retinal dystrophies have different pathologies the strategies for their treatment have had to be similarly varied.

1.6.1 Gene replacement strategies

Autosomal recessive and X-linked recessive mutations result in disease through lack of an essential gene function and therefore treatment requires delivery of a functional copy of the defective gene to the target cell. One autosomal recessive form of RP results from a null mutation in a rod PR cell specific gene that encodes the beta sub-unit of the enzyme cyclic GMP phosphodiesterase (cGMP PDE), a component of the phototransduction cascade involved in the hydrolysis of cyclic GMP (section 1.1.2). In humans some mutations within *βPDE* generate a premature stop codon preventing normal expression of this gene [114]. Two naturally occurring mutations have also been observed in the same gene in the *rd* mouse [115] and *rcd1* dog [93]. In the mouse a nonsense mutation results in the truncation of the normal gene product eliminating more than one-half of the peptide, including the putative catalytic domain. The mutation leads to a deficiency in PDE enzyme activity and, in homozygous mice, elevated levels of cGMP by postnatal day 6. The first pathological changes are detectable under the

electron microscope at postnatal day 8 (P8) and by P13 the photoreceptors are degenerating rapidly. Complete loss of the rod photoreceptor cells approximately occurs by postnatal day 20 (P20). In contrast cone PR cells survive much longer, and other retinal cells remain intact [92].

Conclusive proof that the phenotype of *rd* mice is produced by a defect in the *βPDE* was provided by Lem *et al.* who rescued the degeneration phenotype through the expression of a functional bovine *βPDE* gene in transgenic *rd* mice [116]. Subsequently the *rd* mouse has been the subject of several functional gene therapy trials but it has several drawbacks that make it a difficult model to treat. Firstly the speed with which the degeneration progresses doesn't give a wide window for intervention. Injection of the vector must occur in very young pups, before the eyes are open, in order for the delivered gene (*βPDE)* to be expressed and have an effect before all the rods are lost. It would therefore be surprising if it were possible to slow the rate of degeneration of PR cell ('rescue') in the *rd* mouse using rAAV since this vectors mediates a slow onset of transgene expression. However, this has been reported in one study in which the *βPDE* transgene was expressed with an *opsin* promoter [117]. Rescue has also been reported with adenoviral and lentiviral vectors. An E1, E3 deleted Ad vector (1×10^8 iu/ml) was used by Bennett *et al.* [118] to deliver the *βPDE* transgene expressed from a CMV promoter. The slowing of PR cell loss through expression of *βPDE* was reported to last for 6 weeks after treatment, but is unconvincing since the immune response limits adenoviral-mediated gene expression in the retina to approximately 3 weeks [105]. In addition, adenoviral vectors do not transduce PR cells efficiently – even in pups. This point also applies to the rescues reported by Kumar-Singh and Farber [108], who used a gutless Ad vector to deliver *βPDE* regulated by a section of the human *βPDE* promoter, and Takahashi *et al.* [119], who used two HIV-based vector carrying *βPDE,* one regulated by CMV and the other by a *rhodopsin* promoter. In all of these studies there is no demonstration of *βPDE* expression within the target cell type, the PR cells. The presence of functional PDE in the correct location is inferred from RT-PCR experiments to detect the transgene and PDE activity assays on retinal extracts. In fact the study utilising lentiviral vectors only reported the presence of photoreceptor cells in approximately 50% of the treated eyes and these eyes were not subject to any further assays of function [119].

These experiments highlight not only the need for careful controls in all aspects of the gene therapy strategy, but also the difficulties in determining when and how a therapeutic effect is achieved. Experimental treatment of the *rcd1* dog might be more successful. This strain of Irish setter has a similar phenotype to the *rd* mouse, the result of a non-sense mutation near the C-terminal end of the *βPDE*. As in the mouse this leads to truncation and destabilisation of the gene product [93]. In affected dogs normal photoreceptor development is arrested at P13 but photoreceptor degeneration is not evident until 1 month. Nearly all photoreceptor have degenerated by 5 months, and cone photoreceptor degeneration is complete by approximately 1 year. This provides a better opportunity for delivery of a wild type *βPDE* gene using rAAV. This vector is able to transduce a significantly higher percentage of PR cells than both adenoviral or lentiviral vectors and may mediate a more obvious therapeutic effect. Dog models however are expensive and experiments are relatively long-term.

In contrast to the *rd* mouse the *Prph2*$^{Rd2/Rd2}$ mouse has several advantages that may make it a better model in which to study the effects of gene therapy. The retinal degeneration phenotype in these mice results from an insertion mutation in the third exon of the gene that codes for the peripherin-2 protein (also known as peripherin/RDS) [120]. This is a photoreceptor specific membrane glycoprotein found in both rods and cones that has a role in the stabilisation of the outer segment discs (see section 1.1.3). Mutations within the *peripherin-2* (*Prph2*) have been shown to cause both autosomal dominant RP and macular dystrophy in humans [14, 19, 20]. In the mouse, however, the null mutation causes a semi-dominant phenotype so both the heterozygous and homozygous mice display retinal degeneration. In the homozygous mice there is a failure in the formation of photoreceptor outer segments and degeneration of these cells results. In comparison, the heterozygous mice develop abnormal outer segments and there is a slower degeneration of PR cells. Complete rescue of the homozygous mice was demonstrated by the transgenic introduction of a functional copy of the *Prph2* gene that expressed at the same level as the wild type [121].

The slower degeneration in this mouse strain (over 1 year) combined with the relatively easily observed histological evidence of effectiveness of treatment, through the restoration of outer segments, make the *Prph2*$^{Rd2/Rd2}$ mouse an exciting opportunity for

the investigation of the potential of ocular gene therapy. This thesis aims to further examine this potential.

1.6.2 Strategies for gain of function mutations

Dominantly inherited gain of function mutations present perhaps the biggest challenge to gene therapy. However, an ability to treat them is crucial since they have been identified as causing significant proportion of retinal degeneration (http: //www.sph.uth. tmc.edu/Retnet/disease.htm). The disease mechanism stems from a situation in which the gene product in its mutant form is toxic to the cell either as a result of the gain of an abnormal function or due to the inability of the cell to deliver the mutant protein into its normal location. In order to treat these types of disease by gene therapy it is necessary to deliver genes that prevent the production of mutant protein. It may also be necessary in the homozygous or haploinsufficient condition to deliver a normal copy of the gene.

The removal of the mutant protein can be achieved via the destruction of the mutant mRNA before it is translated. There are two strategies for this: an antisense approach and ribozyme therapy. An antisense approach involves the production of antisense oligonucleotides that are designed to match and therefore bind to the mutant mRNA. The mRNA is thus prevented from being translated and its degradation is promoted. This form of therapy has yet to be combined with gene therapy as there are still several difficulties related to the non-specific binding of synthesised oligos and the short half-life of these molecules within the target cell. Its relatively low efficiency would require high levels of expression and therefore currently ribozyme therapy presents a better chance of success in the treatment of dominantly inherited disease.

1.6.2.1 Ribozyme therapy

First discovered in the early 1980s ribozymes are naturally occurring RNA catalysts that allow the manipulation of RNA in *trans* [122, 123]. Ribozymes have been divided into groups based on their specialised catalytic properties. Two of these types, hammerhead (Hd) and hairpin (Hp) are characterised by their ability to cleave a specific phosphodiester bond within an RNA molecule. Both types recognise specific target sequence mRNA through complementary base pairing and catalytically cleave the mRNA at specific motifs. The hammerhead requires a 5′-NUX sequence for cleavage (where N is any nucleotide and X is A or C) while the hairpin requires a 5′-NBNGUC

sequence (where B is G, C, or U). One of the main advantages of ribozymes over antisense RNA is that as catalysts they have the ability to cleave many transcripts and are therefore much more efficient. In addition the binding of ribozymes to their target occurs with much greater stringency and as a result there is a much greater chance of creating allele specificity, cleaving the mutated transcripts while leaving the wild type transcripts intact.

The majority of work on the use of ribozymes for ocular gene therapy has been carried out on the transgenic rats TgN(P23H)3 (abbreviated P23H-3). This model carries three amino acid changes, one of which is a histidine to proline substitution in codon 23 [95, 124]. This substitution is identical to that found in humans which is responsible for 12% of the cases of autosomal dominant RP in the US [125, 126]. Synthesis of the abnormal rhodopsin protein results in cell death. In the rats expression of the mutated *opsin* transgene begins at about P5 although normal development of the retina is observed until P15. Thereafter photoreceptor cells are lost at a constant rate up until P60, by which time approximately 40% of the photoreceptor cells have been lost. At this point the rate of degeneration slows so that at 1 year the retinas have less than a single row of photoreceptor nuclei.

Both hammerhead and hairpin ribozymes have been designed to recognise and cleave the transcript produced by the P23H transgene. *In vitro* assays demonstrated the ability of these ribozymes to discriminate between the desired substrate while leaving the similar RNA molecules of the wild type sequence intact [127]. More recently ribozymes of the same design have been used *in vivo* in the P23H rat [95]. These experiments used rAAV vectors to deliver the ribozymes genes, driven by a bovine rod *opsin* promoter, to photoreceptor cells after sub-retinal injection. The injections were performed at P14 or P15 and eyes analysed at P60, P75 and P90. Control injections were also performed using the same ribozymes but with disabled catalytic domains. The authors had previously demonstrated a 20-30% transduction rate with the vector carrying a reporter gene [128]. Ribozyme injected eyes had a modest but significant decrease in the accumulation of transcript derived from the P23H transgene. Additionally, the delivery of the virus slowed PR degeneration over a three-month period. However, the catalytically inactive control ribozymes also slowed the retinal degeneration, although to a lesser extent. Further work in this model showed that a ribozyme rescue persisted

until P130, and even slowed the rate of degeneration when injected at later time points such as P30 and P45 [129]. The caveat to these experiments is that the P23H rat contains an engineered site close to the P23H mutation presenting ribozymes with an optimal motif for cleavage. These sites are not present in humans and therefore cleavage might not occur with the same level of efficiency.

O'Neill *et al.* [130] have addressed the problem of the large heterogeneity in the mutations involved in RP using a mutation-independent gene silencing approach. In essence this involves the suppression of wild type and mutant alleles with ribozymes designed against sequences in the untranslated region (UTR) of transcripts or at degenerate (wobble) sites and concurrent introduction of replacement genes with modified UTRs or degenerative sites that escape suppression but code for the wild type protein. *In vitro* analysis showed that the designed ribozymes were able to specifically cleave the mutant alleles, and it is hoped that similar results can be obtained *in vivo*.

While these experiments demonstrate a potentially successful strategy there is still no direct transgenic evidence for rescue of retinal degeneration phenotypes with ribozymes, as there have been for the *rd* and *Prph2*$^{Rd2/Rd2}$ mice. However, proof of principle has been established in another transgenic line: crosses between transgenic mice expressing a human growth hormone and transgenic mice expression a ribozyme against that mRNA resulted in substantial reductions in mRNA levels in doubly transgenic progeny [131].

1.6.3 Non-specific strategies

So far the majority of strategies discussed have been aimed at specific gene defects, however, the specific tailoring of treatments to the extensive array of RP mutations may prove to be impractical. Therefore it is attractive to develop non-specific strategies that are likely to be more versatile and have a widespread utility. These strategies might also be used to complement gene replacement for an additive effect. The two options for this type of strategy involve the delivery of genes encoding either anti-apoptotic factors or neurotrophic factors.

1.6.3.1 Anti-apoptotic factors

Apoptosis has been shown to have a central role in degeneration of retinal cells in animal models and therefore is a logical choice for a non-specific secondary target through which cell death can be prevented. A gene recognised as central to the control of apoptosis in several tissues is *bcl-2*. The release of cytochrome c from the inter-membrane space in mitochondria is known to be an important stage in the pathway that leads to cell death and Bcl-2 is known to exert an anti-apoptotic effect by the blocking of this release. *Bcl-2* is not expressed in mature rat retina although a related protein Bcl-X_L is [132]. Transgenic lines which over-express *bcl-2* in the photoreceptor cells have been generated and crossed with both *rd* mice, and a mutant rhodopsin strain [133, 134]. Studies of the rate of PR cell loss in these animals failed to provide conclusive proof of an increase in PR cell survival in those mice expressing *bcl-2*. However, there was an indication of a slowing in the rate of cell loss in the later stages of degeneration in homozygous *rd* mice over-expressing *bcl-2* in one study [133]. The expression of *bcl-2* above endogenous levels in *rd* mice has also been tested using a gene therapy strategy [135], however, this study also suffers from the use of first generation adenoviral vectors which mediate only short-term transgene expression and do not transduce PR cells efficiently.

In contrast experiments in which transgenic mice carrying the complete human *bcl-2* coding region driven by a mouse *rhodopsin* promoter were crossed onto the *Prph2*$^{Rd2/Rd2}$ homozygous background were much more successful [136]. At 3 months *Prph2*$^{Rd2/Rd2}$ mice expressing *bcl-2* had approximately twice the number of PR cells as the non-transgenic *Prph2*$^{Rd2/Rd2}$ however, this was significantly less than *Prph2*$^{Rd2/Rd2}$ mice rescued through the transgenic delivery of a normal copy of the *Prph2* gene [121]. The relative success in controlling cell death with *bcl-2* in the *Prph2*$^{Rd2/Rd2}$ mouse is attributed to the slower pace of apoptosis in this mutant. However, while the pathways between gene defects and apoptotic cell death are still unidentified it is difficult to predict whether complete prevention of cell death is possible via this strategy. The identification of further genes involved apoptosis in the animal models of RP, such as *caspase-3* [137], present alternatives and it is possible that co-expression at specific levels of more than one factor may be required. In the long run this strategy is promising but it requires a much greater level of understanding of the control of apoptosis in the retina.

1.6.3.2 Neurotrophic factors

Neurotrophic factors are growth factors that have been identified through their ability to inhibit apoptosis by enhancing the viability of different neuronal cell types. A large number of factors have been identified that might be useful specifically in preventing or slowing retinal degeneration. They act over a short range, binding to cell receptors and activating specific metabolic pathways that are not clearly understood. Basic fibroblast growth factor (bFGF) was the first to be shown to slow the progression of PR cell degeneration in the RCS rat [138]. Since then many factors have been shown to have similar effects in different models of retinal degeneration including ciliary neurotrophic factor (CNTF) and brain-derived neurotrophic factor (BNTF) [28]. The neurotrophic factors were delivered by intra-ocular (intra-vitreal or sub-retinal) injections. One of the drawbacks, however, was that the factors have a relatively short half-life, and this made delivery via gene therapy an attractive option since in theory it would allow long-term expression of neurotrophic factors.

Several virally delivered neurotrophic factors have been shown to slow the rate of apoptosis of rod photoreceptor cells in animal models of retinal degeneration. Ciliary neurotrophic factor (CNTF), delivered intra-vitreally in an adenoviral vector has slowed degeneration in the *rd* mouse [139] and the *Prph2*$^{Rd2/Rd2}$ mouse [140]. The latter study additionally demonstrating an increase in concentration of rhodopsin in treated retinas suggesting that CNTF increased PR cell function as well as preventing cell death. However, the mechanism via which CNTF exerts its effect is unclear. Most studies have so far failed to find evidence that mammalian rods express the receptor for CNTF, CNTFα. CNTF has been shown to be expressed in both the developing and mature rat retina [141] where it is predominantly located in the Muller cells. Recent work in a photo toxicity model of retinal degeneration suggested a role for Muller cells as intermediaries that balance the pro- and anti-apoptotic forces [142], but extension of these results to other models is difficult. Neurotrophic factors and their receptors are known to have highly variable effects depending on developmental time point, cell type and species. CNTF has also been delivered to the retina of a rhodopsin knockout mouse in a rAAV vector injected sub-retinally [143]. Expression of CNTF was confirmed in the PR cells by the co-expression of *egfp*, and the treatment shown to significantly enhance their survival. Interestingly the expression of a non-secretable form of CNTF

was reported not to have a survival effect and it was proposed that this supported the role of Muller cells as intermediaries in promoting survival.

Basic fibroblast growth factor (bFGF) has also been shown to rescue PR cells in the RCS rat after delivery in a recombinant adenoviral vector. However, careful controls are required if a positive effect on PR cell degeneration is seen as it has recently been demonstrated that an immune response against adenoviral vectors can slow PR cell degeneration in the *rd* mouse [144]. FGF-2, FGF-5 and FGF-18, delivered to the retina with rAAV vectors, have all been shown to slow the rate of degeneration of PR cells in strains of transgenic rat expressing *rhodopsin* mutations [145, 146].

As with the anti-apoptotic strategies gaining a better understanding of how these factors operate will allow them to be more easily manipulated to positive effect. If they can be used to prevent PR cell death they are likely to be a very useful tool in the future, particularly in maintaining the number of PR cells since their presence is a prerequisite for the success of specific gene therapy strategies.

1.7 Aims of the thesis

Recombinant AAV vectors may have the properties required for the successful targeting of photoreceptor cells in the treatment of retinal disease. Therefore the aim of the work described in this thesis was to examine further the characteristics of rAAV-mediated transduction in the retina after sub-retinal injection into normal mice. More specifically this work would entail the production and use of rAAV virus of a higher titre than previously used in the eye, and the examination of the effects of viral titre and recombinant genome promoter on the onset, location and duration of reporter gene expression.

It was anticipated that these vectors could mediate transgene expression that would be suitable for the treatment of the *Prph2*$^{Rd2/Rd2}$ mouse. The further aim of the thesis was to create rAAV suitable for the treatment of this model and to examine the effects of this treatment on the retinal structure and the degeneration of photoreceptor cells. Functional assessment of the treated animals would be performed through electrophysiology.

2

Materials and methods

2.1 Reagents

All reagents were from Merck Ltd., Leics, UK unless otherwise stated. Recipes for solutions are given in section 2.14. The primers and oligonucleotides were manufactured by Sigma-Genosys Ltd., Cambs, UK, and their sequences are shown in section 2.15.

2.2 Amplification of plasmid DNA in bacteria

2.2.1 Transformation of competent cells

For transformation, DH5α™ competent cells (Invitrogen Ltd., Paisley, UK), or Epicurian Coli® SURE® 2 competent cells (Stratagene Europe, Amsterdam, Netherlands), were thawed on ice. A 100 µl aliquot was incubated with the plasmid DNA (30 minutes on ice) before heat shock at 37°C in a pre-warmed water bath for 45 seconds. LB (Luria-Bertani) medium (0.4 ml during the transformation of a ligation mixture and 0.9 ml during the transformation of a plasmid) at room temperature was added to the mix, and incubated with gentle shaking at 37°C for 1 hour. A 100 µl sample was spread on a LB-agar plate, containing 50 µg/ml ampicillin. In cases where a blue-white colony selection was required (i.e. when using pGEM®-T Easy plasmids) 50 µl of X-gal solution (20 mg/ml) was spread over the plate before addition of the transformation mix. Plates were incubated overnight at 37°C to allow the growth of resistant colonies.

2.2.2 Amplification and recovery of recombinant plasmid DNA

Bacterial colonies from agar plates were inoculated into 5 ml of LB media containing 50 μg/ml ampicillin and incubated at 37°C with agitation for 12-16 hours. For small-scale preparations, nucleic acid was prepared using a QIAprep® Spin Miniprep Kit (QIAGEN Ltd., W. Sussex, UK). For bulk cultures, 200 μl of the 5 ml culture was used to inoculate a further 250 ml of LB, which was incubated as above. Plasmid DNA was recovered with a QIAGEN® Plasmid Mega Kit (QIAGEN Ltd.).

2.2.3 Quantification of nucleic acid

Nucleic acids produced with the QIAGEN Mega Kits were quantified using a Unicam UV 500 spectrometer. An absorption of 1 at OD_{260nm} was taken to equal a concentration of 50 μg/ml double stranded DNA. Nucleic acids produced with QIAGEN Mini Kits were quantified on a 1% agarose gel (section 2.3.2).

2.3 DNA analysis

2.3.1 Restriction enzyme digestion of plasmid DNA

Digestion of DNA was carried out in accordance with enzyme manufacturer's instructions, in a 1 x buffer (New England Biolabs (UK) Ltd., Herts, UK) with an excess of enzyme (5-10 U/μg DNA).

2.3.2 Electrophoresis of DNA

DNA products were separated on a 0.8 – 1.2 % (w/v) agarose gel with 1% (w/v) ethidium bromide using a 1 x TAE buffer. A 1 kb DNA ladder (Invitrogen Ltd.) was run to provide size markers. Samples were loaded using gel-loading buffer. Gels were run using the voltage and time for the separation of the required DNA bands. Gels were photographed on a UVP ultraviolet (UV) transilluminator. The approximate concentration of DNA was assessed through comparison with the 1636 bp band from the DNA ladder, which contains 10% of the mass applied to the gel.

2.4 Cloning in plasmid vectors

2.4.1 Creating appropriate DNA fragments

DNA fragments that were required for cloning protocols were generated with restriction enzyme digests (section 2.3.1). For cloning into plasmids, where possible, non-complementary ends were used to enhance the efficiency and determine orientation of the insertion. Otherwise, to prevent intra-molecular ligation, the vector molecule was pre-treated with calf intestinal alkaline phosphatase (New England Biolabs (UK) Ltd.) to remove 5′-phosphate groups. One microlitre was added after the restriction digest and the mixture incubated at 37°C for 1 hour. Where a blunt ligation was necessary the 5′ overhang was filled using 1 µl of Klenow fragment DNA-polymerase I (New England Biolabs (UK) Ltd.) in the presence of excess (0.1 mM) deoxynucleotide triphosphates (dNTPs – Promega UK, Southampton, UK), both added after the restriction enzyme digest and incubated at room temperature for 15 minutes. These reactions were terminated by the addition of gel loading dye. Samples were run out on an agarose gel (section 2.3.2) and the required bands excised with a scalpel under UV light.

2.4.2 Engineering restriction sites

The sequence of oligonucleotides used is shown in section 2.15.2. Oligonucleotides were rehydrated and then heated at 65°C for 5 minutes to separate the strands. They were then left on ice for 30 minutes to allow them to self-anneal, before use in a ligation (section 2.4.5).

2.4.3 Isolation of DNA fragments from agarose gels

DNA fragments excised from agarose gels were purified away from the agarose using QIAquick™ Gel Extraction Kits (QIAGEN Ltd.). DNA was eluted from the column using 30 µl of TE buffer (supplied by manufacturer). The concentration of the eluted sample was assessed by comparing 5 µl of the sample against the 1636 bp band of the 1 kb DNA ladder (Invitrogen Ltd.) on an agarose gel as described in section 2.3.2.

2.4.4 DNA ligation

The ligation of gel purified DNA fragments was carried out at 16°C for 4-16 hours, using T4 DNA ligase (New England Biolabs (UK) Ltd.) with buffer at concentrations

recommended by the manufacturer and at a vector to insert molar ratio of 3. Where oligonucleotides were ligated into plasmids they were used in excess (100 pM). Where PCR fragments were ligated into pGEM®-T Easy plasmids (Promega UK) ligations were performed according to manufacturer's instructions.

2.4.5 Checking cloned plasmids

A 2 µl sample of the ligation mixture was transformed and amplified in bacteria (section 2.2) and successful ligation determined by restriction digestion analysis of purified plasmid DNA (section 2.3).

2.5 Polymerase chain reaction (PCR)

2.5.1 PCR reaction conditions

The sequence of primers used is shown in section 2.15. All PCR reactions were performed in a volume of 50 µl using 0.2 mM dNTPs (Promega UK), 25 pM of each primer, and 1 unit of enzyme. The enzyme was prepared by mixing *Pfu* DNA polymerase (Promega UK) with *Taq* DNA polymerase (Promega UK) at a ratio of 1:2, to combine the qualities of high fidelity of the former with speed of the latter. The buffer used was that supplied with the *Taq* DNA polymerase, following manufacturer's instructions. Routinely the reaction was performed in triplicate at three different $MgCl_2$ concentrations (0.5, 1.5 and 2.5 mM) with an additional control reaction to which no template DNA was added. The amount of template DNA was approximately calculated to provide $>10^4$ copies of the target sequence, but the final DNA concentration of the reaction was kept to less than 10 ng/µl. Reactions were temperature cycled using a Techne Touchgene Thermal Cycler. All the reaction cycles were based around the following

Initial denaturation	3 minutes at 94°C	
Denaturation	1 minute at 94°C	30 cycles (35 cycles for PCR on genomic DNA)
Annealing	1 minute at X°C	
Extension	X minutes at 72°C	
Final extension	10 minutes at 72°C	

The temperature of annealing for each set of primers was calculated by using the program PrimerSelect™ (DNAStar Inc.). During the extension step 1 minute was

allowed for every kb of amplicon (minimum extension time = 1 minute). Where the primers incorporated restriction enzyme overhangs 5 cycles were inserted prior to the main batch of 30 in which the annealing temperature corresponded to that of the primer without the overhang. The annealing temperature of the entire primer was used in the main batch of 30 cycles. For PCR on genomic DNA a hot start was incorporated. Ten microlitres of each PCR reaction was analysed on an agarose gel (section 2.3.2).

2.5.2 Walking PCR reaction conditions

This protocol utilises the 'universal walking' primers, UNI 28 and UNI 17, as well as the *peripherin-2* promoter specific MUPM and MUPL primers (sequences shown in section 2.15.1). UNI 17 is nested within UNI 28, while MUPM is nested within MUPL. PCR reactions are performed in 50 µl with 1 unit of *Taq-Pfu* mix (as described in secton 2.5.1) in the supplied buffer and supplied $MgCl_2$, with primers at 0.5 µM and nucleotides (Promega UK) at 0.2 mM. Each PCR is done at two different $MgCl_2$ concentrations of 1.5 mM and 3 mM. Control reactions, without template DNA, were also run. Reactions were temperature cycled using a Techne Touchgene Thermal Cycler. For the primary PCR the template DNA (at 10 ng/µl), buffer, nucleotides, $MgCl_2$, dH_2O and the primer, UNI 28, are mixed and the solution divided in half, incubated at 94°C for 1 minute before adding the *Taq-Pfu*. The block temperature was altered to 80°C for 30 seconds, 15°C for 2 minutes, 25°C for 10 minutes, 72°C for 1 minute and 90°C for 1 minute, before addition of the primer MUPL. The tubes were then cycled 35 times through the following stages: 94°C for 10 seconds, 60°C for 30 seconds and 72°C for 30 seconds. There was a final incubation step at 72°C for 10 minutes. A 10 µl sample of the primary PCR was run on an agarose gel (section 2.3.2) to check for the presence of a smear. A 1 µl sample of this PCR mixture was used in a second round of PCR. This sample was mixed with buffer, $MgCl_2$, nucleotides and the primers, UNI17 and MUPM, at the same concentrations used for the primary PCR. Each mixture was divided in half and incubated at 94°C for 10 seconds before addition of the *Taq*. The tubes were then cycled 35 times through the following stages: 94°C for 5 seconds, 58°C for 5 seconds and 72°C for 30 seconds. There was a final incubation step at 72°C for 10 minutes. A 10 µl sample of the second round PCR was run on an agarose gel (section 2.3.2) and the appropriate bands excised and ligated into pGEM®-T Easy vector (Promega UK) (sections 2.4.3 and 2.4.4).

2.6 DNA sequencing

2.6.1 Design of sequencing primers

Primer sequences are shown in section 2.15.3. Those primers with the prefixed MUP- were a kind gift from N. Kanuga. Primers pUC/M13 Forward and pUC/M13 Reverse are commercially available (Promega UK) and bind within the backbone of the pGEM®. The remainder were designed with the program PrimerSelect™ (DNAStar Inc.) to have an annealing temperature of approximately 55-60°C.

2.6.2 Sequencing

Template DNA of the Pac clone 481-K1 used for sequencing was a kind gift from N. Kanuga. Template plasmid DNA was prepared as in section 2.2. Sequencing reactions were prepared with ABI Prism® BigDye™ Terminator Cycle Sequencing Ready Reaction Kit (Perkin Elmer, Warrington, UK) and ethanol precipitated according to manufacturer's instructions. Samples were run overnight on an ABI Applied Biosystems 373A DNA Sequencer. Sequence was analysed using the computer programme Gene Works Release 2.5.1 (Oxford Molecular Group Inc.).

2.7 Tissue culture

2.7.1 Cell lines and viruses

The baby hamster kidney (BHK) cell line was obtained from European Collection of Animal Cell Cultures (ECACC, Porton Down, UK). The disabled single-cycle herpes simplex (DISC-HSV) helper virus (DISC-HSV), PS1, used in the production of rAAV was prepared by M. de Alwis.

2.7.2 Culture of cell lines

BHK cells were grown in BHK-21 media (Invitrogen Ltd.) supplemented with 5 ml of antibiotic-antimycotic (Invitrogen Ltd.), 10% heat inactivated foetal calf serum (FCS - Invitrogen Ltd.), 5 % tryptose phosphate broth (Invitrogen Ltd.), 5 ml of 200 mM L-glutamine (Invitrogen Ltd.) and 4 ml of 50 mg/ml Geneticin (Invitrogen Ltd.). Cells were grown in a Sanyo CO_2 incubator at 37°C with 5% CO_2.

2.7.3 Splitting and counting cells

Prior to passaging plates of BHK cells were washed twice with PBS. The cells were then incubated with a thin covering (approximately 1.5 ml for 15 cm dishes) of trypsin-EDTA (Invitrogen Ltd.) for 10 minutes at 37°C. The trypsinisation was stopped with the addition of 10 volumes of growth medium and the cells were split one in six. These cells were split every 2-3 days and were not allowed to overgrow. Approximate numbers of cells were counted using a haemocytometer.

2.7.4 Long-term storage of cells

Cells were frozen at approximately 1 x 10^6 cells/ml in growth media with 20% FCS (Invitrogen Ltd.) and 10% DMSO (Invitrogen Ltd.) by first cooling slowly to -70°C overnight in a polystyrene box containing pre-cooled isopropanol. The next day cells were transferred to liquid nitrogen for long-term storage. To thaw, cells were warmed quickly in a 37°C water bath, diluted in growth media, pelleted by centrifugation and resuspended in the appropriate medium.

2.8 Manufacture of replication defective rAAV

2.8.1 Production of rAAV

For rAAV production, BHK cells were plated at 4 x 10^6 cells/150 mm dish 1 day earlier so that they were approximately 70-80% confluent on the day of transfection. Twenty dishes were routinely used for large-scale preparation of virus. Cells were transfected with Lipofectin/Integrin targeting peptide/DNA (LID) transfection complexes. These were made by gentle mixing of three components: cyclised integrin targeting peptide 6 (Zinsser Analytic, Maidenhead, UK) at 0.1 mg/ml in Opti-MEM® (Invitrogen, Ltd.), Lipofectin (Invitrogen, Ltd) and plasmid DNA (prepared as in section 2.2), in a weight ratio of 0.75:4:1. The order in which these components are mixed is important for the efficiency of transfection. A total of 60 μg of DNA was transfected into a single 150 mm dish; this total consists of a 1:3 weight ratio of vector plasmid : helper plasmids. The appropriate amounts of each plasmid were mixed and then made up to 6 ml with Opti-MEM®. In a separate tube 45 μl of Lipofectin (1 mg/ml) was added to 6 ml of Opti-MEM®, and then 2.4 μl of integrin targeting peptide (0.1 mg/ml) was added and

mixed gently. The DNA was added to Lipofectin and peptide and then mixed by inverting the tube. Complexes were allowed to form (1 hour at room temperature). Cells were washed twice with Opti-MEM® medium and then each dish was covered with 12 ml of Lipofectin/Integrin targeting peptide/DNA complexes mixture. After 5 hours the transfection media was removed and normal growth media was added containing DISC-HSV (PS1) at 10-20 infectious units per cell. Cells were incubated for a further 32-35 hours. During this period the cells were monitored as the cytopathic process occurred. The cells were harvested by scraping just as they started to lift off from the plate, and they were pelleted by centrifugation (1200 rpm for 10 minutes).

2.8.2 Purification of rAAV through a discontinuous iodixanol gradient

Collected cells from 10 plates were resuspended in 15 ml of TMN buffer. Cells were lysed through three cycles of freeze thawing between dry ice-ethanol and a 37°C water bath, with vortexing between each cycle. Genomic DNA was removed by digestion with Benzonase, (50 Units per 10 plates), incubated at 37°C for 30 minutes. The lysate was clarified by centrifugation (3700 *g* for 20 minutes), and the virus containing supernatant retained. The virus was then purified on a discontinuous step iodixanol gradient. The gradient was created in a Quick-Seal Ultra-Clear 25 mm x 89 mm Beckman centrifuge tube (Beckman Coulter (UK) Ltd., Bucks, UK). Care was taken to avoid making air bubbles. All the cleared lysate was pipetted into the bottom of the centrifuge tube. A peristaltic pump (Pharmacia model P1) was then used to create the gradient by underlaying successively higher percentage iodixanol solutions. The inlet tube from the pump was first inserted into the 15% iodixanol solution and the pump turned on to ensure that the dead volume in the tubing contained this solution. The outlet tube from the pump was then placed into the lysate and 9 ml of the 15% solution was slowly allowed to enter the tube. The flow rate of the pump had been previously calculated and therefore the correct volume could be added to the tube over a timed period. The inlet tube was inserted into the 25% solution iodixanol solution and 6 ml of this solution was allowed to enter the tube. This was repeated with the 40% solution (5 ml), and with the 60% solution (5 – 6 ml), when the tube was filled to the top. Tubes were heat sealed and spun in an ultracentrifuge for 1 hour at 350 000 *g* (without brake) at 18°C. After centrifugation the tube was removed, placed into a clamp stand and pierced at the top with a needle to allow the entry of air. Within the gradient the rAAV

was located in the 40% iodixanol band, the boundaries of which were marked by the phenol red marker in the 25% and the 60% bands. A second needle was thus inserted at the boundary between the 60% iodixanol solution and the 40% solution and the 40% band was allowed to drip from the column into a separate container (approximately 5 ml). This 5 ml was then added to 5 ml of PBS-MK and the solution was put through a 5 μm filter and then a 0.8 μm filter (Millipore Corporation, MA, USA) to remove any large particles, such as the DISC-HSV.

2.8.3 Purification of rAAV through a heparin column

The rAAV was further purified through a 2.5 ml pre-packed Heparin-Agarose column (Sigma-Aldrich Company Ltd.). The existing column buffer was allowed to drip through the column before equilibration with 4 x 5 ml of 1 x PBS-MK. The 10 ml of filtered virus solution (section 2.8.2) was then applied to the column under gravity and allowed to pass through. The column was washed with 10 ml of PBS-MK before elution of the virus through the addition of 6 ml of PBS-MK/1 M NaCl solution. After applying this elution buffer the first 2 ml of the eluate was discarded as dead volume.

2.8.4 Concentration of rAAV

The rAAV within the eluate was concentrated and desalted in a Centricon YM-10 filter device (Amicon Bioseparations, Millipore Corporation), according to the manufacturer's instructions. The eluate was split between two filter devices that were then spun at 4000 *g* for 50 minutes. The high-salt buffer was exchanged by repeatedly diluting the concentrated virus with storage buffer. The elution was discarded and a further 2 ml of storage buffer is added to each before spinning again at 4000 *g* for 50 minutes. The concentrated virus (approximately 150 μl) was then pooled and stored at -70°C.

2.8.5 Examination of viral particles with the transmission electron microscope

A single drop of the viral preparation was placed on glow discharged carbon coated grids and left for 1 minute. After blotting the grids were inverted onto drops of 1% uranyl acetate for 1 minute. The grids were then blotted and examined in a JEOL 1010 transmission electron microscope (TEM).

2.9. Titration of rAAV with photoreceptor cell-specific promoters

2.9.1 Extraction of viral DNA from rAAV particles

Two aliquots of 1 or 5 µl were taken from the rAAV produced in section 2.8. These samples were digested with 100 µg of proteinase K (Promega UK) in a volume of 400 µl with 1 x proteinase K buffer, to liberate the rAAV genomic DNA from the capsid proteins. This digest was incubated at 37°C for 1 hour. The contaminating proteins were removed through phenol extraction. An equal volume of phenol:chloroform:isoamyl alcohol (25:24:1) was thoroughly mixed with the solution and centrifuged for 13000 rpm for 5 minutes to separate organic and aqueous layers. DNA was precipitated from the aqueous layer through the addition of 40 µg of glycogen (Sigma-Aldrich Company Ltd.), 1/10 volume of 3 M sodium acetate and 2.5 volumes of 100% ethanol, and incubation at -70°C for 30 minutes. The DNA was pelleted by centrifugation for 13000 rpm at 4°C for 30 minutes. The resulting pellet was washed with 70% ethanol and then re-spun as above for 20 minutes. The pellet was air-dried and resuspended in 20 µl of dH_2O.

2.9.2 Preparation of dot blot

A standard curve was prepared through the serial dilution of a plasmid containing the section of DNA that was to be used as a probe. Routinely eight samples were prepared ranging from 10^{12} molecules to 10^5 molecules in 10 fold serial dilutions. These were prepared in dH_2O. These samples, and those from section 2.9.1 containing the recombinant viral genomes, were denatured by the addition of 10 µl of alkaline stock solution (10x) with 70 µl of dH_2O, and heating at 100°C for 5 minutes. Samples were then kept on ice to prevent re-annealing. Dot blots were prepared on pre-wetted 0.45 µm Hybond™- N+ membrane (Amersham Pharmacia Biotech. UK, Bucks, UK) in a dot blot manifold (Bio-Rad Laboratories Ltd., Herts, UK). The wells of the manifold were pre-washed with 0.4 ml of dH_2O and the vacuum applied until they were empty. The denatured DNA was added without vacuum and then the vacuum applied. The wells were rinsed with 0.4 ml of alkaline stock solution (1x). The membrane was removed

from the manifold and washed in sodium phosphate buffer (pH 7.2), dried between blotting paper and stored at room temperature.

2.9.3 Preparation of probe

The section of DNA to be used as the probe was excised from the plasmid with a restriction enzyme digest (section 2.3.1), separated on a gel (section 2.3.2) and then extracted from a gel fragment (section 2.4.3). A Prime-It® II Random Primer Labelling Kit (Stratagene Europe) was used to label the probe radioactively with α^{32}P dCTP (Amersham Pharmacia Biotech. UK) according to manufacturer's instructions. Unincorporated dNTPs were removed using a MicroSpin™ G50 Column (Amersham Pharmacia Biotech, UK). Immediately before use the probe was denatured at 96°C for 2 minutes.

2.9.4 Hybridisation of membrane

The dried membrane was wetted in dH_2O, rolled with gauze and then placed in a hybridisation tube with room temperature 0.3 M sodium phosphate buffer. The tube and its contents were heated to 65°C in a hybridisation rotisserie oven. Once at 65°C the buffer was exchanged for Church buffer (pre-warmed to 65°C) and the membrane pre-hybridised for 30 minutes. The radioactively labelled probe (section 2.9.3) was then added to the Church buffer and the membrane hybridised for 5 hours. The membrane was washed with a ten-fold dilution of sodium phosphate buffer (pH 7.2), twice at room temperature (2 minutes) and twice at 65°C (10 minutes) with pre-warmed buffer. Excess liquid was removed and the membrane sealed in plastic. The membrane was then placed in a cassette with Kodak Scientific Imaging BioMax™ MR-1 film (1-4 hours at room temperature), which was later processed in a Fuji RG II X-Ray Film Processor.

2.10 *In vivo* methods

2.10.1 Animals

All normal mice were C57Bl/6 (Harlan Olac Ltd, Bicester, UK). Adult mice were between 6 and 12 weeks old at the time of injection. The *Prph2*$^{Rd2/Rd2}$ mice were originally from stock held by D. Bok. All animals were cared for in accordance with the

Animal Scientific Procedures Act 1986 and procedures were in accordance with the ARVO Statement for the Use of Animals in Ophthalmic and Vision Research.

2.10.2 Anaesthetic for intra-ocular observation and injection

Adult mice were anaesthetised by intra-peritoneal injection of 0.2 ml of Hypnorm (Janssen Pharmaceutical Ltd, Oxford, UK) and Hypnovel (Roche, Welwyn Garden City, UK) mixed 1:1:6 with distilled water. Ten-day old pups were anaesthetised with 0.2 ml of a 1 in 10 dilution of the same Hypnorm/Hypnovel mixture.

2.10.3 Intra-ocular injection

The palpebral fissure was opened if necessary with a small scalpel blade and the pupil dilated with topical 1% Tropicamide (1% Mydriacyl, Alcon Labs, Watford). Surgery was performed under direct retinoscopy through an operating microscope. The eyes were protruded by gentle pressure either side of the eye. Once the eye was proptosed it was held in position by a rubber sleeve that was place around the eye with a pair of forceps. The pressure of the rubber sleeve on the eye was always moderate and did not block the circulation. The eye was covered with 2% hypromellose solution (Moorfields Eye Hospital, London, UK) and a small cover slip was placed over it. The eye was stabilised by holding a section of the conjunctiva and extra-ocular muscle with a pair of fine forceps. For sub-retinal injections the tip of a 1.5 cm, 34-gauge hypodermic needle mounted on a 5 μl Hamilton syringe (Hamilton, Bonaduz, Switzerland) was guided between the coverslip and the rubber sleeve to the sclera of the mouse eye and then inserted tangentially through it, causing a self-sealing wound tunnel. The needle tip was brought into focus between the retina and the RPE and approximately 1-2 μl of viral suspension was injected to produce a bullous retinal detachment covering 30% of the fundus. For intra-vitreal injections the needle tip was advanced through the sclera, 1 mm posterior to the corneo-scleral limbus, into the vitreous cavity. Two microlitres of viral suspension was injected once the needle tip could be seen in the vitreous cavity behind the lens.

2.10.4 Observation with the small animal camera (SAC)

Mice were anaesthetised as in section 2.10.2 and their pupils dilated with 1 drop of 1% Tropicamide and 1 drop of 2.5% Phenylephrine Hydrochloride (both from Chauvin Pharmaceuticals Ltd, Essex, UK). A Nikon photo slip lamp (Tokyo, Japan) and a Kowa

Genesis small animal fundus camera (Tokyo, Japan) were used to photograph the mouse fundus. These were used in conjunction with a Volk 90D-condensing lens mounted between the camera and the eye. White light photographs were taken with Fujichrome Sensia 200 slide film and fluorescent photographs with Fujichrome Provia 1600. The photographic flash on the power pack has seven intensity levels. For fluorescent images of the eye the upper intensity setting was used.

2.10.5 Observation with the confocal laser scanning ophthalmoscope

Mice were anaesthetised as in section 2.10.2 and their pupils dilated with 1 drop of 1% Tropicamide and 1 drop of 2.5% Phenylephrine Hydrochloride (both from Chauvin Pharmaceuticals Ltd, Essex, UK). A prototype Zeiss (Oberkochen, Germany) SM 30-4042 confocal laser scanning ophthalmoscope (cLSO) was used. Confocal images were acquired in a 20° field of view. The cLSO detector is a high-gain Hamamatsu (Tokyo, Japan) photomultiplier, which has an extended red, high-sensitivity multialkali photocathode. The cLSO has two illuminatory wavelengths: an argon laser line at 488 nm and a helium neon line at 633 nm. Fluorescence images were generated by illuminating the fundus with the argon laser line while a high-pass filter (521 nm) was in place in front of the detector. At wavelengths shorter than 521 nm the barrier filter has a blocking transmission of 10^5 or better. Light leakage to the detector was therefore kept to a minimum (less than 20 photo events per frame). An ametropic corrector was used to correct for refractive error. The cLSO images were recorded at 25 frames per second onto a SVHS videotape recorder and digitised at 768 x 576 x 8 bit resolution using a Matrox Millennium frame grabber. Only retinal images that exhibit minimal eye movements were used for analysis and they were automatically aligned most commonly on a retinal blood vessel intersection and averaged to increase the signal to noise of the images by 5.6 times.

2.10.6 ERG method and analysis

Mice were dark-adapted overnight (16 hours) before recording. All of the preparations for recording were carried out under dim red light. The anaesthetic used was a mixture of 667 µl of Ketaset (Fort Dodge Animal Health Ltd., Southampton, UK), with 585 µl of 2% Rompun (Bayer plc, Suffolk, UK) and 1.67 ml of Atropine Sulphate (Phoenix Pharma Ltd, Gloucs, UK) in 10 ml of dH_2O. Animals were anaesthetised with an intra-peritoneal injection of 0.1 ml of anaesthetic per 10 grams of body weight. Mouse eyes

were dilated with 1 drop of 1% Tropicamide and 1 drop of 2.5% Phenylephrine Hydrochloride (both from Chauvin Pharmaceuticals Ltd.). A mid-line reference intra-dermal electrode was placed between the ears and a reference electrode was placed in the skin above the base of the tail. A single drop of 1% of hypromellose was placed on each eye and corneal ring electrodes manuipulated so that they were touching each eye. Sub-dermal electrodes were made of platinum and iridium, while the corneal electrodes were silver on copper with Kynar insulation. All electrodes were obtained from C. Hogg. Stimulation and recordings were carried out using commercially available equipment (Toennies Multiliner Vision, Jaeger/Toennies, Wuerzburg, Germany). Bandpass filter cut-off frequencies were 1 and 300 Hz for all measurements. All data was stored and analysed on the Toenneis Multiliner Vision programme operating on an IBM compatible PC. The standard definitions of an a-wave latency (from point of stimulus to first most negative trough) and magnitude (from point of stimulus to first most negative trough) and b-wave implicit time (from first most negative trough to highest positive peak) and amplitude (from a-wave trough to b-wave peak) were used during analysis.

2.11 Cryo and wax sectioning

2.11.1 Fixation and processing

Animals were sacrificed by cervical dislocation. The eyes were marked with a temporal stitch through the conjunctiva. A scalpel was used to separate the eye from the surrounding tissue. The eyes were immersion fixed in 4% (w/v) paraformaldehyde (4 hours at room temperature). Eyes for cryosectioning were cryoprotected in 20% (w/v) sucrose solution (overnight at 4°C). Eyes were then embedded, stitch upwards, in O.C.T (R A Lamb, E. Sussex, UK) and frozen in iso-Pentane which had been pre-cooled in liquid nitrogen. Specimens were stored at -80°C. Sections were cut with a Bright cryostat and kept frozen until use. Eyes for wax sectioning were dehydrated overnight in a Leica Histokinette processing machine and embedded in wax, stitch upwards. Sections (7 μm) were cut on a microtome and stored at room temperature until use.

2.11.2 Observation of EGFP fluorescence in cryosections

Sections were washed for 10 minutes in tap water to remove O.C.T. and counterstained with propidium iodide (Sigma-Aldrich Company Ltd.) at 1 μg/ml in PBS (5 minutes). After washing (5 minutes in PBS) the sections were mounted in fluorescent mounting medium (Dako Ltd.) and a coverslip secured with spots of nail varnish. Low power images were obtained using a Leica DMIL inverted microscope with a mercury vapour lamp and a GFP excitation filter. Higher power images were captured using a Zeiss LSM 510 confocal microscope operating a multi-tracking mode. EGFP and propidium iodide were detected using a narrow banded FITC (488 nm) filter and a rhodamine/TRITC (543 nm) filter respectively.

2.12 Immunohistochemistry

2.12.1 Blue cone opsin immunostaining

Cryosections were washed for 10 minutes in tap water to remove O.C.T., then left in TBS for 10 minutes. The sections were the left for 30 minutes at room temperature in blocking buffer (TBS with 0.1% (v/v) Tween 20, 3% (w/v) BSA (bovine serum albumin) (Sigma-Aldrich Company Ltd.) and 10% (v/v) normal goat serum (Dako Ltd.). Slides were incubated for 1 hour with the primary antibody (rabbit anti-mouse blue cone opsin antibody – a kind gift from J. Nathans) diluted 1:250 in blocking buffer. After three washes (TBS with 0.1% (v/v) Tween 20, for 5 minutes) the slides were incubated with a secondary antibody (Alexa Fluor® 350 nm goat anti-rabbit IgG conjugate – Molecular Probes Europe BV, Leiden, The Netherlands) at a dilution of 1:40 in blocking buffer (45 minutes at room temperature). Slides were washed twice (TBS with 0.1% (v/v) Tween 20 for 5 minutes) before being counterstained with propidium iodide (Sigma-Aldrich Company Ltd.) at 1 μg/ml in TBS (5 minutes). After washing (5 minutes in TBS) the sections were mounted in fluorescent mounting medium (Dako Ltd.) and a coverslip secured with spots of nail varnish. Images were captured using a Zeiss LSM 510 confocal microscope operating a multi-tracking mode.

2.12.2 Peanut agglutinin staining

Cryosections are washed in tap water to remove the O.C.T., then left in TBS for 10 minutes. The sections were blocked for 30 minutes at room temperature in blocking

buffer (TBS with 0.1% (v/v) Tween 20, 3% (w/v) BSA and 10% (v/v) normal goat serum). Slides were then incubated with biotinylated peanut agglutinin (Vector Laboratories, CA, USA), diluted 1:200 in blocking solution (90 minutes at room temperature). After three washes (TBS with 0.1% (v/v) Tween 20 for 5 minutes) the slides were incubated with a streptavidin-rhodamine conjugate (Dako Ltd.) at a dilution of 1:150 in blocking solution (90 minutes at room temperature). Slide are washed twice (TBS with 0.1% (v/v) Tween 20 for 5 minutes) and then counterstained for 5 minutes with a 1 in 5000 dilution (in dH_2O) of DAPI (Sigma-Aldrich Company Ltd.). Slides were washed once (TBS for 5 minutes) and then mounted with fluorescent mounting medium (Dako Ltd.) with a coverslip secured with spots of nail varnish.

2.12.3 Peripherin-2 immunostaining

Paraffin sections were soaked in xylene to remove the wax, and then rehydrated. For horseradish peroxidase detection endogenous tissue hydrogen peroxidases were inactivated by pre-incubation of the slides for 25 minutes with 0.3% (v/v) hydrogen peroxidase in methanol. These slides were then soaked in tap water for 10 minutes and PBS for 5 minutes. Slides were incubated for 30 minutes in blocking buffer (4% BSA (w/v) and 10% (v/v) normal swine serum (Dako Ltd) in PBS). Slides were incubated for 1 hour with the primary antibody (rabbit anti-mouse peripherin-2 antibody generated against a carboxy-terminal peptide – a kind gift from G.Travis) at a dilution of 1:100. After three washes (PBS for 5 minutes) slides were incubated for 45 minutes with the secondary antibody, biotinylated swine anti-rabbit-Ig antibody (Dako, Ltd) at a dilution of 1:300. The slides were washed again three times (PBS for 5 minutes). Visualisation of the bound antibody was achieved using a horseradish peroxidase (HRP)-streptavidin (Dako Ltd.) or alkaline phosphatase (AP)-streptavidin (Dako Ltd.) conjugated complex for another 30 minutes following manufacturer's instructions. Diaminobenzadine (HRP) or Vector Red (AP) was used for colorimetric detection which yielded brown and red colour respectively. Counterstaining of the nuclei was performed with Meyer's haematoxylin and slides were mounted in DPX. Slides were observed using a Leica DMLS light microscope and images captured with a digital camera.

2.12.4 Peripherin-2 and rhodopsin immunofluorescent staining

Paraffin sections were soaked in xylene and then re-hydrated. Sections were blocked with 3% BSA in TBS and then simultaneously incubated for 1 hour with the two

primary antibodies – a peripherin-2 specific antibody as described in section 2.12.3 at a dilution of 1:100, and a monoclonal rhodopsin-specific antibody (a kind gift from R. Lund) at a dilution of 1:500. Slides were then washed three times (TBS for 5 minutes) before incubation with the secondary antibody for 45 minutes. Fluorescein isothiocyanate (FITC)-conjugated goat anti-mouse-Ig (at a dilution of 1:40, Dako Ltd.) and tetramethylrhodamine isothiocyanate (TRITC)- conjugated swine anti-rabbit-Ig (Dako Ltd.) were both used at a dilution of 1:40 against the corresponding primary antibodies. After two washes (TBS for 5 minutes) DAPI (Sigma-Aldrich Company Ltd.) was used at a dilution of 1:5000 (in dH_2O - 5 minutes) as a nuclear counterstain. Slides were washed once more (TBS for 5 minutes) before mounting in fluorescent mounting medium (Dako Ltd.) with coverslips secured with spots of nail varnish. Slides were kept in the dark as much as possible from the addition of the secondary antibody. Images were captured using a Zeiss LSM 510 confocal microscope operating a multi-tracking mode.

2.13 Semithin and ultrathin sectioning

2.13.1 Marking and fixation of the eye

Mice were killed by cervical dislocation. The orientation of the eye was marked along the sagital plane on the cornea with a cautery. The eyes were immediately fixed by immersion in 3% (v/v) glutaraldehyde with 1% (w/v) paraformaldehyde buffered to pH 7.4 with sodium cacodylate buffer. After 12 hours of fixation the eyes were dissected to remove the anterior part of the eye. The posterior segments were then osmicated for 2 hours with a 1% (w/v) solution of osmium tetroxide (Johnson Matthey, Herts, UK) and dehydrated through ascending alcohols (50%, 70%, 90% and 3 x 100%, 10 minutes per step).

2.13.2 Semi and ultrathin sections for transmission electron microscopy (TEM)

After 3 changes of 100% ethanol, in section 2.13.1, specimens were passed through propylene oxide (2 x 20 minutes) and then left overnight in a 50:50 mixture of propylene oxide and araldite (both from Agar Scientific, Cambs, UK). Following a single change to fresh araldite (5 hours with rotation) the specimens were embedded and cured overnight at 60°C. Semithin and ultrathin sections were prepared with a Leica

ultracut S microtome fitted with a diamond knife. Semithin sections were dried on a 60°C hot plate and stained with 1% (w/v) toluidine blue. The stain was left on until the edge of the drop had begun to dry. Sections were removed from the hot plate, washed with dH_2O and then 95% ethanol. Slides were mounted with DPX after the sections had dried. Slides were viewed with a Leica DMLS microscope and images were captured with a digital camera. The average thickness of the outer nuclear layer was measured using Image Pro Plus 4.1 (Media Cybernetics, MD, USA). Ultrathin sections were sequential contrasted with 1% uranyl acetate (alcoholic solution in 50% ethanol – 5 minutes) and lead citrate (2 minutes), and were then viewed and photographed using a JEOL 1010 TEM, operating at 80 kV.

2.13.3 Scanning electron microscopy (SEM)

Following three changes of 100% ethanol, in section 2.13.1, the retinas were critical point dried to prevent shearing of the specimen, and mounted on stubs (scleral side upwards) with DAG, a conductive adhesive. These were sputter coated with gold. Specimens were characterised using a JEOL 6100 SEM, operating at 15 kV.

2.14 Buffers

Distilled water (dH_2O) was used to prepare all solutions. Sterile solutions were autoclaved at 121°C for 20 minutes unless otherwise stated.

Ampicillin (1000x) 50 mg/ml ampicillin (Sigma-Aldrich Company Ltd.) in dH_2O, sterile-filtered, stored at - 20°C.

Alkaline stock solution (10 x)

4 M NaOH and 100 mM EDTA.

Church buffer 21 g of NaH_2PO_4, 48.55 g of Na_2HPO_4, 70 g of SDS, 0.5 M EDTA and dH_2O to 1 litre.

DNA loading buffer (6x)

0.25% (w/v) bromophenol blue and 30% (v/v) glycerol in water.

Iodixanol (60%) solution

10 ml Opti-Prep™ 60% (w/v) iodixanol solution (Invitrogen, Ltd.) with 30 µl phenol red solution (0.5% - Invitrogen, Ltd).

Iodixanol (40%) solution

10 ml Opti-Prep™ 60% iodixanol solution with 1.5 ml of 10 x PBS-MK and ddH_2O to 15 ml.

Iodixanol (25%) solution

10 ml Opti-Prep™ 60% iodixanol solution with 2.4 ml of 10 x PBS-MK, 525 µl of phenol red solution (0.5%) and ddH_2O to 24 ml.

Iodixanol (15%) solution

5 ml Opti-Prep™ 60% iodixanol solution with 2 ml of 10 x PBS-MK, 10 ml of NaCl and ddH_2O to 20 ml.

LB (Luria-Bertani) bacterial growth medium

10 g Tryptone (Oxoid Ltd., Hampshire, UK), 5 g Yeast Extract (Oxoid Ltd.) and 10 g NaCl, water to 1 litre. 15 g/litre of Bacteriological Agar (No.1) (Oxoid Ltd.) added for LB agar plates.

PBS (1X) 85 g NaCl, 4.3 g KH_2PO_4, 14.8 g Na_2HPO_4, dH_2O to 10 litres, pH 7.2.

PBS (1X) for tissue culture

10 phosphate buffered saline tablets (Oxoid Ltd) dissolved in 1 litre ddH_2O, sterile.

PBS –MK 1 x PBS with 1 mM $MgCl_2$ and 2.5 mM KCl, sterile.

Proteinase K buffer

100 mM Tris (pH 7.4), 50 mM EDTA and 0.5% SDS.

Sodium cacodylate buffer

0.2 M $(CH_3)_2AsO_2Na.3H_2O$ with 0.2N HCl

Sodium phosphate buffer

97.1 g of Na_2HPO_4, 43.6 g of NaH_2PO_4, pH7.2 and dH_2O to 1 litre.

Storage buffer 20 mM Tris pH 8.0, 0.15 M NaCl and 2 mM $MgCl_2$.

TAE (50X) 0.2 M Tris base, 1 M glacial acetic acid, 50 mM EDTA, pH 8.

TBS (1X) 85.3 g NaCl, 60.8 g Tris, 30 ml conc. HCl and dH_2O to 10 litres.

TE (pH 8.0) 10 mM Tris-HCl, pH 8.0, 1 mM EDTA.

TMN 50 mM Tris pH 8.0, 5 mM $MgCl_2$ and 0.15 M NaCl, sterile.

X-gal 20 mg/ml in dimethylformamide, stored at -20°C.

2.15 Sequence of primers and oligonucleotides

2.15.1 PCR primers

Primer	**Sequence 5′ → 3′** (sections in red indicate restriction site overhangs)
GEN UPPER	TGGGACGTCTGGGGATGGTAACT
GEN LOWER	GCCCCAAGCTGAAGAGGACGAT
L PER DOWN	GGGAGGGAGGGTGGAATTGAGAGG
L PER DOWN (*SpeI*)	ACTAGTGGGAGGGAGGGTGGAATTGAG

MUPL	GCTGGGCAGTTCCTGCACGCC
MUPM	GGGAGCTGCTTGAGAGCC
PER UP	GTTCAGCAGCCTCCCACGGTTCAG
PER UP (*AgeI*)	ACCGGTGTTCAGCAGCCTCCCACGG
S PER DOWN (*AflII*)	CTTAAGCCCATGCCCCTTGCTGTGACC
UNI 17	TTTTTGTTTGTTGTGGG
UNI 28	TTTTTTTTTTTGTTTGTTGTGGGGGTGT

2.15.2 Oligonucleotide sequences

Oligonucletide	**Sequence 5′ → 3′**
*Afl*II to *Avr*II	TTAATCCTAGGA
*Afl*II to *Spe*I	TTAATACTAGTA

2.15.3 Sequencing primers

Primer	**Sequence 5′ → 3′**
pUC/M13 Forward	GTTTTCCCAGTCACGAC
pUC/M13 Reverse	CAGGAAACAGCTATGAC
M13R2	GCTAATCTAGGCCGCCGTATCTGC
MUPJ	CGAGCAATACATCTGCCACTG
MUPK	CCCATGCCCCTTGCTGTGACC
PER DOWN 1	CATAGAAGAAGGTACAGGTGATAAATAAG
PER DOWN 2	AACGCTCTGCCCCTCCCCTCTA
PER DOWN 3	GACTGGAAGGCATGGTGGCACAC
PER DOWN 4	GTCGCCCTCTTCTGGTTTCTGTGG
PER UP 1	GTTTTTCTGTCGTGTTTTTCCTTG

The positions of the sequencing primers used for the sequencing of the *Prph2* promoter region are shown in Figure 2.1.

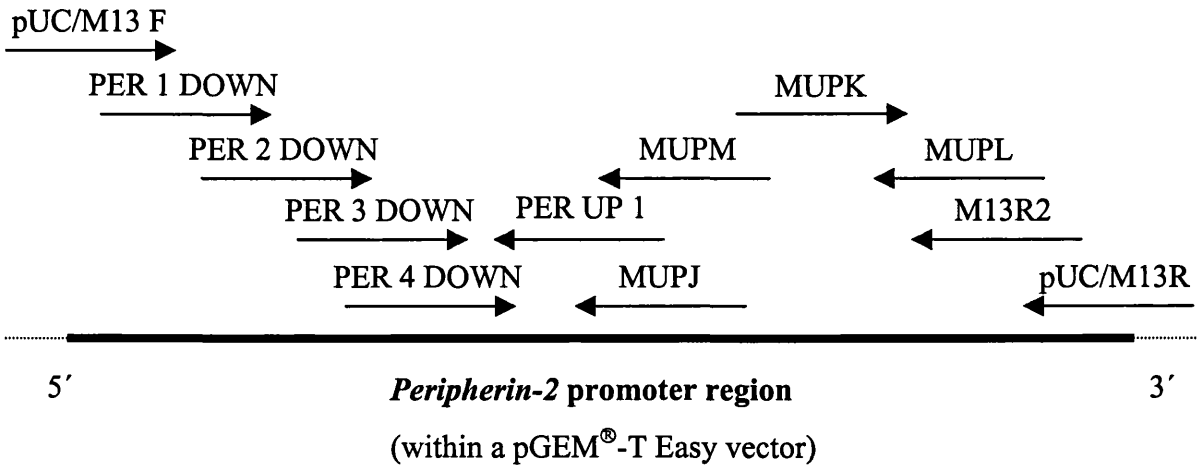

Figure 2.1 The positions of primers used to sequence the *peripherin-2* promoter region. Primers are shown in a 5′ to 3′ direction.

3

Production of recombinant adeno-associated virus

3.1 Introduction

As discussed in section 1.5.2.2, AAV is the most efficient vector for transducing photoreceptor cells and over the past three years its use in sub-retinal gene delivery has expanded. Even at the start of this project it showed much promise in this role [109] and it was therefore the logical choice of vector on which to base attempts to treat retinal dystrophies by gene replacement therapy. The aim of the work described in this chapter was to construct vector plasmids that would facilitate the cloning of constructs for the production of rAAV. These would allow the easy manipulation of genes and promoters within the expression cassette and incorporate features that would aid rAAV production. The plasmids were used to generate rAAV containing PR cell-specific promoters driving reporter genes. These viruses could then be used to study transgene expression *in vivo* following sub-retinal injection.

3.1.1 Life cycle of AAV

AAV is a small DNA virus with a single stranded genome of 4681 bp (section 1.4.5). The primary events in the normal lifecycle of wild type (wt) AAV are the attachment of the virus to the host cell, endocytic uptake, escape from the endosome, un-coating and second strand synthesis of the viral genome. After all of these events have occurred, the virus then forms either a lytic or a latent infection. AAV is naturally defective and requires co-infection with a helper virus, commonly adenovirus or herpes simplex virus (HSV) [147], in order to form a lytic infection (Fig. 3.1). A lytic infection involves the

replication of both the helper and the wtAAV viruses, and the release of progeny virus upon host cell lysis. In the absence of a helper virus the infecting AAV genome integrates into the genome of the host cell where it may remain latent for long periods. During this latent infection the AAV genome can be rescued at any stage by the co-infection of a helper virus.

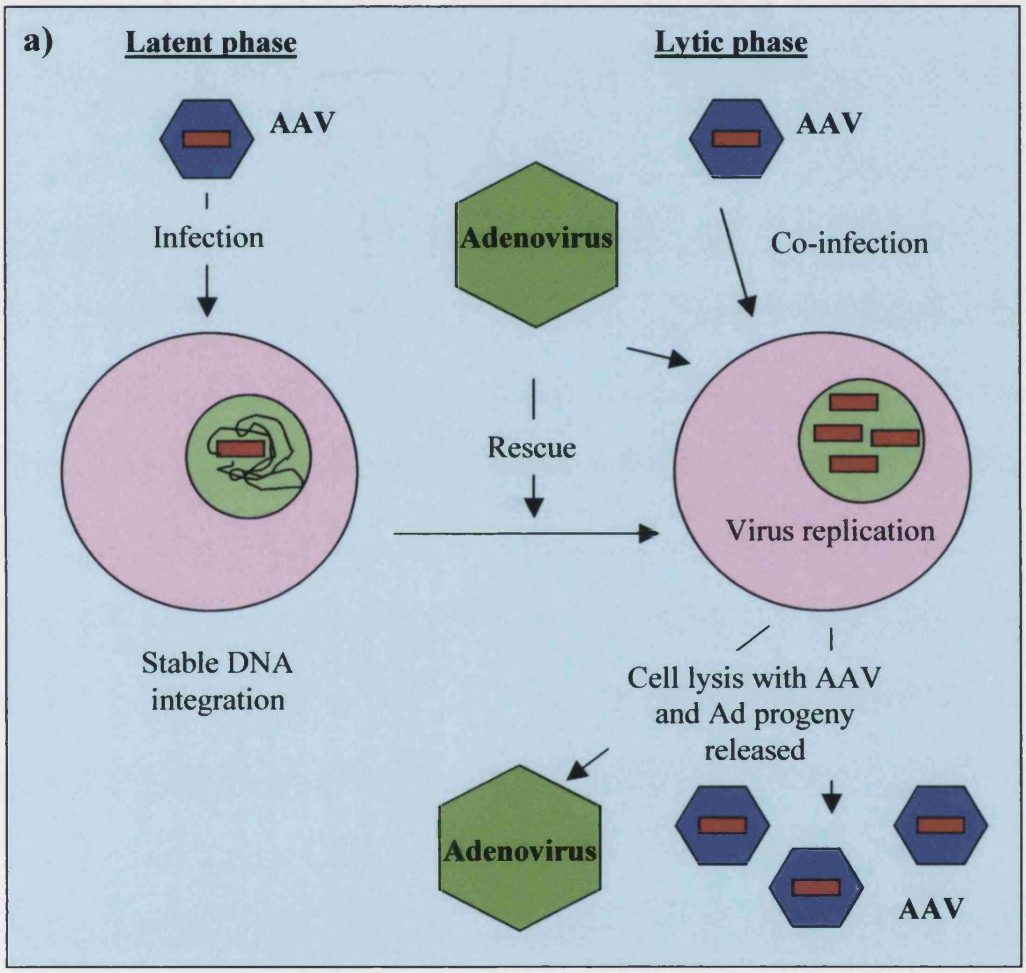

Figure 3.1a Wild type adeno-associated virus life cycle. The latent phase of the AAV life cycle (left half) results when cells are infected in the absence of helper virus, while the lytic phase (right half) occurs when AAV infects in the presence of a helper such as adenovirus. If latently infected cells are subsequently infected with a helper virus then the latent AAV can be rescued and a lytic infection ensues. Adenovirus and AAV particles are produced and at the end of lytic infection they are released on host cell lysis.

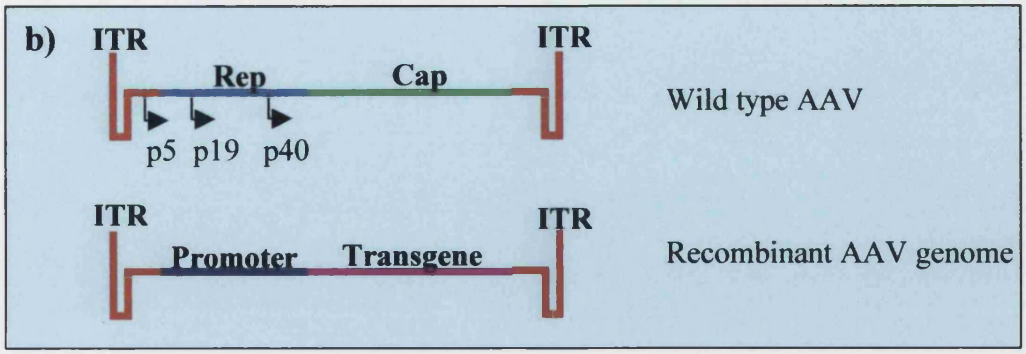

Figure 3.1b Genomic structure of wild type and recombinant AAV. The wild type AAV genome consists of two coding regions *rep* and *cap* flanked by two ITRs. *Rep* and *cap* are transcribed from three promoters, p_5, p_{19} and p_{40}. These genes can be deleted from the recombinant genome, leaving 96% of the particle capacity free for the insertion of therapeutic and promoter sequences. The ITRs are retained in the recombinant genome as they are essential for packaging and second strand synthesis.

The wtAAV genome consists of two open reading frames, *rep* and *cap*, flanked by two 145 bp inverted terminal repeat sequences (ITRs) (Fig. 3.1b). The viral *rep* gene is transcribed from two promoters, p_5 and p_{19}, while *cap* is transcribed from p_{40}. The spliced and unspliced forms of the mRNA transcripts are used in the production of the proteins Rep 68, Rep 78, Rep 40 and Rep 52, and VP1, VP2 and VP3 from the *rep* and *cap* regions respectively. The Rep proteins are non-structural and have a variety of roles including excision and replication of AAV DNA, accumulation of single-stranded-DNA forms, regulation of gene expression, integration and packaging [148-150]. VP1, VP2 and VP3 are the capsid (Cap) proteins that make up the coat of AAV particles. While the viral genome is single stranded the ITRs form T-shaped 'hairpins' as a result of their internal palindromic sequences within the terminal 125 nucleotides (Fig. 3.2). This secondary structure is used as a primer for the initiation of viral DNA replication [151]. The internal 20 bp of the ITR, designated the D-sequence, is not involved in the hairpin formation and required for efficient rescue of the AAV genome [152].

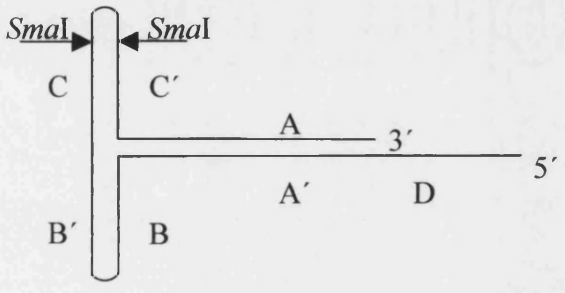

Figure 3.2 The hairpin structure formed by a single stranded AAV ITR. A, A′, B, B′, C, and C′ represent palindromic sequences within the ITR. The two *Sma*I restriction enzyme sites within the ITR are also indicated.

3.1.2 Production of recombinant AAV

Recombinant AAV particles were first generated when it was discovered that the AAV genome could undergo rescue from a plasmid in the same way that the latent virus can be rescued from within the host cell genome [66]. The viral ITRs are the only *cis*-acting sequences required for this rescue and therefore all the viral coding sequence can be replaced with foreign DNA [153] (Fig. 3.1b). Recombinant genomes up to 110% of the wtAAV genome can be efficiently packaged [154].

The conventional method of production of rAAV requires the co-transfection of two plasmids into a producer cell line and infection with Ad as described in Fig. 3.3 [153, 155]. One of the plasmids carries the rAAV construct, this is known as the vector plasmid. The other plasmid, the packaging plasmid, provides the AAV *rep* and *cap* in *trans*. Within the producer cells the adenoviral gene products help in the production of both the Rep and Cap proteins and the rAAV genome is then replicated and packaged. Wild type Ad is also produced. The rAAV is then separated from wtAd by caesium chloride (CsCl) density gradient centrifugation. Using this method titres of between 10^7 to 10^9 iu/ml can be produced. However, there are several problems with this method of preparation. Firstly, the requirement for Ad means there is a risk of contamination with live helper virus or even structural helper virus proteins. It has been suggested that the latter may be the cause of inflammatory processes after intra-muscular injection of rAAV prepared in this way [80]. Secondly, co-transfection is often inefficient and makes the scaling-up of production difficult. In addition the purification processes are slow, and contaminating proteins and wtAd often remain.

The first problem has been addressed through the isolation of the minimum Ad components required for efficient rAAV production. This has led to the generation of Ad mini-plasmids that carry all the essential helper genes but lack Ad structural and replication genes preventing the production of wtAd. It has been demonstrated that these systems do not result in a decrease in rAAV production [156-158]. Methods to increase the titre of the virus produced have also been developed. An obvious solution is the generation of packaging cell lines that bypass the need for co-transfection. Such cell lines have been developed, containing integrated copies of *rep* and *cap*, and requiring only infection with wtAd for rAAV production [159]. These systems, however, yield

approximately 300 to 700 vector particles per cell, the same as co-transfection methods. In comparison, a wtAAV infection yields more than 10^5 particles per cell [160].

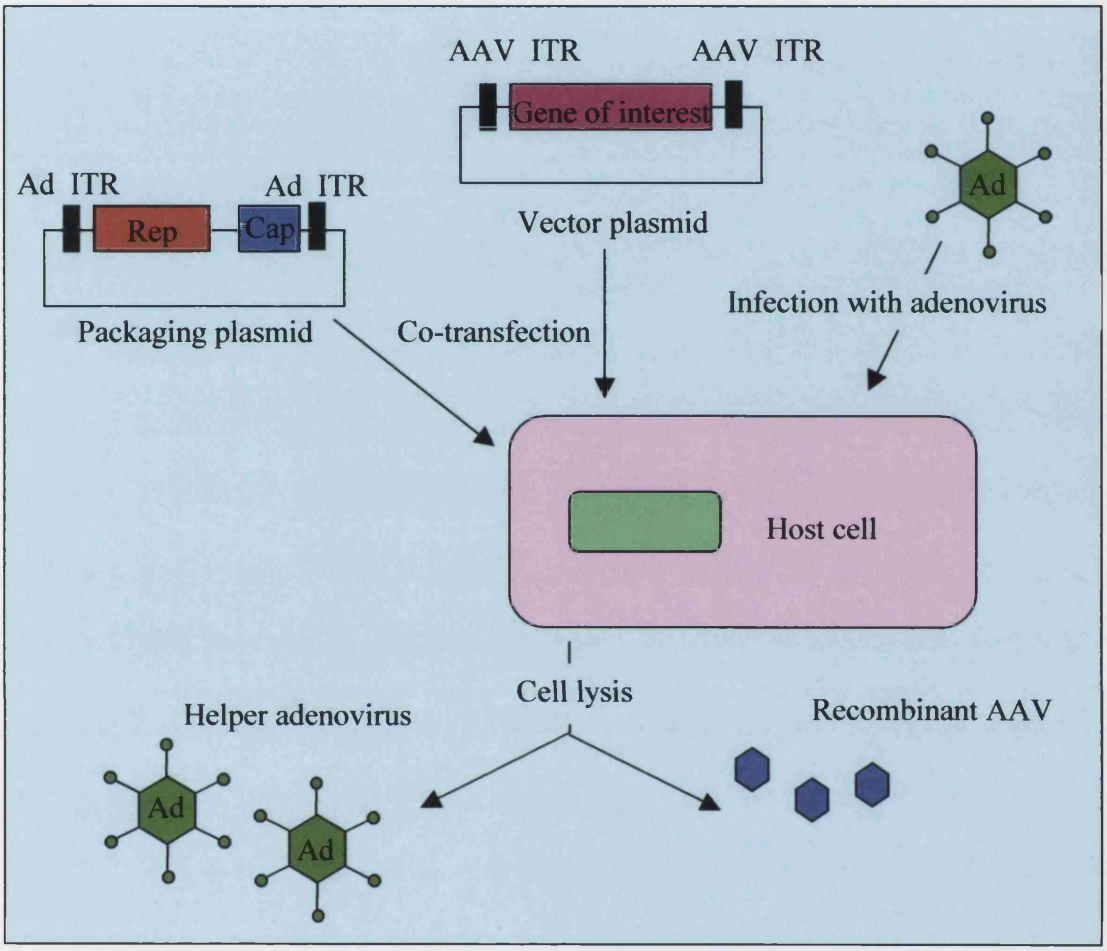

Figure 3.3 Conventional method of production of recombinant AAV. The host cell is infected with the helper adenovirus and then co-transfected with the packaging plasmid, encoding the *rep* and *cap* genes, and the vector plasmid, that contains the recombinant construct between the AAV ITRs. Inside the host cell the adenoviral proteins and the Rep and Cap proteins are produced. The vector construct is replicated and packaged into AAV particles by the action of these proteins. Recombinant AAV and wild type adenovirus are produced, and released on cell lysis. The recombinant AAV particles can then be purified from this mixture by CsCl density centrifugation. Figure based on Ali *et al.*, 1994 [161].

A possible limiting factor for both these cell lines and the transient transfection approaches is related to the copy number of the viral genes that can be used as templates for the proteins required for virion production [162]. In a cell infected with wtAAV and wtAd, replication of the AAV genome results in 10^4 copies of the *rep* and *cap* per cell [160]. In contrast packaging cell lines contain only 10 to 40 copies, since they lack the AAV ITRs necessary for replication, and therefore levels of the Rep and Cap proteins

are correspondingly low. Increased synthesis of the AAV Cap proteins has been shown to improve the yields of rAAV [163, 164], although strategies that rely on the over-expression of viral gene products can be limited by the problems associated with the cellular toxicity of the Rep proteins [165, 166]. Other developments include the use of herpes simplex virus type 1 (HSV-1) as an alternative helper virus [167]. In this study amplicons, plasmids containing the HSV-1 origin of replication, encoding the *rep* and *cap* genes were shown to support the production of rAAV in the presence of wild type HSV-1. It has also been shown that replication of these amplicons within the transfected cell line is not inhibited by expression of the Rep protein [168].

3.2 Initial cloning strategy for the production of rAAV constructs

3.2.1 Choice of basic rAAV construct

The rAAV vector plasmid initially chosen for the experiments was the pTR_{BS}-UF2 recombinant vector construct, obtained as gift from W. Hauswirth. Based on the plasmid pBS(+) (Stratagene) and designated UF for 'user friendly', this vector construct arose from a series of experiments in which a variety of rAAV vectors were produced for the delivery and expression of a 'humanized' green fluorescent protein cDNA (*gfp*$_h$) in mammalian cells [169]. The pTR_{BS}-UF2 vector construct contains a synthetic version of the jellyfish *Aequorea victoria* green fluorescent protein (*gfp10*) cDNA. This has been adapted for high-level expression in mammalian cells primarily by the production of 88 synonymous codon changes to match codons preferentially used in the human genome. The construct also incorporates changes within the sequence preceding the start codon for *gfp*$_h$ that produce a Kozak consensus sequence [170], and a point mutation that produces a Ser-65 to Thr substitution. The latter has been shown to increase the fluorescence of *gfp10* [171]. The *gfp*$_h$ has been cloned between the simian virus 40 (SV40) intron and the SV40 polyadenylation signal. The neomycin resistance gene was also included, driven by the promoter for the HSV thymidine kinase gene and the enhancer from polyomavirus obtained from the plasmid pMC1neo (Stratagene). The resulting cassette has been cloned between the AAV ITRs from the plasmid pTR_{BR} (+)

[172]. This rAAV vector (Fig. 3.4) has been shown to produce efficient transduction and expression of the gfp_h gene *in vitro* in the human 293 cell line [169]. Later studies, involving the exchange of the CMV promoter for a 472 bp proximal section of the murine rod *opsin* promoter, also demonstrate *in vivo* expression specifically in rodent PR cells [128]. The plasmid pTR_{BS}-UF2 was transformed into competent DH5α™ cells (section 2.2.1), and plasmid DNA prepared (section 2.2.2).

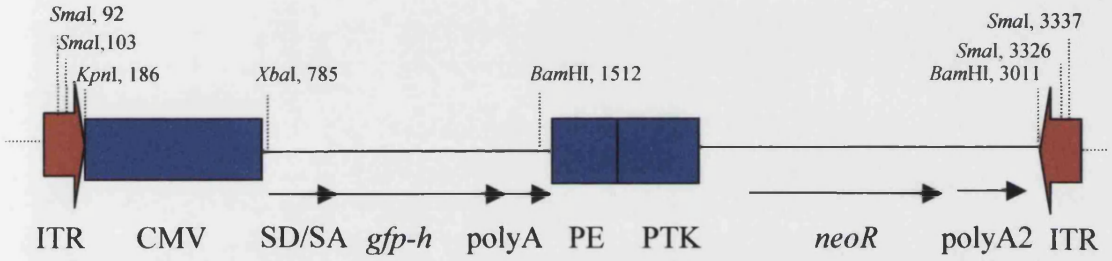

Figure 3.4 Schematic diagram of the rAAV construct, pTR_{BS}-UF2. Only the relevant restriction sites with their positions within the construct are shown. Promoter/enhancer elements are shown in purple. ITR (shown in blue) is the inverted terminal repeat sequence of wild type AAV; CMV is the immediate-early promoter/enhancer of cytomegalovirus; SD/SA is the SV40 late viral protein gene 16S/19S splice donor and acceptor signals; *gfp-h* is the 'humanized' *A.victoria gfp* cDNA; polyA is the SV40 polyadenylation signal from the SV40 genome; PE is a tandem repeat of the enhancer from the polyomavirus mutant PYF441; PTK is the *thymidine kinase* promoter of herpes simplex virus; *neoR* is the neomycin resistance gene; and polyA2 is the bovine growth hormone polyadenylation signal from pRc/CMV (Invitrogen).

3.2.2 Choice of photoreceptor cell-specific promoters

Three different promoters were selected to give photoreceptor cell-specific expression.

3.2.2.1 Sections of the mouse *Prph2* gene promoter

The first two promoters selected were based on the mouse *Prph2* gene promoter. Since the long-term aim of the study was to treat the $Prph2^{Rd2/Rd2}$ mouse through the delivery of a normal copy of the gene for peripherin-2, the investigation of native genomic regulatory sequences of *Prph2* was important. The sequence up to 1851 bp upstream of the start codon has previously been determined by Ma *et al.* and has been directly submitted to the NCBI Entrez database (accession number L42167). However, only the first 430 bp upstream of the translation start point were examined in detail [173] (Fig. 3.5). They scanned this region for recognisable promoter or enhancer motifs and

identified an AT-rich TATA-box-like sequence at position –253 to –246, and a region at position –630 to –611 that is similar to the Ret-1 nuclear-protein binding element upstream of the rat *opsin* gene. Up to 1414 bp of the upstream sequence has been obtained by Cheng *et al.* [174]. Their sequence analysis identified the same TATA-box-like sequence but a different Ret-1-like sequence at position –1349 to –1337, through its 86% homology with the Ret-1 element of the bovine *opsin* gene promoter. They also identified CRS-3-like and Bat-1-like elements. They also identified, through transcription analysis, seven transcription initiation start sites between positions –242 and –219.

Two fragments were chosen for use in rAAV constructs: a 1158 bp section of the upstream region from position –1172 to –14, and a 2803 bp section from position –2817 to –14. The shorter 1158 bp fragment had been obtained previously in this laboratory, as a PCR fragment, by N. Kanuga and contained the Ret-1-like elements and the TATA-box-like element described above. The longer 2803 bp fragment was isolated using a walking PCR method (section 2.5.2) adapted from Dominguez and Lopez-Larrea [175] on the Pac clone 481-K1. This clone had previously been identified by N. Kanuga using the HGMP Mouse Genomic Pac Library, RPCI21, through screening using a fragment from exon I of the mouse *Prph2* gene as a probe. The 2803 bp fragment is approximately the longest section of DNA that could be incorporated in this rAAV construct. Both PCR fragments were gel purified and sub-cloned into pGEM®-T Easy Vectors (Promega) (section 2.4). The clones were sequenced using a dideoxymediated chain termination method (section 2.6), with oligonucleotide primers synthesized in a sequential overlapping manner. Final sequence was determined for one strand and the sequence comparisons were made using the GeneWorks Release 2.5.1 programme. The identified upstream sequence (Fig. 3.5) corresponded with that of L42167 for the region that includes the 1158 bp of the short *Prph2* promoter fragment. However, at position –1442 the two sequences diverge and there is no sequence similarity upstream of this point.

Figure 3.5 The nucleotide sequence of the 5′ region of the mouse *Prph2* gene. Full legend overleaf.

Figure 3.5 The nucleotide sequence of the 5′ region of the mouse *Prph2* gene. The start of the long *Prph2* upstream fragment, at position –2817, and the start of the short *Prph2* upstream fragment, at position –1172, are marked with green arrowheads. At position -1442 the long *Prph2* upstream sequence diverges from that of the Entrez clone, L42167, and is marked with a pink arrowhead. The 5′ limit of the sequence described by Cheng *et al.*[174] is marked with a red arrowhead at position –1414. The significant sequences noted by this group, Bat-1-like, Ret-1-like, CRS3-like, and TATA-box-like, are marked in red. In comparison the Ret-1-like element described by Ma *et al.* [173] is marked in blue, although this group also identified the same region as TATA-box-like as Cheng *et al.* [174]. In total seven transcription initiation sites have been identified by Cheng *et al.* [174] by RNase protection assay, 5′ RACE and primer extension. These are marked with bold letters along with the start of translation.

In order to further investigate the different upstream sequences NIX analysis was performed. This is a bioinformatics application, available at the Human Genome Mapping Project (HGMP) Resource Centre web site (http://www.hgmp.mrc.ac.uk), which runs many DNA analysis programmes on DNA sequence, helping in the identification of interesting regions. These programmes will recognise possible promoter elements, introns and exons, and repeat sequences and match the submitted sequence to previously sequenced clones and expressed sequence tags. The *Prph2* upstream sequence results are shown in Figure 3.6. One program predicted a region containing polymerase II promoter elements within the long fragment from position –1880 to –1591. The quality of prediction was rated as good and suggests that even this far upstream of the *Prph2* start codon there may be regulatory sequences that are important in the control of expression. The analysis also shows that 5′ of position -1442, where our sequence diverges from that of clone L42167, there is a Sine/B2 repeat sequence. These are short interspersed elements that constitute approximately 0.7% of the mouse genome [176], and may be the cause of recombination. Further, the NIX analysis suggested that the sequence of clone L42167 was the result of a recombination event since the sequence of this clone, upstream of position -1442, matched 229 bp of two genomic clones from mouse chromosome 11 (NIX results not shown). To confirm that our sequence for the longer upstream fragment was correct, a PCR was performed on mouse genomic DNA using a forward primer from position -1608 to -1585, GENUPPER, and a reverse primer, GENLOWER, from position +115 to + 94 (section 2.5.1). This PCR produced a 1.7 kb band as expected (Fig. 3.7), confirming the long fragment of the *peripherin-2* promoter was correct.

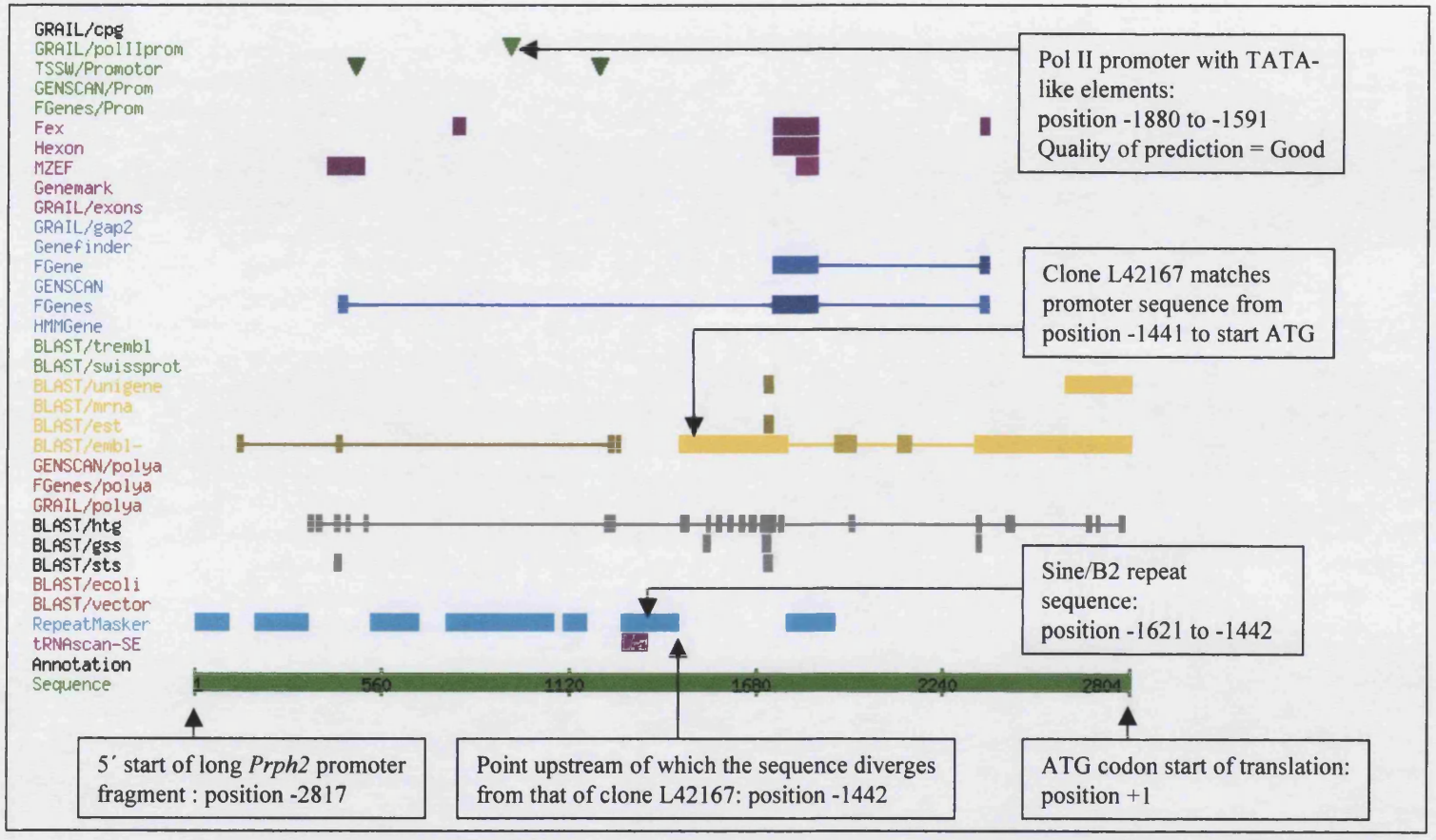

Figure 3.6 NIX analysis predictions for the 5′ region of the mouse *Prph2* gene. NIX analysis was performed on the complete sequence of the long *peripherin-2* upstream fragment. The prediction programmes included in NIX are shown on the left hand side of the figure. The regions of interest predicted by each programme are highlighted, the brighter colours indicating better predictions. The diagram has been annotated to show that the clone L46167 matches the sequence of the long promoter fragment from position -1442 onwards. Just upstream of this point RepeatMasker has detected a Sine/B2 repeat sequence This may have been the cause of the recombination of clone L46167. The GRAIL/polII promoter analysis program has found a region which contains TATA-like elements indicating that the longer fragment of the *Prph2* upstream region may contain additional sequence important for the control of *Prph2* expression.

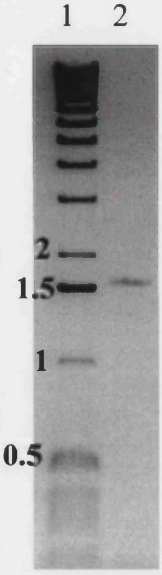

Figure 3.7 Confirmation of the long *peripherin-2* promoter fragment. A PCR reaction to amplify the long *peripherin-2* promoter fragment was performed on mouse genomic DNA and the results run on an agarose gel.
Lane 1 – Marker (sizes in kb).
Lane 2 – 10 µl of a PCR reaction. Expected fragment size = 1722 bp as described in the text.

3.2.2.2 Bovine *rhodopsin* promoter

The *Prph2* promoter fragments have not been used in transgenic studies to drive gene expression and therefore it was important to select a third promoter fragment from which specific expression of a reporter gene has been demonstrated *in vivo.* The promoter selected was a large fragment of the upstream region of the bovine *rhodopsin* gene. In a study to characterise the *cis*-acting DNA elements required for *rhodopsin* expression, a –2174 to +70 bp fragment was shown to produce strong expression of the reporter gene *β-galactosidase* in the PR cells of transgenic mice [177]. This study compared transgenic lines made with three different lengths of the upstream region of this gene, all of which showed photoreceptor cell-specific expression. However, the average expression levels were reported to be highest with the –2174 to 70 bp fragment. It is clear from these experiments that the similarity between the upstream region of the bovine *rhodopsin* gene and that of the murine *rhodopsin* gene is sufficient to result in conservation of biological function. For these transgenic studies the fragment had been cloned upstream of the gene for *β-galactosidase* to create the plasmid gBR200-lacF. This plasmid was a gift from D. Zack. The plasmid, gBR200-lacF, was transformed into competent DH5α™ cells (section 2.2.1), and plasmid DNA prepared (section 2.2.2).

3.2.3 Introduction of a bovine *rhodopsin* promoter into pTR$_{BS}$-UF2

The 2246 bp fragment containing the bovine *rhodopsin* promoter was removed from the gBR200-lacF plasmid by restriction enzyme digestion (section 2.3.1) with *Kpn*I and *Xba*I. A similar restriction enzyme digest was carried out on pTR$_{BS}$-UF2 with *Kpn*I and *Xba*I, removing the existing CMV promoter (for diagram of pTR$_{BS}$-UF2 see Fig. 3.4). Restriction fragments were separated on an agarose gel; fragments were purified, ligated and transformed (section 2.4). The resulting colonies were propagated and plasmid DNA extracted (section 2.2). In order to pick the colonies containing the *rhodopsin* promoter *Sma*I digests (section 2.3.1) were performed on the extracted DNA, and the results separated on an agarose gel (section 2.3.2). *Sma*I cuts four times within the *rhodopsin* promoter fragment, and four times within the pTR$_{BS}$-UF2 cassette – twice within each ITR. Therefore the expected fragments from the clone containing the correct insertion of the *rhodopsin* promoter into pTR$_{BS}$-UF2 are 2 x 11, 410, 426, 725, 760, 2549 and 3009 bp (from the plasmid backbone) as shown in Figure 3.8. The result of this digest is shown in Figure 3.9.

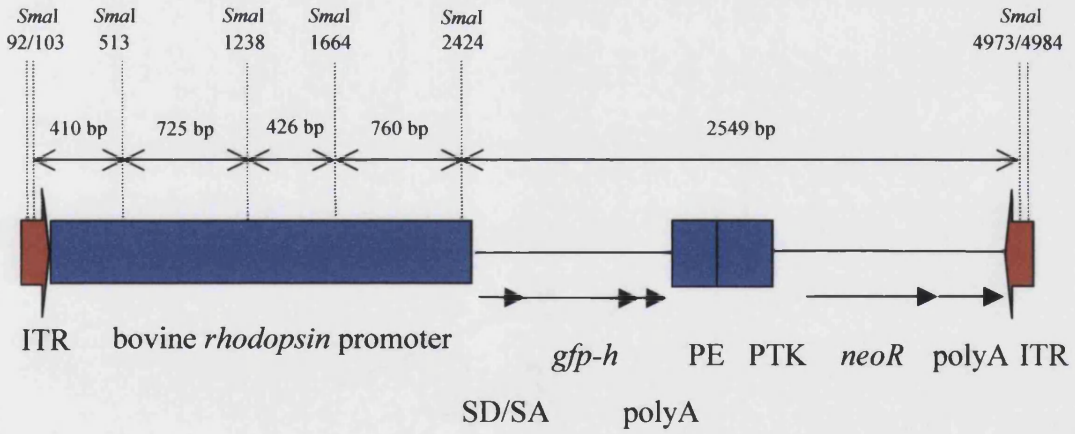

Figure 3.8 Schematic showing the positions of *Sma*I sites within pTR$_{BS}$-UF2 after the insertion of the bovine *rhodopsin* promoter. Each *Sma*I site is marked along the top with their bp location within the plasmid. The single line arrows below them show the expected fragment sizes generated on digestion with this restriction enzyme. ITR is the inverted terminal repeat sequence of wild type AAV; SD/SA is the SV40 late viral protein gene 16S/19S splice donor and acceptor signals; *gfp-h* is the 'humanized' *A.victoria gfp* cDNA; polyA is the SV40 polyadenylation signal from the SV40 genome; PE is a tandem repeat of the enhancer from the polyomavirus mutant PYF441; PTK is the *thymidine kinase* promoter of herpes simplex virus; *neoR* is the neomycin resistance gene; and polyA2 is the bovine growth hormone polyadenylation signal from pRc/CMV (Invitrogen).

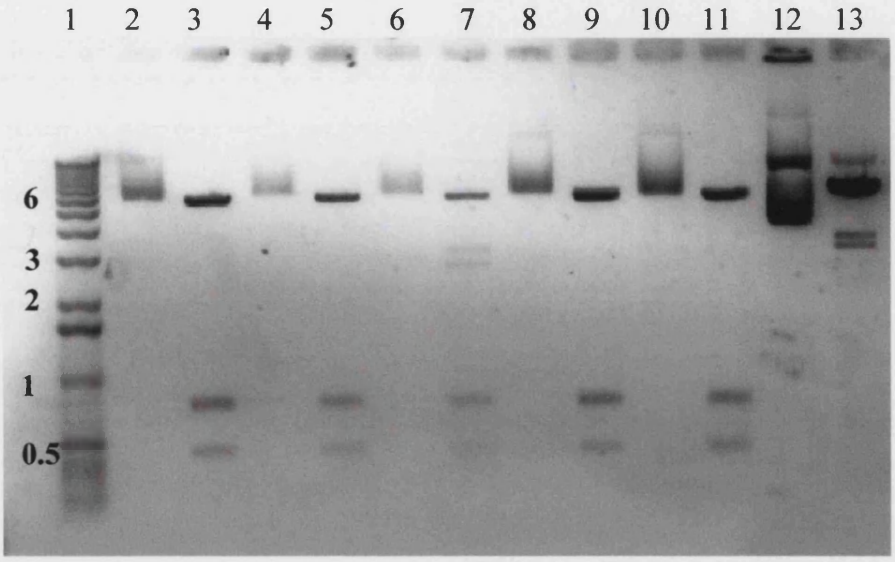

Figure 3.9 *Sma*I digest to check the ITRs within the plasmids produced from the ligation of the bovine *rhodopsin* promoter into pTR_{BS}-UF2. Lane1 – marker (sizes in kb); Lanes 2 to 11 – uncut (even numbered lanes) and *Sma*I cut (odd numbered lanes) clones 1 to 5; Lane 12 and 13 - uncut and *Sma*I cut pTR_{BS}-UF2 respectively.

The ~ 750 bp and ~ 400 bp bands in lanes 3, 5, 7, 9 and 11 (Fig. 3.9) suggest that the *rhodopsin* promoter fragment is present in all the clones. However the absence of the 2549 bp and the 3009 bp fragments in all of those lanes except lane 7 indicates that in these clones the two *Sma*I sites within one of the ITRs have been lost. This could be due to a complete or partial loss of the 3′ ITR. In fact even in clone 3 (lane 7) the digest indicates that the plasmid copies containing two complete ITRs are only a sub-population. The digest of the original pTR_{BS}-UF2 clone (lane 13) shows that in this plasmid too, a large number of copies appear to have lost one set, and in some cases both sets of *SmaI* sites. In repeated attempts to clone the bovine *rhodopsin* promoter into pTR_{BS}-UF2 there was frequent loss of all or part of at least one ITR and the generation of recombination products (data not shown).

3.2.4 Instability of ITRs

The apparent instability of the ITRs was tested by simultaneous transformation (section 2.2.1) of pTR_{BS}-UF2 into two different bacterial strains. Stratagene's Epicurain Coli® SURE®2 competent cells, and GibcoBRL's Library Efficiency® Competent DH5α™ cells were used. The SURE®2 cells have mutations in both the *recB* and *recJ* genes.

These genes are involved in the rearrangement and deletion of irregular DNA sequences such as those containing inverted repeats and those with secondary structure. The mutations therefore confer a recombination deficient phenotype that greatly reduces the number of homologous recombination events in comparison to the number that would occur within the DH5α™ cells, even though these cells contain a *rec*A1 mutation to increase insert stability. After transformation eight colonies were picked from each bacterial strain and plasmid DNA extracted (section 2.2.2). Restriction digest analysis with *Sma*I (section 2.3) shows the ratio of plasmids containing two complete ITRs, indicated by the doublet at 3 kb, to plasmids containing, at most, one complete ITR, represented by the single band at 6 kb for each colony picked (Fig. 3.10). In all bacterial clones tested, including the original sample (not shown), there are plasmids that have lost the *Sma*I sites from one ITR. However, the ratio of those plasmids that retain both sets of *Sma*I sites to those that retain only one set remains relatively constant in those clones transformed and grown in SURE®2 cells. In contrast a significant proportion of plasmids isolated from clones transformed and grown in the DH5α™ cells appear to have lost the *Sma*I sites from one ITR, so that the 6 kb band was much stronger on *Sma*I digestion of these clones. Although the loss of *Sma*I sites may not represent the loss of the entire ITR in our laboratory, the use of these plasmids in the production of rAAV has consistently resulted in recombinant virus with titres substantially lower than expected (M. de Alwis - unpublished results).

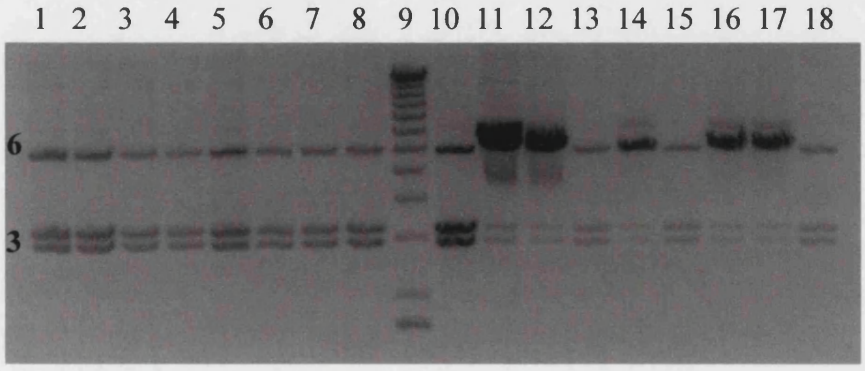

Figure 3.10 *Sma*I digests to check the ITRs of pTR$_{BS}$-UF2 clones transformed into two differenct bacterial strains. Lanes 1 to 8 - *Sma*I digests of clones transformed into SURE2® cells; Lane 9 – marker (sizes in kb); Lanes 10 to 18 - *Sma*I digests on clones transformed into DH5α™cells.

3.3 An alternative strategy for the production of rAAV constructs

Having established that the use of pTR_{BS}-UF2 as the vector plasmid for rAAV production was complicated by the instability of sequences within the ITRs, it was necessary to produce an alternative vector plasmid that would have more stable ITRs and would allow the easy cloning of a variety of constructs.

3.3.1 D sequence-deleted ITRs

As shown in Figure 3.2, the ITRs of AAV type 2 are 145 bp in length, with the terminal 125 bp forming a palindromic hairpin. The stretch of 20 bp not involved in the hairpin is designated the D sequence (section 3.1.1). This sequence has been shown to play an essential role in the efficient rescue, replication and packaging of the AAV genome from a recombinant plasmid [152, 178]. However, further mutation analyses revealed that only the 10 nucleotides adjacent to the hairpin structure are necessary and sufficient for these roles, and that the distal 10 nucleotides could be deleted [179]. The plasmid resulting from this deletion is designated pD-10 and has had nt 11 to 20 of the D sequence removed and an *Eco*RV site engineered in its place (Fig. 3.11).

D sequence	5′	CTCCA	TCACT	AGGGG	TTCCT	3′
	3′	GAGGT	AGTGA	TCCCC	AACGA	5′
D-10	5′	CTCCA	TCACT	**GATAT**	CACTT	3′
	3′	GAGGT	AGTGA	**CTATA**	GTGAA	5′

Figure 3.11 Sequence of the wtAAV D sequence and the deleted sequence, D-10. The sequence in bold letters marks the position of the engineered *Eco*RV site. Plasmids generated by Wang *et al.* [179].

The deletion of these nucleotides has greatly increased the stability of the ITR sequence [180], making it more appropriate for use in a vector plasmid.

3.3.2 Cloning of a multiple cloning site into pD-10

In order to easily utilise pD-10 in the generation of rAAV vector plasmids, a multiple cloning site was introduced between the deleted ITRs (for general cloning methods see section 2.1 to 2.4). The plasmid pD-10 (a kind gift from X-S Wang and A Srivastava) was transformed into competent DH5α™ cells and plasmid DNA prepared. Plasmid DNA was digested with *Eco*RV to remove the viral genome and leave a blunt ended fragment containing the plasmid backbone and the ITRs. A multiple cloning site polylinker was selected from the plasmid LITMUS 28 (New England BioLabs Cat. No. N3628S). This polylinker region was excised with *Sna*BI and *Stu*I, generating a blunt ended fragment. The fragments were gel purified, ligated and transformed. However, on transformation no colonies were obtained. The polylinker fragment is only 153 bp in length and it is possible that the ITRs, in double stranded form, may have some secondary structure that causes a steric hindrance to the ligation, thus preventing the polylinker ligating to both ITRs efficiently in the context of a blunt ligation. A stuffer fragment was therefore included into the polylinker region to increase the size of the fragment to be ligated between the ITRs (Fig. 3.12). This stuffer fragment was excised from pTR_{BS}-UF2 with *Bam*HI and ligated into the *Bam*HI site in the centre of the polylinker. This increased the polylinker size to 1445 bp. Following blunt ligation into the *Eco*RV bacterial colonies were obtained after transformation.

The resulting construct designated pD10-MCS was checked by restriction digest analysis with *Eco*RI, *Pac*I and *Sma*I and the results are shown in Figure 3.13. The presence of the stuffer fragment within the multiple cloning sites restricts the number of unique sites available for cloning into pD10-MCS, since one enzyme site either side of the stuffer fragment must be used in order for the fragment to be removed from the final recombinant genome. Nevertheless, compared with the original plasmid, pD-10, there is an increase in the number of unique restriction sites available making the cloning of vector constructs easier. These unique sites are shown in Figure 3.12.

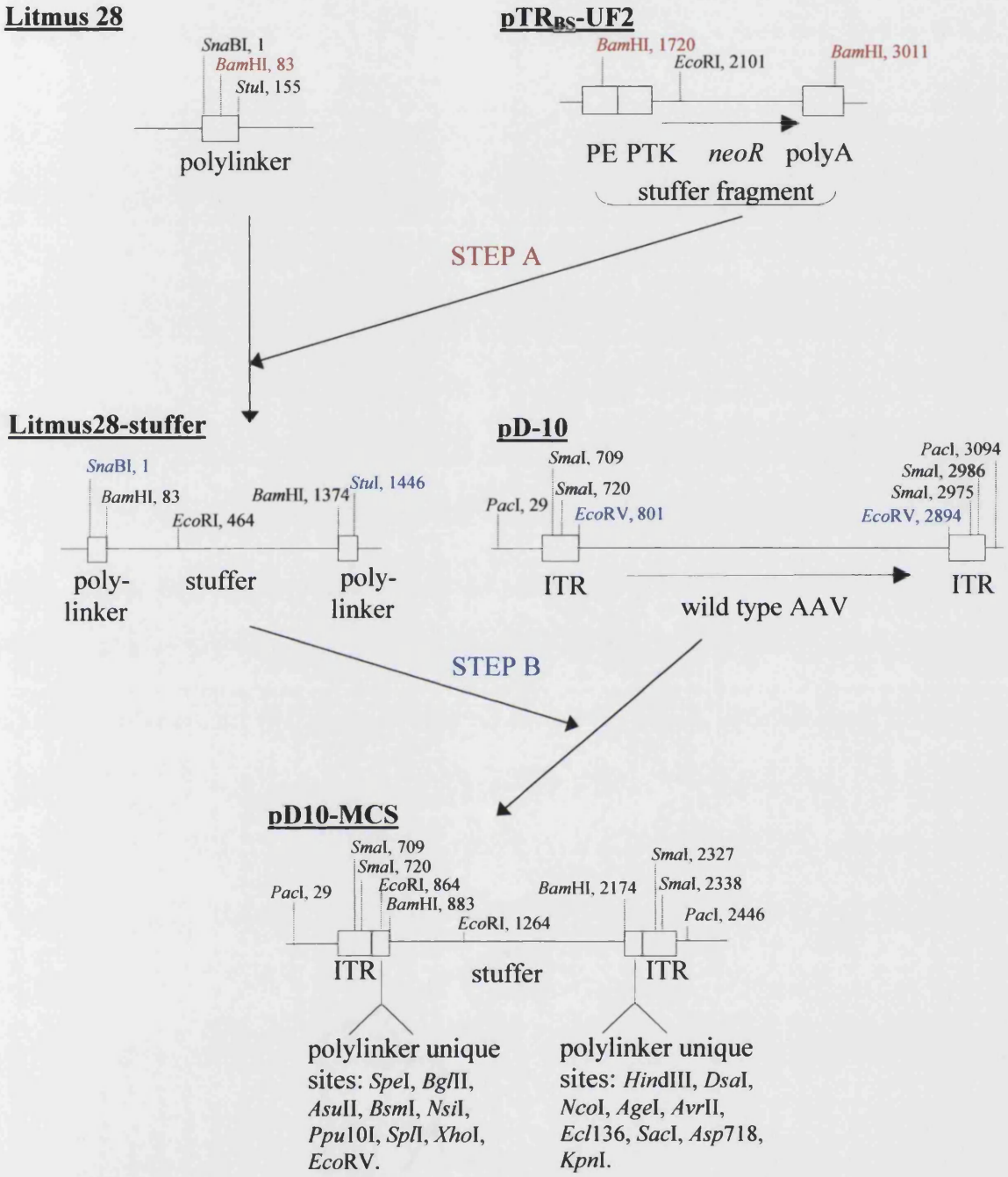

Figure 3.12 Cloning strategy for the production of pD10-MCS.
Step A : a *Bam*HI fragment from pTR$_{BS}$-UF2 was cloned into the *Bam*HI site within the poly-linker of Litmus 28. The resulting plasmid was called Litmus28-stuffer.
Step B : the AAV genome was removed from pD-10 by digestion with *Eco*RV. *Stu*I/*Sna*BI digest of Litmus 28-stuffer gave the stuffer fragment flanked by sections of the polylinker. This fragment was then cloned into the *Eco*RV sites to give **pD10-MCS**.
PE is the enhancer from the polyomavirus; PTK is the *thymidine kinase* promoter; *neoR* is the neomycin resistance gene: polyA is the SV40 polyadenylation signal; and ITR is the rAAV inverted terminal repeat.

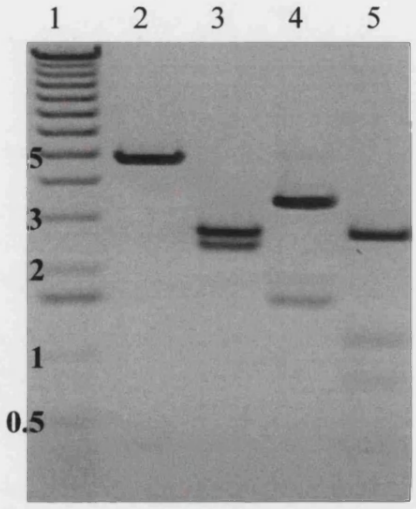

Figure 3.13 Confirmation of the plasmid pD10-MCS (5075 bp) with restriction enzyme digests. Lane 1 – marker (sizes in kb); Lane 2 - pD10-MCS digested with *Eco*RI, expected fragment sizes are 400 bp and 4675 bp; Lane 3 - digested with *Pac*I, expected fragment sizes are 2419 bp and 2656 bp; Lane 4 - digested with *Sma*I, expected fragment sizes are (2 x 11 bp), 1607 bp and 3446 bp; Lane 5 - digested with *Eco*RI and *Pac*I, expected fragment sizes are 400 bp, 835 bp, 1182 bp and 2658 bp.

3.3.3 Construction of vector plasmids containing *egfp* driven by photoreceptor cell-specific promoter constructs

All the constructs utilise the *egfp* gene from the vector pEGFP (Clontech Cat. No. 6077-1) for ease of cloning. This *egfp* gene has been engineered in a similar manner to that of *gfp-h* (see section 3.2.1). The double amino acid substitutions of Phe-64 to Leu and Ser-65 to Thr optimise fluorescence [181] and 190 silent base changes make the codon usage more suitable for expression in human cells. The upstream sequence directly flanking the gene has been converted to a Kozak consensus translation initiation site [170]. This plasmid does not contain a polyA sequence and therefore an SV40 polyA was taken from the plasmid pTRE (Clontech Cat. No. K1620-1).

3.3.3.1 *Egfp* driven by the *rhodopsin* promoter

The bovine *rhodopsin* promoter from gBR200-lacF, discussed in section 3.2.2.2, had been sub-cloned into the *Kpn*I and *Xba*I sites within the polylinker site of LITMUS 28, and the resulting plasmid designated pLitRho. A schematic diagram of the subsequent cloning steps for the production of the rAAV construct containing *egfp* driven by the *rhodopsin* promoter is shown in Figure 3.14. The SV40 polyA sequence was removed from pTRE by digestion with *Xba*I and *Hin*dIII, and sub-cloned into the *Xba*I and *Hin*dIII sites of LITMUS 28. The resulting plasmid was designated pLitA. The *egfp* gene was excised from pEGFP by digestion with *Xba*I, and sub-cloned into the re-formed *Xba*I site upstream of the polyA sequence in pLitA. The *egfp*-polyA fragment was excised from this plasmid by digestion with *Xba*I and *Hin*dIII and directionally

cloned into the same sites downstream of the *rhodopsin* promoter in pLitRho. The resulting construct was designated pLitRhoEgfp.

A 56 bp section of 5′ polylinker from the plasmid pEGFP that separated the *rhodopsin* promoter and the *egfp* gene in pLitRhoEgfp was removed to prevent it interfering with expression. This was achieved by restriction digest with *Bpu*1102 and *Age*I, blunting of the plasmid with DNA polymerase I, and then self-ligation of the resulting fragment. This deletion resulted in the shortening of the untranslated region of the *rhodopsin* promoter from +72 to + 33 and removal of one of the *Sma*I sites within the promoter at position 2473.

In order to clone this construct into pD10-MCS a *Spe*I site was engineered at position 210 of pLitRhoEgfp upstream of the start of the *rhodopsin* promoter. This was achieved by the insertion within the *Afl*II site at position 216 of an oligonucleotide (designated *Afl*II to *Spe*I) containing the *Spe*I site. The resulting cassette was then cloned into pD10-MCS by digestion of both plasmids with *Spe*I and *Hin*dIII, and ligation of the *rhodopsin-egfp* and D-10 ITR fragments. Restriction digest analysis with *Pac*I, *Sma*I, *Xba*I, and a double digest with *Hin*dIII and *Spe*I, was used to show the correct clone, pD10RhoEgfp (Fig. 3.15). The *SmaI* digest of pD10RhoEgfp showed that all the expected sites within the ITRs were present.

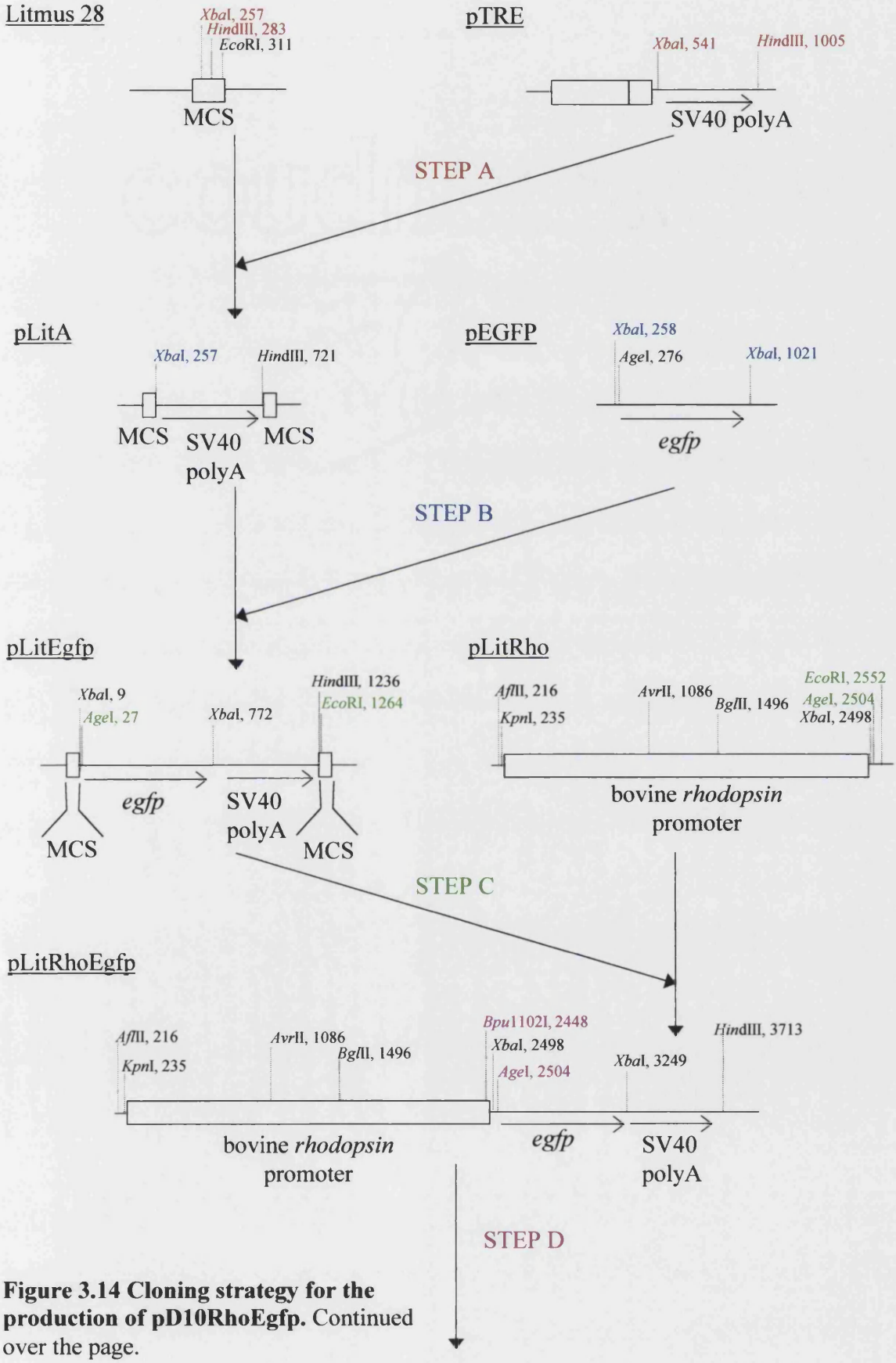

Figure 3.14 Cloning strategy for the production of pD10RhoEgfp. Continued over the page.

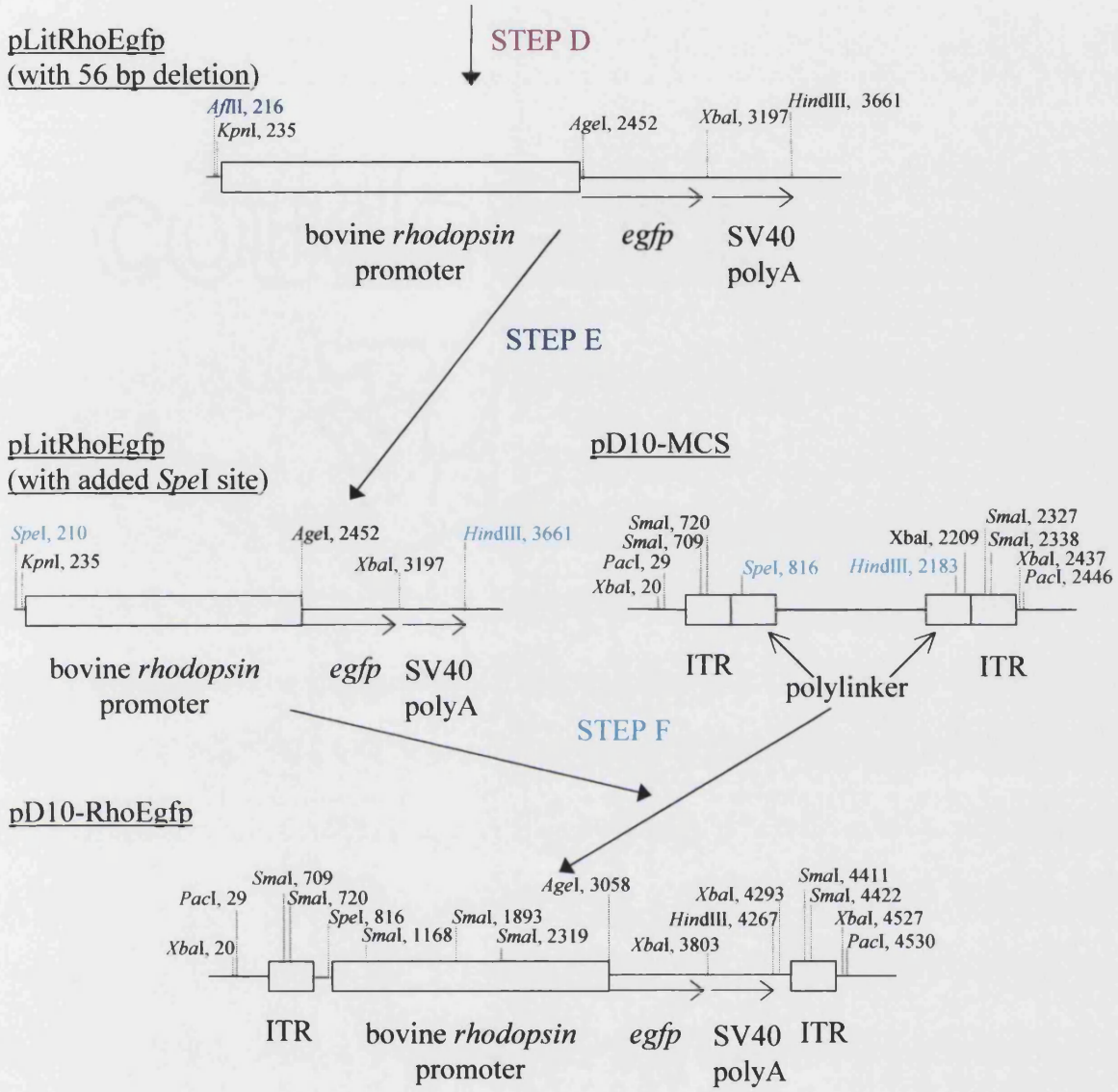

Figure 3.14 Cloning strategy for the production of pD10RhoEgfp.
Step A : the SV40 poly adenylation signal was removed from the plasmid pTRE by digestion with *Xba*I and *Hin*dIII and cloned into the same sites within Litmus 28, to produce pLitA.
Step B : the *egfp* gene was removed from the plasmid pEGFP by digestion with *Xba*I and ligated into the *Xba*I site upstream of the polyA sequence in pLitA producing pLitEgfp.
Step C : the *egfp*-polyA sequence was excised from pLitEgfp by digestion with *Age*I and *Eco*RI and ligated into the corresponding sites downstream of the bovine *rhodopsin* promoter in pLitRho to produce pLitRhoEgfp.
Step D : pLitRhoEgfp was digested with *Bpu*1102I and *Age*I and then religated to remove a 56 bp fragment between the bovine *rhodopsin* promoter and *egfp*.
Step E : pLitRhoEgfp resulting from Step D was cut with *Afl*II and an oligonucleotide containing an *Spe*I site was ligated upstream of the bovine *rhodopsin* promoter.
Step F : the resulting plasmid was cut with *Spe*I and *Hin*dIII and ligated into the corresponding sites within the ITRs of pD10-MCS to produce **pD10RhoEgfp**.
MCS is the multiple cloning site polylinker; SV40 polyA is the polyadenylation signal from SV40; *egfp* is the gene from Clontech's enhanced green fluorescent protein; and ITR is the rAAV inverted terminal repeat.

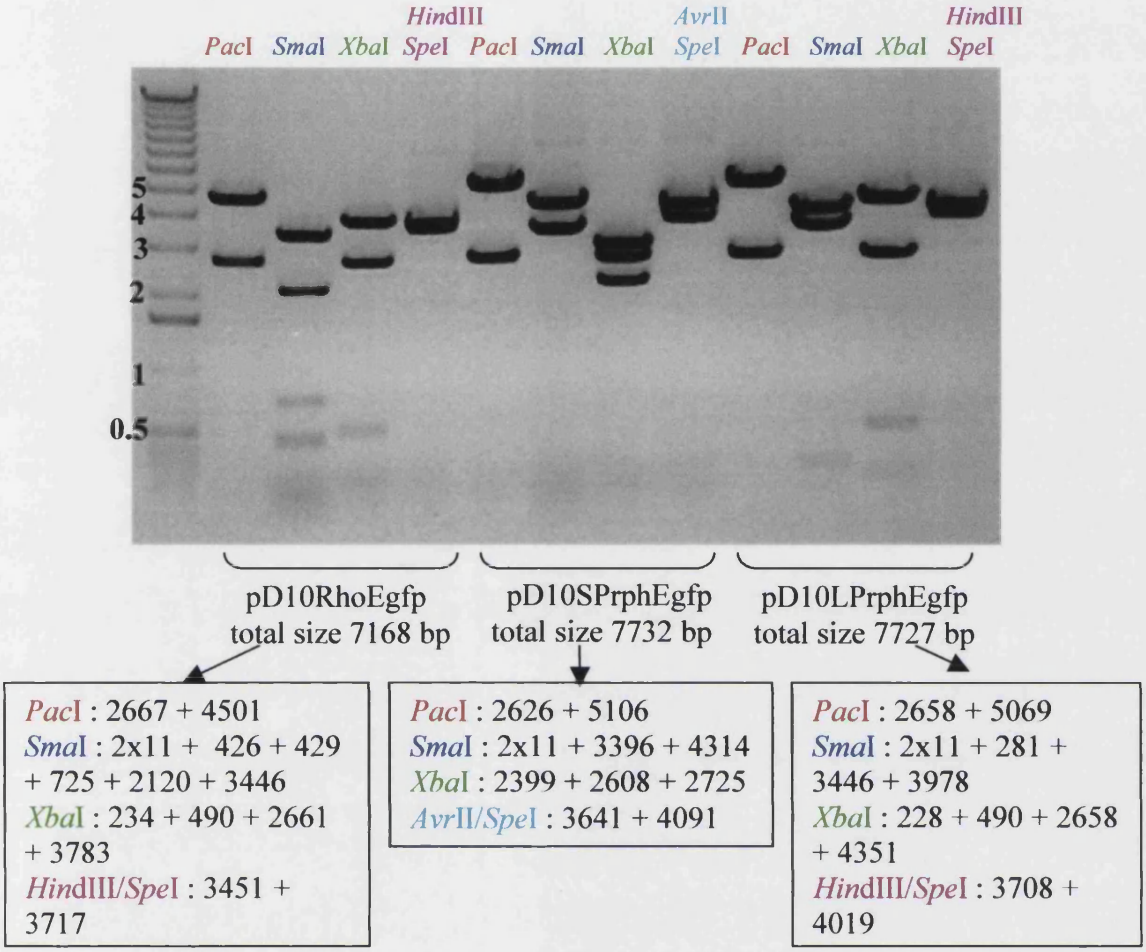

Figure 3.15 Confirmation of the plasmids pD10RhoEgfp, pD10SPrphEgfp and pD10LPrphEgfp with restriction enzyme digests. Lane 1 – marker (sizes in kb). Predicted fragment sizes from a correct clone for each digest are shown in the boxes.

3.3.3.2 *Egfp* driven by the short *Prph2* promoter fragment

The short 1158 bp *Prph2* promoter fragment, described in section 3.2.2.1, was re-amplified from pGEM®-T Easy by PCR with the primers PERUP*Age*I and SPERDOWN*Afl*II (section 2.5.1). The upstream primer (PERUP*Age*I) included an overhang that contained an *Age*I site, whereas the downstream PCR primer (SPERDOWN*Afl*II) included an *Afl*II site overhang. The resulting PCR fragment was cloned into pGEM®-T Easy to produce the plasmid pGEM-short and checked by sequencing (section 2.6). Subsequent cloning steps are shown in Figure 3.16. The plasmid pGEM-short was cut with *Age*I and *Afl*II giving the promoter fragment that could be cloned into the previously described plasmid pLitRhoEgfp (Section 3.3.3.1 also shown in Fig. 3.14 as the product of step D) after the removal of the *rhodopsin* promoter with an *Age*I-*Afl*II digest. The resulting construct was designated

pLitSPrphEgfp. This expression cassette was too small to insert directly into pD10-MCS and therefore a 1660 bp stuffer fragment was added. This fragment was obtained from the plasmid pCMVβ (Clontech Cat. No. 6177) by digestion with *SplI* and *Eco*RV and contains part of the 3′ end of the *β-galactosidase* gene. This fragment was cloned into the *SplI* and *Eco*RV sites downstream of the polyA tail in LitSPrphEgfp. In order to clone the resulting expression cassette into pD10-MCS an *Avr*II site was created by ligation of an oligonucleotide (designated *Afl*II to *Avr*II) into the *Afl*II site at position 216. This plasmid was then cut with *Avr*II and *Spe*I and ligated into the corresponding sites within the multiple cloning site in pD10-MCS. Restriction digest analysis with *Pac*I, *Sma*I, *Xba*I, and a double digest with *Avr*II and *Spe*I, was used to show the correct clone of pD10SPrphEgfp (Fig. 3.15).

3.3.3.3 *Egfp* driven by the long *Prph2* promoter fragment

The long 2803 bp *Prph2* promoter fragment described in section 3.2.2.1 was re-amplified from pGEM®-T Easy with the primers PERUP*Age*I and LPERDOWN*Spe*I (section 2.5.1). The upstream primer (PERUP*Age*I) included an overhang that contained an *Age*I site, whereas the downstream PCR primer (LPERDOWN*Spe*I) included an *Spe*I site overhang. The resulting PCR fragment was cloned into pGEM®-T Easy to produce the plasmid pGEM-long and two different clones were checked by sequencing (section 2.6). The following cloning steps are shown in Figure 3.17. The pGEM-long plasmid was digested with *Age*I and *Spe*I giving the promoter fragment that could be cloned into the previously described plasmid pLitRhoEgfp (section 3.3.3.1 also shown in Fig. 3.14 as the product of step E) after the removal of the *rhodopsin* promoter with an *Age*I-*Spe*I digest. The resulting construct was designated pLitLPrphEgfp. This plasmid was then cut with *Spe*I and *Hin*dIII and ligated into the corresponding sites within the multiple cloning site in pD10-MCS. Restriction digest analysis with *Pac*I, *Sma*I and *Xba*I, *Hin*dIII and *Spe*I was used to show the correct clone of pD10LPrphEgfp (Fig. 3.15).

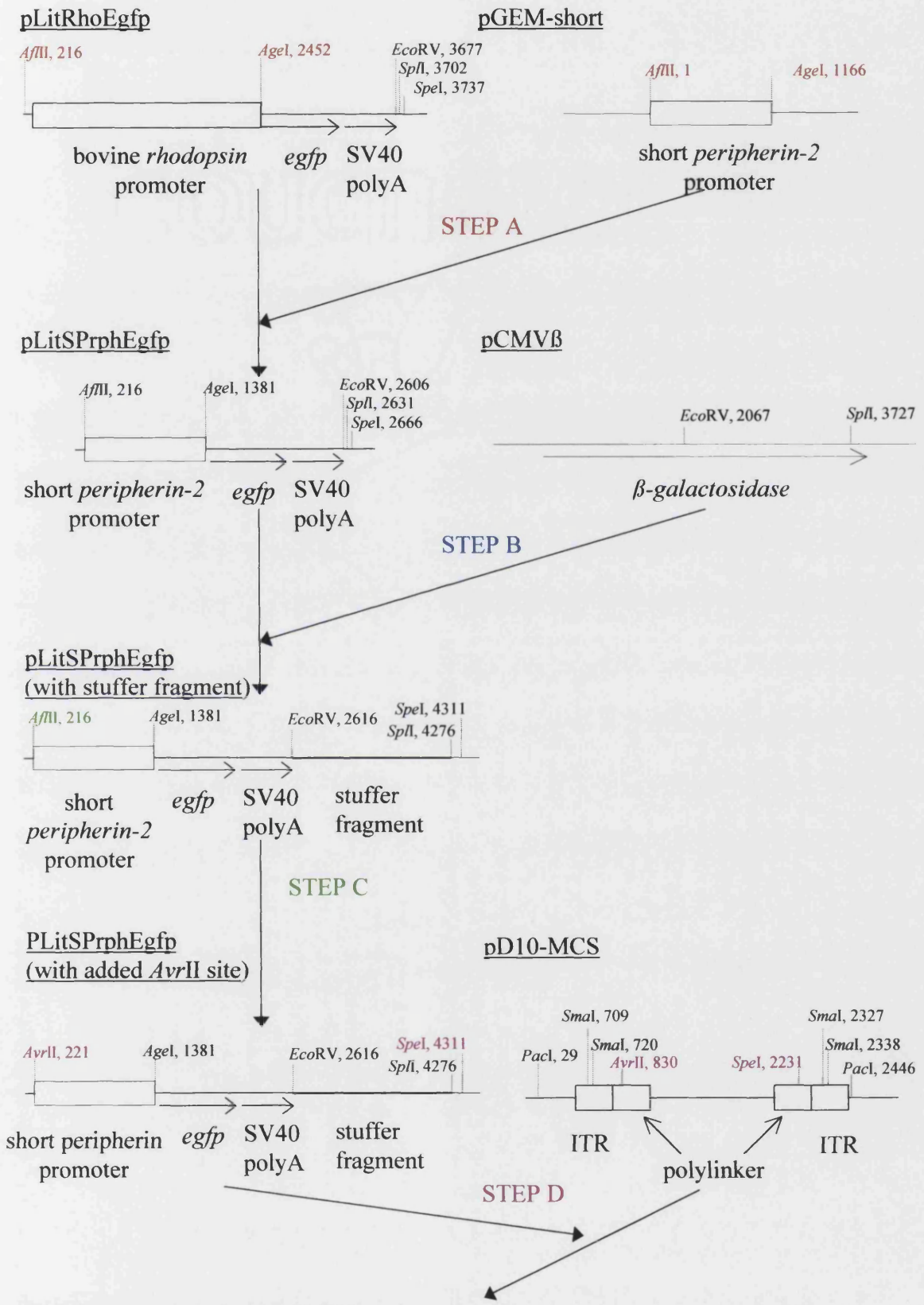

Figure 3.16 Cloning strategy for the production of pD10SPrphEgfp. Continued over the page.

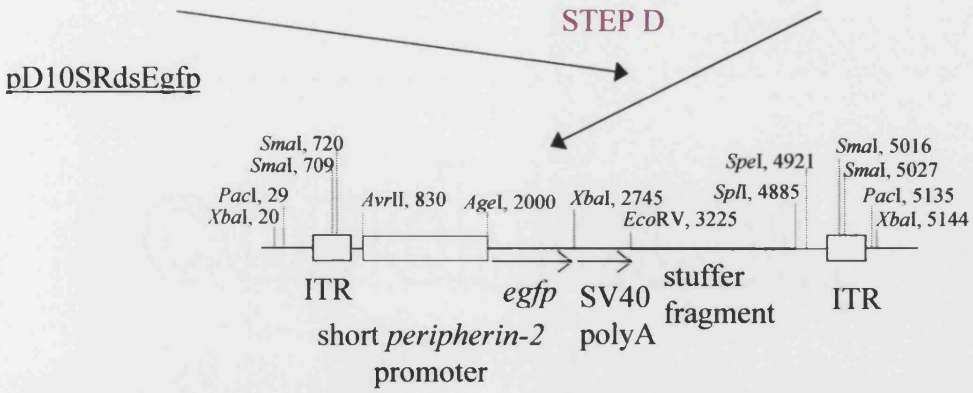

Fig 3.16 Cloning strategy for the production of pD10SRdsEgfp.
Step A : the short *peripherin-2* promoter was excised from pGEM-short by digestion with *Afl*II and *Age*I. The bovine *rhodopsin* promoter is removed from pLitRhoEgfp with an *Afl*II/*Age*I digest and the short promoter was ligated in its place, creating pLitSPrphEgfp.
Step B : a stuffer fragment was cut from pCMVß by digestion with *Eco*RV/*Spl*I and cloned into the corresponding sites downstream of the polyA signal in pLitSPrphEgfp.
Step C : pLitSPrphEgfp (stuffer) was cut with *Afl*II and an oligonucleotide containing an *Avr*II site was ligated in its place, upstream of the short *peripherin-2* promoter fragment.
Step D : pLitSPrphEgfp (*Avr*II) was cut with *Avr*II and *Spe*I and cloned into the corresponding sites between the ITRs of pD10-MCS to create **pD10SPrphEgfp**.
MCS is the multiple cloning site polylinker; SV40 polyA is the polyadenylation signal from SV40; *egfp* is the gene for Clontech's enhanced green fluorescent protein; and ITR is the rAAV inverted terminal repeat.

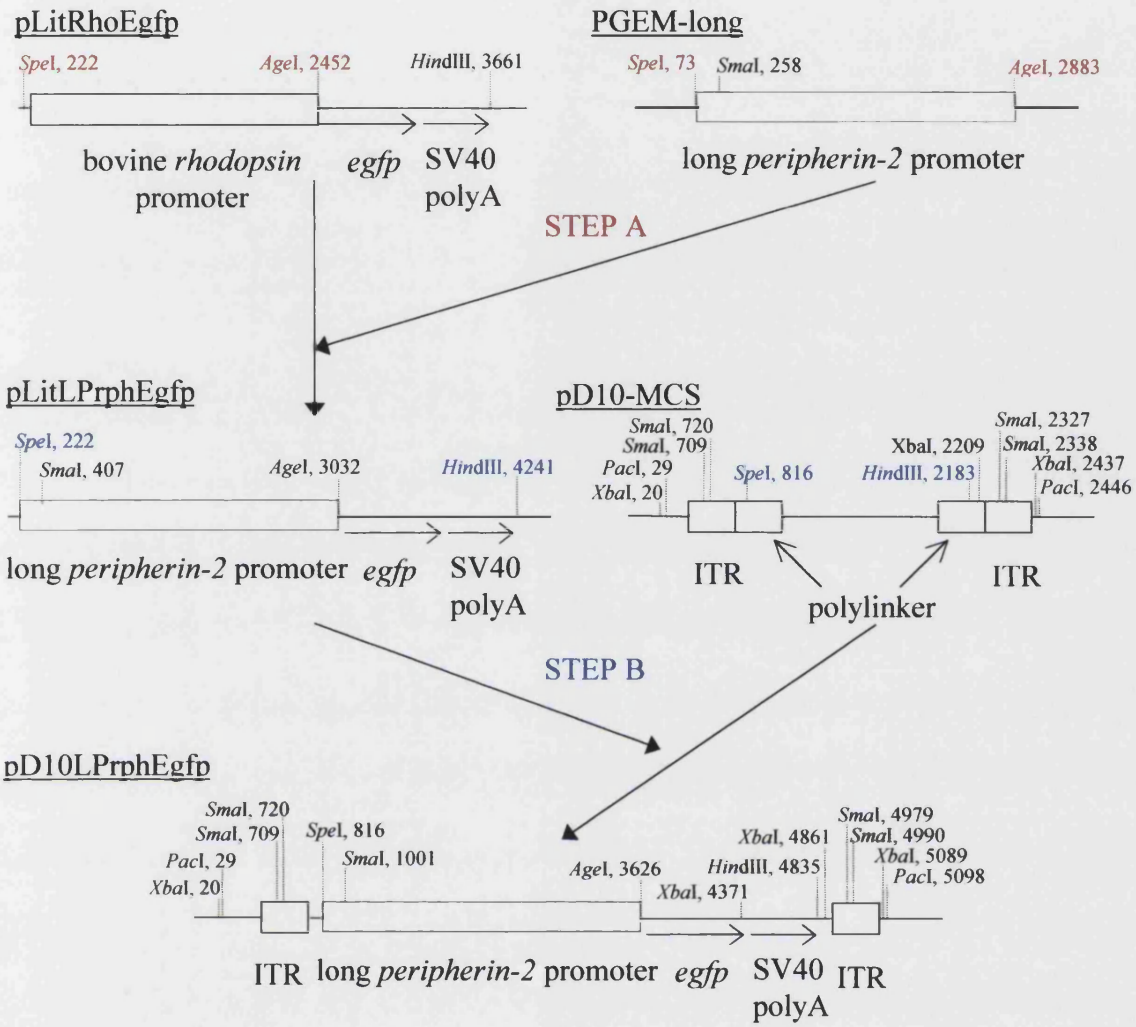

Figure 3.17 Cloning strategy for the production of pD10LPrphEgfp.
Step A : the long *peripherin-2* promoter fragment was excised from pGEM-long by digestion with *Spe*I and *Age*I. The bovine *rhodopsin* promoter was removed from pLitRhoEgfp with a *Spe*I/*Age*I digest and the long *peripherin-2* promoter fragment ligated in its place, creating pLitLPrphEgfp.
Step B : pLitLPrphEgfp was cut with *Spe*I and *Hin*dIII and cloned into the same sites between the ITRs of pD10-MCS to create **pD10LPrphEgfp**.
MCS is the multiple cloning site; SV40 poly A is the polyadenylation signal from SV40; *egfp* is the gene for Clontech's enhanced green fluorescent protein; and ITR is the rAAV inverted terminal repeat.

3.4 Production of purified high titre rAAV

3.4.1 The DISC-HSV system for production of high titre rAAV

During the time that we established that the ITRs within the pTR-UF2 plasmid were unstable our group was developing a new method for the production of rAAV to replace the conventional method described in section 3.1.2. Transduction efficiency with all recombinant viruses has been shown to correlate with titre and therefore improvements in the production process of rAAV that allow the manufacture of higher titres are desirable. The new method utilises the AAV helper functions of a disabled single cycle herpes simplex virus (DISC-HSV). The vector plasmid and the packaging plasmid contain the HSV origin of replication and are called amplicons. These plasmids are co-transfected into the producer cells that are then infected with DISC-HSV. The presence of the origin of replication on the vector and packaging plasmids allows the amplification of both the *rep* and *cap* genes and the rAAV genome inside the producer cell line. This feature to some extent simulates the amplification of the AAV genome that occurs during a wild type infection. The helper virus, DISC-HSV, has been genetically modified by the deletion of the gene for *glycoprotein H* (*gH*). This virus can be propagated to high titre as an infectious virus in cells expressing *gH* in *trans*, but in permissive non-complementing cell lines (*gH*$^-$) although the virus replicates effectively it is non-infective on release [182]. After transfection of a baby hamster kidney (BHK) cell line with the vector and packaging amplicons, and infection with the DISC-HSV, our group [183] demonstrated an increase in the total number of rAAV particles produced per cell (approximately 10^5 particles per cell). Figure 3.18 illustrates this method in detail. The best yields were obtained when using the vector genome and the helper AAV genome on separate amplicons. In these experiments the virus produced contained the reporter gene *egfp* driven by the CMV promoter. The vector amplicon for this virus was designated pHAV-5, and the packaging amplicon carrying the *rep* and *cap* regions was designated pHAV-7.3. Both of these constructs are illustrated in Figure 3.19. These plasmids are based on the amplicon plasmid pW7-TK [184].

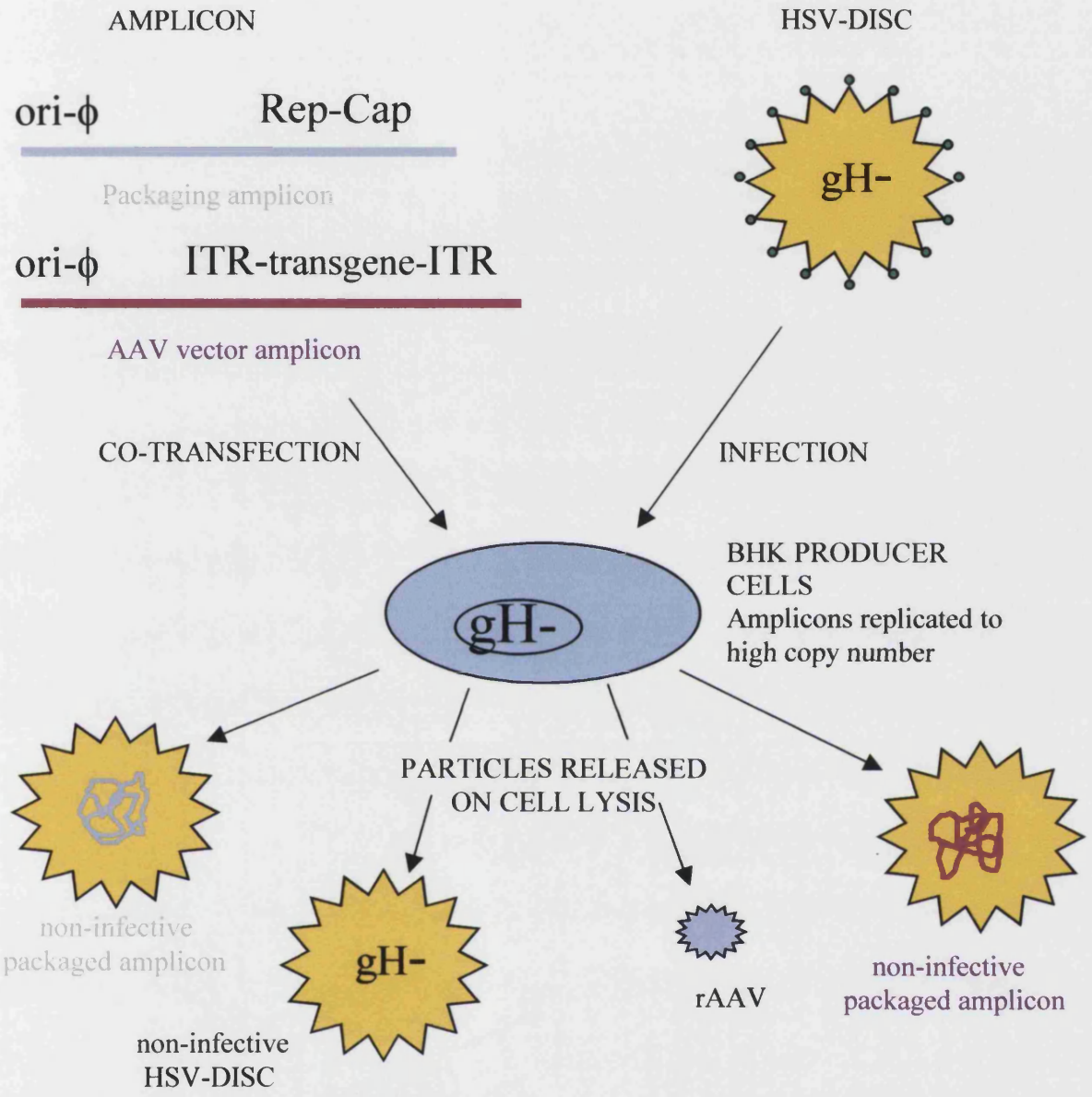

Figure 3.18 Production of high titre rAAV from replicating amplicons and DISC-HSV. The packaging plasmids, containing the *rep* and *cap* sequences, and the rAAV vector plasmids all contain the origin of replication for HSV, ori-ϕ, and are known as amplicons. These amplicons are co-transfected into a BHK producer cell line that is later infected with disabled single-cycle herpes simplex virus (DISC-HSV). This virus is produced in a complementing cell line and is infective. However, the BHK producer cell line is non-complementing and therefore any HSV produced from is non-infective. The DISC-HSV replicates the amplicons to high copy number within the producer cell and performs the helper functions necessary for the production of rAAV. On cell lysis rAAV particles are released, along with several varieties of non-infective HSV particle, that can be purified for use *in vivo*.

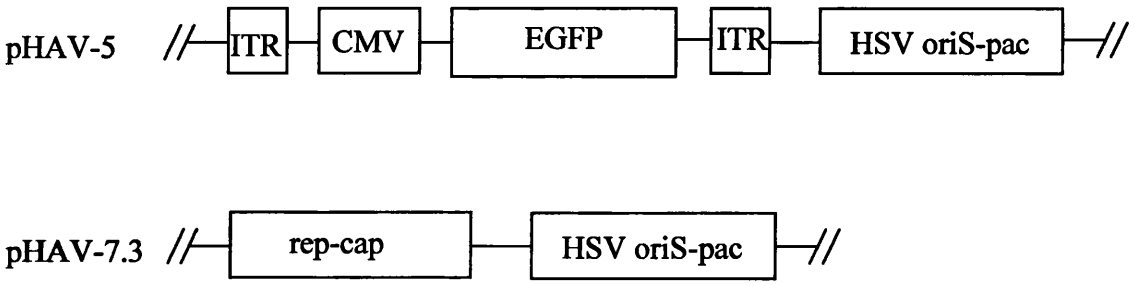

Figure 3.19 Schematic representations of the amplicons, pHAV-5 and pHAV-7.3. HSV amplicons retain the HSV replication origin and packaging signal (represented as HSV oriS-pac). The ITR represents the rAAV inverted terminal repeats; CMV represents the cytomegalovirus immediate-early promoter; and EGFP represents Clontech's *egfp* gene. Figure redrawn from Zhang *et al.* [183].

3.4.2 Cloning of rAAV constructs into the amplicon plasmid, pW7

In order to utilise this new method of producing high titre virus it was necessary to clone the photoreceptor cell-specific rAAV genomes into the amplicon plasmid. The pD-10 plasmid described in section 3.3.1 was engineered to contain two *Pac*I sites outside the viral cassette flanked by the ITRs. These sites were retained through the cloning of the photoreceptor-cell specific constructs (Fig. 3.15). Therefore the final cloning step for pD10RhoEgfp, pD10SPrphEgfp, and pD10LPrphEgfp was digestion with *Pac*I followed by cloning into the unique *Pac*I site within the amplicon plasmid pW7. The resulting colonies were checked by digestion with *Pac*I (data not shown). These plasmids were designated pW7RhoEgfp, pW7SPrphEgfp and pW7LPrphEgfp.

3.4.3 Generation of rAAV

AAV.RHO.EGFP, AAV.SPRPH.EGFP and AAV.LPRPH.EGFP were made using the vector plasmids generated in section 3.4.2 and the helper plasmid pHAV-7.3 discussed in section 3.4.1. For each of these viral preparations a small-scale virus isolate was prepared in parallel using the vector plasmid pHAV-5 (Fig. 3.19). Since this plasmid contains a CMV driven *egfp* gene it produces a visible marker of gene expression within the cell lines used, and therefore provides a control both for the transfection efficiency and the generation of rAAV particles. This is in contrast to the photoreceptor cell-specific *rhodopsin*, and *peripherin-2* promoter fragments that are not active in the producer cell line.

For full details of preparation and purification see section 2.8. To prepare rAAV, BHK cells, which are permissive to HSV infection, were seeded onto twenty, 15 cm dishes (4 x 10^6 cells) 16 hours before transfection so that they were 70-80% confluent on the day of transfection. Cells were then transfected with Lipofectin/Integrin targeting peptide/DNA (LID) complexes. These complexes were made by mixing cyclised integrin targeting peptide 6 ([K^{16}] GACRRETAWACG), plasmid DNA and Lipofectin in a weight ratio 0.75:4:1. The LID transfection complexes improve the transfection efficiency of the BHK cells, increasing the transfection rate to approximately 25% in comparison to the 10-15% achieved with Lipofectamine/DNA complexes [185]. Each dish was routinely transfected with a total of 60 μg of DNA, with the vector amplicon and the packaging amplicon mixed at the ratio 1:3. A single 15 cm dish was transfected with pHAV-5 as the control. After incubation (5 hours) the medium was exchanged for fresh medium containing DISC-HSV at a multiplicity of infection (MOI) of 10. The control dish was assessed for *egfp* expression 16–20 hours after super-infection with the helper virus (Fig. 3.20). The incubation was continued for 32-35 hours post-super-infection. During this period the cells were monitored as the cytopathic effect progressed. At completion of the lytic process, cells were harvested by centrifugation, and lysed by repeated freeze-thaw. The final cell lysate was treated with Benzonase to digest the genomic DNA.

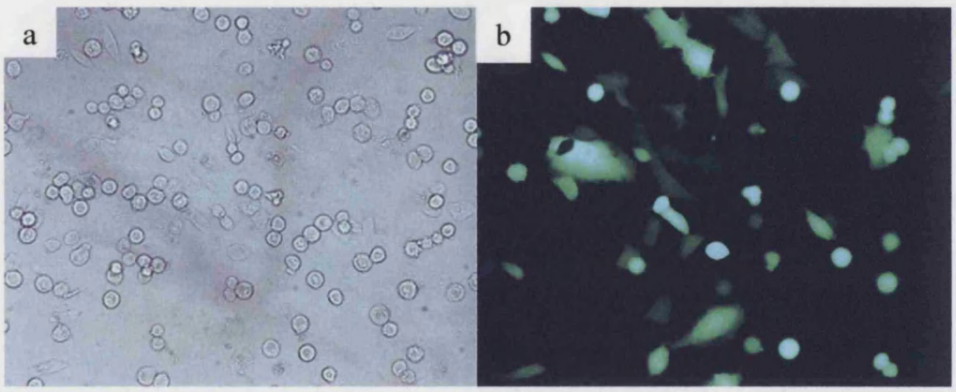

Figure 3.20 BHK cells transfected with the control plasmid pHAV-5, 20 hours after infection with the helper virus, DISC-HSV. Those cells transfected with pHAV-5 were checked for expression of *egfp* to confirm that the transfections had been successful. **(a)** Light image showing cells infected with DISC-HSV undergoing a cytopathic effect and rounding up. **(b)** Fluorescent image of the same area showing the cells successfully transfected with pHAV-5 expressing *egfp* from the CMV promoter.

3.4.4 Purification of rAAV

Recombinant AAV vector stocks were purified through a discontinuous iodixanol gradient (section 2.8.2), as an alternative to multiple CsCl gradients. This method is based on the work of Zolotukhin *et al.* [186] who attempted to reduce the loss of particle infectivity that is often associated with traditional purification procedures. They demonstrated that their strategy of an ionic iodixanol gradient in combination with ion exchange or heparin affinity chromatography resulted in more than 50% recovery of the rAAV from the crude lysate, and consistently produced rAAV with a good particle number to infective particle ratios of less than 100:1. In addition this method is quicker since the virus is centrifuged on the iodixanol gradient for only 1 hour in comparison to the two 48 hour steps on the CsCl gradients. After removal of the virus-containing fraction from the iodixanol column, the solution was passed through filters to remove any large contaminating particles, such as HSV-1 helper.

The next purification step was to pass the virus through a heparin-agarose column (section 2.8.3). Once bound to the column the virus was washed to remove contaminants before elution. For the final stage of the process the virus was concentrated and the buffer exchanged using a protein centrifugal concentrator (section 2.8.4). The purity of the produced virus was confirmed with the transmission electron microscope (section 2.8.5 - Fig. 3.21).

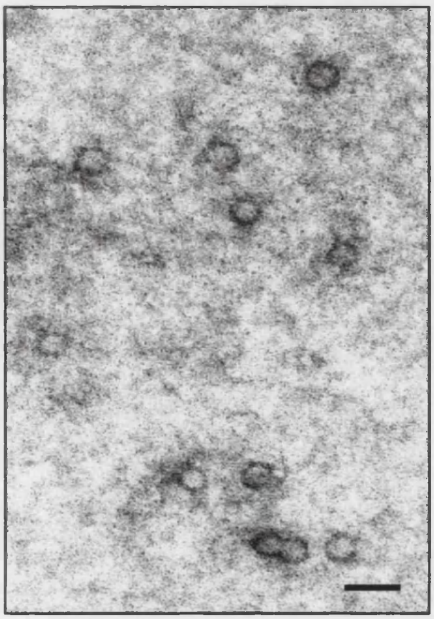

Figure 3.21 Transmission electron microscope image of rAAV particles. Scale bar represents 50 nm.

3.4.5 Titration of rAAV

The viruses were titred by dot-blot hybridisation using a probe encoding the *egfp* gene (section 2.9) (Fig. 3.22). A sample of AAV.CMV.EGFP of known titre was included on the same blot. This virus had been prepared in the same way and titred at $1x10^{10}$ iu/ml, on HeLa cells. Therefore, it could be used to give an estimation of the particle-to-infectivity ratio. From the two blots this control virus was shown to be approximately 10^{12} particles per ml, which, compared to iu/ml titre, gives a particle-to-infectivity ratio of approximately 100:1. This ratio is consistent with those obtained by Zolotukhin *et al.* [186] who developed the method of purification used in section 3.4.4. However, it can only be taken as an approximate figure when applied to other viral preparations. Titres for those viruses carrying photoreceptor cell-specific promoters were calculated by comparing the strength of the hybridisation of the probe to the DNA extracted from 1 µl of virus to the strength of its hybridisation to dots containing a known number of copies of the probe sequence. These titres are then given in the units particles/ml.

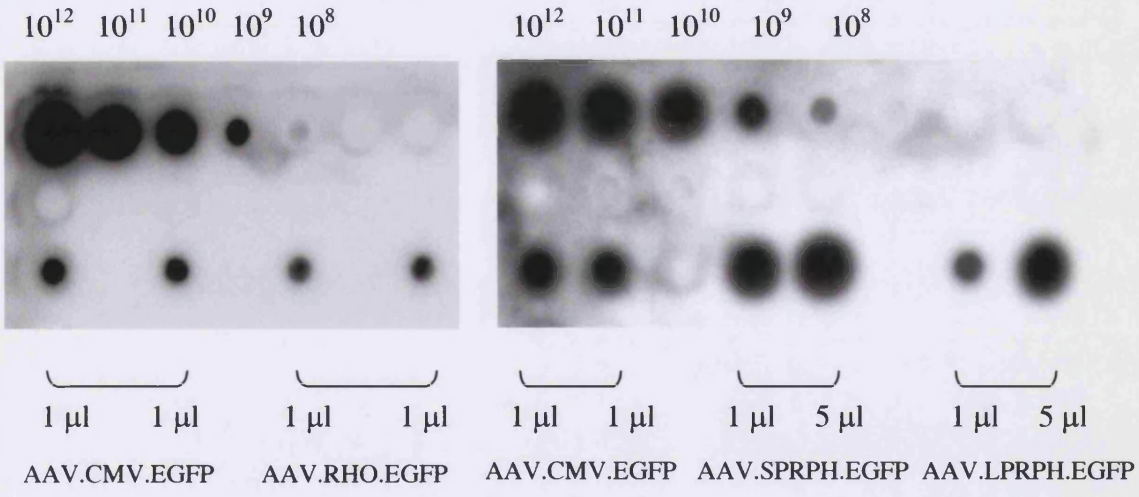

Figure 3.22 Autoradiograms of a dot blot assessing the titre of preparations of AAV.RHO.EGFP, AAV.SPRPH.EGFP and AAV.LPRPH.EGFP. The upper line of dots shows increasing dilutions of the plasmid pD10RhoEgfp starting at 10^{12} molecules. The lower line of dots is the DNA extracted from either 1 µl or 5 µl of the viral preparations. The dots from a preparation of AAV.CMV.EGFP on the left hand side of both autoradiograms are also included as a reference. This virus has been previously titred on HeLa cells at $1x10^{10}$ iu/ml.

Virus type	Particles/ml
AAV.RHO.EGFP	1×10^{12}
AAV.SPRPH.EGFP	1×10^{13}
AAV.LPRPH.EGFP	1×10^{12}

3.5 Discussion

The value of rAAV as a vector for gene delivery to photoreceptor cells has become apparent over the last five years and with protocols advancing rapidly towards the clinic there is a heightened interest in rAAV vector design and production. This chapter describes the cloning of three rAAV constructs, containing photoreceptor cell-specific promoters and incorporating deleted ITRs for increased stability, and the production of high titre rAAV via a novel method.

3.5.1 Inverted terminal repeat elements

The problem of the partial loss of ITRs within the plasmid pTR_{BS}-UF2 is thought to be due to their ability to recombine. This theory is supported by an increase in the retention of *Sma*I sites in clones that are grown within recombination deficient bacterial strains. It has been reported that mutant viruses, that contained deletions within either the left or right terminal repeats, were viable and able to produce AAV virons that contained wild type AAV DNA [187]. Of the four mutants examined that contained deletions in both termini, only one was viable. From this study it was concluded that there is an efficient mechanism for correcting deletions within the AAV termini, with the complete ITR acting as a template for the partially deleted one. However, the precise effect of the partial or complete loss of an ITR on the production of rAAV is not known. Despite the fact that this plasmid has been successfully used to create AAV.CMV.GFP in past experiments [128, 186], it has been found by our group that use of pTR_{BS}-UF2 in the manufacture of rAAV produces virus of inferior titre (unpublished data). In order to overcome the problem of the ITR instability alternative vector plasmids were produced using the D sequence deleted ITRs. The *Sma*I sites within these ITRs remained through all of the cloning steps in the generation of the rAAV constructs. Since high titre rAAV was prepared using vector plasmids with these ITRs it was concluded that they are capable of supporting efficient rescue, replication and packaging of the rAAV genome

as reported by Wang *et al.* [179]. A second advantage of the deleted ITRs is a possible reduction in the number of wild type AAV-like particles that are generated during recombinant viral vector production. Studies have shown that in conventional production of rAAV these contaminating particles are the result of recombination events between the AAV ITRs in the vector plasmid and AAV sequences within the helper plasmid [180]. All of these recombination events in the particles examined involved the AAV D sequence distal to the viral hairpin structure. This study also showed that the use of rAAV vector plasmids lacking these nucleotides helped in the complete elimination of wild type particles from rAAV stocks [180]. However, while the exact function of the D sequence is still unknown it is possible that the removal of the 10 nucleotides distal to the hairpin structure may have an effect on another function of the ITR, such as genomic integration.

3.5.2 Production of photoreceptor cell-specific constructs

Two regions of the *Prph2* promoter have been isolated and cloned upstream of the reporter gene *egfp* in rAAV constructs. A third construct has been made that incorporates a previously studied section of the bovine *rhodopsin* promoter driving the *egfp* reporter gene. The longer section of the upstream region of the *Prph2* gene was shown to be different from the Entrez published clone, accession number L42167, upstream of position –1442 (relative to the start of translation). However, it was possible to amplify the longer section from mouse genomic DNA, suggesting that it was the sequence of L42167 that was incorrect. NIX analysis showed that the long *Prph2* promoter sequence contained a SINE/B2 repeat sequence directly upstream of position –1442 that may have facilitated a recombination event, resulting in the L42167 clone. Further clarification of the promoter sequence would require the screening of a cosmid library with a probe from exon one of the mouse *Prph2* gene and sequencing upstream of the first exon.

3.5.3 Production of rAAV

The conventional method of production for rAAV as described in section 3.1.2 is now seen as relatively inefficient and efforts to increase production have focused around two areas: ways of bypassing the need for co-transfection of the vector and packaging plasmids, and methods of increasing the replication and expression of AAV *rep* and *cap* gene products within the producer cell line. The method described in this chapter

addresses the latter point by utilising herpes-derived amplicons to support the replication of both the packaging plasmid and the vector plasmid, in combination with a DISC-HSV as the helper virus. This strategy has been shown to increase the number of transducing rAAV particles recovered from the producer cell line, an increase that is attributed in part to the enhanced level of production of Rep and Cap proteins in the presence of DISC-HSV [183]. This method has been used to produce three, high-titre rAAVs for expression of *egfp* in the retina after sub-retinal injection.

The DISC-HSV method still requires the co-transfection of plasmids. In contrast a method has been developed by Inoue and Russell [188] that achieves inducible amplification of chromosomally integrated vector and packaging sequences by incorporation at these sites of the SV40 origin without the need for co-transfection. These sequences can then be amplified by expression of SV40 T antigen under the control of a reverse tetracycline trans-activator [189]. While this method has the advantage of a stable packaging cell line, removing the need for transient transfection, recovered titres of rAAV are still at least tenfold lower than those obtained using herpes amplicons. As a result the method used in this chapter is currently our method of choice, but its dependence on co-transfection is an obvious area for improvement. The success of rAAV as a vector has meant that many gene therapy trials are being extended to larger animals. These will require a much greater amount of virus, as will clinical trials, and currently methods of production are time consuming. The future success of rAAV vectors is therefore largely dependent on continued efforts to understand and advance production methods.

Aknowledgements

I would like to thank Sascha Fauser for his help with cloning, Mahesh de Alwis for his help with virus production and Peter Munro for electron microscopy.

4

Adeno-associated virus-mediated gene expression in the retina

The experiments described in this chapter were designed to examine the following:

- The use of *egfp* as a reporter gene to follow gene expression within the eye,
- The temporal and spatial pattern of expression of a reporter gene driven by a CMV promoter after sub-retinal injection of rAAV,
- The effect of viral titre on the number and type of cells transduced and,
- The expression pattern from the rAAVs, produced in Chapter 3, which carry photoreceptor cell specific promoters, in both normal and *Prph2*$^{Rd2/Rd2}$ mice.

The results of these experiments should make it possible to assess the potential of rAAV, in combination with these promoters, to produce the expression required for treatment of the *Prph2*$^{Rd2/Rd2}$ mouse.

4.1 Introduction

As *in vivo* studies in the eye using rAAV have progressed quickly there have been major advances in vector and reporter gene technology. As a result, publications from different groups on reporter gene expression after delivery with a rAAV vector are hard to compare, and the literature presents a rather confused picture. For the treatment of many diseases a therapeutic effect will only result from a specific temporal and spatial pattern of gene expression. Expression from a delivered gene is dependent on several factors that are related to the type of viral vector used, as well as the promoter chosen to drive transgene expression. Therefore, a clear understanding of these factors is

important in assessing the potential of rAAV in the treatment of inherited retinal disease.

4.1.1 Cell types transduced after sub-retinal injection of rAAV

After sub-retinal injection the rAAV is directly in contact with only PR cells and the RPE. Early studies with rAAV carrying the reporter gene *β-galactosidase*, driven by a CMV promoter (AAV.CMV.LacZ) in albino mice, showed consistent transduction of a large area of RPE, but relatively few photoreceptor cells [109, 190]. Simultaneously, Flannery *et al.* [128] performed a similar study, following *gfp* expression in albino rats from a construct driven by a proximal murine rod *opsin* promoter (AAV.mOp.GFP). They reported GFP fluorescence extending over 10-20% of the retina, with almost all of the PR cells being fluorescent in the area immediately surrounding the site of injection. The higher number of transgene expressing PR cells was attributed to the use of a *rhodopsin* promoter instead of a CMV promoter, although the latter is known to be active within PR cells [191]. Studies using an HIV lentiviral vector have also shown *egfp* expression in PR cells to be more efficient with a *rhodopsin* promoter than with a CMV promoter [113]. However, Flannery *et al.* did not directly compare the transduction rates gained with AAV.mOp.GFP, with an AAV.CMV.GFP virus. While the virus they used was at a titre of 4.6×10^9 iu/ml and contained the reporter gene for GFP, the rAAV injected in the initial study by Ali *et al.* [109] was 1×10^7 iu/ml and contained the reporter gene *β-galactosidase*. More recent work with AAV.CMV.EGFP in mice [111], dogs [192] and primates [112], all demonstrated substantial transduction of PR cells using rAAV at titres of around 1×10^9 iu/ml. Although these results suggest that titre plays a significant part in the ability of rAAV to transduce PR cells there are still results that indicate otherwise. Rolling *et al.* [193] have performed sub-retinal injections with rAAV of a similar titre in rats and they report no transduction of neuroretina in 8 out of 10 rat retinas.

Another issue yet to be properly examined is the transduction of cones. The most convincing evidence to date that cones are not infected by rAAV is the lack of EGFP-positive cone cells found after injection of AAV.CMV.EGFP into non-human primates [112]. The monkey is a good model in which to study this feature of rAAV since its retina contains a fovea, similar to that found in humans, where there are a high percentage of cone photoreceptors. In contrast, the retina of a normal mouse contains

approximately 97% rods and only 3% cones [194, 195] and therefore it is harder to be sure that transduced cones have not simply been overlooked.

4.1.2 Temporal expression patterns of reporter genes after sub-retinal injection of rAAV

The onset of AAV-mediated transgene expression has a characteristic time lag in many tissues (see section 1.4.5) and has also been demonstrated in PR cells and the RPE [110]. As in other tissues, this time lag has been shown to be reduced in mice by the administration of DNA-damaging agents [196]. Normal onset of expression is apparent in mice from about 1-3 weeks after injection and in dogs from 2-4 weeks [192]. In contrast, expression in primate retinas took between 8-18 weeks in four animals studied [112]. The reason for this difference between species is not known but it has been speculated that it may relate to conditions in the cell affecting the conversion of single stranded to double stranded DNA [192]. Primate, dog and mouse studies have all shown long-term stable expression of *egfp* in the retina. However, there is little data on the increase of expression over time, the spread of transduction away from the area of detachment and the percentage of photoreceptor cells transduced.

4.1.3 Promoter effects on reporter gene expression

The promoter chosen to drive transgene expression obviously has an important role to play in the location, strength and duration of expression. Many rAAV studies in a wide variety of tissues have utilised the CMV promoter. This promoter has been shown to be active in many tissues. Whilst in some tissues, such as muscle, this promoter has remained active for more than a year [67], it has also been shown to be down regulated in different areas of the brain, including the hippocampus [197]. This phenomenon has been attributed to either hyper-methylation or lack of endogenous activating transcription factors [197]. Further studies in the brains of rats compared rAAV carrying the CMV promoter with rAAV, of the same titre, carrying a neuron-specific promoter [198]. The rAAV vectors containing the neuron-specific promoter appeared to transduce significantly more neurons than those vectors carrying the CMV promoter. Moreover, the incorporation of an additional element, the woodchuck hepatitis virus post-transcriptional regulatory element (WPRE), further increased the number of transgene expressing neurons by approximately two-fold. These results highlight the role of the promoter in visualising all of the cells transduced by rAAV and demonstrate the

possibility of reducing viral titre while maintaining the levels of transgene expression. These results also support the suggestion by Flannery *et al.* [128] that the *rhodopsin* promoter may be more active than the CMV promoter in photoreceptor cells. However, the levels of rhodopsin within the rod photoreceptor cells and the constant turnover of the outer segments indicate that there should be high levels of transcription from this promoter. This has been confirmed by transgenic studies [177]. If the amount of a protein is taken as an indication of the activity of its promoter, then the activity of the *peripherin-2* promoter could be expected to be lower than that of the *rhodopsin* promoter, since peripherin-2 is only present in the rims of the outer segment discs, whereas rhodopsin is distributed throughout the whole disc membrane. However, the *peripherin-2* promoter fragments described in Chapter 3 should be active within both the rod and cone PR cells, whereas the *rhodopsin* promoter should only be active in rods.

4.1.4 Transduction and expression within the *Prph2*$^{Rd2/Rd2}$ mouse

As discussed in the introduction (section 1.6.1) the *Prph2*$^{Rd2/Rd2}$ mouse is a good model in which to test gene therapy since the degeneration of photoreceptor cells is slower than that of the *rd* mouse. However, even in the *Prph2*$^{Rd2/Rd2}$ mouse degeneration begins early, with the peak of apoptosis of photoreceptor cells occurring around post-natal day 14 (P14). This factor, in combination with the relatively slow onset of expression from rAAV vectors, requires that the delivery of rAAV be performed as soon after birth as possible. Sub-retinal injection into a mouse pup eye is very difficult and therefore the need for early injection must be weighed against the success rate. Grant *et al.* [190] have compared gene transfer in normal and homozygous *Prph2*$^{Rd2/Rd2}$ mice and noted that gene transfer to photoreceptor cells was enhanced in mice with retinal degeneration. It was suggested that this was due to the lack of outer segments, which may allow better access of the rAAV to the inner segments. An increase in the number of rAAV genomes per cell may also have an effect on the time of onset of gene expression.

The treatment of the *Prph2*$^{Rd2/Rd2}$ mouse will obviously require photoreceptor cell-specific expression, and the experiments in this chapter will examine the potential of the *rhodopsin* promoter and the *peripherin-2* promoter for achieving this aim. Although the *peripherin-2* promoter has yet to be studied in detail, the *rhodopsin* promoter has been extensively analysed. *Rhodopsin* mRNA levels, and rhodopsin rates of synthesis and

localisation have been studied by Nir *et al.* [199] throughout the degeneration of photoreceptor cells in the retina of the *Prph2*$^{Rd2/Rd2}$ mouse. While they were able to detect *rhodopsin* mRNA in *Prph2*$^{Rd2/Rd2}$ retina up to P210, rhodopsin synthesis could be demonstrated in these mice only up to 90 days of age. It was suggested that the absence of rhodopsin synthesis in older retinas might be due to translational down-regulation or some defect in the capacity to synthesise rhodopsin, rather than inactivation of the *rhodopsin* promoter.

4.1.5 Following reporter gene expression *in vivo*

Until recently, *lacZ*, the bacterial *β-galactosidase* gene, has been the marker of choice for many studies of gene expression in mice, including those in the field of gene therapy. Over the past six years there has been a shift in interest towards green fluorescent proteins, novel autofluorescent genetic reporters derived from the bioluminescent jellyfish. GFP is now widely used as a reporter of gene expression, tracer of cell lineage and as a fusion tag to monitor protein localisation within living cells. When expressed in either eukaryotic or prokaryotic cells and illuminated with blue or UV light, GFP emits a bright green fluorescence. It does not require any cofactors, substrates or additional gene products from *A.victoria* or the host and, therefore, is species independent. In addition the *gfp* gene is relatively small. GFP is easily detectable in fixed samples but its real advantage lies in the fact that visualisation is non-invasive and therefore it is possible to observe its presence *in vivo*. This presents a unique opportunity in the context of the eye. The human fundus is routinely observed in the clinic using ophthalmoscopes. These techniques have been extended to the observation of the mouse fundus, allowing the study of both the temporal and spatial pattern of expression in the eye after injection of rAAV. The advantage of this type of study is that it requires far fewer animals than one that utilises a histological approach, and there is even the potential for quantification of GFP.

The *gfp* gene has been engineered to form *enhanced gfp* (*egfp*) (as described in section 3.3.3). The EGFP protein is a red-shifted variant of wild type GFP; its major excitation peak is approximately 490 nm encompassing the excitation wavelengths of commonly used filter sets. There are two pieces of equipment available for the observation of the mouse fundus with this wavelength of fluorescent light, a confocal laser scanning ophthalmoscope (cLSO), and a small animal fundus camera (SAC). A prototype Zeiss

cLSO is routinely used within The Institute of Ophthalmology to study the fundus autofluorescence associated with retinal disease [200]. Fluorescent images are generated by illuminating the fundus with an argon laser line (which produces light at a wavelength of 488 nm), and are then recorded onto an SVHS videotape recorder. Alternatively, as the EGFP has similar absorption-emission characteristics as fluorescein, the techniques of indirect ophthalmoscopic examination and photography used in fluorescein angiography studies can also be applied. Some studies have used a human fundus camera in conjunction with a condensing lens to assess EGFP in the retina of treated mice [110] and rats [193]. More recently, however, Hawes *et al.* [201] have documented the use of a Kowa Genesis SAC (Tokyo, Japan) that has been specifically designed to meet the special needs for photographing small eyes, the mouse eye being only 3 mm in diameter. The group compared the Genesis SAC to both a Nikon photo slit lamp and a Kowa RC-2 human fundus camera and described the SAC as providing the best fundus images. In their studies the SAC camera was used to document the ocular abnormalities in several mutant mouse strains as well as abnormal vascular leakage by fluorescein angiography. We have produced a similar set-up to this using an external condensing lens, mounted 5 cm below the camera.

4.2 Non-invasive *in vivo* monitoring of rAAV-mediated *egfp* expression

4.2.1 Method

In order to analyse the potential for the SAC and the cLSO in monitoring the expression of EGFP in the retina, sub-retinal injections and intra-vitreal injections (section 2.10.3) were performed in adult C57Bl/6 mice (section 2.10.1). Two microlitres of AAV.CMV.EGFP (5×10^9 iu/ml) was injected. At several time points after injection mice were anaesthetised and their pupils dilated (section 2.10.2), and the fundus observed using either the cLSO (section 2.10.5) or the SAC (section 2.10.4). After observation over a period of eight weeks the mice were sacrificed and their eyes processed (section 2.11.1) for histological examination of EGFP (section 2.11.2).

The cLSO and SAC set-ups (Fig. 4.1) had not been used previously in this laboratory and therefore it was necessary to develop methods for their use. For observation, using either the cLSO or the SAC, the mouse was hand held and the eye gently proptosed. The use of a rubber sleeve to proptose the eye (as used for sub-retinal injections see section 2.10.3) resulted in corneal clouding and loss of a fundus image and so was not used for this procedure. The cLSO set-up (Fig. 4.1a) included a platform on which to rest the mouse and focusing was achieved by moving the cLSO unit backwards and forwards. The cLSO could also be moved from side to side to study different parts of the retina. However, this movement was quite limited and the position and angle of the mouse were also changed in order to obtain images of more peripheral areas of the retina. This method of observation required two people and the simultaneous view of the images being recorded on video allowed a real-time assessment of the image quality. In contrast there was no hand-rest with the SAC (Fig. 4.1 b and c) and focusing was primarily achieved by altering the position and angle of the mouse. Video imaging was not available with this set-up so fundus images were captured on film and therefore there was less quality control as the film then had to be processed before images could be assessed. However, one person could manage this set-up, with the use of a foot pedal to operate the shutter button.

4.2.2 Assessment of the potential of both methods

It was possible to detect EGFP within the retina using either the cLSO or the SAC. The cLSO images were acquired in a 40° field of view and therefore only show a relatively small area of the fundus. However, a number of pictures could be aligned into a collage to give an impression of a large central area (Fig. 4.2a, b and c). Pictures of the peripheral retina were harder to align. Preliminary images showed good detail of the fluorescence pattern and the ability to focus on fluorescence from both the inner (Fig. 4.2d) and outer retinal layers (Fig. 4.2a and c). The quality of the cLSO images, however, was undoubtedly affected by changes in the cLSO set-up that was also being used for other unrelated experiments. In comparison, the wider field of view with the SAC gave a much better overall picture of the retina (Fig. 4.2 e and f) although careful rotation of the animal was required to gain clear pictures of peripheral areas. In all cases the site of sub-retinal injection could be identified as a small area of scarring on the periphery of the retina.

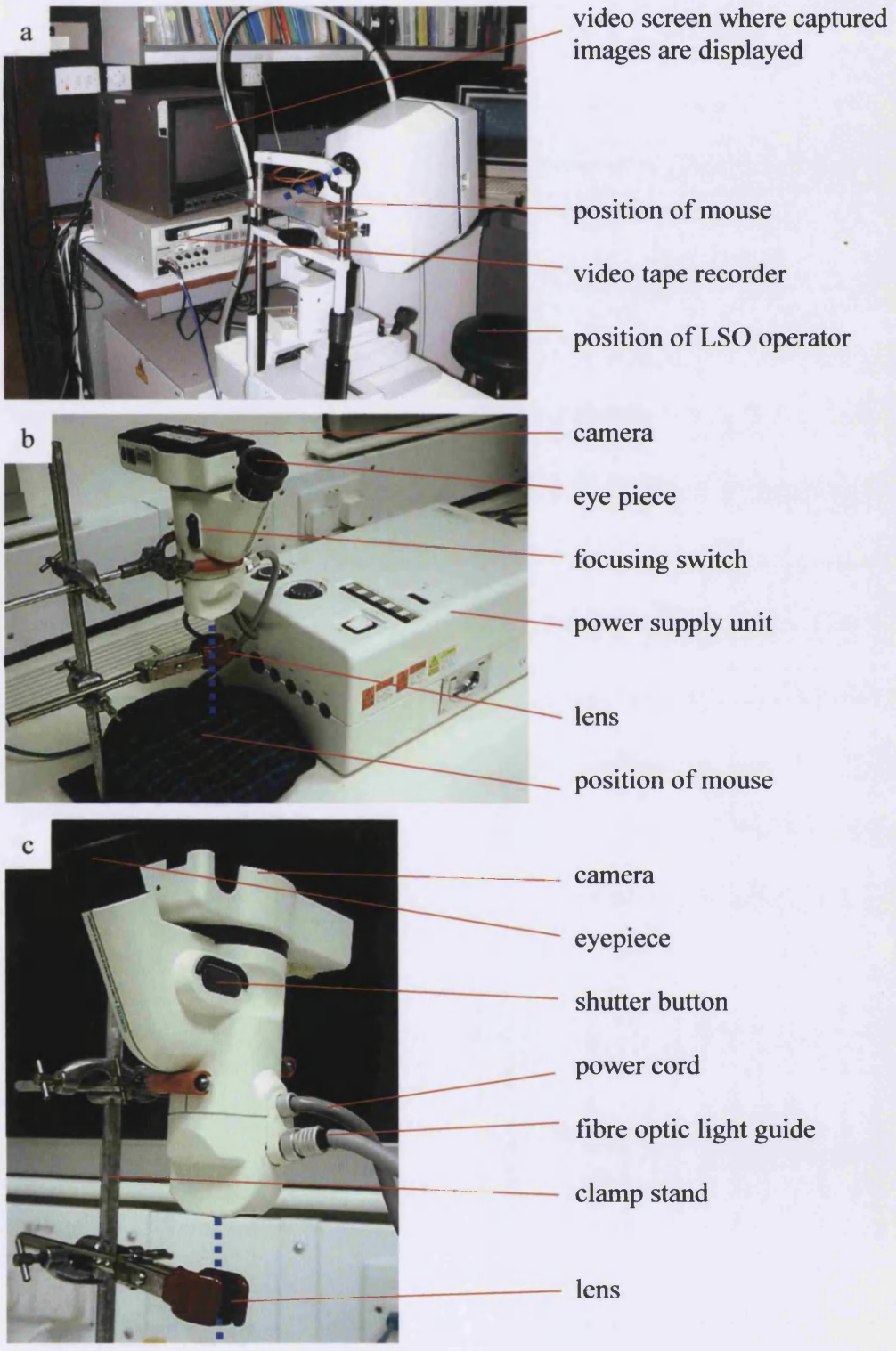

Figure 4.1 The set-up of the cLSO (a) and the SAC (b and c) for the recording of *in vivo* fundus images. The excitation beam of light is shown for each set-up as a dotted blue line.

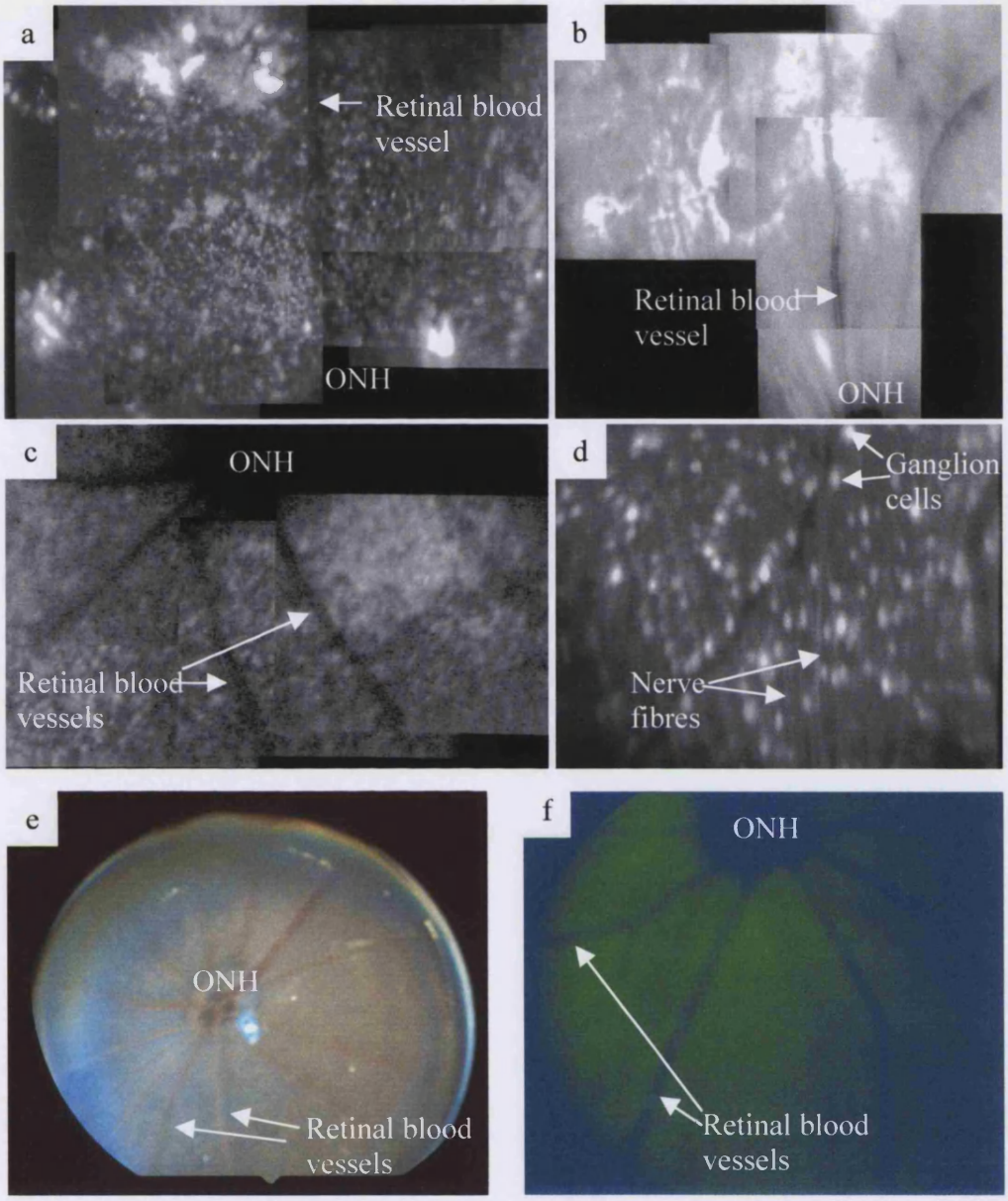

Figure 4.2 Assessment of the potential of the cLSO and the SAC for the detection of EGFP in the retina. *In vivo* images of the mouse fundus obtained approximately 8 weeks after sub-retinal (**a-c**, **e** and **f**) or intra-vitreal (**d**) injection. Images from the cLSO are shown in **a-d**. Images from the SAC are shown in **e** and **f**. Collage of fluorescent images from the injected portion of the retina (**a**), with the corresponding reflectance image (**b**). Collage of fluorescent images from the uninjected portion of the retina (**c**). The fluorescence from the inner nuclear layer (**d**) after intra-vitreal injection, shows EGFP positive nerve fibres and ganglion cell bodies. Light image (**e**) and fluorescent image (**f**) of fundi through the SAC; ONH = optic nerve head.

The strength of fluorescence was observed to increase over eight weeks starting at a very low level. The cLSO set-up was sensitive, detecting and recording these early low levels of fluorescence. Fluorescence resulting from the intra-vitreal injections was first detected one week after injection. In comparison, fluorescence was not detectable with the SAC until two weeks after injection. Even when inner retinal fluorescence was faintly visible with a 'starry sky' appearance through the eyepiece, images were hard to record. The image quality varied between time points and was influenced by corneal clouding, particularly if the gap between anaesthetising the mouse and observing the fundus was longer than 10-15 minutes.

Both methods provided useful ways of looking at the mouse fundus and studying the onset of gene expression. However, they do not provide an easy method by which to quantify fluorescence, or to localise the fluorescence to a specific retinal layer, and the amount of light entering the eye is hard to control.

4.2.3 Correlation with histological sections

Cryosections of the eyes examined with the SAC and the cLSO showed that after sub-retinal injection, the EGFP was located in both the RPE and PR cells with most of the fluorescence coming from the latter (Fig. 4.3a and b). Within the PR cells the EGFP appears to be primarily located in the inner segments and the cell bodies. In the RPE the EGFP is visible in the nucleus and around the areas of pigmentation. In all the sections studied the EGFP positive PR cells were spread evenly through the full thickness of the outer nuclear layer. After intra-vitreal injection EGFP is primarily located in the ganglion cells and nerve fibres of the inner retinal layers although transduced inner retinal nuclei and PR cells can also be seen (Fig. 4.3c and d). The technique of intra-vitreal injection is important as a slight perforation of the retina can result in rAAV in the sub-retinal space and efficient transduction of the PR cells (Fig. 4.3c).

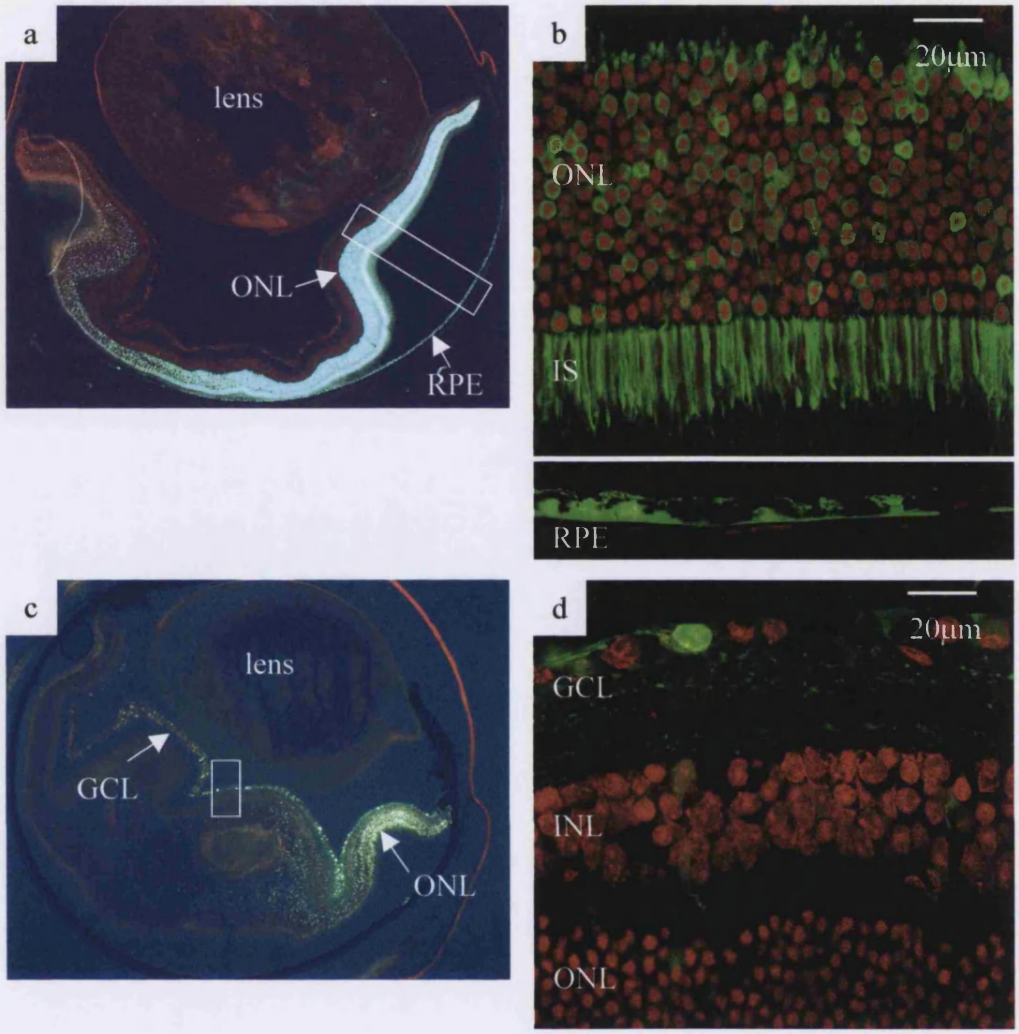

Figure 4.3 Location of EGFP after sub-retinal and intra-vitreal injection of AAV.CMV.EGFP. After sub-retinal injection EGFP fluorescence is visible at low power in the outer nuclear layer and the RPE (**a**). At high power magnification the EGFP can be seen to be localised primarily within the inner segments and cell bodies of the photoreceptor cells, while within the RPE, EGFP fluoresces around the areas of pigmentation (**b**). After intra-vitreal injection fluorescence is seen in the ganglion cell layer, although there is some localised fluorescence in the outer nuclear layer where the injection has perforated the retina (**c**). At high power magnification, away from the localised detachment, there is strong EGFP fluorescence in the ganglion cells and the nerve fibres but also faint fluorescence from a few cells in the inner and outer nuclear layers (**d**). Sections are counterstained with propidium iodide to show the cell nuclei (red). The regions selected for high magnification (**b** and **d**) are shown in white boxes on the lower power images (**a** and **c**). ONL = outer nuclear layer; INL = inner nuclear layer; RPE = retinal pigment epithelium; IS = inner segments; and GCL = ganglion cell layer

4.3 Identification of pattern of expression of *egfp* after sub-retinal injection

4.3.1 Method

To examine cell transduction after sub-retinal delivery of high titre rAAV, sub-retinal injections (section 2.10.3) were performed in the right eye of 14 normal adult C57Bl/6 mice (section 2.10.1). A volume of 2 µl of AAV.CMV.EGFP at a titre of 5 x 10^9 iu/ml (i.e. approximately 10^7 infectious particles) was injected into the sub-retinal space. Several of the mice were observed over the time course with the SAC and the cLSO (section 4.2). Two mice were sacrificed at each time point - 3, 7, 28, 64, 120, 180 and 360 days after injection - and the eye's orientation marked with a temporal stitch. After enucleation the eyes were fixed and cryoprotected for frozen sectioning (section 2.11.1).

In order to examine the spread of transduction through the retina over time in more detail each eye was serially sectioned at 25 µm with sections taken every 350 µm for observation of EGFP fluorescence (section 2.11.2). Approximately six points, evenly spaced around the length of the retina in each section (Fig. 4.4a), were selected. At each of these points the percentage of positive photoreceptor cells was calculated and RPE fluorescence scored. Percentages were calculated by capturing an image at a x 63 magnification (Fig. 4.4a) and counting the number of photoreceptor cell nuclei and the number of EGFP positive PR cells within a 100 µm square. The extent of RPE fluorescence was graded numerically from 0 to 3 (Fig. 4.4b):

0 = no detectable fluorescence

1 = isolated positive cells

2 = several positive cells together

3 = continuous positive cells

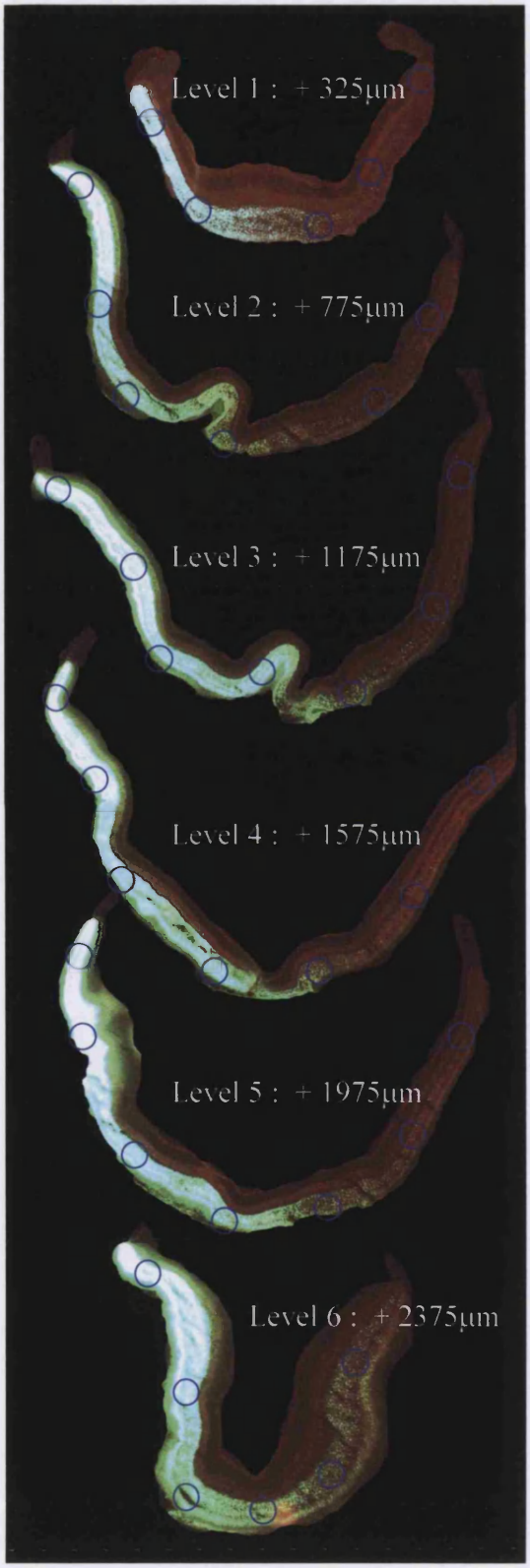

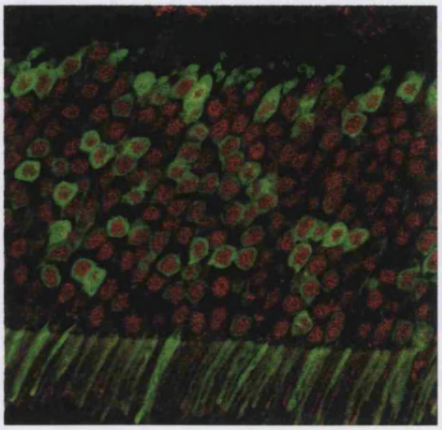

Figure 4.4a Method used for calculating the spread of photoreceptor cell transduction. Eyes were serially sectioned and six sections evaluated per eye (shown to the left). Five to seven areas – as represented by purple circles – were selected, evenly spaced along the horizontal extension of the retina in each section. A confocal image (shown above) was captured in each of these areas. The numbers of photoreceptor cell nuclei (red, propidium iodide counterstain) and the numbers of EGFP-positive cells (green) were counted. The image above shows an area of the retina where the transduction rate is around 45%.

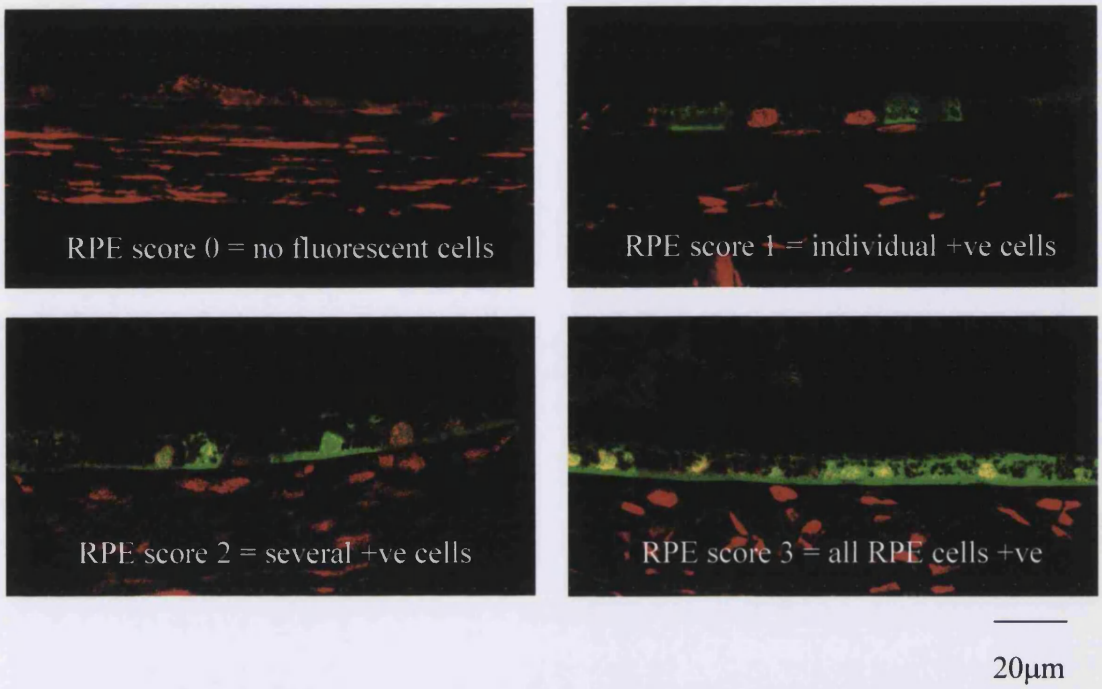

Figure 4.4b Method used for the scoring of RPE transduction. The section of RPE adjacent to each area of retina captured (Fig. 4.4a) was scored numerically from 0 to 3, with increasing intensity and spread of EGFP fluorescence.

4.3.2 Results

In vivo observation of the mice with the SAC and cLSO on a weekly basis after injection revealed that EGFP could be detected at one week after sub-retinal injection with the cLSO, although only very faintly and in a region adjacent to a retinal scar which was taken to be the site of injection (Fig. 4.5a and b). In a separate eye the fluorescence was observed to increase from week to week, although it always remained strongest in the region of sub-retinal detachment (Fig. 4.5c, d and e). By nine weeks after injection EGFP fluorescence can clearly be seen in more than two thirds of the retina and covers the total area captured by the SAC (Fig. 4.5f). A year after injection the levels of fluorescence are so strong that a light SAC photograph of the fundus has a green tinge and the whole mouse eye appears to fluoresce (Fig. 4.5g and h).

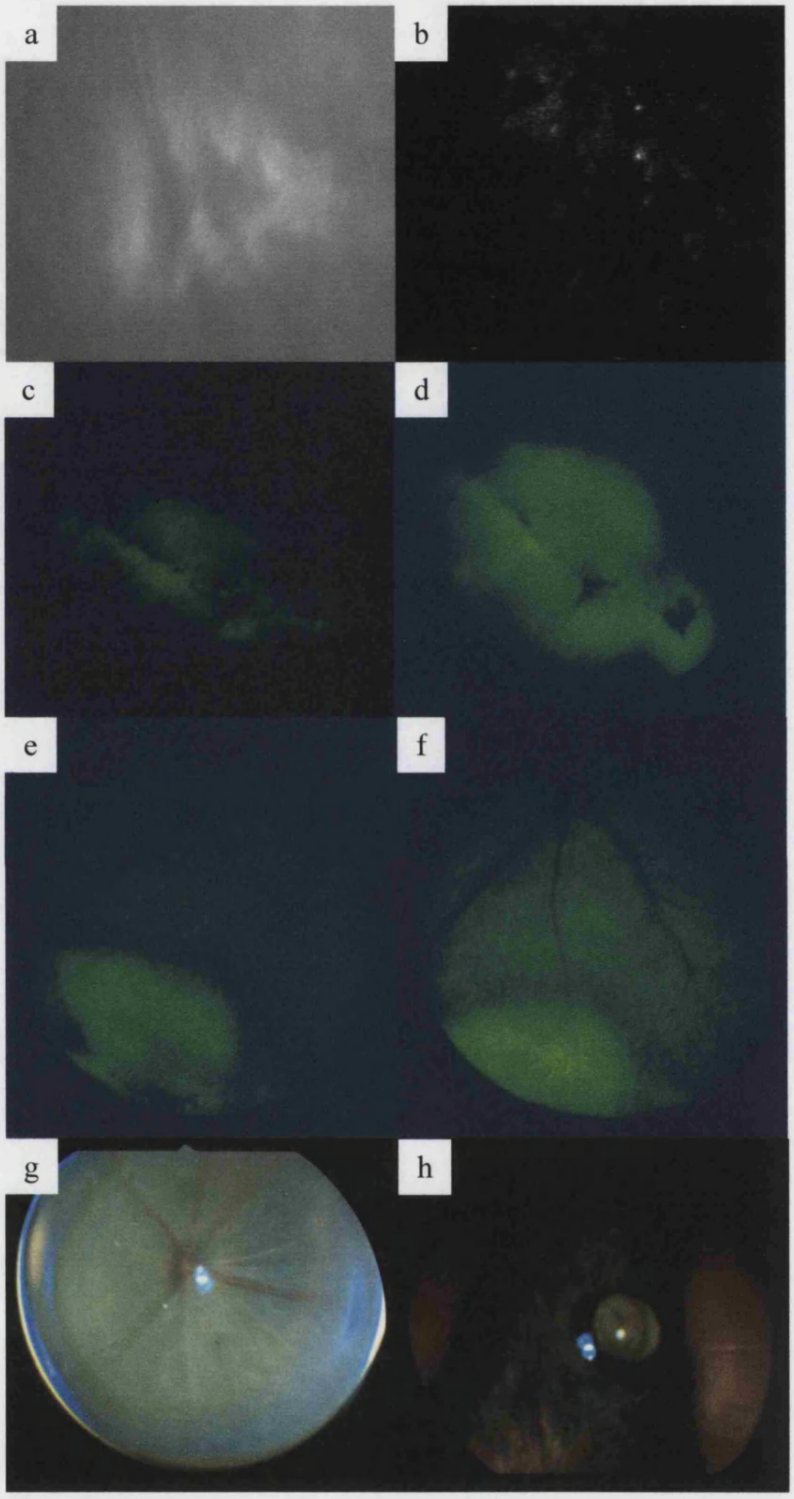

Figure 4.5 *In vivo* images of increasing EGFP fluorescence in mouse eyes over time after sub-retinal injection of AAV.CMV.EGFP. A reflectance image from the cLSO (**a**) shows the retinal scar from the injection and (**b**) the first area to demonstrate fluorescence one week after injection. Fluorescent images from one eye taken with the SAC, 3 weeks (**c**), or 9 weeks (**d, e** and **f**) after injection. The intensity of fluorescence increases over time (**c** and **d**), and is particularly strong in the area surrounding the point of injection (**e**). By 9 weeks post-injection the fluorescence has spread away from the area of detachment (**f**). At one year after injection the fundus appears green under white light (**g**) and the mouse's eye visibly glows green (**h**).

The histological data supports the findings with the cLSO and SAC (Fig. 4.6 and Fig. 4.7). Fluorescent PR cells were visible as early as 3 days after injection (Fig. 4.6), although the RPE was not recorded as positive until one week after injection. This may be due to the pigmentation masking the early stages of *egfp* expression as by 7 days the RPE was strongly positive (Fig. 4.7a). The highest percentages of positive PR cells, counted in the areas of strongest expression, increased rapidly over the first 64 days to approximately 80-90% and then levelled off. This high percentage of transduced cells was maintained up to a year. Strong RPE fluorescence was also maintained, and there are still areas of RPE that are scored as a 3 after one year. RPE fluorescence was sometimes hard to score particularly on sections where the fluorescence from the PR cells was strong. In these areas it was impossible to capture one image containing both positive PR cells and RPE since the scan settings required to prevent bleaching of the EGFP fluorescence are too low to capture fluorescence from the RPE (Fig. 4.7 b and d). It was also impossible to tell whether EGFP in the RPE had come from the PR cells through the natural process of disc shedding and RPE phagocytosis, although the lack of EGFP in the outer segments, even in strongly positive areas of the ONL, suggests that EGFP is turned over within the PR cells themselves. In some areas the intensity of fluorescence in the PR cells appeared to correlate well with that in the RPE with high percentages of transduction of the PR cells adjacent to areas where the RPE is strongly positive (Fig. 4.7b), while areas of lower percentages are adjacent to fainter RPE fluorescence (Fig. 4.7c). However, there are also many areas where there is no correlation between the two (Fig. 4.7d).

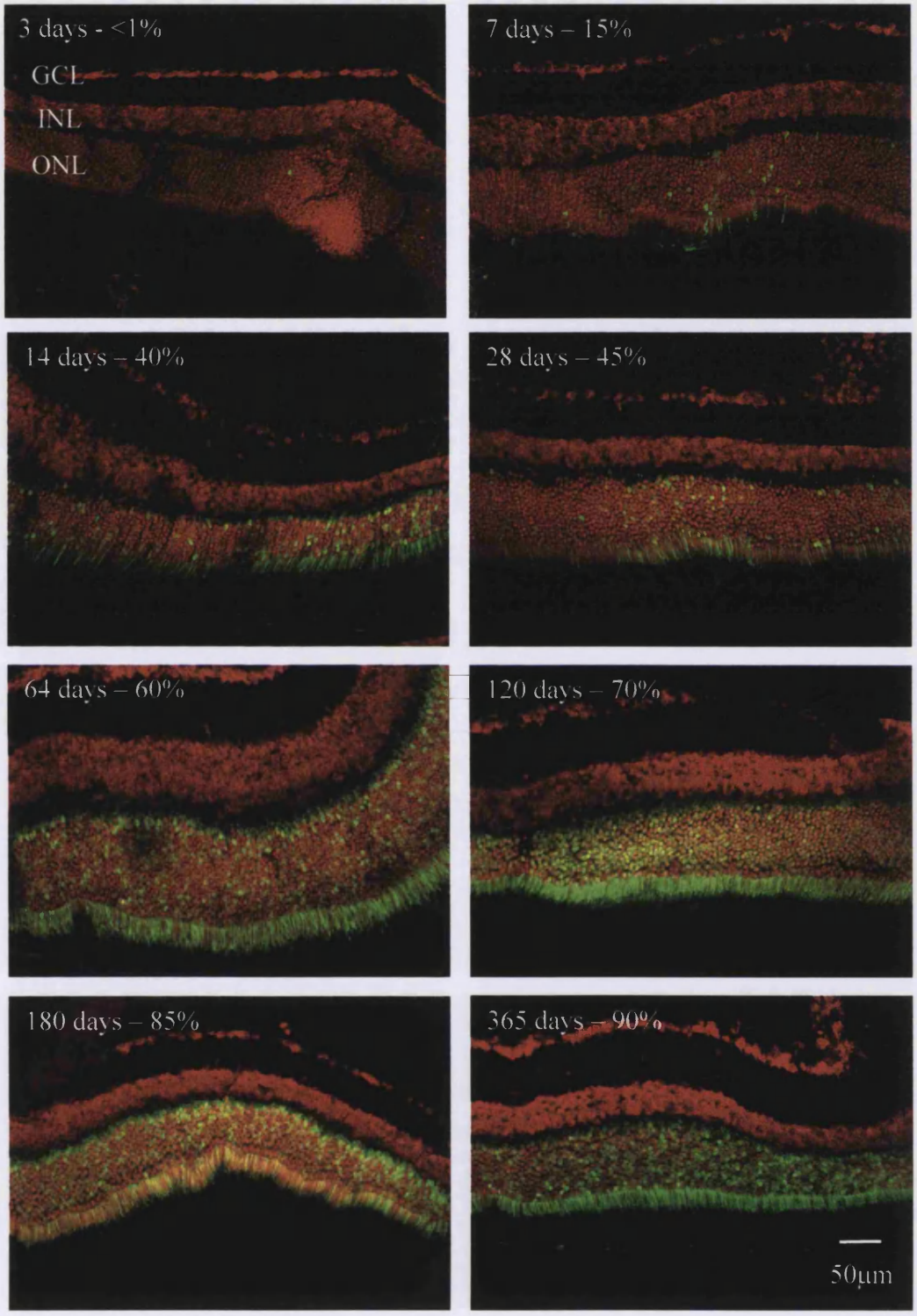

Figure 4.6 Increasing numbers of EGFP-positive photoreceptor cells in wild type mouse retina following sub-retinal injection of AAV.CMV.EGFP (titre 5 x 10^8 iu/ml). Representative confocal images were selected from the regions of the retina with the highest percentages of photoreceptor cell transduction at 3 to 365 days post-injection. Propidium iodide nuclear counterstain (red). The percentage transduction rate is indicated at each time point. Retinal layers: GCL = ganglion cell layer; INL = inner nuclear layer; and ONL = outer nuclear layer.

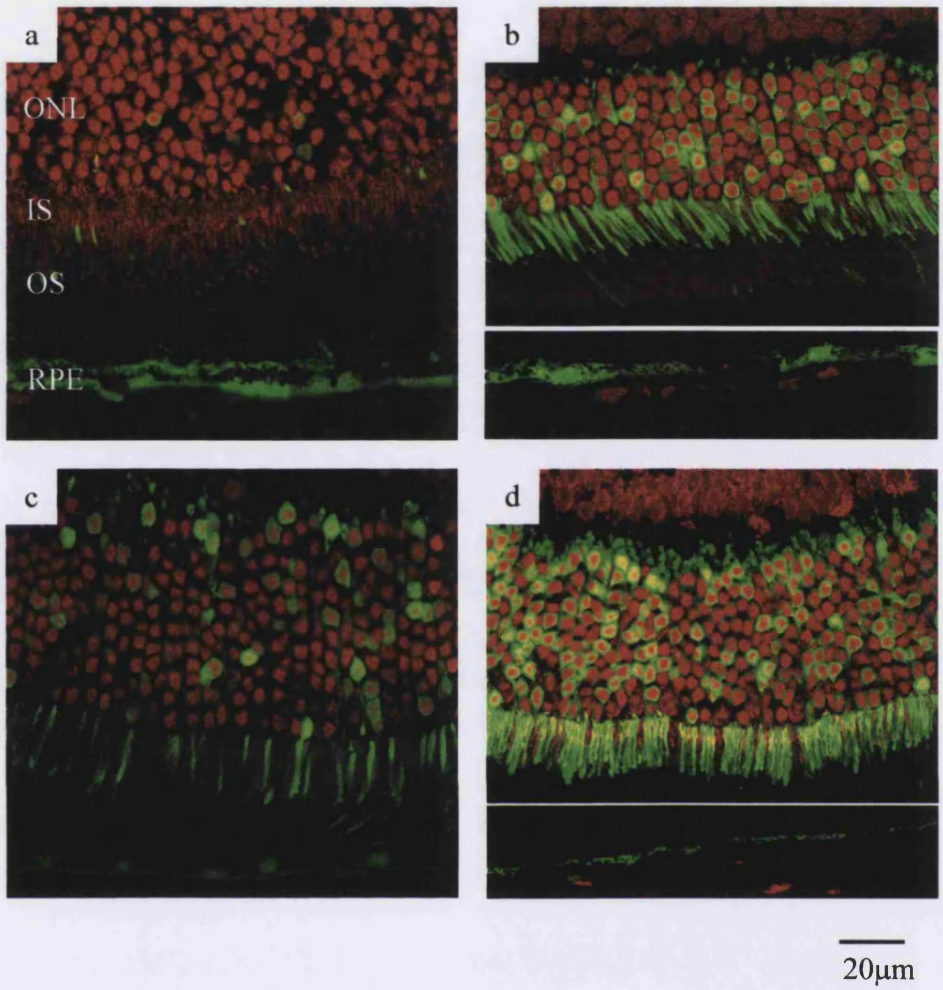

Figure 4.7 Expression of *egfp* in the retinal pigment epithelium after sub-retinal injection of AAV.CMV.EGFP and correlation with transduction of photoreceptor cells. Strong expression of EGFP is observed in areas of the RPE 7 days after injection of rAAV (**a**). Over time, EGFP fluorescence from the RPE correlates well with the percentage transduction of the outer nuclear layer (**b** and **c**). However, in some areas there is no correlation (**d**), the PR cells are strongly EGFP-positive but the RPE itself appears negative although its anterior surface is coated in fluorescent material. Sections were counterstained with propidium iodide (red). Retinal layers are marked on image **a**. ONL = outer nuclear layer; IS = inner segments; OS = outer segments; and RPE = retinal pigment epithelium.

To further examine the distribution of transduced photoreceptor cells the percentage transduction rates from the six sections of 16 eyes were combined to create graphical plots using MatLab 5.3 and the MatLab 4 grid data method to generate surface fits. The resulting colour graded plots are shown in Figure 4.8. The plots show that up to 64 days after injection transduced photoreceptor cells were confined to the region of the retinal detachment induced by the procedure. At later time points, however, a substantial spread over almost the entire retina could be observed although with a lower transduction efficiency. These findings strongly suggest that viral particles have the ability to spread well beyond the area of the original detachment. In a few eyes focal photoreceptor cell loss was observed and is represented by horizontal red bars (Fig. 4.8). All of these areas were adjacent to the parts of the retina showing the highest transduction efficiencies.

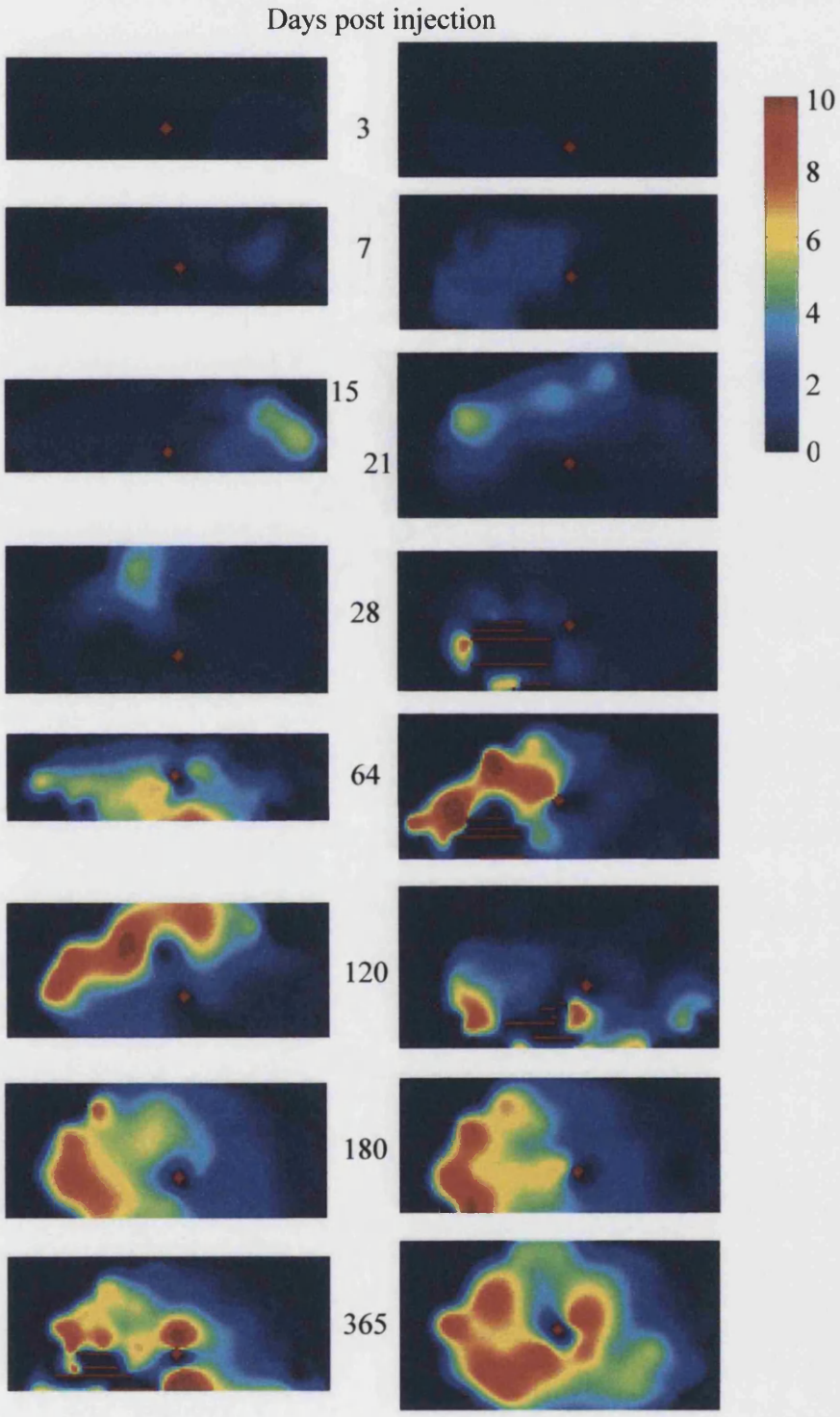

Figure 4.8 Colour coded plots showing the geographical spread of EGFP-positive cells throughout the retina as a function of time. Smoothed plots are shown which geographically reconstruct the photoreceptor cell transduction rates of approximately 30 retinal locations from 16 wild type mouse retinas following sub-retinal injection of AAV.CMV.EGFP (titre 5 x 10^9 iu/ml). These mice have been sacrificed at various time points between 3 and 365 days post-injection. Transduction rates are colour coded as indicated by the bar. The retinal boundaries and the optic nerve are represented by red squares and red horizontal bars indicate areas where data is missing.

4.4. Effect of viral titre on the transduction efficiency of photoreceptor and RPE cells

4.4.1 Method

To investigate the effect of viral titre on transduction efficiency a batch of AAV.CMV.EGFP at an original titre of 2 x 10^{10} iu/ml was diluted to 2 x 10^{8} iu/ml and 2 x 10^{6} iu/ml prior to sub-retinal injection. Two microlitres of each virus was injected into the right eyes of 8 normal adult C57Bl/6 mice. Two mice from each group were sacrificed at 7, 14, 28 and 84 days after injection. Before enucleation the eye's orientation was marked with a temporal stitch. Each eye was fixed and serially sectioned (section 2.11.1) at 25 μm with sections taken every 350 μm for observation of EGFP (section 2.11.2). Areas of highest fluorescence were located and the percentage of positive photoreceptor cells in that area was calculated (Fig. 4.4). The highest RPE rating (section 4.3) from the same section was also recorded.

4.4.2 Results

The results of this study are shown in Table 4.1. In addition, confocal images showing areas with maximal transduction rates are shown in Figure 4.9, and a graph of the increase in percentage of transduced PR cells over time is shown in Figure 4.10. Titre appears to have a substantial effect on both the transduction of PR and RPE cells. Both the lower titres (2 x 10^{6} and 2 x 10^{8} iu/ml) only reach a maximum transduction rate in the ONL of approximately 15% after 84 days, following a slow increase in the number of EGFP-positive cells. In contrast, the virus of the highest titre (2 x 10^{10} iu/ml) shows a relatively rapid increase in numbers of transgene expressing cells from 30% at 14 days to 60% at 28 days, reaching 75% at 84 days. The reduction in titre also appears to have a substantial effect on the transduction of RPE with lower titres producing very few visible EGFP-positive cells.

Time point	Titre (2 x) iu/ml	Highest % of +ve cells	RPE rating
7 day	10^{10}	8%	3
		25%	3
	10^{8}	<1%	0
		<1%	0
	10^{6}	<1%	0
		<1%	0
14 day	10^{10}	31%	3
		53%	2
	10^{8}	8%	1
		17%	1
	10^{6}	5%	2
		<1%	0
28 day	10^{10}	70%	3
		59%	2
	10^{8}	7%	0
		7%	1
	10^{6}	<1%	0
		15%	2
84 day	10^{10}	75%	3
		72%	3
	10^{8}	23%	1
		12%	1
	10^{6}	17%	0
		6%	0

Table 4.1 The effect of rAAV titre on the transduction efficiency of photoreceptor and RPE cells. At each time point two eyes were injected sub-retinally with varying titres of AAV.CMV.EGFP. Shown are the percentages of transduced PR cells and the rating of RPE transduction at the site of the highest PR cell transduction efficiency. The injection of lower titres of rAAV results in a reduction in the numbers of photoreceptor and RPE cell scored as EGFP-positive.

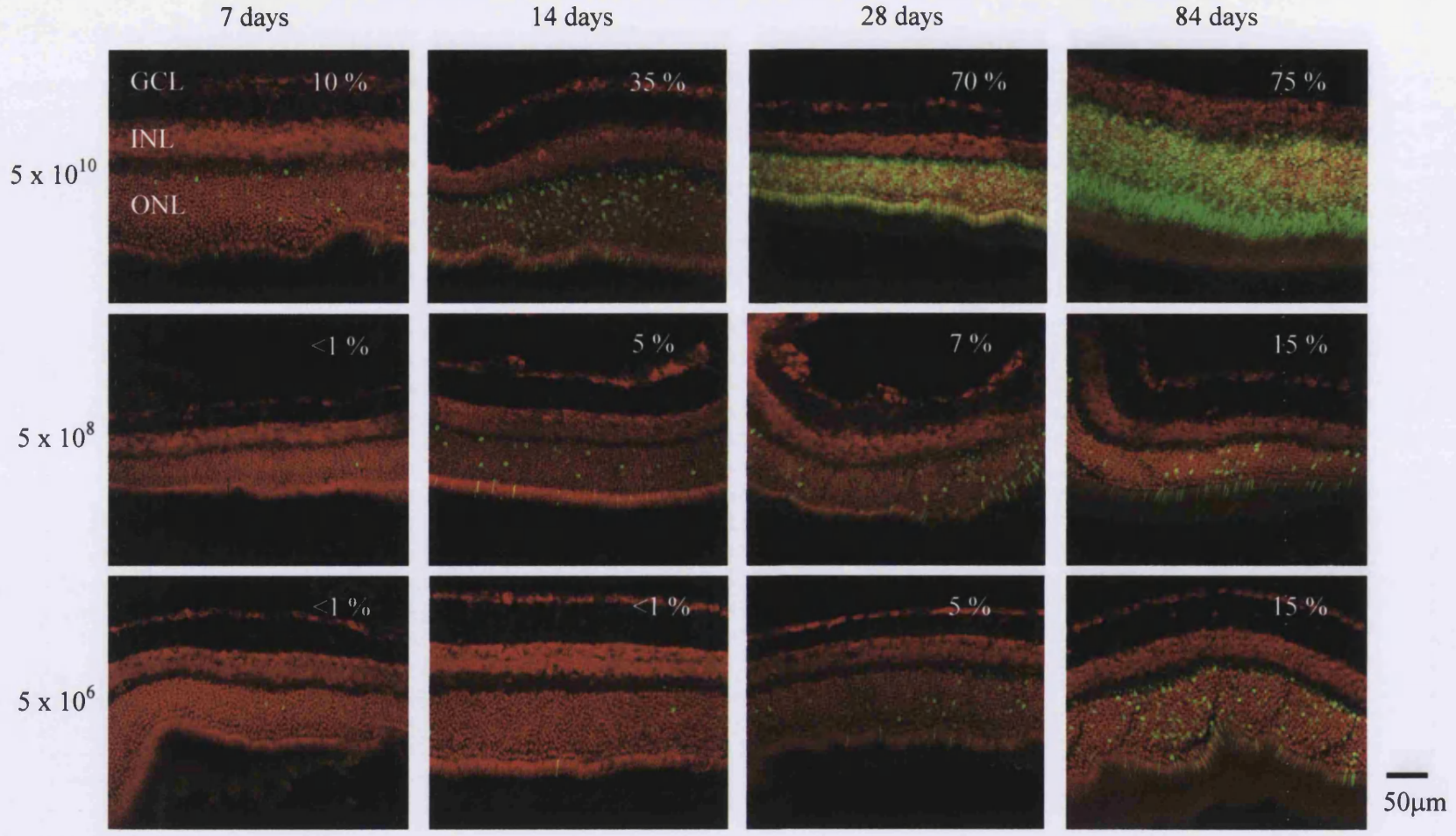

Figure 4.9 Increasing numbers of EGFP-positive photoreceptor cells in normal mouse retinas over time after sub-retinal injection of three different titres of AAV.CMV.EGFP. Representative confocal images were selected from the areas with the highest transduction rates at 7, 14, 28 or 84 days after injection of virus of 2 x 10^{10}, 2 x 10^8 or 2 x 10^6 iu/ml. Sections are counterstained with propidium iodide (red). The transduction rates are indicated at each time point. The retinal layers are indicated on the first image. GCL = ganglion cell layer; INL = inner nuclear layer and ONL = outer nuclear layer

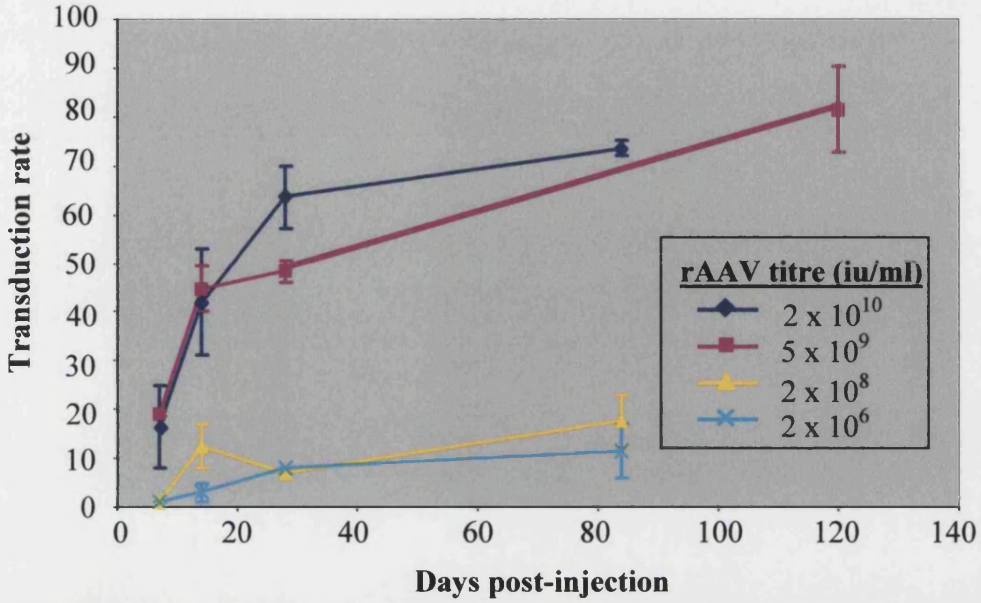

Figure 4.10 Maximal transduction rates of photoreceptor cells in wild type mouse retina as a function of time following sub-retinal injection of AAV.CMV.EGFP at four different titres. At each time point for four titres (2×10^{10}, 5×10^{9} (section 4.3), 2×10^{8} and 2×10^{6} iu/ml) two eyes were evaluated and the maximal transduction rates calculated. The vertical bars represent the two individual values for each data point.

4.5 Transduction of cone photoreceptor cells

4.5.1 Method

To test whether cones are transduced by rAAV, frozen sections from eyes that had been injected with AAV.CMV.EGFP, and used in experiments described in section 4.3, were selected on the basis that they were known to contain areas of retina in which a percentage of PR cells were expressing *egfp*. These sections were either immuno-stained with antibodies against blue cone opsin (section 2.12.1), or stained with peanut agglutinin (section 2.12.2), a lectin that specifically binds to glycoprotein on the outside of cone inner and outer segments [202]. When this work proved inconclusive sub-retinal injections were performed on the *rd* mouse. The *rd* mouse has served as a model for human RP for many years and its phenotype is well described (see section 1.6.1). The retinal degeneration is characterised by a rapid initial loss of the rod PR cells so that by postnatal day 20 the majority of PR cells are cones. The cones survive much longer and the other retinal cells remain intact [92]. Therefore, this phenotype presents an interesting opportunity to test the transduction of cone PR cells with rAAV since the percentage of cones in the retina is much higher. Injections were performed in a single eye of three, 10-day old homozygous *rd* mice, and in a single eye of three, 29-day olds. Two microlitres of AAV.CMV.EGFP at a titre of 5×10^{9} iu/ml was injected. In three

more 29-day old mice, 2 µl of AAV.LPRPH.EGFP, at a titre of 1 x 10^{12} particles/ml, was injected. It was anticipated that these injections would produce a relatively high dosage of virus, due to the smaller number of PR cells present, and this would result in a rapid onset of *egfp* expression. All mice were sacrificed at 14 days post-injection since the duration of cone PR cell survival within the *rd* mouse retina is reported to be variable [203]. The eyes were marked, fixed and serially cryosectioned (section 2.11.1).

4.5.2 Results

The results of the blue cone opsin and lectin immunostaining, on retinal sections from normal mouse eyes (Fig. 4.11), show that it was difficult to co-localise either stain with EGFP. The blue cone opsin staining (Fig. 4.11a) was particularly difficult since this stain marks the outer segment of the cone while EGFP primarily accumulates in the inner segments and cell body. Whilst the lectin staining (Fig. 4.11b) indicated that there might be some cones expressing *egfp,* particularly when the image is rotated so that it is viewed through the ONL towards the outer segments (Fig. 4.11c), this was far from clear. If it is assumed that rAAV transduces rods and cones at the same efficiency then the chances of finding a cone that is EGFP-positive in a section of retina in which the transduction rate is low, are relatively small. However, finding conclusive evidence of co-localisation in sections where there was a high percentage of photoreceptor transduction (Fig. 4.11d) was also difficult since there is a large amount of overlap between fluorescent inner segments.

The *egfp* expressing sections of retinas from injected *rd* mice, shown in Figure 4.12, demonstrate that assessment of cone transduction within this model also has its difficulties. Frozen sections taken from the eyes of mice that were injected with AAV.CMV.EGFP at 10 days old, when the retina contained both rod and cone PR cells, are shown in Figure 4.12 a, b and c. These mice were sacrificed at 24 days old and the sections show that the distinctive distance between the outer and inner nuclear layers is still visible. Therefore, it is clear that there are some positive photoreceptors. However, there is still the possibility that these might be rods. Unfortunately in the sections taken from *rd* mice that were injected at 29 days it is not possible to tell whether the *egfp* expressing cells are cells within the outer or inner nuclear layer (Fig. 4.12d, e and f). Recombinant AAV in which *egfp* expression is driven by a section of the *peripherin-2* promoter (virus produced in Chapter 3, tested in experiments described in section 4.6)

should limit expression to PR cells. However, retinal sections from *rd* mice injected with AAV.LPRPH.EGFP at 29 days showed no expression of *egfp* (Fig. 4.12g and h).

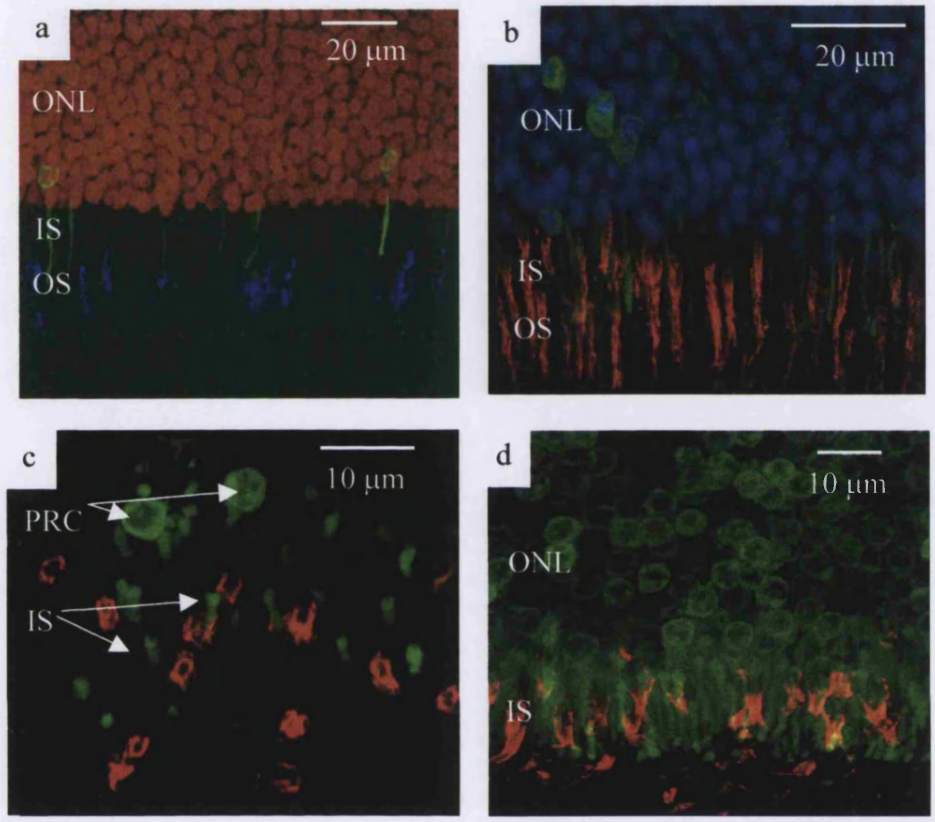

Figure 4.11 Assessment of possible rAAV-mediated cone transduction in wild type mouse retina after sub-retinal injection of AAV.CMV.EGFP. All the images show photoreceptor cells containing EGFP (green) and are stained with cone-specific markers, either blue cone opsin (blue) (**a**) or peanut agglutinin (red) (**b-d**). Co-localisation of opsin stain in outer segments with EGFP in inner segments is difficult (**a**). Staining with peanut agglutinin (red) marks the inner and outer segment membrane of cones but co-localisation here is also difficult (**b-d**) even with optical tangential cuts (**c**) and in areas of the retina where there are a large number of EGFP-positive cells (**d**). Cell nuclei were counterstained in (**a**) with propidium iodide (red) and in (**b**) with DAPI (blue). Retinal layers: INL = inner nuclear layer; IS = inner segments; OS = outer segments; and PRC = photoreceptor cells.

Figure 4.12 (shown on the next page) Assessment of possible cone transduction in in the *rd* mouse retina after sub-retinal injection of AAV.CMV.EGFP (a-f) or AAV.LPRPH.EGFP (g and h). Images, at increasing magnifications, taken of sections of *rd* retina from mice injected at P10 days and sacrificed 14 days later (**a, b** and **c**). EGFP positive cells in these images may be rods. Images, at increasing magnifications, taken of sections of *rd* retina from mice injected at P28 days and sacrificed 14 days later (**d, e, f, g** and **h**). Positive retinal cells in these images may be from the inner nuclear layer. No positive cells are seen after injection of rAAV carrying a *peripherin-2* promoter. Propidium iodide (red) counterstain was used. Retinal layers: GCL = ganglion cell layer; INL = inner nuclear layer; ONL = outer nuclear layer; and RPE = retinal pigment epithelium.

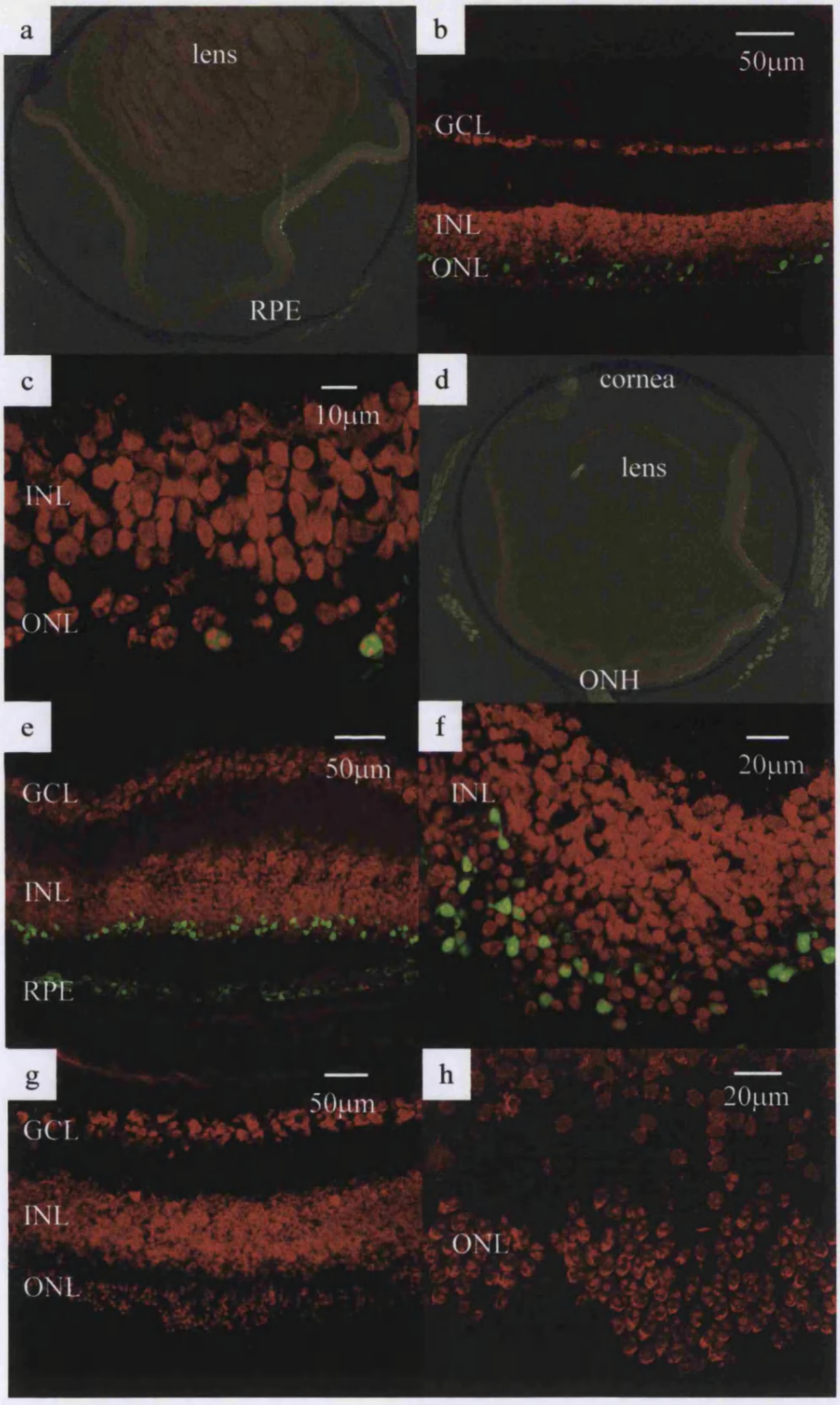

Figure 4.12 Assessment of possible cone transduction in the *rd* mouse retina after sub-retinal injection of AAV.CMV.EGFP (a-f) or AAV.LPRPH.EGFP (g and h). Full legend shown on previous page.

4.6 Comparison of photoreceptor cell-specific promoters

4.6.1 Method

The expression of *egfp* driven by photoreceptor cell-specific promoters was compared with *egfp* expression gained with a CMV promoter. AAV.RHO.EGFP at a titre of 1 x 10^{12} particles/ml, AAV.SPRPH.EGFP at a titre of 1 x 10^{13} particles/ml and AAV.LPRPH.EGFP at a titre of 1 x 10^{12} particles/ml were sub-retinally injected into a single eye of twenty-two adult C57Bl/6 mice. The *egfp* expression from the long and short *peripherin-2* promoter fragments was studied in two mice sacrificed at each time point (14, 28 and 64 days after injection). The *egfp* expression from the *rhodopsin* promoter was studied in two mice sacrificed at 7, 14, 28, 64 and 180 days after injection. On sacrifice the eyes were processed (section 2.11.1) for histological examination of EGFP (section 2.11.2). The eyes were analysed as described in section 4.4.

4.6.2 Results

Sectioning of the eyes injected with photoreceptor specific promoters showed that, as anticipated, expression from the long and short sections of the *peripherin-2* promoter was not as strong as that from the *rhodopsin* promoter. Therefore, the confocal images of the retinal sections from eyes into which AAV.RHO.EGFP had been injected were captured on the same laser intensity settings as those from eyes into which AAV.CMV.EGFP had been injected (described in section 4.3). These images are shown in Figure 4.13. Confocal images of sections from AAV.SPRPH.EGFP and AAV.LPRPH.EGFP injected eyes are shown in Figure 4.14. These images were captured using higher laser intensity settings. The highest percentages of positive PR cells were recorded for both eyes at each time point and are presented graphically (Fig. 4.15), with a line linking the average maximal transduction rate at each point.

There was a characteristic increase in the maximal transduction rates over time with all the vectors. Overall, in contrast with the findings of Flannery *et al.* [128], the AAV.CMV.EGFP vector mediated the highest percentages of transduction of PR cells, despite a slightly lower titre of 5 x 10^9 iu/ml. The onset of expression also appeared to be quicker after injection of this virus. In contrast, those eyes injected with rAAV

carrying photoreceptor cell-specific promoters initially showed a slow increase in the number of EGFP-positive cells although transduction rates after injection of AAV.RHO.EGFP were comparable with those of AAV.CMV.EGFP. Transduction rates with vectors carrying the long *peripherin-2* promoter fragment increased rapidly between 3 weeks and 9 weeks and resulted in a final transduction rate at 64 days that was substantially higher than that seen for the short fragment despite a titre that was ten-fold lower. No positive RPE cells were found in any of the sections taken from eyes injected with PR cell-specific promoters, including those injected with the vector carrying the *rhodopsin* promoter construct where the percentage of transduced PR cells was at its highest, at around 75%.

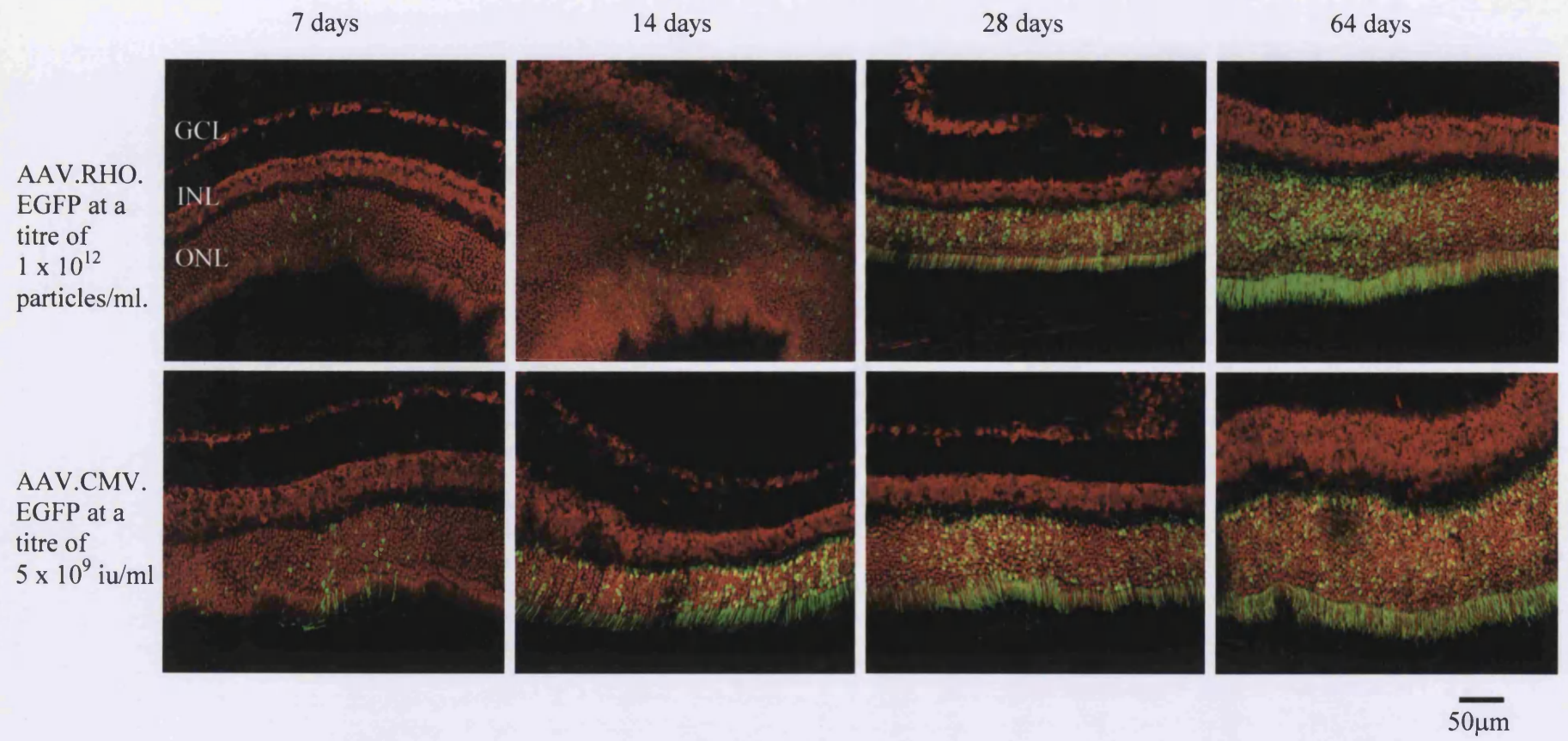

Figure 4.13 Comparison of EGFP-positive photoreceptor cells in normal mouse retina as a function of time following sub-retinal injection of AAV.RHO.EGFP or AAV.CMV.EGFP. Representative confocal images from the areas of maxiamal tranduction are shown at four timepoints, 7, 14, 28 and 64 days post injection. The upper row of pictures represents the eyes injected with AAV.RHO.EGFP, while the lower row represents those treated with AAV.CMV.EGFP. The time after injection is shown along the top edge of the figure. Propidium iodide (red) counterstain was used. Retinal layers: GCL = ganglion cell layer; INL = inner nuclear layer; and ONL outer nuclear layer.

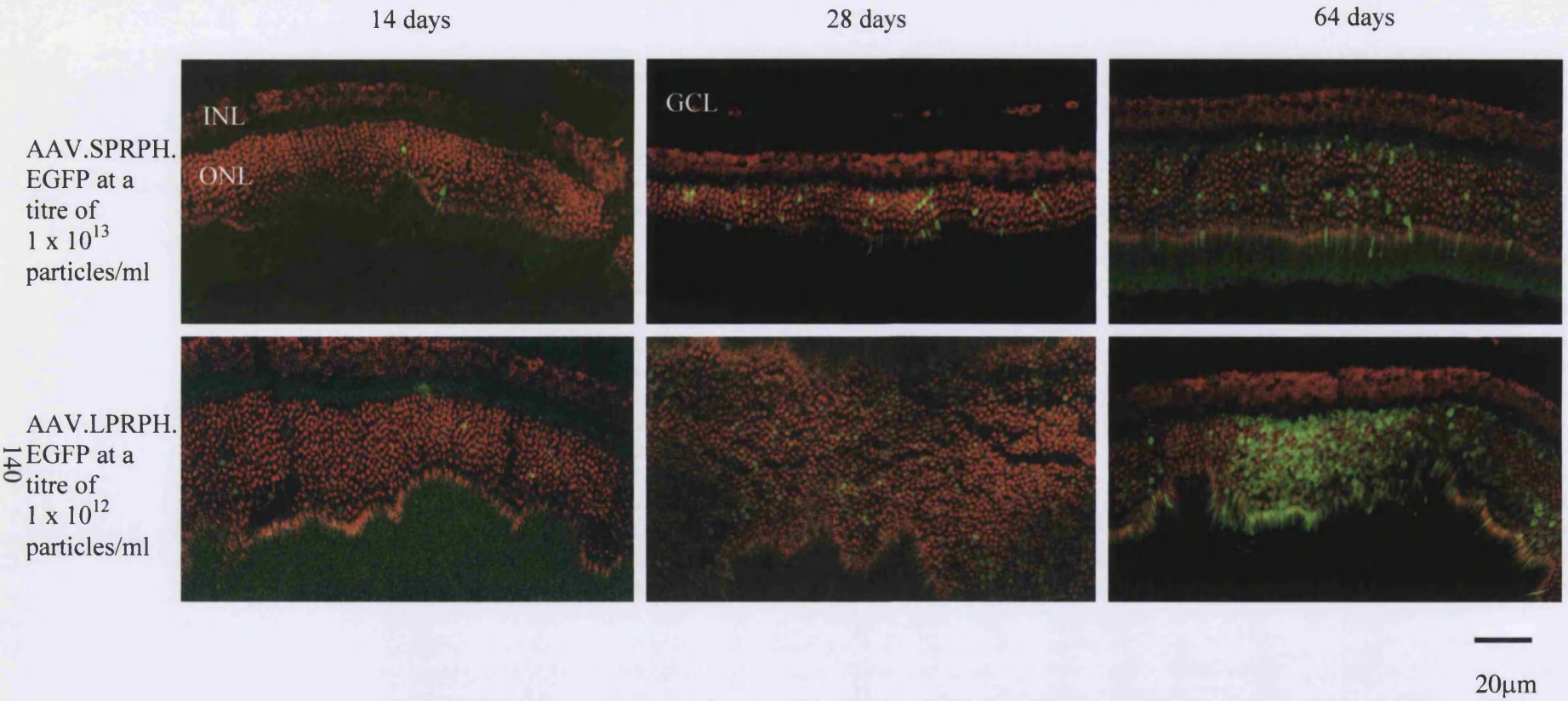

Figure 4.14 Comparison of EGFP-positive photoreceptor cells in normal mouse retina as a function of time following sub-retinal injection of AAV.SPRPH.EGFP or AAV.LPRPH.EGFP. Representative confocal images from the areas of maximal transduction rate at three time points, 14, 28 and 64 days post-injection, are shown. The upper row of pictures represents the eyes injected with AAV.SPRPH.EGFP, while the lower row represents those injected with AAV.LPRPH.EGFP. The time after injection is shown along the top edge of the figure. Propidium iodide (red) counterstain was used. Retinal layers: GCL = ganglion cell layer; INL = inner nuclear layer; and ONL = outer nuclear layer.

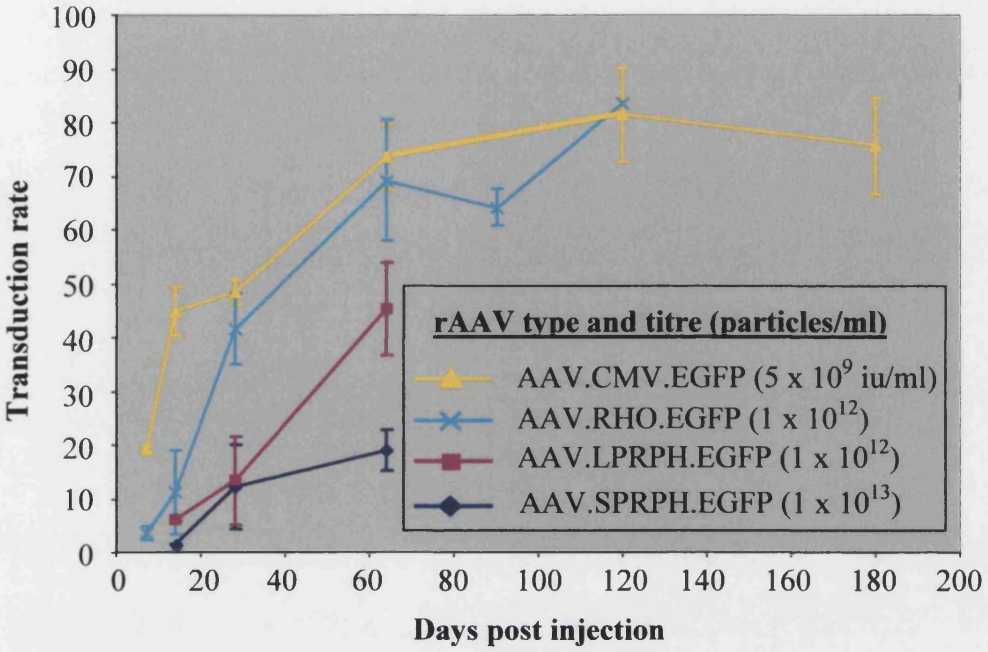

Figure 4.15 Maximal transduction rates of photoreceptor cells in wild type mouse retina as a function of time following sub-retinal injection of AAV.CMV.EGFP, AAV.RHO.EGFP, AAV.LPRPH.EGFP or AAV.SPRPH.EGFP. At each time point and for each virus two eyes were examined and the maximal transduction rates calculated. The vertical bars represent the two individual values for each data point.

4.7 Expression of *egfp* after injection of AAV.RHO.EGFP into *Prph2*$^{Rd2/Rd2}$ pups

4.7.1 Method

On the basis of the above experiment the *rhodopsin* promoter was selected for use in driving expression of functional constructs because of the more rapid onset of expression that it mediated. We wished to determine the activity of the *rhodopsin* promoter in the *Prph2*$^{Rd2/Rd2}$ mouse retina after its sub-retinal delivery in rAAV into 10-day old *Prph2*$^{Rd2/Rd2}$ mice. Therefore 2 µl of AAV.RHO.EGFP at a titre of 1 x 10^{12} particles/ml was sub-retinally injected into eight 10-day old *Prph2*$^{Rd2/Rd2}$ mice (section 2.10.3). These mice were sacrificed at 7, 14, 28 or 120 days after injection. Additionally three 90-day old *Prph2*$^{Rd2/Rd2}$ mice were also injected and sacrificed 30 days later to determine whether the *rhodopsin* promoter could still drive expression of *egfp* at this late stage in the degeneration of the retina. These injections also controlled for the possibility that any fluorescence seen at the 120-day time point from the 10-day old

injected *Prph2*$^{Rd2/Rd2}$ mice was only the result of EGFP that had not been degraded. Six 10-day old normal C57Bl/6 pups were also injected in the same way as controls, and sacrificed at 7, 14 and 28 days after injection. Before enucleation of all eyes their orientation was marked with a temporal stitch. Eyes were processed and sectioned (section 2.11.1) and examined for EGFP fluorescence (section 2.11.2) according to the method described in section 4.4.

4.7.2 Results

The expression of *egfp* after injection into 10-day old and 90-day old *Prph2*$^{Rd2/Rd2}$ mice is shown in Figure 4.16. EGFP was detected in retinal sections at all of the time points including the earliest and latest time points. Consistent with the findings of Nir *et al.* [199] there does not appear to be any down-regulation of the *rhodopsin* promoter in 120-day old mice. In *Prph2*$^{Rd2/Rd2}$ and normal mice the rates of transduction characteristically increase over time (Fig. 4.17). The transduction rate at day 7 in *Prph2*$^{Rd2/Rd2}$ mice is substantially higher than that obtained following injection into normal pups and this difference is maintained over the time-course. This might, in part, be attributed to a better transduction rate in the degenerating retina but it should also be noted that although the batches of rAAV injected into the control and *Prph2*$^{Rd2/Rd2}$ mice were the same titre, they were prepared and injected on different occasions. The batch that was injected into the *Prph2*$^{Rd2/Rd2}$ mice had previously been used to study expression of *egfp* in normal adults (see section 4.6) where levels of transduction comparable to those observed here were also recorded. This suggests that the state of the PR cells is not necessarily the only cause of differences in transduction rates. Factors such as injection technique, and the form of the needle i.e. position and size of bevel, may have an impact on the quality of the sub-retinal injection and therefore transduction rate. This is particularly so for pups where the eyes are smaller and injection more difficult. During the injections into the control pup eyes we noted that there was more reflux of virus after sub-retinal detachment and, as a result, less virus remained between the PR cells and RPE. This is may account for some of the lower transduction rates observed in these animals but is unlikely to account for all of it.

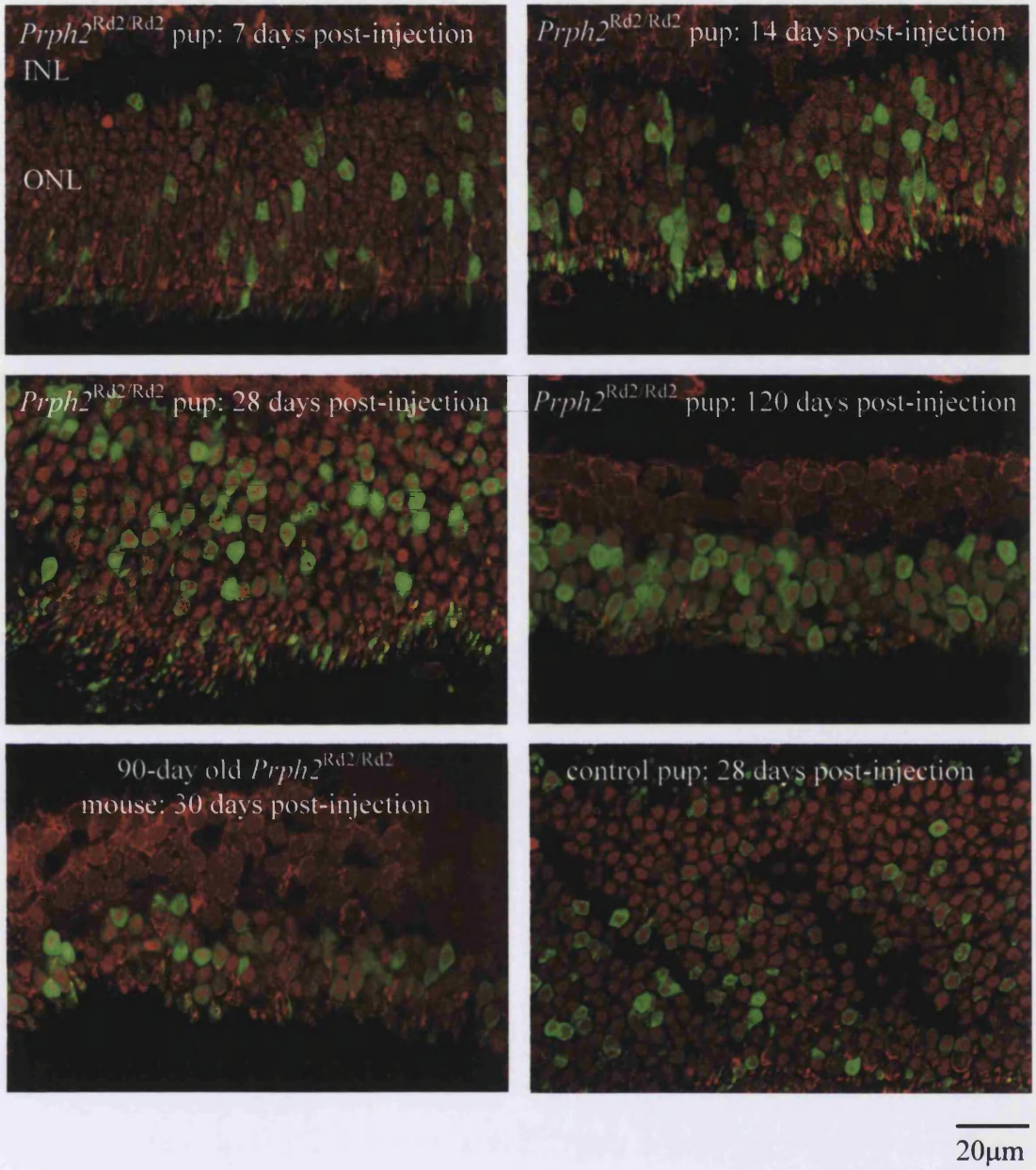

Figure 4.16 Assessment of *egfp* expression in photoreceptor cells after sub-retinal injection of AAV.RHO.EGFP into *Prph2*$^{Rd2/Rd2}$ and normal pups, and 90-day old *Prph2*$^{Rd2/Rd2}$ mice. Expression of *egfp* is seen at every time point indicating that the *rhodopsin* promoter in AAV.RHO.EGFP is active even at the later stages of degeneration. Each image is labelled according to the age of the mouse and the time point post-injection. Pups were all injected 10 days after birth. Sections are counterstained with propidium iodide (red). Retinal layers: INL = inner nuclear layer; and ONL = outer nuclear layer.

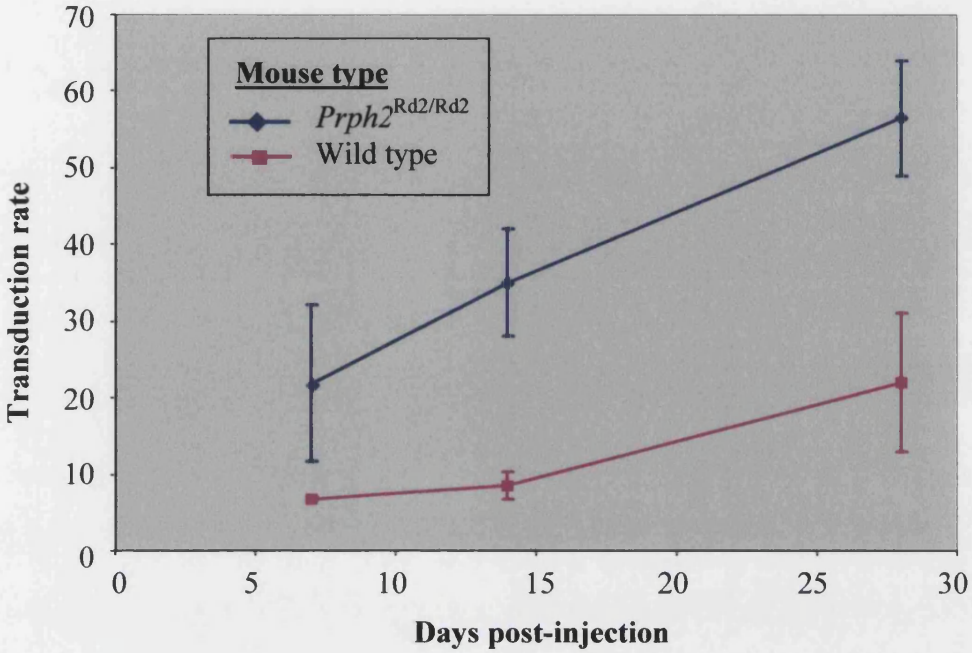

Figure 4.17 The increase in the maximal transduction rate of photoreceptor cells over time in wild type and *Prph2*$^{Rd2/Rd2}$ pups after sub-retinal injection of AAV.RHO.EGFP (1 x 10^{12} particles/ml). At each time point and for each virus two eyes were examined and the maximal transduction rates calculated. The vertical bars represent the two individual values for each data point. Mouse pups were injected at 10 days old.

4.8 Discussion

4.8.1 Potential for *in vivo* monitoring of *egfp* expression

Both the SAC and the cLSO set-ups were evaluated for their ability to detect and record expression of *egfp* after retinal gene transfer. While the cLSO provided a more sensitive method of detecting fluorescence from the retina and a relatively flexible method of recording images, the results it produced were of more variable quality than those produced by the SAC. In contrast, the SAC provided a better overall picture of the retina allowing an easier assessment of the area and location of fluorescence. The two methods complement each other well and, in combination with the use of the new reporter gene *egfp*, provide an important method of studying the onset and increase in transgene expression over time. However, the size of the mouse eye may limit the value of these techniques in the quantification of fluorescence since it is difficult to

standardise the amount of light entering the eye. In addition, the strong fluorescence at the later time points is difficult to measure.

4.8.2 Transgene expression after sub-retinal injection of rAAV

The delay in onset of reporter gene expression following delivery with rAAV is a well-characterised feature of this viral vector. Dudus *et al.* [192] have reported low levels of transgene expression at 3 weeks post-injection with levels peaking and stabilising around 6 weeks post-injection. This study has shown that expression is detectable as early as 3 days after injection, although at very low levels. Over time transduction rates increase with all of the promoters used. The stronger *rhodopsin* and CMV promoters showed rapid increase over the first 3 months post-injection before the rate of increase slowed and expression levels appeared to be relatively stable. This long-term stability of expression has also been reported by Bennett *et al.* [204] in mice, dogs and primates. These findings are consistent with studies in the eye that show no detectable humoral immune response to EGFP after sub-retinal delivery in rAAV and a lack of a strong cellular response to the rAAV capsid proteins [192]. In some retinal sections studied in the experiments described here there were focal areas of photoreceptor cell loss. The reasons for this are not clear, although it is possible to exclude immune-mediated damage since high percentages of transduced photoreceptor cells remain in these eyes even at 1 year after injection. Since these areas tend to occur adjacent to the areas of maximal transduction efficiency, EGFP or vector toxicity at high concentrations are possible explanations.

The lower transduction rates, of both the RPE and PR cells, associated with sub-retinal injection of rAAV at a reduced titre provides a possible explanation for the disagreement on the ability of rAAV to transduce PR cells. The apparent lack of RPE transduction in eyes injected with lower titre virus would indicate that rAAV is not as efficient at transducing RPE cells as PR cells, assuming that the CMV promoter is equally efficient in both of these cell types. Rolling *et al.* [205] reported that after sub-retinal injection in rats, *egfp* expression was maintained in some areas of the RPE while almost completely disappearing in others. In the context of many studies showing the lack of immune response stimulated by rAAV they proposed that the CMV promoter could be shut down in these cells according to the number of viral constructs present in the nucleus. The apparently less efficient transduction of RPE compared to PR cells

may also simply be due to the pigment granules in the RPE. Dampening of fluorescence would cause the RPE to be scored as negative when the levels of EGFP are low.

When comparing results from various groups the method of virus production must be considered, as it may be a factor in the varying results obtained. Early studies with rAAV used virus that had been purified through CsCl gradients [109, 110, 190]. These preparations have been shown to be contaminated by proteins from the production process and may result in the rAAV forming aggregates (M. de Alwis – unpublished results). These factors may affect the transduction, as clumps of virus may be less efficient at transducing PR cells while contaminating adenoviral proteins may increase transduction of the RPE. In contrast recently developed methods of purification, such as those used to prepare the virus used in these studies, result in less protein contamination.

The spread of transduction around the retina away from the area of injection is an interesting result and is previously unreported. The method of virus production used in this study has been shown to produce replication-competent AAV at levels of 0.01-1%. This level has been reported to be reduced further by the deletion of the distal 10 nucleotides within the D sequence of the ITR [180](see section 3.3.1). Therefore, it is unlikely that the consistent spread is due to replication competent virus, which would need to incorporate the *egfp* gene and would require the presence of a helper virus for its production. The half-life of rAAV particles and the method for their movement within retina is not known. However, the longer time delay in onset of expression in areas away from the site of sub-retinal detachment may be the result of transduction with fewer viral particles. As demonstrated by the comparison of *rhodopsin* and *peripherin-2* promoters, the strength of the promoter can have a significant effect on the perceived transduction rate, with cells being scored negative if the levels of EGFP are outside the limits of detection. These results are encouraging for the use of rAAV as a vector to deliver genes to PR cells, demonstrating that a single sub-retinal injection can target cells both within and outside the area of detachment.

4.8.3 Transduction of cones

The study of cone transduction in normal and *rd* mice has proved inconclusive and shown the difficulties in confirming the identity of EGFP-positive cones. In the light of

these results it would seem that the mouse is not an ideal model in which to assess this due to the low percentage of cones in its retina. However, the use of cone-specific promoters, transmission electron microscopy or immunohistochemistry with a cone cell body specific antibody, for example one specific for X-arrestin, may provide a solution if this work is continued in mice. There are a number of reasons why EGFP-positive cones have not been seen. It is unlikely that the virus or transgene are specifically toxic to cone photoreceptor cells particularly since expression is maintained for so long in rods. It is possible that the CMV promoter is not active in cone PR cells; however, it is unlikely that the *peripherin-2* promoter is also not active. Lack of *egfp* expression in *rd* mice after injection of AAV.LPRPH.EGFP might be due to the relatively short time between injection and sacrifice (14 days). However, the vastly reduced numbers of PR cells remaining at the time of injection should mean a substantial increase in the number of copies of the viral genome in each cell, at least in the area of detachment, in comparison to injection into a normal mouse eye. The most plausible explanation is that cones lack the receptors necessary for rAAV infection. The even spread of transduced PR cells throughout the full thickness of the outer nuclear layer at any one point suggests that the receptors important for rAAV transduction are present on the outer and inner segments. However, the transduction rates within the *Prph2*$^{Rd2/Rd2}$ mouse model, where outer segments are absent, would indicate that some receptors are present on the inner segments or cell body. Although a few of the receptors for rAAV have been identified [206-208] their presence on PR cells has not been assessed.

4.8.4 Photoreceptor cell-specific expression

The use of both the long and short sections of the *peripherin-2* promoter, and of the *rhodopsin* promoter, demonstrates the potential for PR cell specific gene expression. The lack of expression of *egfp* in RPE cells also confirms that this cell type is truly transduced after an injection of AAV.CMV.EGFP and is not positive as a result of phagocytosis of EGFP produced in the adjacent PR cells. The *peripherin-2* promoter has not previously been used to drive *in vivo* expression and both versions of this promoter have been shown here to be capable of expressing *egfp* in PR cells. The direct comparison of promoters in an *in vivo* setting is difficult. Despite consistency in the procedure of sub-retinal injection each injection is slightly different and in a small mouse eye it is difficult to inject an exact quantity of virus, particularly if there is some reflux or leakage of virus through the needle track. The size and form of the

detachments also vary as a result of the way in which virus is injected. To allow for these variations larger numbers of animals will need to be examined for each time point. However, these preliminary results suggest that the longer section may direct stronger expression. In comparison to the *rhodopsin* and CMV promoters the increase in transduction rates over time is relatively slow. Therefore, the AAV.RHO.EGFP was chosen for injection and expression studies in the *Prph2*$^{Rd2/Rd2}$ mouse since attempts at treatment of the retinal degeneration phenotype of this model will require rapid onset of transgene expression. Transduction rates increased more quickly in the *Prph2*$^{Rd2/Rd2}$ pups than in control pups that may be partially due retinal degeneration phenotype, as previously reported by Grant *et al.* [190]. The long-term expression of *egfp* from the *rhodopsin* promoter in 120-day old *Prph2*$^{Rd2/Rd2}$ mice confirmed the findings of Nir *et al.* [199] that the reduction in levels of rhodopsin in older *Prph2*$^{Rd2/Rd2}$ mice is not a result of reduced mRNA transcription from the *rhodopsin* promoter. While the *rhodopsin* promoter is unlikely to provide the exact therapeutic level of peripherin-2 in the treatment of the *Prph2*$^{Rd2/Rd2}$ mouse, it is a good starting point from which to investigate the effects of treatment.

4.8.5 Future work

Recombinant AAV has been shown by this study and others to be an effective vector for the delivery of genes to photoreceptor cells. The importance of the promoter and reporter genes in the detection of transduced cells has been highlighted. Titre has also been shown to play an important role and virus that is further concentrated may allow a more rapid onset in transgene expression. It would be of interest to establish the number of viral copies in all of the cells transduced. Since it is hard to imagine how multiple transduction events of a single cell could be avoided, the promoter system used will be the key to establishing the correct level of gene expression. Research is beginning to focus around the use of inducible promoter systems that allow induction of expression with a specific drug, such as tetracycline, administered to the patient (to be discussed further in Chapter 7).

Aknowledgements

I would like to credit Mahesh de Alwis for producing most of the rAAV used in the work described in this chapter, and Jim Bainbridge for performing the sub-retinal and intra-vitreal injections. I would also like to thank Geno Sarra for his assistance with sectioning and analysing the injected eyes, and Professor Phil Luthert for his assistance in creating the colour plots shown in Figure 4.8. For the *in vivo* work with the cLSO we collaborated with Professor F. Fitzke and Tony Halfyard, and I would like to thank both of them for their time and input.

5

A gene therapy strategy for the treatment of the *Prph2*$^{Rd2/Rd2}$ mouse

The aims of the experiments described in this chapter were as follows:

- to produce a rAAV vector carrying a wild type *Prph2* gene driven by a photoreceptor cell-specific promoter,
- to establish expression of *Prph2* after sub-retinal injection of this virus in the *Prph2*$^{Rd2/Rd2}$ mouse,
- to examine the histological and ultrastructural changes caused by this expression in transduced photoreceptor cells,
- to investigate the effect of this treatment on retinal degeneration in this model.

5.1 Introduction

The *Prph2*$^{Rd2/Rd2}$ mouse is a relatively well-defined model of retinal degeneration and therefore a good one in which to begin to assess the potential of gene therapy for treatment of RP. Moreover, the mutation in this model results in the complete absence of protein (section 1.6.1). As a result treatment is not complicated by the need to remove a mutant protein at the same time as replacing a functional copy of the gene. In addition, the mutation results in an ultrastructural defect, which when corrected allows an unambiguous assessment of the efficacy of therapy. The loss of PR cells occurs slowly in this model giving time for therapeutic intervention. However, the commitment of a cell to the degeneration process is not fully understood and it is unclear whether gene therapy will be successful in preventing or slowing PR cell loss.

5.1.1 The *Prph2*$^{Rd2/Rd2}$ mouse – genotype and phenotype

The mouse gene *Prph2* consists of 3 exons located on chromosome 17 [120] and is expressed in both rods and cones [209]. In the *Prph2*$^{Rd2/Rd2}$ mouse there is an insertion of a 9.2kb repetitive genomic element into exon II [173]. Although the entire inserted element is included in the transcribed mRNA no translation products are detectable [173], and the defect is therefore considered to be a null mutation. The wild type *Prph2* gene encodes a 36-kDa PR cell-specific membrane glycoprotein, peripherin-2, which is 92% homologous at the amino acid level to its human analogue [210]. The protein has four transmembrane segments and is located in the rims of rod and cone outer segment discs (Fig. 5.1). Within rods it is associated, in a heterotetrameric complex, with a homologous protein, Rom-1 [21].

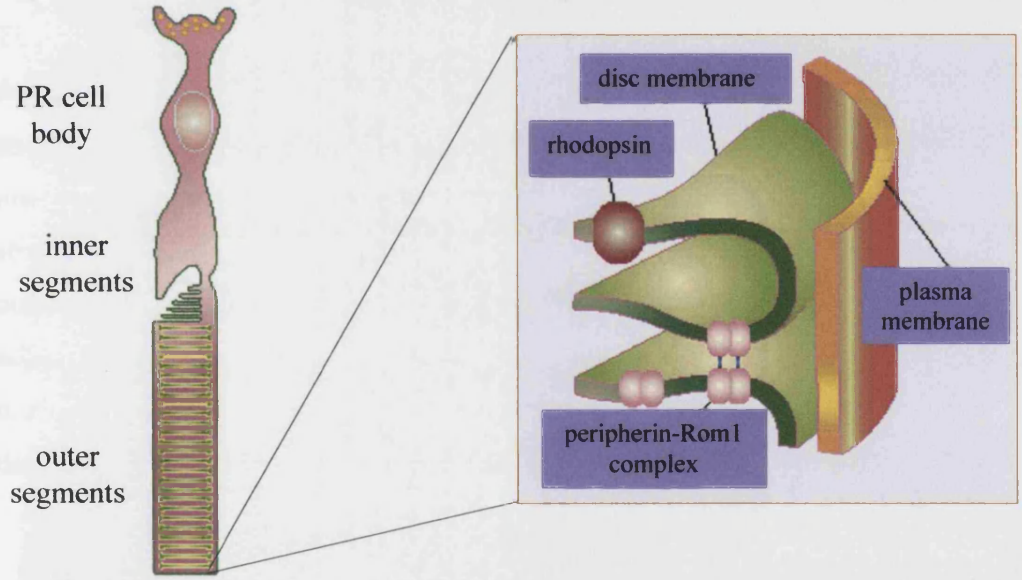

Figure 5.1 Location of peripherin-2 in the membrane of rod outer segment discs. Figure taken from Gregory-Evans and Bhattacharya [211]

The *Prph2* $^{Rd2/Rd2}$ mouse highlights the importance of this complex in maintaining the flattened forms of the discs. In the absence of peripherin-2 the PR cells are unable to develop outer segments [212, 213], and cell death results. The defect is in fact a semi-dominant trait and the protein produced from one functional allele is insufficient to support normal PR cells. The heterozygous animals have outer segments but they are shorter and disorganised with characteristic irregular whorls of membranes. Their PR cell degeneration is slower than that observed in mice that are homozygous for the mutation [214].

In the retina of a normal mouse the PR cells undergo their final round of mitosis between postnatal day 2 and 3 and outer segments appear after this during the first postnatal week. Synthesis of the opsin visual pigments follows. As previously discussed in section 1.2.3 PR cell loss in *Prph2* $^{Rd2/Rd2}$ mouse, as in other models of PR cell degeneration, occurs via apoptosis. Apoptosis is an integral part of the development of the retina, but in the *Prph2*$^{Rd2/Rd2}$ mouse the failure to produce outer segments appears to result in a dramatic increase in the number of apoptotic PR cells around P10, which peaks at approximately P18 [23]. Degeneration is most rapid up to the age of 2-3 months, and the inner layer is reduced to half its original thickness. Thereafter it progresses more slowly. By 12 months the 11 rows of PR cells present in the retina at P10 have been reduced to a single row [212] (Fig. 5.2). In contrast, the outer nuclear layer of heterozygous animals is only half its original thickness by 18 months [214]. The apoptotic cells detected in homozygous mice at any one time during the degeneration are spread evenly through the retina and are not clustered in patches [23], and there does not appear to be a preferential loss of either rods or cones. Opsins are initially synthesised at a rate comparable to normal [199] and are seen in vesicular structures between the PR inner segments and the RPE [213]. However, the absence of outer segments means that the vesicles are subject to continuous phagocytosis by the adjacent RPE and therefore the opsin content of the retina is lower than that of a normal mouse. Over time it appears that synthesis of opsin ceases although mRNA can still be detected [199] (section 4.1.4).

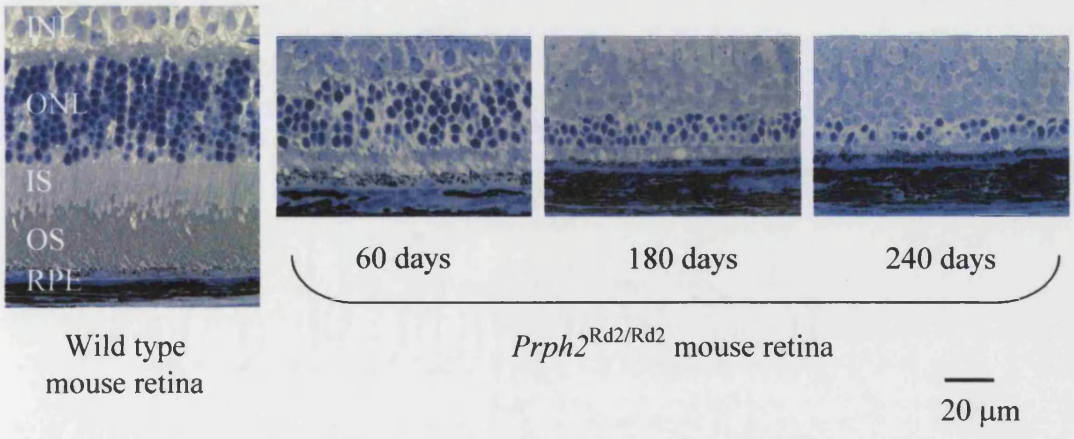

Figure 5.2 Progress of photoreceptor cell loss in the *Prph2*$^{Rd2/Rd2}$ mouse retina. Semithin sections showing the appearance of the outer retinal layers in wild type mice and in *Prph2*$^{Rd2/Rd2}$ mice over the course of PR cell degeneration. The retinal layers are marked on the section of the wild type mouse retina. There is no layer of outer segments in the *Prph2*$^{Rd2/Rd2}$ mouse retina. INL = inner nuclear layer; ONL = outer nuclear layer; IS = inner segments; OS = outer segments; and RPE = retinal pigment epithelium.

5.1.2 Mechanism of degeneration

Although the mechanism of degeneration is thought to be apoptosis for this and other models, the upstream processes that lead to the initiation of cell death are unclear. Photoreceptor cells appear to be very sensitive to small changes both in their internal and external environment. It has been suggested that in the case of the *Prph2*$^{Rd2/Rd2}$ mouse the absence of outer segments cause an increase in the concentration of oxygen to toxic levels [215]. Travis [215] has proposed that the PR cells are subjected to a much higher concentration of oxygen for two reasons. Firstly, the lack of outer segments results in the cells being physically closer to the supply of oxygen, the capillaries in the choroid. Secondly, the absence of the cGMP-gated channels of the outer segments causes a reduced cation influx and an unloading of the Na+/K+-ATPase pumps. Therefore there is a reduced consumption of oxygen by the mitochondria in the inner segments, which causes a much flatter pO_2 gradient across the outer retina. The link between apoptotic cell death and reactive oxygen species is well established and it has long been suggested that oxidative stress causes metabolic disruption in many neurological degenerative disorders, including Alzheimer's and Parkinson's diseases [216]. This type of theory suggests that the cell death occurs as a result of cumulative damage, and therefore the probability of death increases over time. Clarke *et al.* [217] have recently demonstrated that this may not be the case. They studied 11 animal models of inherited retinal degeneration and, disregarding the mechanism of degeneration, used regression analysis to examine cell death. They showed that in the *Prph2*$^{Rd2/Rd2}$ mouse there is an exponential decline in PR cell number (Fig. 5.3) that is consistent with a constant or decreasing risk of cell death. They argue against the idea of accumulation of damage causing cell death, instead proposing a "mutant steady state" in which a " single rare catastrophic event" triggers the commitment to the apoptotic pathway – a so called " one-hit" model. The corollary of this theory is that the chance of successfully rescuing a mutant PR cell does not decrease with age.

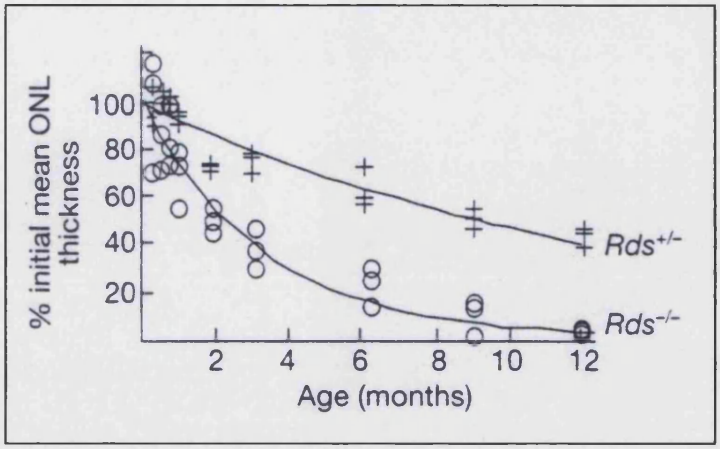

Figure 5.3 Kinetics of photoreceptor cell death in *Prph2*$^{Rd2/Rd2}$ homozygous and *Prph2*$^{Rd2/+}$ heterozygous mice. The graph shows that in mice homozygous for the null mutation in *Prph2* there is an exponential decline in the thickness of the ONL over the course of the PR cell degeneration. This is consistent with a constant or decreasing risk of cell death. Figure taken from Clarke *et al.* 2000 [217].

There are several strands of evidence, however, that suggest that there are environmental changes occurring within the retina over the period of degeneration, which may also have a role to play in cell death. Cheng *et al.* [218] compared the effect of haploinsufficiency on rods and cones by observing the numbers of surviving PR cells, the retention of ERG amplitudes and the maintenance of mRNA levels in these two cell types over the course of the degeneration in heterozygous animals. They concluded that the *Prph2*$^{Rd2/+}$ mutation has a greater impact on rods than on cones, a finding which may reflect the slightly different outer segment structure of the rod PR cell i.e. the longer and more rigid structure of individual discs. More interestingly, it was also proposed that in this model cone degeneration arises primarily as a result of rod degeneration. While this is obviously not the case in the homozygous mice, the concept of a cell undergoing apoptosis as a result of its surroundings is supported by the phenotype of rod and cone degeneration in RP patients where the genetic defect is in rod specific genes (section 1.2.1). In addition to this, chimeric mice, in which there is a mosaic pattern of mutant and wild type PR cells, show uniform thinning and degeneration of the outer nuclear layer [25, 26]. These observations point to environment factors influencing the PR cell degeneration either through the release of pro-apoptotic factors or the withdrawal of neurotrophic factors. This indicates that retinal degeneration is not a simple " one-hit " process, but is complicated by the

involvement of cell-cell interactions so that cell death may be, at least in part, non-autonomous. The origin and importance of these pro- and anti- survival factors are still unknown. Nir *et al.* [199] speculate that the loss of 65% of PR cells in the *Prph2*$^{Rd2/Rd2}$ retina within the first 3 months, followed by the relatively slow loss of the remaining cells over the next 9 to 12 months, could reflect initial competition for a neurotrophic factor which is in short supply. Once the cell number is reduced the remaining cells can function for longer periods of time in an environment where there are more survival factors to go around. This type of theory is consistent with the even distribution of apoptotic cells in the degenerating retina, a feature that suggests that these survival factors are spread evenly through the outer nuclear layer and may have their origins there. These factors may equally be pro-apoptotic. Microglial cell-derived nerve growth factor has been shown to cause cell death in developing chick retina [219] and microglia cells are known to be up regulated in degenerating retinas [220]. This suggests that the apoptosis of PR cells could be stimulated by factors released by activated microglial cells. In addition other layers of the retina may also be involved. For example, ciliary neurotrophic factor (CNTF) has been reported to promote PR cell survival in the *Prph2*$^{Rd2/Rd2}$ mouse [140], although its receptor is not found in PR cells. Its effect is thought to be mediated through Muller cells in the inner nuclear layer (see section 1.6.3.2).

5.1.3 Assessment of therapy

Travis *et al.* [121] have previously corrected the morphological phenotype of the *Prph2*$^{Rd2/Rd2}$ mouse through the microinjection into fertilized eggs of the wild type *Prph2* gene coding region driven by a segment of the *opsin* promoter. Retinas from two transgenic lines on the *Prph2* $^{Rd2/Rd2}$ background were shown to be indistinguishable from normal retinas both at 2 and 5 months of age. Despite this, the success of gene transfer to fully differentiated PR cells is far from assured. It is certain that a combination of slow onset of transgene expression from a rAAV vector and sub-retinal injection at P10 will result in production of peripherin-2 at a later time point than occurs in normal mice. The constant turn over of outer segments in retinas indicates that normal PR cells do not lose the ability to incorporate peripherin-2 into functional outer segments. It is therefore likely that the PR cells of young *Prph2*$^{Rd2/Rd2}$ mice will be able to construct outer segments after the expression of *peripherin-2*. However, it will be interesting to establish whether this ability changes over the course of the degeneration.

Will mice injected at P50 or P100 be able to produce outer segments as suggested by the models of Clarke *et al.* [217]? What is also unknown is whether the delivery of a normal copy of the *Prph2* gene and production of outer segments will slow or halt the progress of degeneration. This feature is relatively hard to assess, particularly if it is considered that only a percentage of the cells is transduced, and will be influenced by the time points chosen to sacrifice treated animals. In order to be certain that any effect on the rate of degeneration of PR cells is detected, assessment of cell number should be made over the period when cell loss is usually occurring most quickly i.e. over the first two months (see Fig. 5.3), and will therefore only involve animals injected before P40.

5.2 Production of AAV.RHO.PRPH2

5.2.1 Cloning of the pW7RhoPrph2 construct

The rAAV construct containing a copy of the *Prph2* cDNA driven by the bovine *rhodopsin* promoter was based on the construct pLitRhoEgfp generated during the cloning of the construct pD10RhoEgfp (section 3.3.3.1). The *Prph2* cDNA (1.1-kb sequenced PCR product) had previously been ligated into the polylinker site in LITMUS 28 (NEBiolabs) by S. Fauser to form the plasmid pLitPrph2. This plasmid was transformed into competent DH5α™ cells (section 2.2.1), and DNA was prepared from ampicillin resistant colonies (section 2.2.2). A schematic diagram of the subsequent cloning steps is shown in Figure 5.4. The plasmid pLitRhoEgfp was digested with *Xba*I (section 2.3.1), excising the *egfp* gene. The *Prph2* cDNA was excised from the plasmid pLitPrph2 by digestion with *Spe*I and *Avr*II. This fragment was ligated (section 2.4.4) into the *Xba*I sites within pLitRhoEgfp to generate the plasmid pLitRhoPrph2. Within the construct the untranslated region of the *rhodopsin* promoter extends to +72 bp. Thirteen bp from the 5′ untranslated region of the *Prph2* gene are also included. This plasmid was cut with *Afl*II and *Sna*BI to isolate the expression cassette, and then blunted with DNA polymerase I (section 2.4.1). This fragment was subcloned between the ITRs in the plasmid pD-10 (section 3.3.1), after pD-10 had been digested with *Eco*RV to remove the viral genome. The resulting plasmid was designated pD10RhoPrph2. This

plasmid was checked by single restriction enzyme digests with *Bgl*II, *Sac*II, *Sma*I and *Pac*I. The results of this are shown in Figure 5.5a.

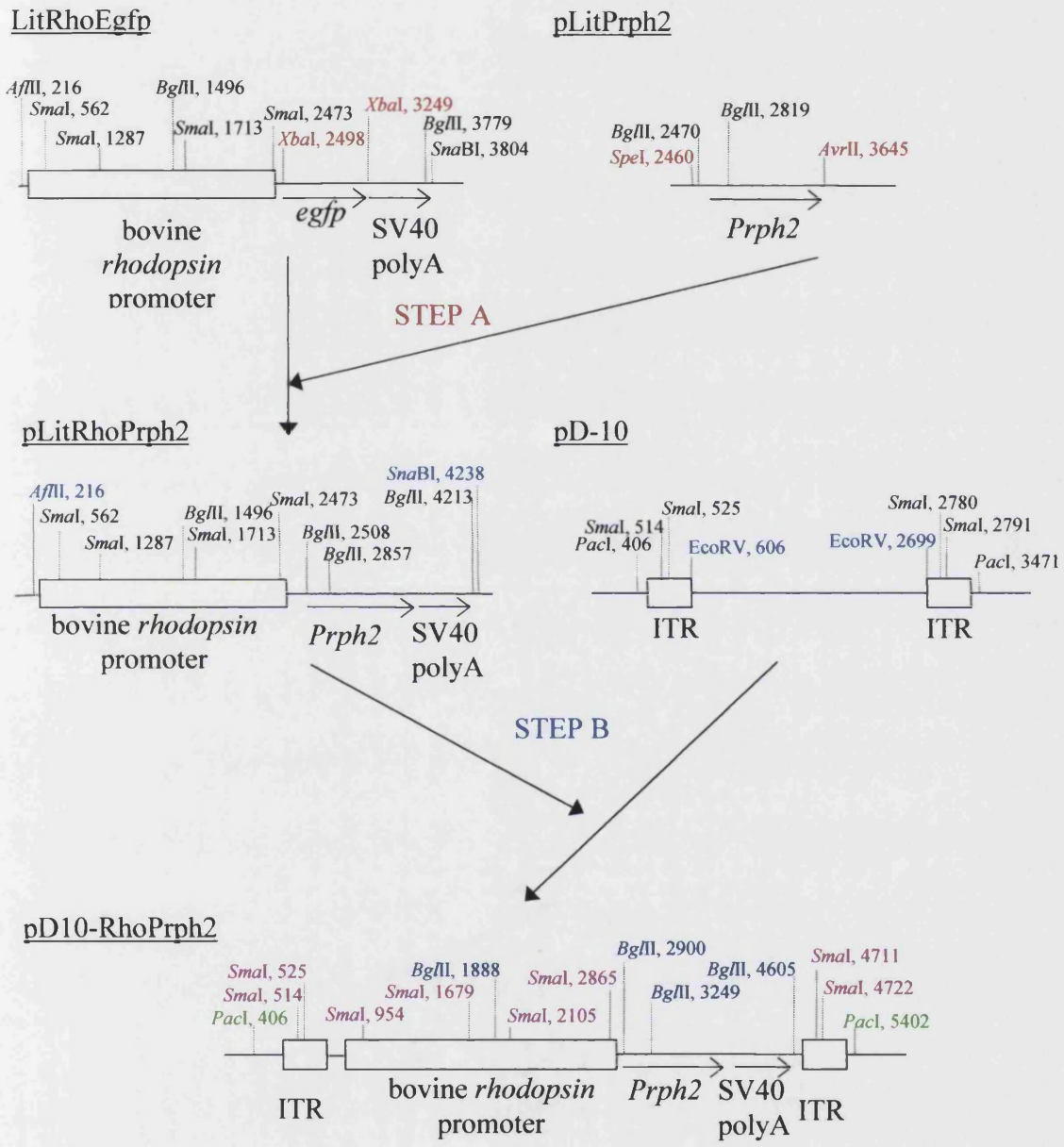

Figure 5.4 Cloning strategy for the production of pD10RhoPrph2.
Step A : the *Prph2* gene was removed from the plasmid pLitPrph2, by digestion with *Avr*II and *Spe*I, and ligated into the *Xba*I sites in pLitRhoEgfp (see Figure 3.14) to produce pLitRhoPrph2.
Step B : pLitRhoPrph2 was cut with *Afl*II and *Sma*BI, blunted, and ligated into the *Eco*RV sites within the ITRs of pD-10 to produce **pD10RhoPrph2**.
MCS is the multiple cloning site polylinker; SV40 polyA is the polyadenylation signal from SV40; *egfp* is the gene for Clontech's enhanced green fluorescent protein; ITR is the rAAV inverted terminal repeat; and *Prph2* is the gene for peripherin-2.

In the final cloning step (not shown in Fig. 5.4) the ITR-Rho-Prph2-ITR fragment was inserted into the amplicon plasmid pW7 (section 3.4.1). This was done by digestion of both plasmids with *Pac*I, purification of the appropriate fragments and ligation together. The final plasmid, pW7RhoPrph2, was checked by digestion with *Pac*I (Fig. 5.5b).

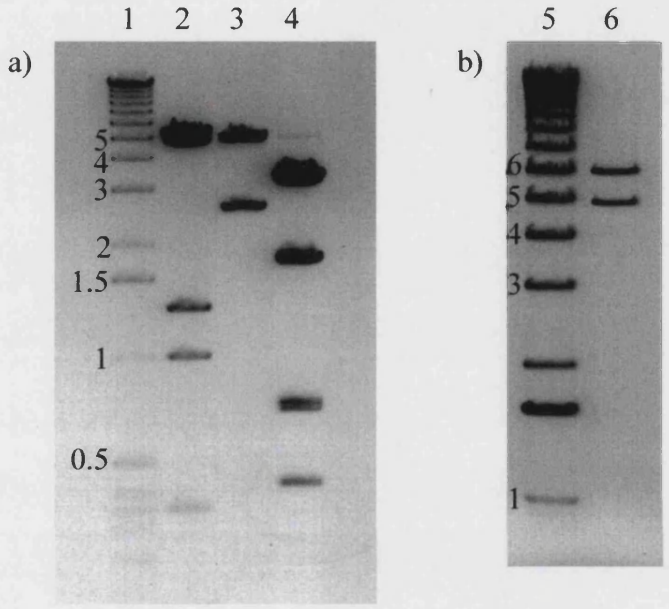

Figure 5.5a and b Confirmation of the plasmids (a) pD10RhoPrph2 (7654 bp) and (b) pW7RhoPrph2 (approximately 11 000 bp) by restriction enzyme digest analysis. Lanes 1 and 5 – marker (sizes in kb); Lane 2 - pD10RhoPrph2 digested with *Bgl*II, expected fragment sizes of 349 + 1012 + 1356 + 4937 bp; Lane 3 - pD10RhoPrph2 digested with *Pac*I, expected fragment sizes of 2658 + 4996 bp; Lane 4 - pD10RhoPrph2 cut with *Sma*I, expected fragment sizes of (2x11) + 426 + 429 + 725 + 760 + 1846 + 3446 bp; Lane 6 – pW7RhoPrph2 digested with *Pac*I, expected fragment sizes are 4996 bp and approximately 5900 bp.

5.2.2 Production of rAAV

Several batches of recombinant AAV were produced and purified by the methods described in sections 3.4.3 and 3.3.4 (full description in section 2.8). Each preparation of AAV.RHO.PRPH2 was titred by dot blot hybridisation of a probe encoding the *Prph*2 gene (section 2.9). The same virus batch was used throughout any one experiment.

5.3 Expression of *Prph2*, and localisation of peripherin-2, after sub-retinal injection of AAV.RHO.PRPH2 into 10-day old *Prph2* $^{Rd2/Rd2}$ mice

5.3.1 Method

One microlitre of AAV.RHO.PRPH2 at a titre of $1x10^{12}$ particles/ml was sub-retinally injected (section 2.10.3) into litters of 10-day old homozygous CBA *Prph2*$^{Rd2/Rd2}$. A bullous retinal detachment was produced, covering 30-40% of the fundus. For immunohistochemistry two mice were sacrificed each week, from the first to the eighth week following the injections. These eyes were orientated and processed for wax sectioning (section 2.11.1). Uninjected fellow eyes were used as untreated controls. Each treated eye was serially sectioned at 5 μm. Immunostaining for peripherin-2 (section 2.12.3) was performed on 5 to 10 consecutive sections from 5 different levels in each of these eyes. Immunofluorescent staining for peripherin-2 and rhodopsin (section 2.12.4) was performed on eyes taken six weeks post-injection, on slides adjacent to those which stained most strongly for peripherin-2. Four mice were sacrificed at 2, 4, and 6 weeks post-injection, two for transmission electron microscopy (TEM) and two for scanning electron microscopy (SEM). In addition, to investigate the long-term expression of the transgene, ten more animals were injected and sacrificed 18, 24, 32 or 42 weeks later. Eyes for TEM were processed (section 2.13.1) for sectioning. From each specimen serial semithin and ultrathin sections were cut at 10 different levels through the eye, and viewed (section 2.13.2). For SEM, eyes were processed (section 2.13.1) and viewed (section 2.13.3). For both TEM and SEM eyes from one month old, untreated *Prph2*$^{+/+}$, *Prph2*$^{+/Rd2}$, and *Prph2*$^{Rd2/Rd2}$ mice were used as controls.

5.3.2 Immunohistochemical detection of peripherin-2

Immunoreactivity for peripherin-2 was first detectable at two weeks post-injection, and became stronger and more extensive over the time course (Fig. 5.6). At this time there is a sharp demarcation in immunostaining between the treated and untreated areas of the retina (Fig. 5.7), allowing untreated parts of the eye to be used as internal controls. This staining was restricted to the regions adjacent to the inner segments, indicating that peripherin-2 localised to the correct layer of the retina. There was no evidence of inflammation on any of the slides studied.

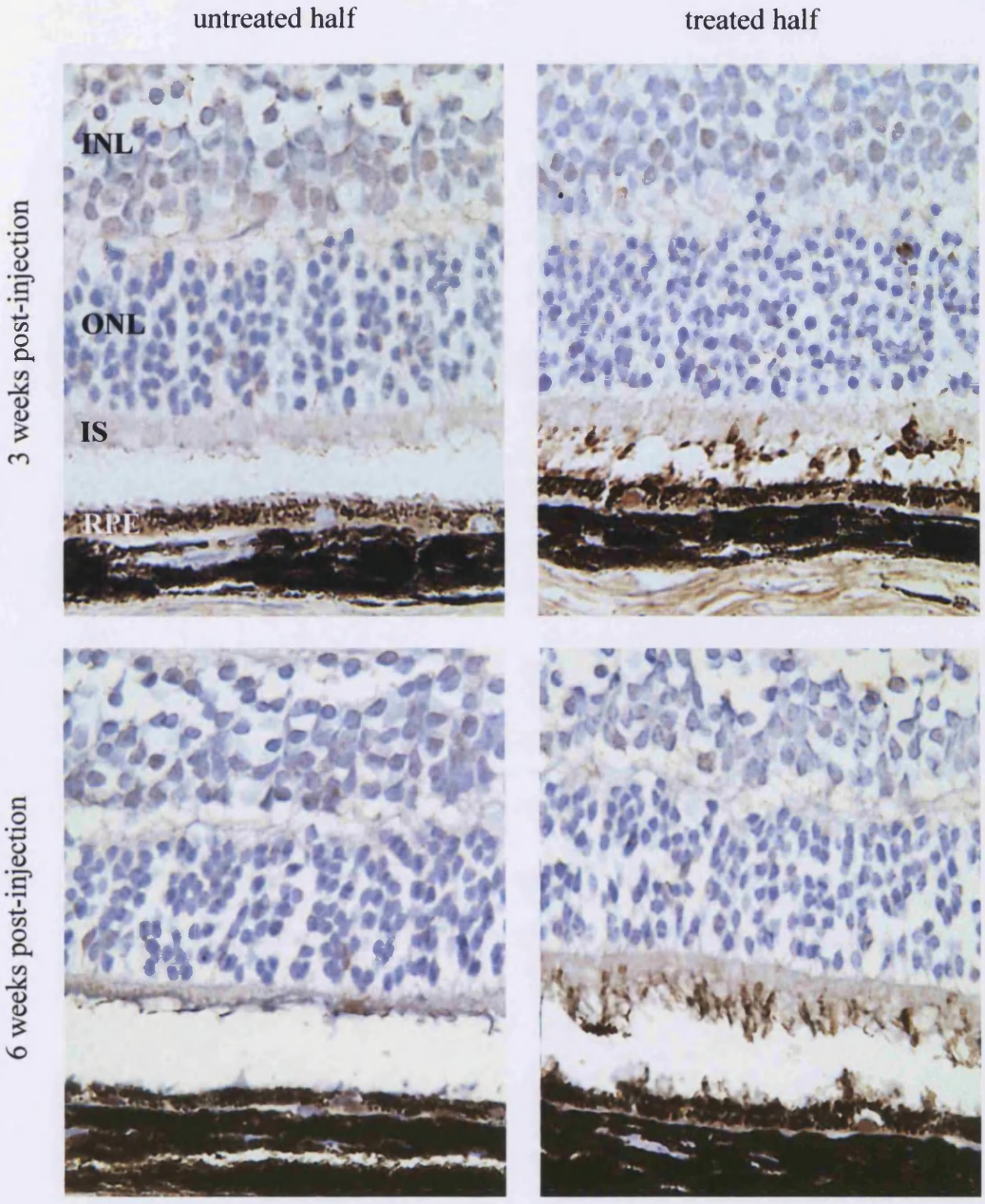

Figure 5.6 Comparison of *Prph2* expression in *Prph2*$^{Rd2/Rd2}$ mice 3 and 6 weeks after sub-retinal injection of AAV.RHO.PRPH2. Peripherin-2 was detected using a peripherin-2-specific antibody with DAB (brown staining) as a chromogen. The sections are counterstained with haemotoxylin. Although the ONL is thinner after 6 weeks than after 3 weeks, the absolute number of outer segments does not seem to be significantly reduced after 6 weeks and the putative outer segments appear to be longer. No immunoreactivity is discernable in the untreated areas. The retinal layers are marked on the first section; INL = inner nuclear layer; ONL = outer nuclear layer; IS = inner segments; and RPE = Retinal pigment epithelium.

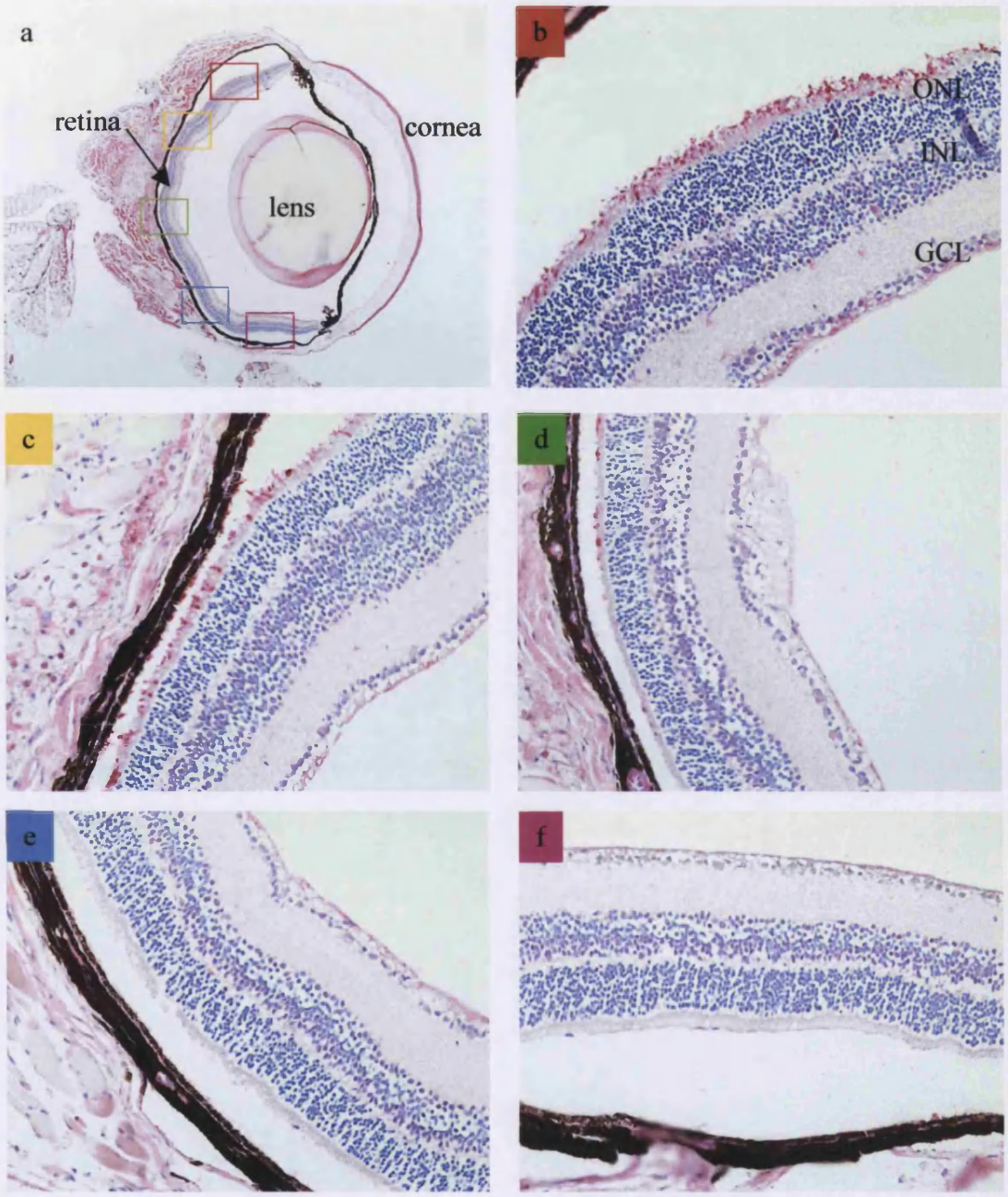

Figure 5.7 Immunohistochemical detection of peripherin-2 in a *Prph2*$^{Rd2/Rd2}$ mouse six weeks after sub-retinal injection of AAV.RHO.PRPH2. (a) Paraffin section of *Prph2*$^{Rd2/Rd2}$ mouse eye injected with AAV.RHO.PRPH2 in the superior half of the retina. Peripherin-2 as detected using a peripherin-2 specific antibody with Vector Red as a chromogen. Sections are counterstained with haematoxylin. The coloured rectangles in (**a**) represent the higher magnifications shown in (**b-f**). Note that peripherin-2 immunostaining is restricted to the upper half of the retina (**b-d**) and totally lacking in the lower aspect (**e** and **f**).

5.3.3 Immunohistochemical co-localisation with rhodopsin

Immunofluorescent staining with antibodies against rhodopsin shows that this protein co-localises with peripherin-2 to the layer between the inner segments and the RPE (Fig. 5.8). Moreover, in the areas where peripherin-2 staining is strongest there is also a larger amount of rhodopsin staining in comparison to the non-injected half of the same eye.

5.3.4 Ultrastructural analysis of treated eyes

Transmission electron microscopy revealed that the peripherin-2 staining regions of the treated eyes contained structures which are composed of membranous discs enclosed in a cell membrane, and are connected to the inner segment of PR cells through a cilium. These outer segment-like structures are not as abundant as those seen in either wild type or heterozygous retina (Fig. 5.9). However, a proportion of them closely resemble the elongated structure of wild type outer segments. In comparison to heterozygous animals the outer segments of treated mice contain fewer whorls and vesicular structures. Evidence of the presence of interactions between the outer segment and the RPE can also be found in treated areas of retina. The outer segments interdigitate with the RPE microvilli (Fig. 5.10) and phagosomes in the RPE of treated animals appear to contain engulfed material from disc shedding. These features are a preliminary indication that some level of normal function has been restored by the presence of newly formed outer segments.

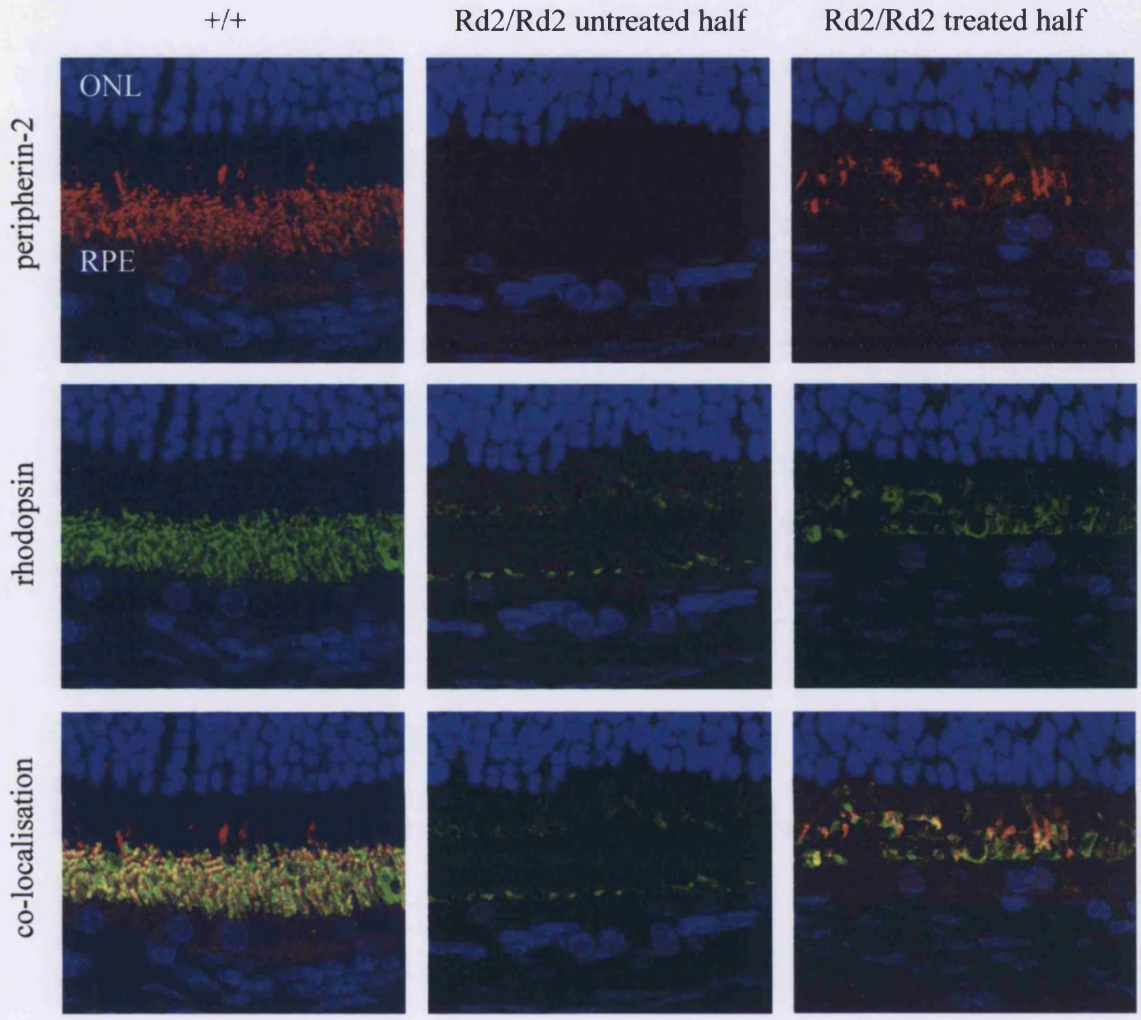

Figure 5.8 Co-localisation of peripherin-2 and rhodopsin in *Prph2*$^{Rd2/Rd2}$ mice 6 weeks after sub-retinal injection of AAV.RHO.PRPH2. Confocal images of immunofluorescence from double-labelled sections using a peripherin-2-specific antibody (red) and a rhodopsin-specific antibody (green). Sections are counterstained with DAPI (blue). Extensive peripherin-2 and rhodopsin immunostaining is observed in the outer segments of wild-type mice, whereas there is no peripherin-2 and little rhodopsin immunostaining in the untreated portion of injected *Prph2*$^{Rd2/Rd2}$ mice. In the treated area, where peripherin-2 is expressed, a substantial increase in the concentration of rhodopsin is observed.

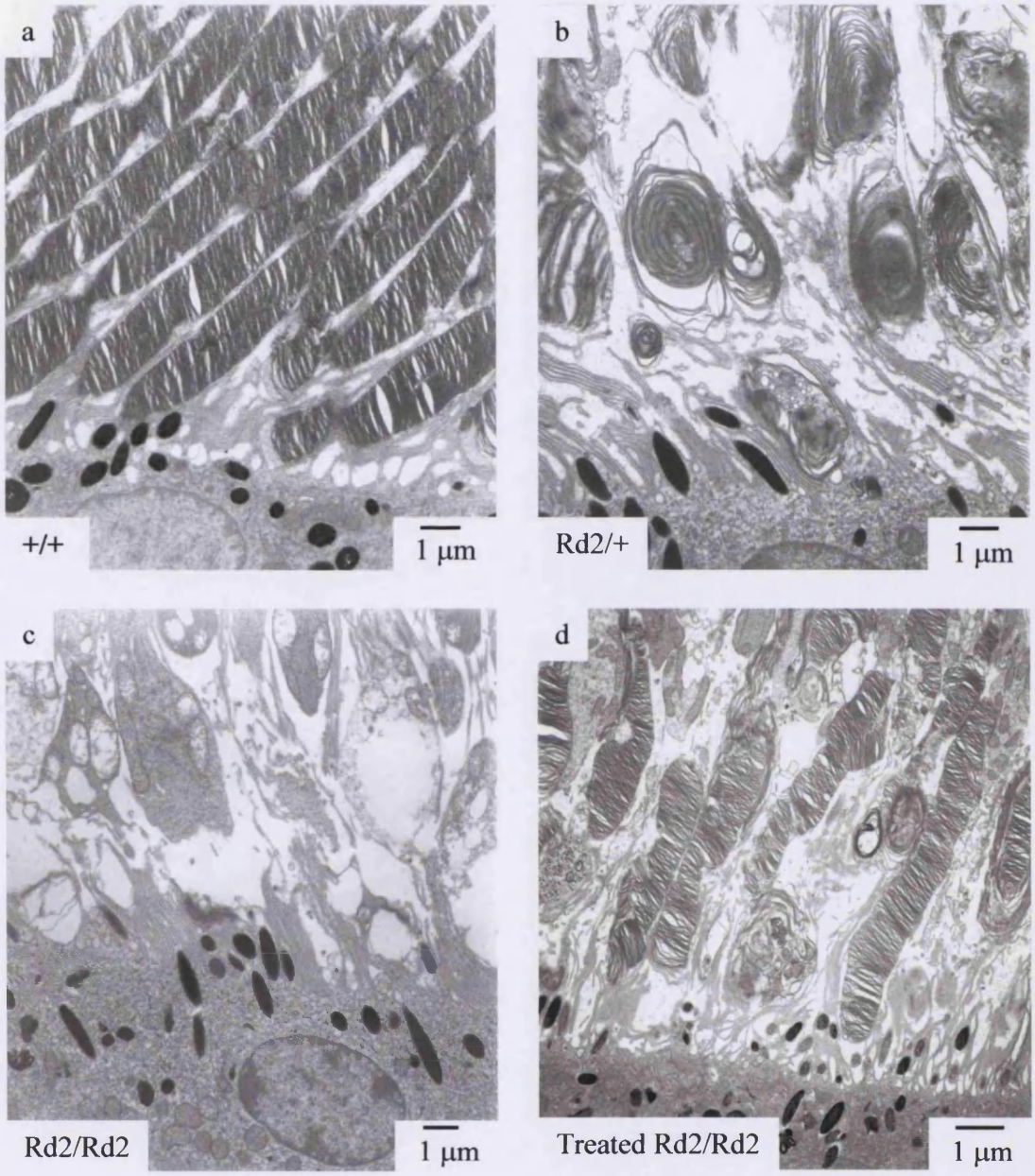

Figure 5.9 Comparison of TEM images of the outer retina of treated *Prph2*$^{Rd2/Rd2}$ mice with images from the retinas of untreated *Prph2*$^{Rd2/Rd2}$, *Prph2*$^{Rd2/+}$ and wild type mice. All images are taken in the region between the RPE and the PR cell bodies and inner segments. **(a)** Image of the densely packed outer segments of a wild-type mouse. (**b**) Disc whorls seen in a *Prph2*$^{Rd2/+}$ mouse retina. (**c**) Degenerating inner segments in an un-treated *Prph2*$^{Rd2/Rd2}$ mouse. (**d**) Outer segment structures seen in a treated *Prph2*$^{Rd2/Rd2}$ mouse retina, 6 weeks post sub-retinal injection.

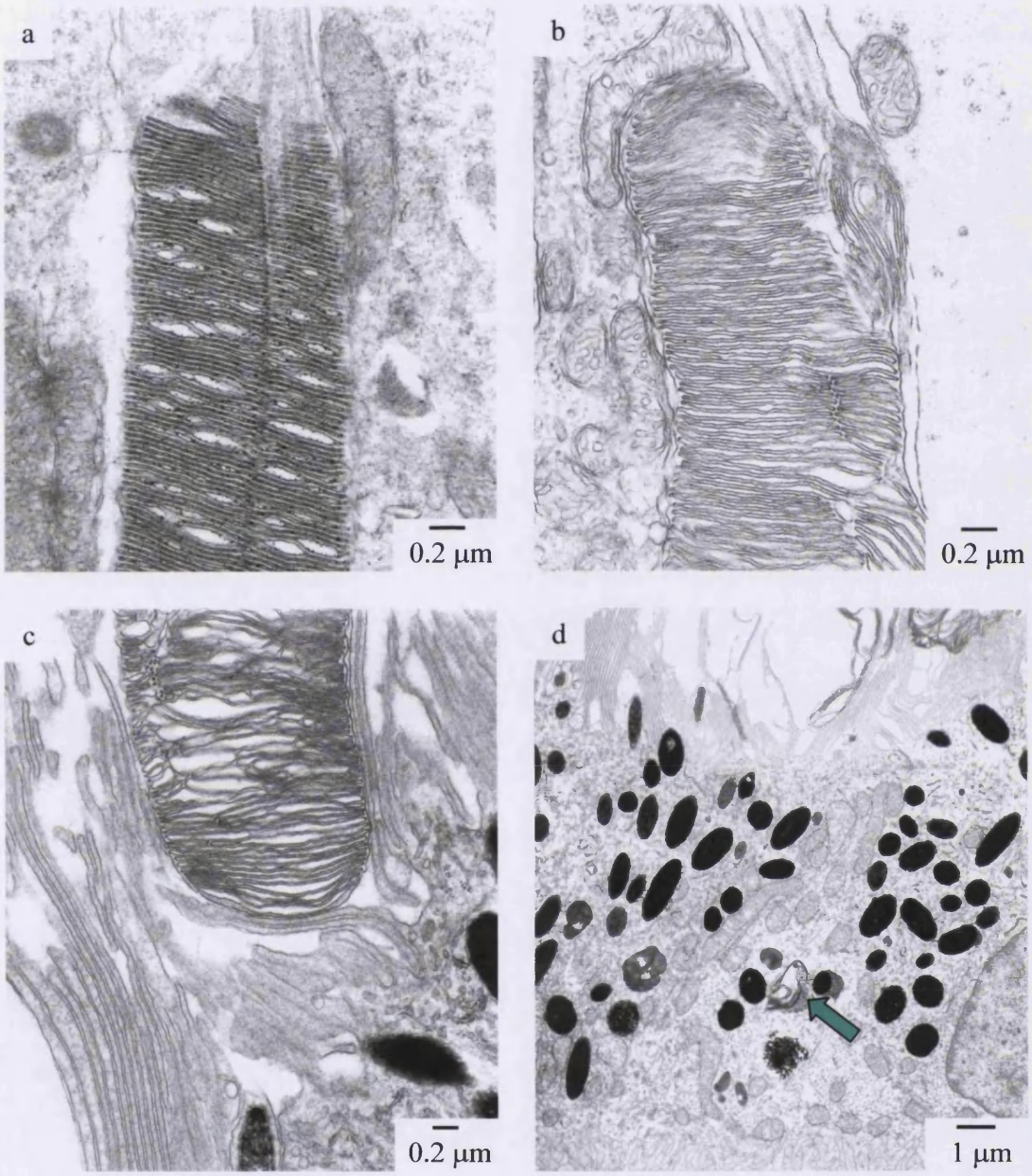

Figure 5.10 Comparison of detailed TEM images of the outer retina of treated *Prph2*$^{Rd2/Rd2}$ mice with those from a normal mouse. (**a**) Outer segments of a wild type animal with the membrane discs evolving from the cilium. (**b**) Newly formed PR outer segment in injected area of a treated *Prph2*$^{Rd2/Rd2}$ mouse. These outer segments can be seen to be interdigitating with the apical processes of the RPE cells (**c**). Moreover the RPE cells adjacent to transduced PR cells contains phagosomes with injected disc material (arrow) (**d**).

Following removal of the retina, it is possible to examine the surface of the outer retina, which is normally in contact with the RPE. A scanning electron microscope was used to determine the extent and shape of the newly formed outer segments in treated mice. As shown in Figure 5.11 in the untreated parts of the *Prph2*$^{Rd2/Rd2}$ retina, bare cilia are visible projecting from the inner segments. In comparison, in the treated areas the cilia are largely obscured by the presence of the outer segments. These images show, in accordance with the TEM results, that the shape of these outer segments is very variable. Most are typically more spherical than the wild type and only a proportion have the elongate, worm-like appearance of normal rods. Scanning electron microscope images can also be utilised to make an approximate estimate of the rate of transduction in the injected area. Assuming that the outer segment structures do not obscure more than one cilium, the total number of PR cells in any one image can be counted by adding the number of visible cilia to the number of outer segment structures. The percentage of cells with outer segments can then be calculated. By this method the percentage of *Prph2*-positive cells, at two weeks post injection, in the area of sub-retinal detachment is between 30 and 40%. This is comparable to the figures gained in section 4.7 where the highest transduction rates have been estimated following injection of AAV.RHO.EGFP into normal 10-day old pups.

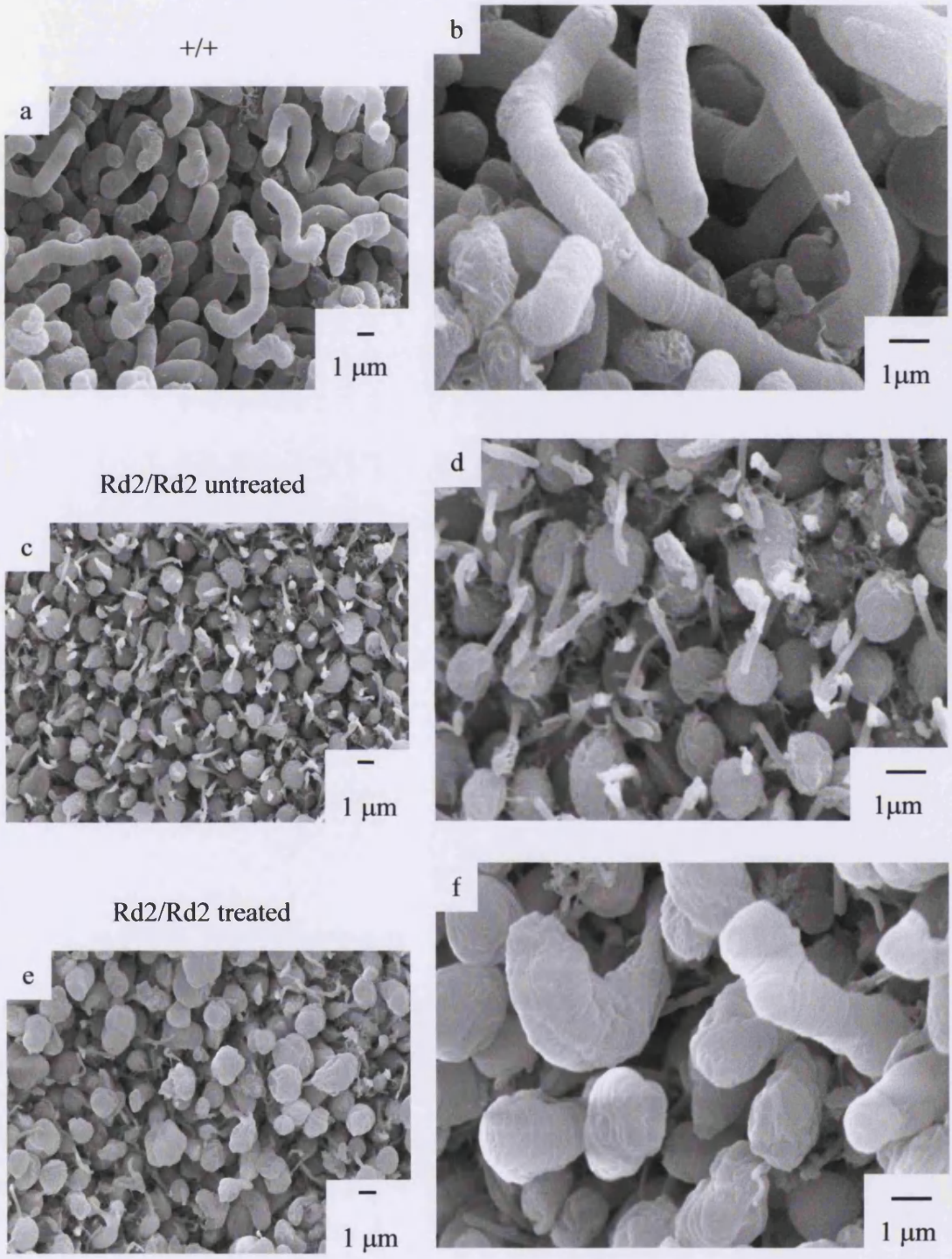

Figure 5.11 Comparison of SEM images of the outer surface of the retina of wild type, *Prph2*$^{Rd2/Rd2}$ untreated and *Prph2*$^{Rd2/Rd2}$ treated mice. Views of the wild type neuroretina (**a** and **b**), show the smooth worm-like appearance of normal outer segments. In the untreated *Prph2*$^{Rd2/Rd2}$ retina (**c** and **d**) there are no outer segment structures, and inner segments and projecting cilia are visible. In contrast, in treated *Prph2*$^{Rd2/Rd2}$ retina (**e** and **f**), approximately one-third of the inner segments show attached outer segments. Images are shown at lower power on the left hand side and at higher magnification on the right hand side.

Scanning electron microscope images also show clearly that the newly induced outer segments from eyes taken 2 weeks after injection have a much better shape than those from eyes taken 4 and 8 weeks post injection (Fig. 5.12). In general newly formed outer segments are more elongate. Over time they appear to become thicker and more disorganised.

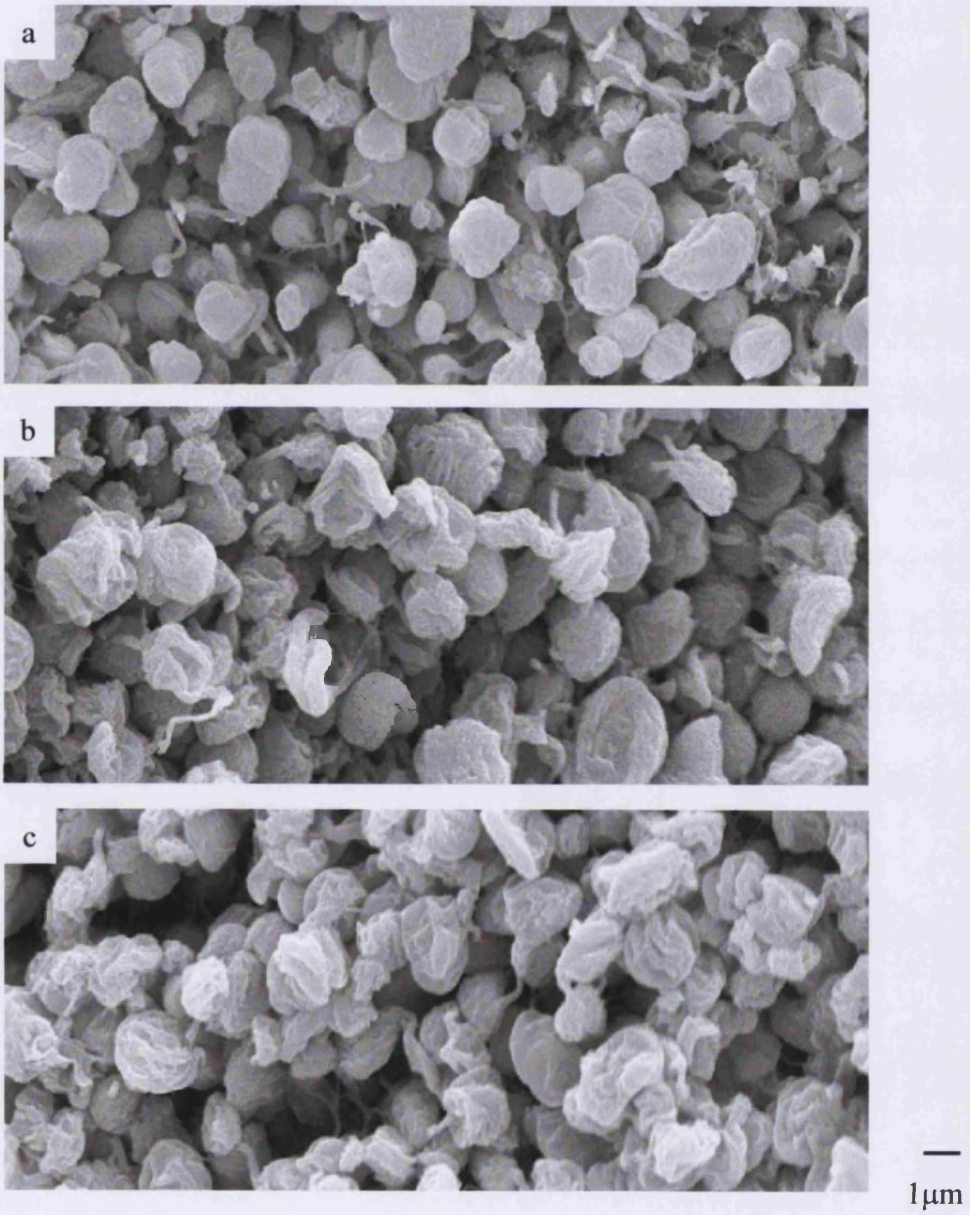

Figure 5.12 SEM images of the neuroretina of treated *Prph2*$^{Rd2/Rd2}$ mice, showing the deterioration of the form of the induced outer segment structures over time. The outer segment structures seen 2 weeks after injection (**a**) are relatively smooth, but it appears that over time, they become more disorganised so that at 4 weeks (**b**) and 8 weeks (**c**) after injection they are progressively more irregular.

5.3.5 Long-term expression of *Prph2*

Consistent with the long-term expression of *egfp* after sub-retinal injection of AAV.RHO.EGFP (section 4.7), expression of *Prph2* appears to persist through all of the time points studied since outer segments are still observed up to 42 weeks after injection (Fig. 5.13). However, in general there are fewer outer segment structures at these time points than at 3 or 6 weeks after injection. The form of these 'old' structures is not as good as those that have been newly produced, the discs being less well aligned in their stacks.

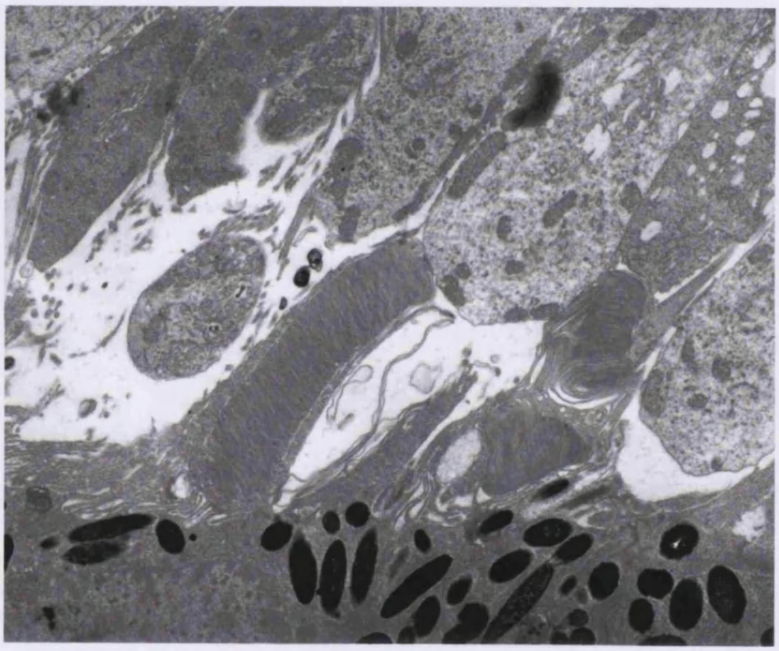

Figure 5.13 TEM image showing outer segment structures in the retina from a *Prph2*$^{Rd2/Rd2}$ mouse 42 weeks after sub-retinal injection of AAV.RHO.PRPH2. The animal was injected at P10.

5.4 Induction of outer segments in older *Prph2*$^{Rd2/Rd2}$ mice

5.4.1 Method

One microlitre of AAV.RHO.PRPH2 at a titre of $1x10^{12}$ particles/ml was sub-retinally injected (section 2.10.2 and 2.10.3) into homozygous CBA *Prph2*$^{Rd2/Rd2}$ mice of various ages to investigate whether outer segments could be induced in older animals. Three mice were injected at day P5, 4 at P10, 3 at P20, 3 at P40, 2 at P80 and 4 at P95. All mice were sacrificed 32 days post-injection. In total, 25 untreated age matched *Prph2*$^{Rd2/Rd2}$ mice were also analysed as controls. The thickness of the outer nuclear layer and the quality of the outer segment structures in treated areas were assessed by semithin sectioning and TEM. Mice were killed by cervical dislocation, and the eyes processed and sectioned (section 2.13.1 and 2.13.2).

5.4.2 Results

Sub-retinal injection of *Prph2*$^{Rd2/Rd2}$ mice at P10 results in the induction of a number of fairly well organised outer segments as demonstrated in section 5.3.3. As shown in Figure 5.14 the age of the animal at the time of injection appears to have a substantial effect on the quality and number of outer segments induced. While animals that have been treated when they are older and in a relatively more advanced state of degeneration are still able to produce outer segments, these structures are, in general, fewer and less well organised than those induced in younger animals. Strong expression of the *egfp* reporter gene after sub-retinal injection of AAV.RHO.EGFP into P90 *Prph2* $^{Rd2/Rd2}$ mice has already been demonstrated (section 4.7), indicating that the PR cells can still be transduced and that the *rhodopsin* promoter is still functional in these cells at these later time points.

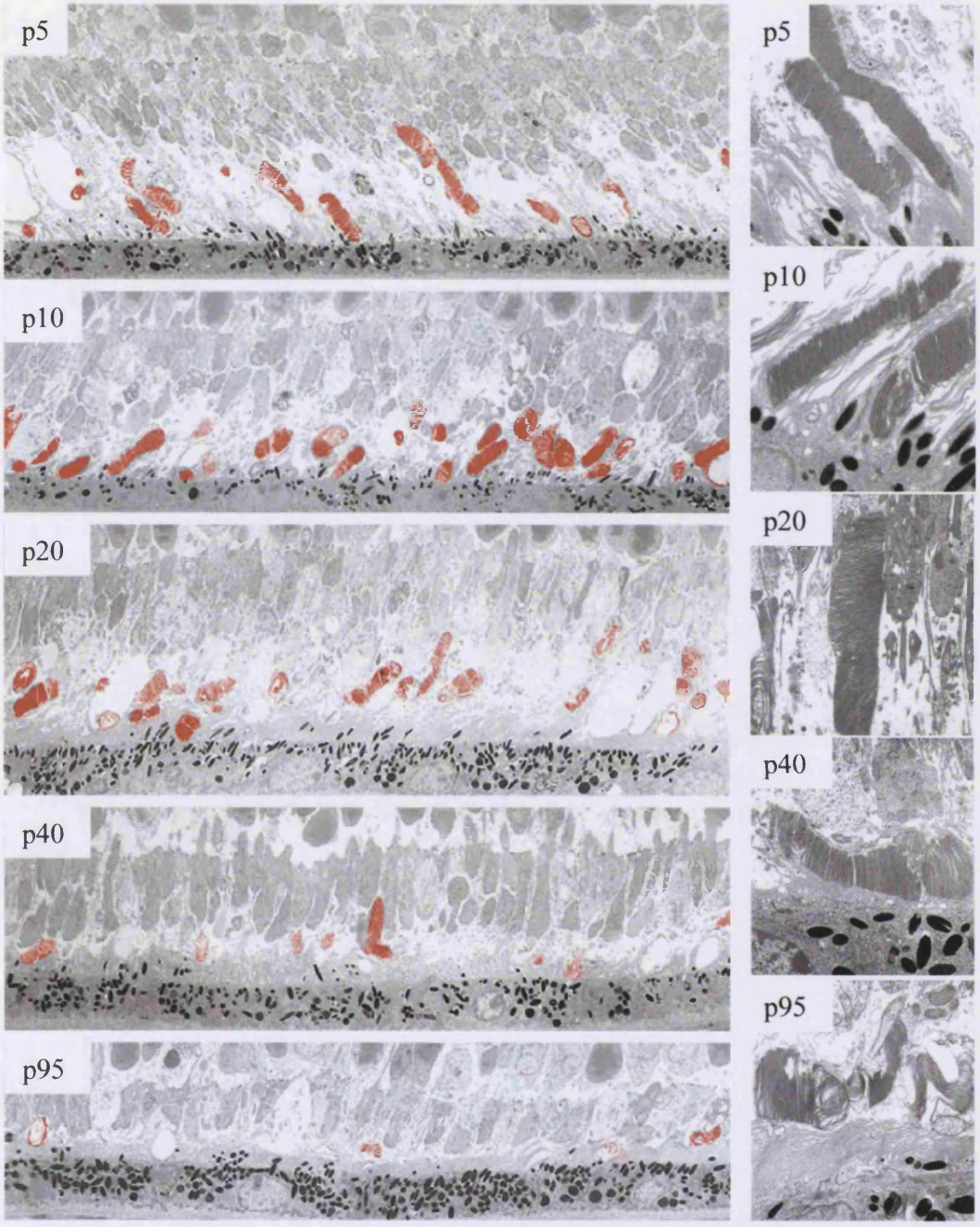

Figure 5.14 TEM analysis of *Prph2*$^{Rd2/Rd2}$ mouse retina after sub-retinal injection of AAV.RHO.PRPH2 at five different time points. Representative areas of retina are shown for mice injected at P5, P10, P20, P40, and P95, and sacrificed 32 days later. The outer segment structures seen in the micrographs in the left hand column are highlighted in red. The right hand column of pictures shows some higher power images of the outer segments induced at the different time points. There is a visible decrease in the quality and number of the outer segments generated after injection into older animals.

5.5 Assessment of the rate of degeneration in the injected areas of treated eyes

5.5.1 Method

In order to assess whether the rate of photoreceptor degeneration was affected in the treated areas of retina, sections were taken from the P5, P10, P20 and P40 eyes injected in experiments described in section 5.4. In addition to this a total of 25 untreated age-matched control *Prph2* $^{Rd2/Rd2}$ mice were also analysed. The method for assessment is shown in Figure 5.15. For each eye ten semithin and six ultrathin sections were cut (section 2.13.2) at 10 different levels through the whole horizontal extension of each retina. Semithin sections were stained and images captured with a digital camera on a light microscope. Each ultrathin section was also stained and assessed for outer segment induction and matched to the appropriate semithin picture. For measurement purposes only sagitally oriented central sections through the optic nerve head (ONH) were used. On each side of the ONH at three different points (400 μm, 1000 μm and 1600 μm from the edge of the ONH) a high power field of the outer nuclear layer (ONL) was captured with a digital camera, and the area of the ONL measured using Image Pro Plus 4.1 (Media Cybernetics, MD, USA). In order to determine the average thickness of the ONL the area was divided by the length of the section (between 130 to 150 μm) following the contour of the outer limiting membrane (Fig. 5.15). Three to six different eyes per time point were then averaged and plotted against the untreated controls.

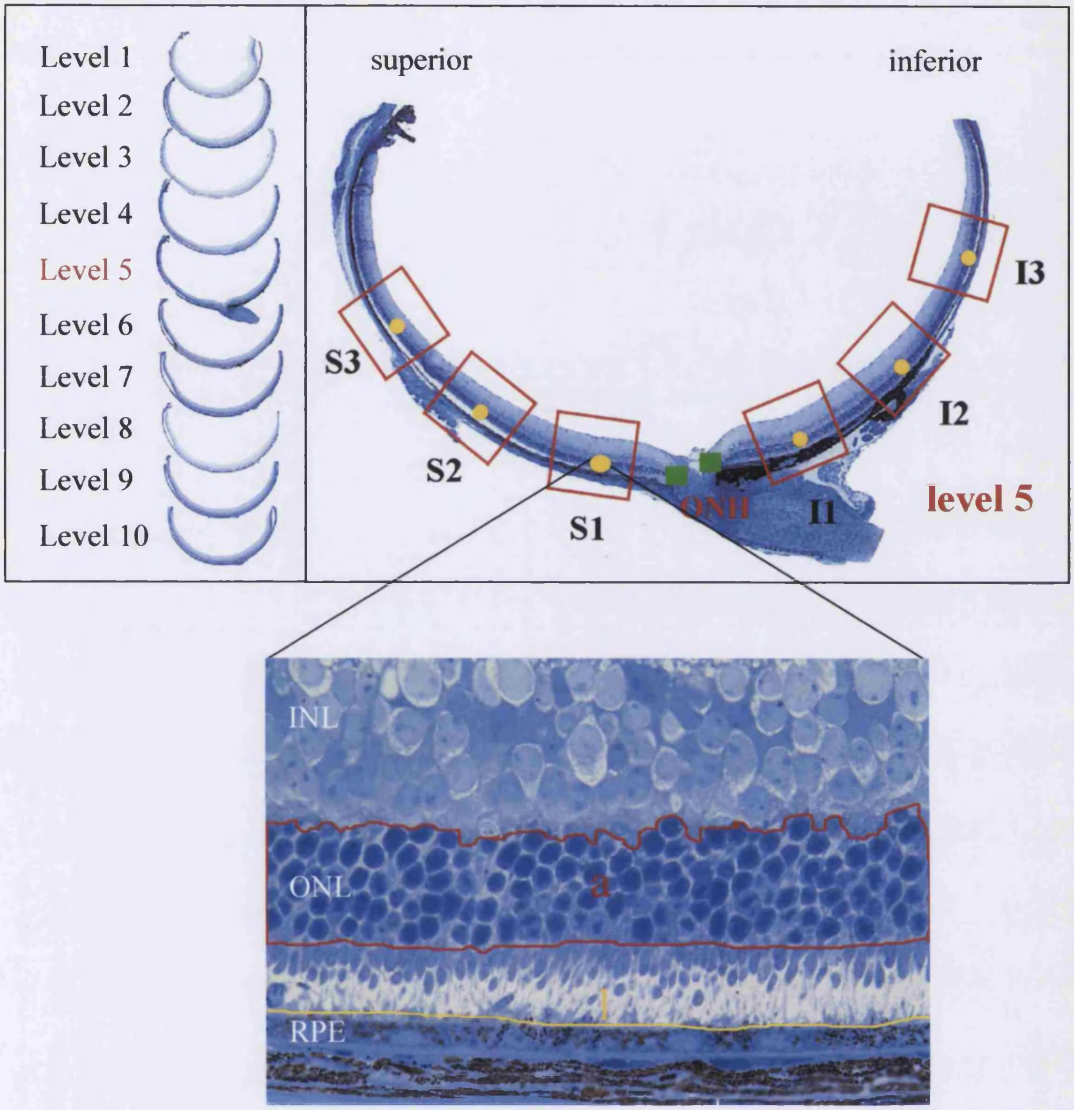

Figure 5.15 Method for assessing outer nuclear layer (ONL) thickness in treated and control animals. All eyes were serially sectioned with sections taken at 10 different levels through the horizontal extension of each eye. For measurement purposes, only sagitally orientated central sections through the optic nerve head (ONH) were used (i.e. in this example level 5). On each side of the ONH at three different points (S1, S2 and S3 in the superior half and I1, I2 and I3 in the inferior half) a high power image of the ONL was captured with a digital camera and the area (a) of the ONL measured using a computer program. In order to determine the average thickness of the ONL the area was divided by the length of the section (l) following the contour of the outer limiting membrane. This value was between 130 – 150 µm.

5.5.2 Results

The complete data sets for the average thickness of each eye examined, at points S1, S2, S3, I1, I2, and I3, are shown in Appendix I. As shown in Table 5.1, the values at each of these points for the treated and age matched control eyes have been averaged across several eyes. Paired t-test between the treated and control columns of numbers at each time point revealed no significant difference ($p > 0.05$) in average thickness of the retina, even when the mice have been treated at P5 or P10. Since every sub-retinal injection is in approximately the same place in the superior half of the eye it might be expected that a particular retinal location (e.g. S3) might show a difference in thickness between treated and control animals. However, when paired t-tests were performed between treated and control rows of numbers at each retinal location (across all time points) no significant difference ($p > 0.05$) was detected. The decrease in the average thickness of the outer nuclear layer for control and treated eyes is shown in Figure 5.16.

Point on retina	**Average of eyes injected at P5**		**Average of eyes injected at P10**		**Average of eyes injected at P20**		**P value**
	treated	control	treated	control	treated	control	
	(n = 3)	(n = 3)	(n = 4)	(n = 3)	(n = 3)	(n = 4)	
S3	37.17	37.73	32.29	34.01	26.43	28.53	**0.09**
S2	38.78	39.71	37.75	35.36	30.82	30.58	**0.62**
S1	42.45	41.87	32.21	39.04	33.26	31.74	**0.61**
I1	43.14	43.75	38.72	42.93	36.69	35.88	**0.47**
I2	41.82	42.98	38.60	39.97	34.66	34.87	**0.12**
I3	41.01	40.55	34.51	37.15	34.76	33.38	**0.85**
P value	**0.26**		**0.11**		**0.64**		

Table 5.1 Average thickness of the retina for all treated and age-matched controls over six retinal locations (S1-S3, and I1-I3). The number of eyes (n) analysed per time point is shown in each column. At each time point paired t-tests were performed between the treated and control sets of data. There was no significant difference ($p > 0.05$) between the treated and age-matched controls at any of the time points studied or across the points on the retina.

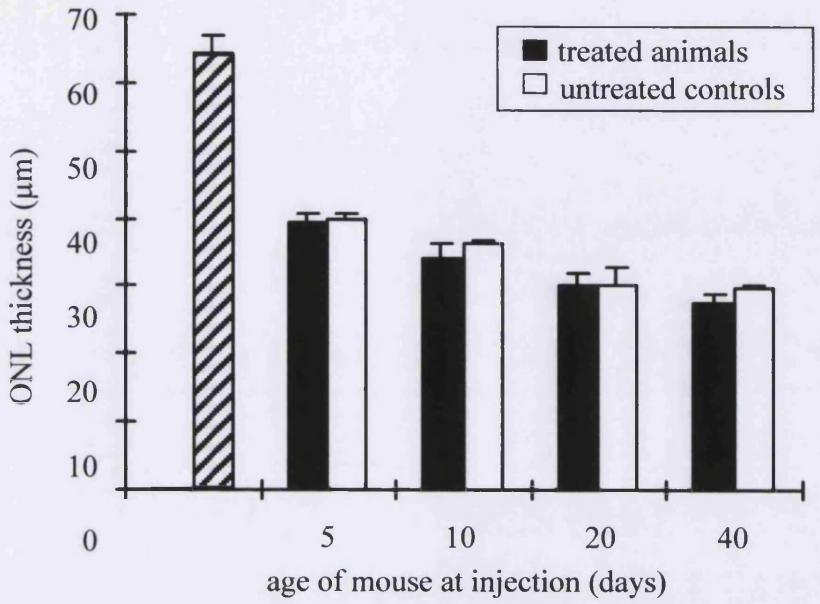

Figure 5.16 The average outer nuclear layer (ONL) thickness in *Prph2*$^{Rd2/Rd2}$mice 32 days after injection. The average superior ONL thickness is shown in animals injected at P5, P10, P20 or P40, and sacrificed 32 days later (black bars). The average thickness for age-matched control mice (white bars) is also shown. The decrease in thickness in control and treated animals is well matched. Each time point represents data from three to six eyes. The average superior ONL thickness for untreated 10-day old *Prph2*$^{Rd2/Rd2}$mice is shown as a reference (hashed bar).

It was concluded that the current treatment does not appear to increase or decrease significantly the rate of PR cell loss, despite the partial correction of the ultrastructural defect in individual transduced cells.

Calculations of the mean and the standard error for control and treated eyes (Appendix I) show that there is substantial variation in the average thickness of the outer nuclear layer between animals of the same age, indicating variation in the rate of degeneration. As a result, a small increase or decrease in thickness may not be revealed using this method. Assuming the rate of degeneration is the same for both eyes in the same animal it would be better, in future studies, to utilise untreated left eyes as the control instead of eyes from age-matched animals.

5.6 Discussion

In these experiments we show that we are able to deliver and express a copy of *Prph2* in the PR cells of *Prph2*$^{Rd2/Rd2}$ mice, and obtain the correct localisation of peripherin-2 in these PR cells. Furthermore, the production of peripherin-2 results in the generation of outer segments that would otherwise be absent in these animals. This is the first time that a complex ultrastructural defect has been partially corrected with gene therapy. However, we have not been able to show that the rate of degeneration is slowed in treated areas of the retina. The final section of this chapter will therefore discuss the possible reasons why the treatment does not appear to have a significant impact on cell death.

The possibility that the positive effects of treatment are outweighed by physical damage to the retina, caused by the process of sub-retinal injection and detachment, cannot be excluded. Work within our laboratory has shown that injection of both PBS and rAAV into normal adult mice does not result in a loss of PR cells except in the area directly in contact with the needle. However, this sort of investigation, which involves counting the number of apoptotic cells and observing rhodopsin relocation in the region of detachment, is more difficult in *Prph2*$^{Rd2/Rd2}$ mice since these processes are already occurring as part of the degeneration. More in depth studies using semithin sections and measuring the average thickness of the outer nuclear layer take a long time and have not yet been completed, but this aspect of treatment is being further investigated.

A second possible cause for the continued degeneration of PR cells after treatment is the relatively late onset of *Prph2* expression. Whilst it is unlikely that all of the PR cells become committed to the pathway of degeneration during the first month of life, the later than normal onset of *Prph2* expression in treated retinas cannot be overlooked. For those mice injected at P10 significant expression of *Prph2* does not occur until approximately P24, 6 days after the peak of apoptosis. During this period there are changes within the retina: for example microglial cells are up regulated, which may predispose PR cells to apoptosis, imposing a limit to what our treatment can achieve. If this is the case then an alternative approach may be necessary. Sub-retinal injection before postnatal day 10 has several major drawbacks. The needle is proportionately

larger in size in these smaller pups and therefore causes direct physical trauma to a larger area of the developing retina. In addition, the smaller size of the eye makes injection technically more difficult and therefore the success rate is reduced. The relatively long lag phase before the onset of expression of the transgene is an inherent property of the rAAV vector, the only vector system, thus far, that has shown reliable transduction of PR cells *in vivo*. Studies conducted in Chapter 4 have shown that by increasing viral titre transduced cells can be detected much earlier and, therefore, higher titre AAV.RHO.PRPH2 might be used to gain earlier expression of *Prph2*. However, increased viral load may be toxic to the PR cells or RPE. Despite these drawbacks these attempts at gene therapy are still useful; the treatment of the *Prph2*$^{Rd2/Rd2}$ mouse is not a goal in itself. Larger animal models and humans show a much slower rate of retinal degeneration to which expression achieved through rAAV vectors will probably be better suited.

Another possible cause why the rate of degeneration is not slowed could be related to the low proportion of the PR cells that are transduced. The immunostaining for peripherin-2 shows a sharp demarcation between the cells with outer segments staining positive for peripherin-2 and those that are negative. In addition the SEM pictures suggest a relatively low transduction rate, assessed by counting outer segment structures, which is approximately 10% of the entire retina. The widespread expression of *egfp* observed in Chapter 4 only occurs after several months. If changes in the microenvironment of the retina are brought about by the release of pro-apoptotic factors, or the withdrawal of the neurotrophic factors, by degenerating PR cells a lethal environment may exist for the transduced, inherently viable PR cells. In this situation a threshold level of transduction might need to be reached before the rate of degeneration can be successfully slowed. The rate of transduction could be increased through the simultaneous injection of different areas of the retina, and/or multiple injections over several time points in a single area.

A fourth possible reason why degeneration is not slowed may be that an incorrect expression level of *Prph2* is damaging to transduced PR cells. We have observed that there is a variation in strength of EGFP fluorescence in transduced PR cells, with cells closer to the site of injection fluorescing brighter than those that are further away

(section 4.2 and 4.3). This is probably due to the different copy numbers of *egfp* within these cells that results from infection with multiple viral particles. The variation in the outer segment structures observed in these experiments might therefore be related to the variation in *Prph2* expression levels achieved after injection with AAV.RHO.PRPH2. At all stages of the study individual PR cells with well organised outer segments can be found, indicating that some of the transfected cells may be expressing *Prph2* to appropriate levels. Those outer segments with whorls may be considered to be due to under-expression, as is the case for heterozygous animals, whereas those with very tightly packed discs would be due to over-expression. However, the change in shape of outer segments over time, becoming less structured than newly formed ones, hints that there may be problems with the long-term expression levels of *Prph2*. An obvious reason could be over-expression as a result of *rhodopsin* promoter directed *Prph2* expression, and multiple transfections of the same cell. This is in line with transgenic studies in which the ultimate consequence of *Prph2* over-expression – more than 4 times the endogenous level – is PR cell loss (G. Travis – personal communication). A down regulation of *Prph2* is another possible cause for the loss of PR cell morphology. The mechanism through which a PR cell controls levels of peripherin-2 is not known and it is not clear whether the *Prph2* transgene is subject to the same control mechanisms as the endogenous gene. Our work (section 4.7) has shown that the *rhodopsin* promoter from AAV.RHO.EGFP is still active after injection into *Prph2*$^{Rd2/Rd2}$ mice at P90. Despite this it is clear from the work of Nir *et al.* [199] that levels of rhodopsin in the degenerating retina are initially reduced as a result of a lack of synthesis and not a down regulation of transcription. The same mechanism may also reduce the levels of peripherin-2 at later time points.

Piecing together the requirements for a successful and complete rescue of the *Prph2* $^{Rd2/Rd2}$ phenotype is difficult in the absence of knowledge of the processes that are occurring in the degenerating retina, but it is clear that there is much potential for future work. As previously mentioned, multiple injections could be performed on the same mouse in different areas of retina to increase the number of transduced PR cells. This treatment may also be combined with other forms of therapy. Although the mechanism through which intra-ocular neurotrophic factors affect the rate of degeneration has not been elucidated, there is some evidence (see section 1.6.3.2) to suggest that these factors may be able to support PR cells and prevent their commitment to apoptotic pathways.

Their use both before sub-retinal injection of rAAV and after may aid the survival of treated PR cells. The effect of different promoters for the expression of *Prph2* should also be examined. Work is ongoing to develop inducible promoter systems that may allow further dissection of the role of over-expression of *peripherin-2* in degeneration. Ultimately these inducible systems are likely to provide the most precise way of regulating gene expression.

Acknowledgements

I would like to acknowledge the work of Mahesh de Alwis in producing the recombinant virus and of Jim Bainbridge in performing the sub-retinal injections. Peter Munro cut all the semithin and ultrathin sections, and prepared SEM specimens with the assistance of Robin Howes. Wax sectioning and immunostaining were performed by Geno Sarra who also conducted the analysis on the semithin, TEM and SEM sections.

6

Electroretinography

The aims of the work described in this chapter are the following:

- To establish a system for obtaining accurate and reproducible ERG recordings from mice within the laboratory,
- To compare the ERG responses from untreated and treated *Prph2*$^{Rd2/Rd2}$ mice in order to determine whether the ultrastructural improvement in treated mice results in improved photoreceptor function.

6.1 Introduction

In Chapter 5 experiments were described in which the treatment of the *Prph2*$^{Rd2/Rd2}$ mice with gene therapy resulted in the production of outer segment structures. The presence of these structures, which are normally absent in *Prph2*$^{Rd2/Rd2}$ mice, suggests that the treatment may also result in an improvement in the level of photoreceptor function. Therefore the next step in the evaluation of the treatment is to establish whether this partial rescue of the histological phenotype is associated with an increase in retinal function. As described in Chapter 1 (section 1.1.2) electroretinography (ERG) is frequently used in the clinics in both the diagnosis and monitoring of retinal disorders, providing information on the ability of the photoreceptor cells, and other layers of the retina, to respond to the stimulus of light. Therefore, although it cannot be used to determine whether the animals have improved vision, ERG is a suitable tool to begin assessing retinal function in the treated eyes.

Reuter and Sanyal [221] first examined the ERG responses from *Prph2* $^{Rd2/Rd2}$ mice in 1984. They showed that in spite of the absence of outer segments small ERG responses were still detectable in these animals. They attributed this to phototransduction brought about by the small amount of rhodopsin that is present in the plasma membrane surrounding the cilia at the distal ends of the inner segments. The a- and b- wave responses in young *Prph2*$^{Rd2/Rd2}$ mice are lower in amplitude than those of age-matched normal mice and these amplitudes decline to zero over the course of the degeneration [221]. The low amplitude of the ERG recordings from these animals means that the a- and b- waves, particularly the former, are hard to distinguish from the background noise. Reuter and Sanyal achieved their results through the use of an intra-ocular electrode, and by averaging the responses from 100 light flashes. With this method they were able to detect a-waves until 2 to 3 months and b-waves at 6 to 7 months. They concluded that the detection of an ERG response indicated the 'presence of the anatomical substrates necessary for the transmission of the impulse from the PR cells to the second order neurons'. Subsequently, ERGs from *Prph2*$^{Rd2/Rd2}$ mice have also been recorded by Cayouette *et al.* [140], using corneal surface electrodes, to examine retinal function in *Prph2*$^{Rd2/Rd2}$ mice after treatment with CNTF. In untreated mice at P21 they detected a- and b-wave amplitudes of only ~10% and 7%, respectively, of the average a- and b- wave amplitudes recorded from wild type mice. More importantly they simultaneously recorded responses from the right, treated eye and the left, untreated or control treated eye. The strength of this method is that, assuming that the background interference is the same for both the right and left eyes, the ERG trace from the control eye can be subtracted from that of the treated eye. This will remove the small endogenous signal and the background noise and leave a trace that is purely the result of the treatment, thus providing a more sensitive evaluation of whether treatment has a positive effect on retinal function.

6.2 Recording electroretinograms and establishing the range of responses from the eyes of wild type mice.

6.2.1 Method

The process of recording electroretinograms had not been carried in our laboratory before and it was therefore necessary to develop protocols for its use. The ERG set-up, illustrated in Figure 6.1, is based on one established in E. Zrenner's laboratory in Tuebingen, Germany. A standard stimulating Ganzfeld bowl (Fig. 6.1a), used to generate the flashes of light, is commercially available, and was adapted by the removal of the chin and head rests (used in the clinic), and the addition of a platform on which to place the mouse. The platform and electrodes were enclosed within a metal box in order to shield the recorded responses from background electrical potentials. Mice were dark-adapted overnight and then the preparations for the ERG carried out under dim red light illumination. Each mouse was anaesthetised and its pupils dilated before it was placed on the platform. Sub-dermal reference and ground electrodes were inserted centrally at the back of the head and just above the base of the tail, respectively (Fig. 6.1b). Care was taken to ensure that the reference electrode was always placed centrally along the midline of the mouse to ensure concordant recordings from the right and left eyes. A single drop of 2% hydroxy-propyl-methyl-cellulose (HPMC) was placed on each eye to keep the eye hydrated during the procedure. Two ring electrodes were manipulated so that there were touching the right and left corneas (Fig. 6.1b). The platform was then manoeuvred so that the mouse was facing the source of the flashes with its head at the mouth of the bowl. The door of the metal box was then closed before recordings were made.

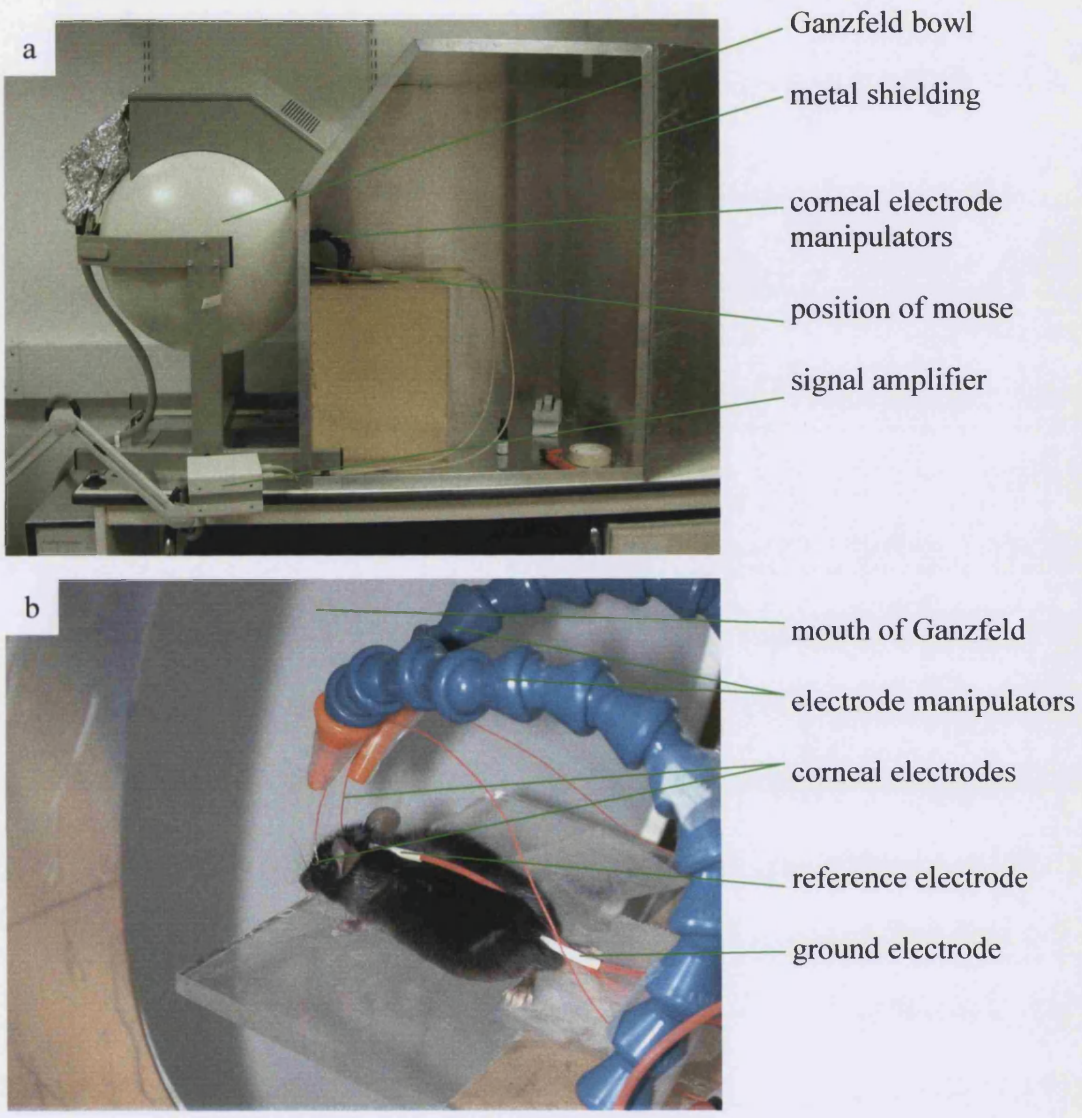

Figure 6.1 Equipment set-up for recording ERGs from mice. The mouse is placed in the mouth of the Ganzfeld bowl, inside a metal box to shield the electrodes from background electrical activity (**a**). Reference and ground electrodes are inserted sub-dermally along the midline of the mouse, and corneal electrodes are manipulated so that they are touching the surface of the eye (**b**).

To assess the consistence of the data recorded with this set-up, simultaneous recordings were taken from the right and left eyes of normal uninjected C57Bl/6 mice over a period of several weeks (section 2.10.6). Mice were dark-adapted overnight, and then anaesthetised and their pupils dilated. Scotopic ERG responses were then recorded after stimulation with flashes of light of increasing intensity – an intensity series. Each series consisted of flashes of 0.1, 1, 10, 100, 1000 and 3000 millicandellas/metre^2 (mcd/m^2). The final trace produced at each intensity setting is the average of the responses to five or ten flashes, depending on the intensity of the stimulus. An inter-stimulus interval of 2 seconds (for 0.1, 1, 10 and 100 cds/m^2) or 5 seconds (for 1000 and 3000 cds/m^2) was used. For isolating cone photoreceptor function, mice were light adapted and 15 Hz flicker ERGs evoked with white flash stimuli of 2500 mcd/m^2 on a background of 30 cd/m^2. The standard definitions of an a-wave latency (from point of stimulus to first most negative trough) and amplitude (from point of stimulus to first most negative trough), and b-wave implicit time (from first most negative trough to highest positive peak) and amplitude (from a-wave trough to b-wave peak) were used for analysis.

6.2.2 Normal form of mouse ERG

Seven adult wild type mice were used to examine the normal form of a mouse ERG. Representative tracings of scotopic (rod-mediated) responses are shown in Figure 6.2. These show a typical increase in the amplitude of the a- and b- waves, and a decrease in the b-wave peak implicit time, as the intensity of the flashes is increased. In these animals the average a- and b-wave amplitudes in response to the 1000 mcd/m^2 flash are 179.3 μV (SD = 20.5; n = 14) and 494.9 μV (SD = 40.1; n = 14) respectively. The corresponding a-wave latency and b-wave implicit time are 15.8 ms (SD = 0.9; n = 14) and 58.8 ms (SD = 10.7; n = 14) respectively. Average b-wave amplitudes for the 100 mcd/m^2 and 3000 mcd/m^2 flashes are 452.7 μV (SD = 38.2; n = 14) and 488.15 μV (SD = 51.3; n = 14) respectively. The mean b-wave amplitude for the highest flash intensity of 3000 mcd/m^2 is lower than that for the 1000 mcd/m^2 flashes. This is probably due to a conditioning flash effect that is reported to affect dark-adapted ERGs unless there is a minimum inter-stimulus interval of 10 seconds [222, 223]. This will have a greatest effect on the response to flashes of 3000 mcd/m^2, but also, to a lesser extent, on the responses to lower intensity flashes. However, the inter-stimulus interval was not increased due to the difficulty of lengthening the period of anaesthesia without altering the retinal responses. Although the conditioning flash effect should be equal for both

eyes the responses to flashes of 3000 mcd/m^2 was not used for comparative quantitative analysis. Photopic flicker responses were also recorded in the same seven mice. Representative traces of photopic (cone-mediated) responses are shown in Figure 6.3. The average cone flicker amplitude, measured between successive negative and positive peaks, is 58.5 μV (SD = 13.4; n = 14).

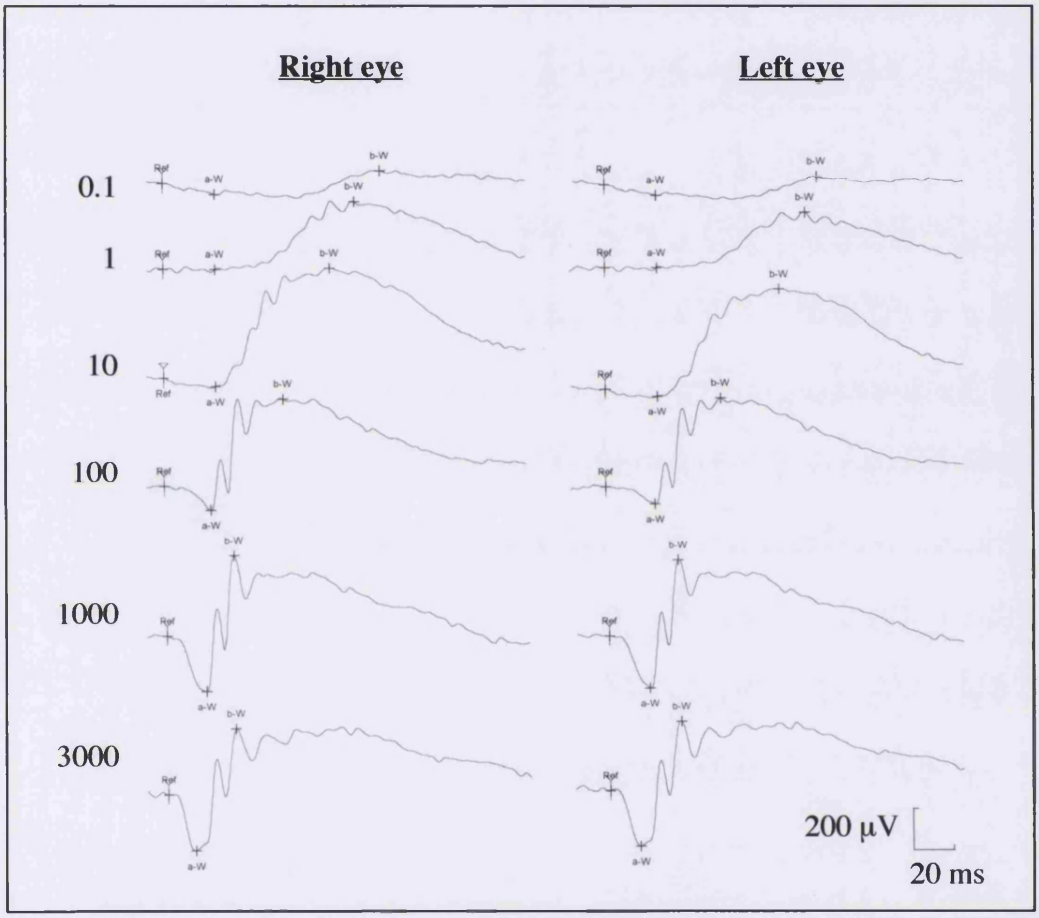

Figure 6.2 Representative electroretinographic intensity-responses obtained from the eyes of a dark-adapted wild type mouse. Simultaneously recorded left and right eye ERG responses are shown for a wild type mouse over a series of six increasing intensity flashes. The intensity of the flash in mcd/m^2 is shown on the left-hand side of the traces. Each waveform is marked at three successive points. From left to right along each trace these represent the flash onset (Ref), the a-wave trough (a-W) and the b-wave peak (b-W).

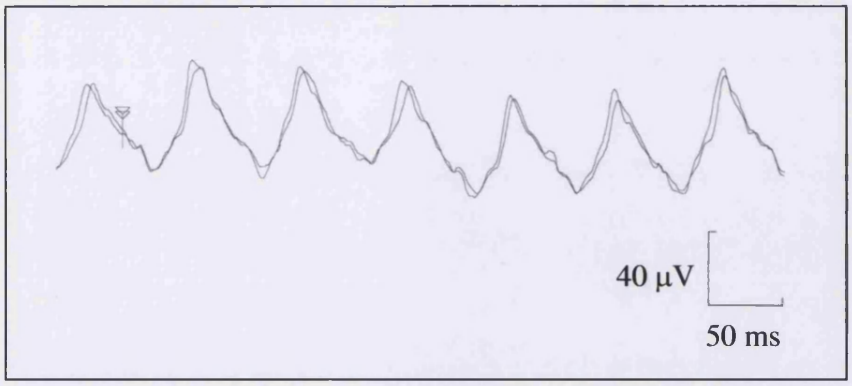

Figure 6.3 Representative flicker electroretinographic responses from a wild type mouse. A 15 Hz flicker was evoked with white flash stimuli of 2500 mcd/m^2 on a 30 cd/m^2 background. Simultaneously recorded left and right eye flicker response are overlaid to show correlation in the response between the two eyes. The traces are marked with the stimulus onset for the second peak. Amplitudes were measured between successive negative and positive peaks.

6.2.3 Concordance between ERGs from the right and left eyes of the same animal

The scotopic responses recorded simultaneously from the right and left eyes of individual mice and described in section 6.2.1 were also analysed to determine the degree of concordance between eyes. The responses from the mice were grouped according to the intensity of the flash. Four measurements were taken for each trace: a-wave amplitude, b-wave amplitude, a-wave latency and b-wave implicit time. Paired t-tests were performed on the groups of values from the right and left eyes at each intensity (Appendix II). Examples of the data analysis performed on the responses to flashes of 100 and 1000 mcd/m^2 are shown in Table 6.1a and b respectively. Analysis revealed that there was no statistically significant difference ($P < 0.05$) between any of the values recorded for the right and left eyes, even though the P values for the difference in b-wave amplitude between the right and left eye at both 100 and 1000 mcd/m^2 is very close to 0.05. Thus there appears to be no significant bias within the recording equipment.

a)

	a-Wave				b-Wave			
	Maximum amplitude (μV)		Latency (msec)		Maximum amplitude (μV)		Implicit time (msec)	
Mouse	Right	Left	Right	Left	Right	Left	Right	Left
1	59.7	62.4	17.6	18.8	438.5	494.3	65.2	66.8
2	80.6	82.3	20.8	21.6	393.0	399.3	63.6	64.0
3	77.8	82.6	20.4	20.0	465.6	481.3	68.0	71.2
4	37.2	40.9	18.8	19.6	398.3	413.0	62.0	63.2
5	32.7	41.0	18.4	17.6	452.9	479.0	66.4	64.0
6	61.8	67.8	17.6	17.6	457.0	506.0	69.2	68.4
7	63.2	54.4	18.8	20.4	486.2	473.4	60.0	60.0
P value	0.25		0.22		0.05		0.53	

b)

	a-Wave				b-Wave			
	Maximum amplitude (μV)		Latency (msec)		Maximum amplitude (μV)		Implicit time (msec)	
Mouse	Right	Left	Right	Left	Right	Left	Right	Left
1	162.7	159.4	14.8	15.6	561.8	563.5	60.0	60.0
2	193.1	199.4	17.2	17.2	495.1	502.3	56.0	55.6
3	173.5	183.5	16.4	15.6	455.3	474.5	41.6	41.2
4	146.0	146.7	16.0	16.0	444.2	462.7	69.2	70.4
5	170.0	206.0	15.6	15.6	447.0	489.7	48.8	47.2
6	184.5	210.8	14.4	14.8	483.0	554.2	70.8	70.0
7	191.8	182.5	15.6	16.8	501.5	493.5	66.0	66.0
P value	0.17		0.39		0.08		0.41	

Table 6.1a and b Comparison of the a-wave and b-wave values from the right and left eyes of individual wild type mice following flashes of (a) 100 mcd/m^2 and (b) 1000 mcd/m^2. The maximum amplitude of the a- and b- waves and their implicit times are shown for each mouse, produced in response to flashes of 100 and 1000 mcd/m^2. The P value was produced by performing a paired T test between each group of right and left eye trace data. There is no significant difference between those values recorded for the left eye and those recorded for the right ($P \leq 0.05$).

6.2.4 Variation in size of ERG potentials between recording sessions

The ERG responses to an intensity series of flashes in seven adult wild type mice were recorded at four different time points over the period of a month in order to establish the consistency of our recordings. The b-wave amplitudes produced, from the left eye of each animal were statistically analysed (Appendix III). Example data for flash intensities of 100 and 1000 mcd/m^2 is shown in Table 6.2a and b respectively. Repeated measure ANOVA (analysis of variance) tests showed that there was no significant variation ($P > 0.05$) in the b-wave amplitudes over the 4 recording sessions at 1000 mcd/m^2 ($P = 0.12$ respectively). At this intensity the variability in b-wave amplitude between recording sessions was not significantly larger than the variability in b-wave amplitude within the groups of mice. However, at 1, 10 and 100 mcd/m^2 there was a significant variation ($P = 0.03$, $P = 0.0006$, and $P = 0.02$ respectively). This was due to a drop in b-wave amplitudes on the third recording session, which was not significant with the higher intensity flashes. The reason for this was not identified, but it demonstrated that there was some variability in the values recorded from the same mice at different recording sessions that was larger than the values recorded from different mice at the same recording sessions. That there was a statistical significance at these lower intensities but not at 1000 mcd/m^2 is presumably due to the higher levels of variation within groups of mice at this intensity.

a) 100 mcd/m^2

	Maximum amplitude of b-wave from left eye (μV)			
Mouse	**Week 1**	**Week 2**	**Week3**	**Week 4**
1	490.6	359.9	312.1	355.1
2	399.3	421.4	368.9	451.7
3	481.3	452.7	427.7	478.6
4	413.0	424.7	297.9	323.9
5	400.0	431.2	358.5	381.9
6	479.3	483.6	253.7	426.6
7	400.0	297.3	363.1	448.8

P = 0.01 (repeated measures ANOVA)

b) 1000 mcd/m^2

	Maximum amplitude of b-wave from left eye (μV)			
Mouse	**Week 1**	**Week 2**	**Week3**	**Week 4**
1	418.1	507.7	322.2	415.9
2	502.3	521.3	361.1	455.3
3	474.5	462.7	496.7	563.2
4	462.7	517.0	355.9	335.2
5	350.4	397.3	444.0	**444.7**
6	489.7	535.6	321.7	**422.9**
7	554.2	356.6	424.4	435.7

P = 0.14 (repeated measures ANOVA)

Table 6.2a and b Analysis of left eye b-wave amplitudes of seven wild type mice over 4 different recording sessions in response to flashes of (a) 100 mcd/m^2 and (b) 1000 mcd/m^2, to assess the consistency of recordings. The maximum amplitude of the b- wave from the left eye is shown for four mice over four weeks, produced in response to flashes of 1000 mcd/m^2. Table (a) shows that at 100 mcd/m^2 the variability between recording sessions is significantly larger than the variability within the groups of mice at each time point. In contrast, at 1000 mcd/m^2 the variability between recording sessions is not significantly larger than the variability within the groups of mice at each time point.

6.3 Electroretinograms from untreated *Prph2* $^{Rd2/Rd2}$ mice.

6.3.1 Method

To determine the ERG responses from untreated, 8-week old *Prph2*$^{Rd2/Rd2}$ mice, dark-adapted ERG responses were recorded (section 2.10.6), using an intensity series consisting of 10, 100, 250, 500, 1000 and 3000 mcd/m^2 flashes. For isolating cone function the mice were light-adapted and 15 Hz flicker ERG evoked with white flash stimuli (2500 mcd/m^2) on a background of 30 cd/m^2.

6.3.2 Form of ERG from *Prph2*$^{Rd2/Rd2}$ mice

The responses for a representative animal are shown in Figure 6.4. As previously reported [221] in the traces from these animals the a- and b-wave amplitudes are reduced, and the time from the stimulus to the b-wave peak is longer than in ERG traces of wild type mice. In addition the a-wave amplitudes are often difficult to detect above the level of background noise, particularly at the lower intensities. Therefore, the amplitude of the b-wave was measured from the most negative point in the trace prior to the b-wave peak. A comparison of the variation in the average b-wave amplitudes for 8-week old *Prph2*$^{Rd2/Rd2}$and normal mice is shown in Table 6.3.

Intensity (mcd/m^2)	Mouse type	Mean b-wave amplitude (μV)	Standard deviation (SD)
100	*Prph2*$^{Rd2/Rd2}$	31.4	26.8
100	Wild type	452.7	38.2
1000	*Prph2*$^{Rd2/Rd2}$	69.8	29.9
1000	Wild type	494.9	40.1
3000	*Prph2*$^{Rd2/Rd2}$	55.2	18.75
3000	Wild type	488.2	51.3

Table 6.3 Comparison of the mean b-wave amplitude of 8-week old *Prph2*$^{Rd2/Rd2}$ and wild type mice in response to flash intensities of 100, 1000 and 3000 mcd/m^2. The table demonstrates that in *Prph2*$^{Rd2/Rd2}$ mice the standard deviation is a substantial proportion of the mean. For the *Prph2*$^{Rd2/Rd2}$ mice n = 8 and for wild type mice n = 14.

The standard deviation represents a substantial fraction of the mean b-wave amplitudes of the *Prph2*$^{Rd2/Rd2}$ mice. This indicates a relatively large amount of variation between animals in proportion to the size of their b-waves. As previously noted for the wild type mice (section 6.2.1), the b-wave amplitudes appear to be greater at 1000 mcd/m^2 flash intensity than at 3000 mcd/m^2.

No responses were detectable above background level in any mice to a flicker ERG (data not shown). This is likely to be due to the saturation of phototransduction by the background illumination.

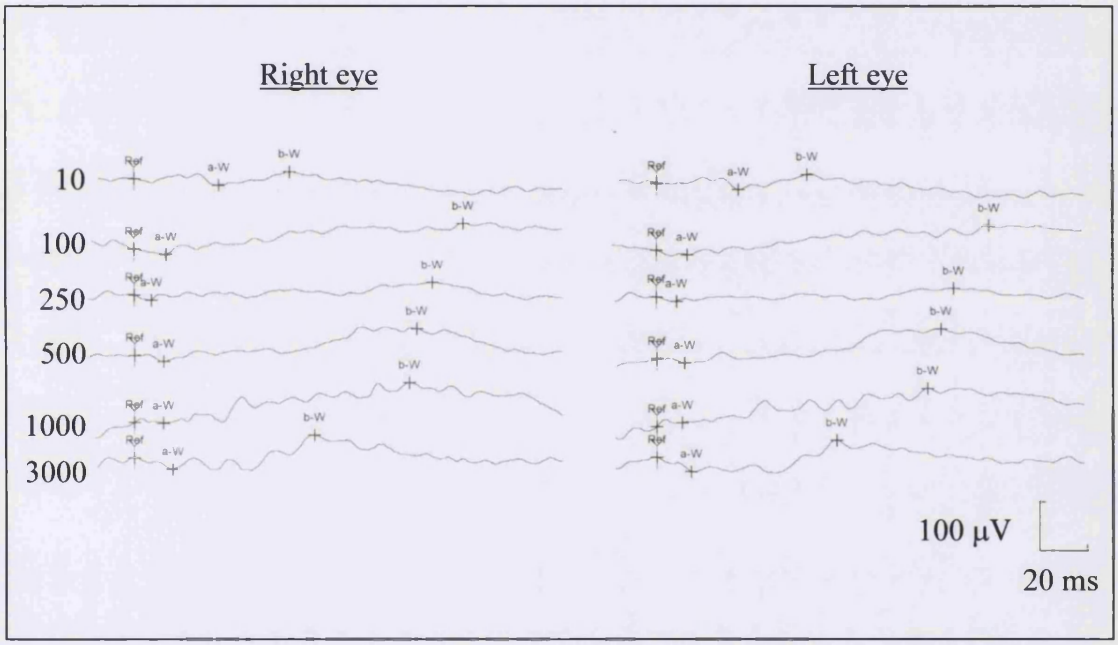

Figure 6.4 ERG responses from an eight-week old, untreated *Prph2*$^{Rd2/Rd2}$ mouse. Responses are shown to an intensity series of flashes of 10, 100, 250, 500, 1000 and 3000 mcd/m^2. Each trace is marked with the onset of the stimulus (Ref) and the approximate negative and positive peaks of the a-wave (a-W) and b-wave (b-W). On many traces the a-W and, at the lower flash intensities, the b-W cursors are difficult position. In these cases the cursors cannot represent the actual a- and b-waves but are positioned to allow comparisons between the traces from the left and right eye.

6.3.3 Concordances between ERG responses of the right and left eyes in the same animal

The responses recorded simultaneously from the right and left eyes of individual mice were also analysed to determine the degree of concordance between eyes. This will establish whether the left eye can be used as an untreated internal control in later experiments. Across all intensities there was no significant difference ($P > 0.05$) between the b-wave responses of pairs of eyes (paired t test). Data is shown in Table 6.4.

Mouse	b-wave amplitudes									
	10 mcd/m^2		100 mcd/m^2		250 mcd/m^2		500 mcd/m^2		1000 mcd/m^2	
	Right	Left	Right	Left	Right	Left	Right	Left	Right	Left
1	20.5	19.1	58.6	57.5	31.7	25.6	60.9	66.6	75.5	63.6
2	82.6	77.2	55.2	53.0	12.0	5.9	98.4	91.2	101.3	121.8
3	26.0	32.0	0.1	1.0	57.4	68.3	15.3	20.9	71.1	34.1
4	7.2	2.8	12.2	13.4	13.9	19.1	111.4	113.0	45.4	44.7
P value	**0.83**		**0.74**		**0.83**		**0.67**		**0.58**	

Table 6.4 Concordance between the amplitude of the b-wave in the right and left eyes of untreated, eight-week old *Prph2*$^{Rd2/Rd2}$ mice. Paired t-tests between the values from the left and right eye at each intensity showed that there was no significant difference ($P > 0.05$) between the two.

These results demonstrate that while the variation in the size of the ERG response between age-matched animals is high there is consistency in the responses from the right and left eyes of the same animal. This emphasises the importance of judging any possible effect of treatment against the response from an untreated control eye in the same animal.

6.4 ERG response following gene transfer in *Prph2*$^{Rd2/Rd2}$ mice

6.4.1 Method

In the light of the results described in Chapter 5 the impact of sub-retinal injection of AAV.RHO.PRPH2 on the retinal function of *Prph2*$^{Rd2/Rd2}$ mice has been evaluated. Sub-retinal injections of AAV.RHO.PRPH2 (titre of 1 x 10^{13} particles/ml) were carried out on a litter of eight, 10-day old *Prph2*$^{Rd2/Rd2}$ pups (section 2.10.3). Two injections were performed on the right eye of each animal, and 1 µl of virus was injected into both the superior and inferior halves of the eye. ERG recordings were performed at 1, 3, 4, 6, 8, 10 and 12 weeks after injection. Eyes were taken at 4 weeks for TEM examination (section 2.13.1 and 2.13.2). Control ERG recordings were performed on seven, 10-day old *Prph2*$^{Rd2/Rd2}$ pups from a second litter. Four of these received double sub-retinal injection of AAV.CMV.EGFP (5 x 10^9 iu/ml) in one eye, while the other three were injected twice with PBS in one eye. ERG recordings on these mice were made at 3, 4, and 5 weeks post-injection. Dark-adapted and flicker ERGs were recorded and analysed as before (section 6.3).

6.4.2 Results

The responses from the treated and control eyes to flashes of 1000 mcd/m^2 were chosen for analysis since in the control animals this intensity had given b-waves with the greatest amplitudes. These values for all treated and control animals up to 8 weeks post-injection are shown in Table 6.5 and 6.6 respectively.

Treated Mice	Maximum amplitude of b-wave (μV) in right and left eyes									
	Week 1		Week 3		Week 4		Week 6		Week 8	
	Right	Left	Right	Left	Right	Left	Right	Left	Right	Left
1	64.9	52.4	187.2	87.0	151.0	65.5	117.3	68.3	72.9	74.5
2	49.9	25.7	88.0	55.7	156.5	104.8	135.1	121.8	45.0	45.8
3	51.1	43.2	159.3	91.0	194.4	135.9	136.0	76.6	133.4	75.0
4	90.4	73.3	184.0	102.0	37.9	38.2	72.7	89.3	*	*
5	65.8	56.7	177.9	80.7	182.5	74.5	*	*	*	*
6	119.2	110.3	123.2	32.5	100.9	66.7	*	*	*	*
7	*	*	124.8	94.1	115.5	87.6	117.6	119.9	*	*
8	102.6	81.7	145.6	40.1	31.3	61.9	132.5	49.7	59.6	65.9
Mean	77.7	63.3	148.8	72.9	121.3	79.4	118.5	87.6	77.7	65.3
SD	26.7	27.8	35.1	26.4	61.8	30.0	24.0	28.8	38.8	13.7
P value	0.17		0.0001		0.05		0.03		0.28	

Table 6.5 Amplitude and analysis of b-waves in the right and left eyes of *Prph2*$^{Rd2/Rd2}$ mice after sub-retinal injection of AAV.RHO.PRPH2 into the right eye. All mice were treated at P10 and recordings made 1, 3, 4, 6 and 8 weeks post-injection. Asterisks indicate where it was not possible to make recordings. Paired t-test performed between the sets of data for the right and left eyes at each time point show that the amplitude of the b-wave from the right eye is significantly larger at 3, 4 and 6 weeks post-injection but not at 1 and 8 weeks post-injection.

Paired t-tests were used to analyse the difference in b-wave amplitudes between the injected (right) eye and the uninjected (left) eye of all the animals. The ERG responses in right eye of the seven AAV.RHO.PRPH2 treated mice were maximal at 3 weeks post-treatment when injected eyes showed a b-wave mean amplitude (mean +/- s.d. = 148.8 +/- 35.1 μV; n = 7) significantly larger (P = 0.0001) than those recorded from untreated eyes (mean +/- s.d. = 72.9 +/- 26.4 μV; n = 7). Moreover these amplitudes were approximately 30% of those amplitudes from wild type mice (mean +/- s.d. = 494.9 +/- 40.1 μV; n = 14). The differences between the treated and untreated eyes were also significant at 4 and 6 weeks post-injection ($P < 0.05$). However the effect was transient and the difference was no longer apparent at 8 weeks post-treatment, although one animal showed larger responses in the right eye until week 10 (data not shown). In contrast, the control mice where the right eye had been injected with AAV.CMV.EGFP

or PBS did not show any significant difference in the b-wave amplitudes between right and left eyes at any of the time points studied (Table 6.6).

Control treated mice		Maximum amplitude of b-wave (μV) in right and left eyes					
		Week 3		Week 4		Week 5	
		Right	Left	Right	Left	Right	Left
AAV.CMV. EGFP injected mice	1	95.2	97.5	0.8	6.5	107.0	110.9
	2	58.6	39.6	78.6	75.5	33.7	59.6
	3	52.7	58.4	54.1	53.9	*	*
	4	106.2	102.7	53.6	74.1	*	*
Mean		78.2	74.6	46.8	52.5		
SD		26.5	30.6	32.8	32.2		
P value		0.55		0.36			
PBS injected mice	5	24.1	14.0	54.9	56.8	60.6	28.8
	6	210.3	207.5	*	*	*	*
	7	14.5	15.7	40.6	69.2	19.7	19.1
Mean		83.0	79.1				
SD		110.4	111.2				
P value		0.36					
Combined control P value		0.28		0.15		0.96	

Table 6.6 Amplitude and analysis of b-waves in the right and left eyes of *Prph2*$^{Rd2/Rd2}$ after sub-retinal injection of AAV.CMV.EGFP and PBS into the right eye. All mice were treated at P10 and recordings made 3, 4 and 5 weeks post-injection. Asterisks indicate where it was not possible to make recordings. The calculations of the standard deviation and paired t-tests could not be performed with less than three data points therefore the data from PBS and AAV.CMV.EGFP injected animals was combined to give an overall P value at each time point. All P values indicate that there is no significance ($P > 0.05$) between the responses from treated and untreated eyes at any of the time points studied.

The ERG traces of a single AAV.RHO.PRPH2 treated animal over the time course are shown in Figure 6.5. This figure clearly shows that at 1 and 8 weeks post-injection the form and amplitude of the right and left eyes are well matched. However, at 3, 4 and 6

weeks post-injection there are substantial differences between the two eyes that are consistent over all of the flash intensities.

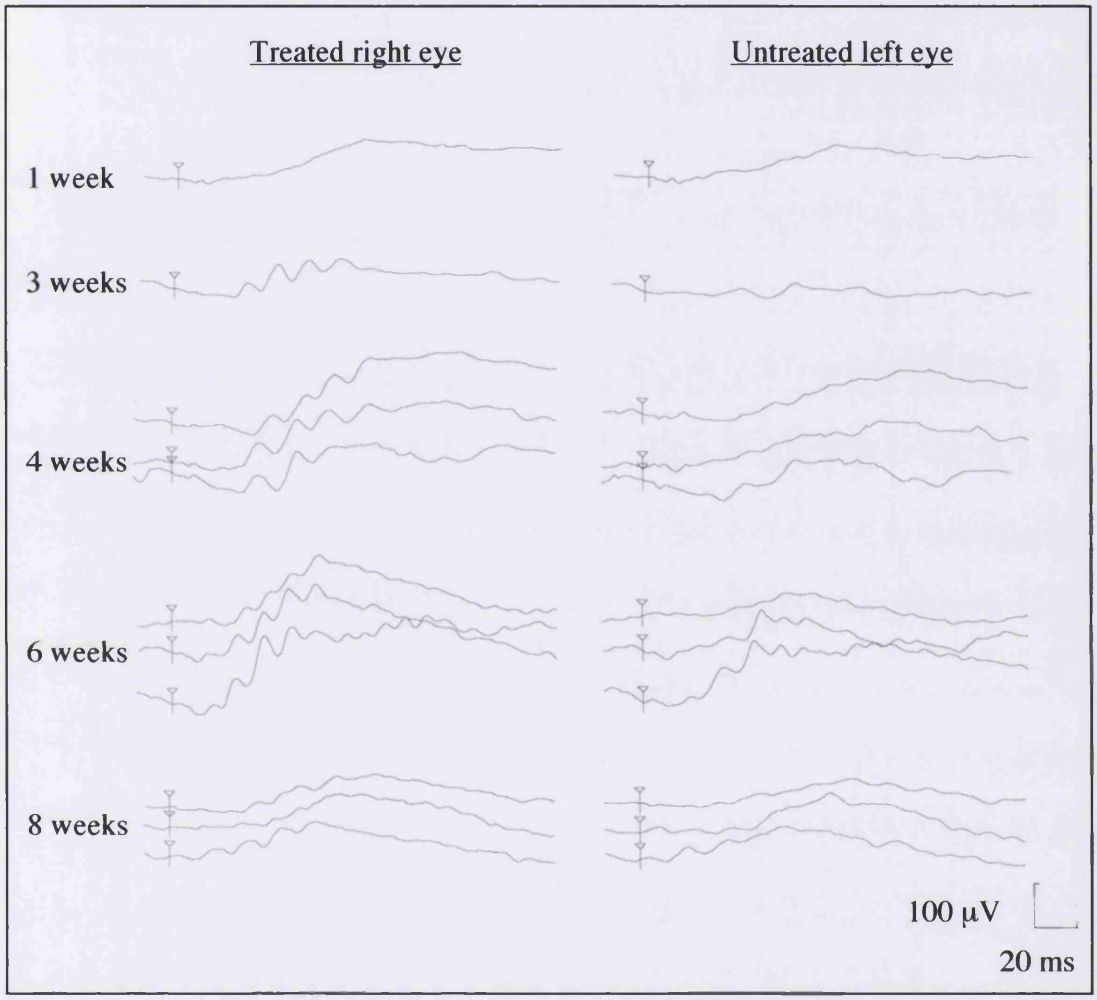

Figure 6.5 ERG responses from a treated *Prph2*$^{Rd2/Rd2}$ mouse at 1, 3, 4, 6 and 8 weeks post-injection. The mouse was treated at P10 by sub-retinal injection of AAV.RHO.PRPH2 into the right eye. ERG responses to flashes of 1000 mcd/m^2 are shown at 1 and 3 weeks. At all other time points the responses to flashes of 500, 1000 and 3000 mcd/m^2 are shown. Each trace is marked with the onset of the stimulus and represents the average of the responses to five flashes. The response from the right eye increases over that of the left over time and peaks between 4 and 6 weeks. However, at 8 weeks the response is reduced and approximately equal to that of the left.

The differences between the responses from treated and untreated eyes are shown in detail in Figure 6.6, an example of a complete intensity series at four weeks post-injection. The form of the ERG traces from the right eye are more similar to that of a wild type mouse (Fig. 6.2), with clear oscillatory potentials and an a-wave which is more pronounced against the background noise at flash intensities of 1000 and 3000 mcd/m^2. Outer segment structures consistent to those observed in Chapter 5 were seen in the right, treated eye of this animal after TEM (data not shown). No similar structures were observed in the left, untreated eye. The presence of oscillatory potential was not consistent throughout all of the treated animals. Figure 6.7 shows 1000 mcd/m^2 intensity traces from all of the treated and control mice. Four of the eight treated mice showed visible oscillatory potentials. These potentials were not visible on any of the traces of animals from the either of the control groups. Flicker ERGs performed at 4 weeks post-injection in AAV.RHO.PRPH2 treated animals showed no improvement over untreated *Prph2*$^{Rd2/Rd2}$ mice (data not shown).

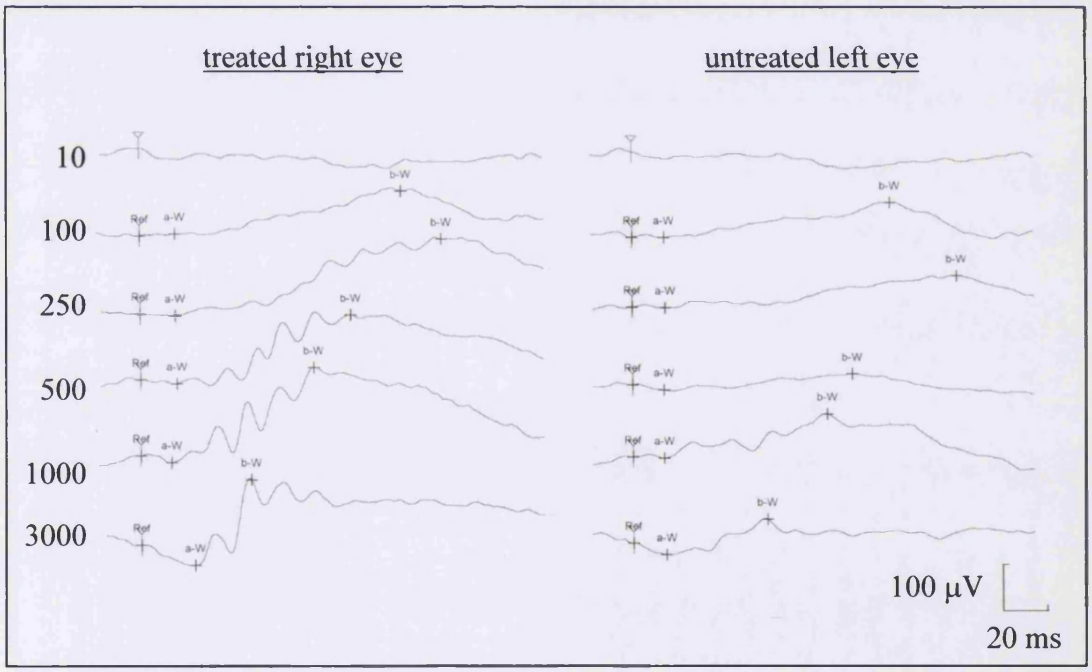

Figure 6.6 Representative electroretinographic responses from a *Prph2*$^{Rd2/Rd2}$ mouse four weeks after treatment. Responses are shown to an intensity series of flashes of 10,100, 250, 500, 1000 and 3000 mcd/m^2. Across all flash intensities the amplitudes and forms of the b-waves from the treated eye are increased over those from the untreated eye. Each trace is marked with the onset of the stimulus (Ref) and the peaks of the a-wave (a-W) and b-waves (b-W). As with the untreated *Prph2*$^{Rd2/Rd2}$ mice (section 6.3 and Fig. 6.4) at most flash intensities the a-wave is not distinguishable. Therefore, in order to obtain a value for the b-wave amplitude, the a-W cursor is placed at the most negative point in the trace between the Ref and b-W cursors.

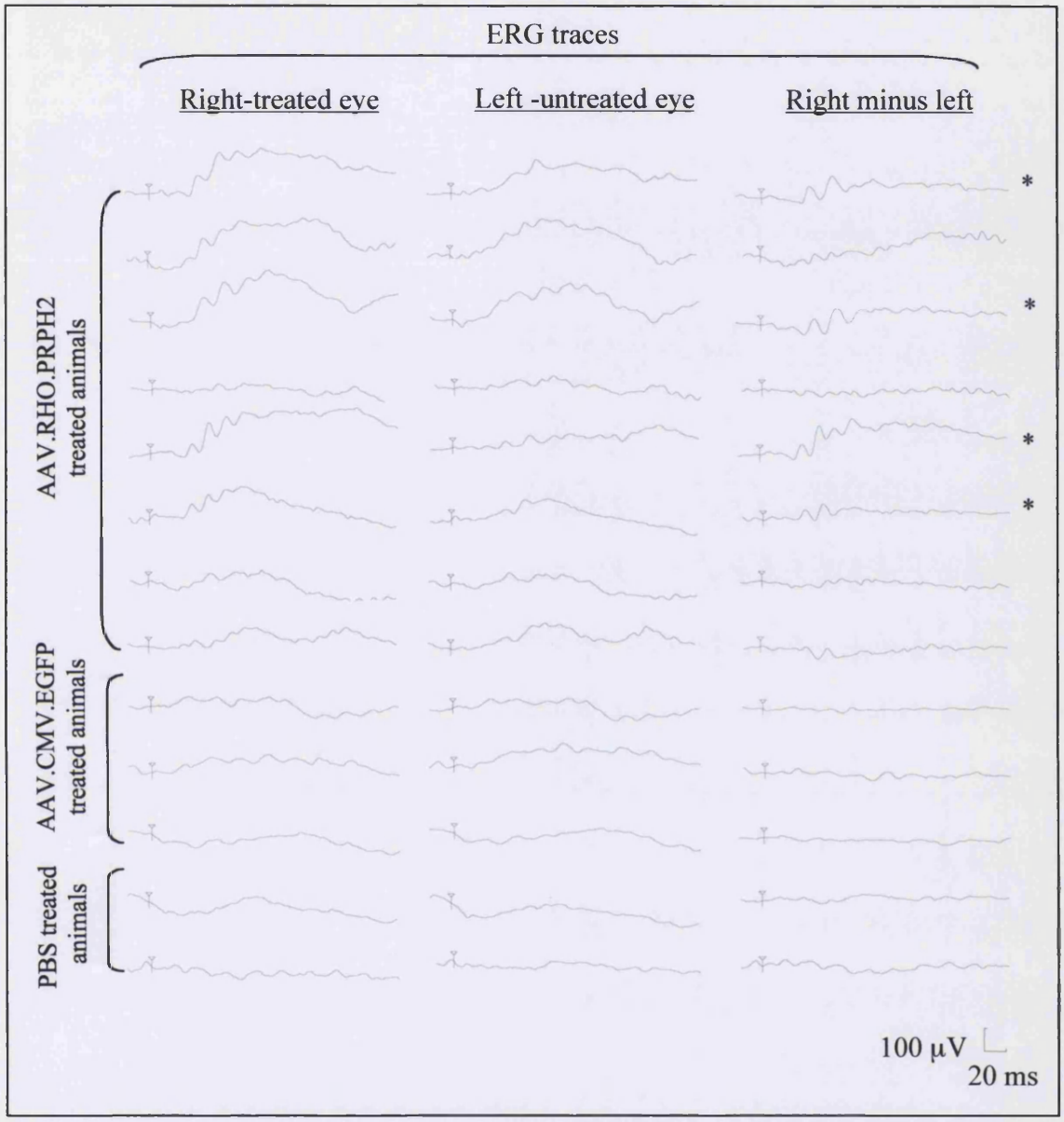

Figure 6.7 ERG responses from individual treated and control *Prph2*$^{Rd2/Rd2}$ mouse eyes following a flash intensity of 1000 mcd/m^2. All animals were treated at P10 and the ERGs recorded 4 weeks later. Each trace represents the average of the responses to five flashes. All of the AAV.RHO.PRPH2 treated and control treated AAV.CMV.EGFP and PBS animals are shown. The third column of traces was produced after the response from the left (untreated) eye had been subtracted from the response from the right (treated) eye. At least four out of eight AAV.RHO.PRPH2 treated animals showed clear oscillatory potentials above the level of the response from the left eye. These animals are marked with an asterisk. In comparison no traces from either of the control groups showed these oscillatory potentials.

6.5 Discussion

The main aim of this chapter was to investigate the effect of a sub-retinal injection of a recombinant adeno-associated virus carrying the *Prph2* gene under the control of a *rhodopsin* promoter on the ability of the retina to respond to light. The results showed that the histological changes observed in the treated areas of retina, such as the presence of outer segment structures, and the increase in the amount of rhodopsin, reported in Chapter 5 are accompanied by a significant increase in the amplitude of rod-mediated responses to light. Treated eyes demonstrated maximal b-wave amplitudes that were approximately 200% of the levels in the untreated contralateral eyes and up to 30% of wild type levels. In addition, these traces showed ERG characteristics that are also present in traces from wild type mice – discernible a-waves and oscillatory potentials. A *rhodopsin* promoter was used to drive gene expression and, as expected, no improvement in the cone function, as measured by the flicker response, was seen.

The improvement in photoreceptor function was first statistically significant at around 3 weeks post injection. The slow increase in amplitude between 1 and 3 weeks post-treatment with AAV.RHO.PRPH2 correlates well with the gradual onset of both *egfp* and *Prph2* expression mediated by rAAV vectors injected into P10 *Prph2*$^{Rd2/Rd2}$ mice (see section 4.7 and 5.3 respectively). However, the effect of an increased response in the treated eye did not last, and by 12 weeks post-treatment the responses from the treated and untreated eyes were approximately equal. The reasons behind this are not clear, but it correlates with the finding that injection of AAV.RHO.PRPH2 does not slow the rate of degeneration in *Prph2*$^{Rd2/Rd2}$ mice (see section 5.5). It has been estimated that between the ages of 3 and 12 weeks old, which corresponds to the period of our examination, these mice lose approximately 60% of their PR cells [199]. The loss of PR cell function may therefore be related to the loss of PR cells.

It has been shown that in a rat light damage model of retinal degeneration a lesion of the retina, made by inserting a dry needle or injection of PBS, can cause the rescue of local photoreceptors [224]. It has been suggested that this is due to the release and diffusion of some endogenous survival-promoting factors from the site of injury in the retina. However, this effect is reported to be absent in the murine retina [28] and, in support of

this, no such rescue was seen here in control-injected eyes. The responses from AAV.CMV.EGFP and PBS treated eyes matched those from the uninjected control eye in each mouse. Although the titre of AAV.CMV.EGFP was approximately 100 fold less than that of AAV.RHO.PRPH2 it is unlikely that the higher concentration of viral particles would cause a therapeutic effect.

The demonstration of the restoration of photoreceptor function is central to assessing the potential of treatment. The work in this chapter has shown that the measurement of ERG response can be a valuable way of doing this. Further work should include the assessment of those mice that have received multiple injections of AAV.RHO.PRPH2 and co-injections with vectors encoding neurotrophic factors as suggested in section 5.6.2. In addition, there may be the possibility of recording focal ERGs in which the response from a particular area of retina may be extracted. However, this recording technique is very difficult to perform in such a small eye and has only been utilised by one group [225]. Behavioural tests, which might identify an increase in visual function, are also difficult to perform in mice, particularly in this model since variable, residual levels of function are retained throughout much of the degeneration. Studies that involve the measurement of visually evoked potentials in the superior colliculus should at least add information on the ability of the treated retina to transmit the electrical stimulus to the brain. It should, however, be noted that since *Prph2*$^{Rd2/Rd2}$ mice have poor retinal function they might not have developed the appropriate synaptic connections to properly process visual information.

Aknowledgements

I would like to acknowledge Mahesh de Alwis for his assistance in producing the virus used in these experiments, and Jim Bainbridge for performing the sub-retinal injections. I would like to thank Lyndon da Cruz, with whom all the ERG recordings were performed, and Graham Holder, Chris Hogg and Matheus Seeliger for their advice on the ERG set-up.

7

Discussion

The aim of the work described in this thesis was to study the application of gene therapy for the treatment of inherited retinal degeneration. Work in Chapter 3 focused around the production of rAAV vectors. This virus was used to assess the dynamics of transduction and the expression of a reporter gene in the retina after sub-retinal injection (Chapter 4). The aim was to establish spatial and temporal levels of expression that would be suitable for attempts to treat retinal degeneration in the *Prph2*$^{Rd2/Rd2}$ mouse, one of the mouse models available for retinitis pigmentosa. The effect of injecting rAAV carrying a functional copy of *Prph2* into the mutant mice is described in Chapters 5 and 6. These studies showed that the treatment was capable of restoring partially the ultrastructural defect seen in these mice, and this was associated with an increase in retinal function as measured by an electroretinogram. However, the treatment did not slow the rate of the photoreceptor cell degeneration in *Prph2*$^{Rd2/Rd2}$ mice.

7.1 Prospects for rAAV in gene therapy

As discussed in the Introduction (section 1.3), the first 10-15 years of research in the field of gene therapy have been heavily focused around obtaining efficient gene transfer – adapting viruses into vectors that are able to transduce efficiently the target cell type. The original vectors gave short-lived, inefficient expression and, as a result, a large number of the early clinical studies were conducted in cancer patients. These trials involved simpler *ex vivo* transduction protocols, often with the aim of killing disease related cells. However, the research effort has paid off and vector technology is advancing rapidly. Recent progress in methods of production and purification of rAAV

described in Chapter 3 has enabled the production of high titre virus. As demonstrated in Chapter 4 and in work by other groups [110, 128], sub-retinal injection of rAAV into the eye results in the efficient long-term transduction of large numbers of photoreceptor cells and is now the vector of choice for targeting this cell type.

The ability of rAAV to provide long-term transgene expression in the retina is consistent with the results of researchers using rAAV to target other tissues. Sustained expression in the liver of Factor IX (F.IX) has been demonstrated after a single intra-portal injection of rAAV.F.IX, successfully correcting a bleeding disorder in haemophilia B dogs for at least 7 months [226]. Another group also achieved over 17 months of therapeutic levels of expression of the same gene after intra-muscular injection [227]. The latter study has been extended to a clinical trial in which the same virus was injected into three haemophilia B patients [228]. The results were encouraging if only in that there was no evidence of toxicity related to vector administration or inadvertent germ-line transmission. Moreover, muscle biopsy of the injected sites followed by immunofluorescent staining demonstrated that there was gene expression, although very low amounts of F.IX were being secreted. Studies such as this one are important in establishing the safety of rAAV before more detailed analysis of therapeutic effects, and have confirmed it as a promising vector. However, there are still problems associated with its manufacture that need to be overcome. The lack of clinical protocols that involve the use of rAAV is largely due to difficulties associated with the scaling-up of production in order to meet the demands of clinical trials. Moreover, production will eventually require methods of quality assurance and control as pharmaceutical companies become involved.

Despite these drawbacks, the advantages of rAAV as a vector have been recognised and attempts are being made to extend the virus's original tropism, allowing it to be used in the transduction of other cell types. Mutation analysis of the AAV-2 capsid genes have identified the regions of the capsid that are potentially responsible for receptor binding and sites that are suitable for epitope insertions [229]. Some regions of the capsid proteins are important in DNA packaging and capsid formation and therefore will not tolerate alterations. However, an insertion of an epitope into one region has already been shown to allow AAV-2 to infect previously non-permissive cell lines [230]. An alternative strategy also under investigation is the use of bispecific antibodies that bind

to the virus and mediate a novel interaction with the vector and a specific cell surface receptor. This type of targeting has shown promise in *in vitro* studies [231], the preliminary results suggesting that the adaptor also decreased the effectiveness of AAV infection into previously permissive cells. In the long-term this will be the aim - to alter, rather than extend, the viral tropism so that vectors can be more specifically targeted to a particular cell type.

Perhaps even more ambitious are those studies in which AAV is being used to create chimeric vectors that utilise elements from different viral families. This type of manipulation, in theory, should allow the production of vectors that combine the strengths of their various components. This is a relatively new area of research. However, work in progress includes adenoviral-AAV chimeras [232, 233], which are based on combining the advantageous features of high titre and transduction efficiencies of rAd with the long-term transduction potential of rAAV. While the search for alternative viruses to use as vectors continues it is clear that AAV vectors will have a significant part to play in the future of gene therapy.

7.2 Gaining appropriate levels of transgene expression

With the improvement in the ability to transduce target cells efficiently and the rapid progress of the vector field, some of the emphasis of research has moved towards gaining appropriate transgene expression post delivery. This type of work is particularly relevant where the gene product is not secreted and a relatively precise level of regulation is required. The use of the promoter region associated with the transgene in the wild type is often complicated by long regulatory sequences and, as with the case of the *peripherin-2* promoter, a lack of understanding of the important elements. Further difficulty is added by the inability to control the number of particles infecting any one cell. Ideally, regulation of the transgene should allow expression to be turned on or off in response to the symptoms of the disease. A possible solution is an inducible gene promoter system in which the expression of the therapeutic gene is regulated by the inducible co-expression of a transcription factor. Currently there are several different systems under investigation but at the forefront of these is the Tet system. This is based on the bacterial tetracycline resistance regulation with the bacterial protein TetR

binding to its target the *tet* operator (*tetO*) only in the absence of tetracycline or its analogues. The requirements for inducible systems are that the induction is reversible and that the inducer is non-toxic, with the capacity to have effect when taken orally. The Tet system, engineered for use in eukaryotic cells, has the potential to meet these criteria. Tetracycline has been used for many years both in humans and animals without deleterious effects except at very high doses; its analogues, doxycycline and anhydrotetracycline, appear to have all the properties of tetracycline yet act at much lower doses. Gossen *et al.* [189] have modified the system to allow transgene expression to be turned on instead of off in the presence of the inducer. Recently this type of system has been incorporated into rAAV, with an *egfp* reporter gene, and delivered to the rat retina [234]. The results were promising with a preliminary correlation of the level of EGFP expression with the dosage of doxycycline. Further refinements of the system should allow more sensitive control over expression levels.

7.3 Prospects for retinal clinical trials

The results in Chapters 5 and 6 have added weight to the prospective use of gene therapy in the treatment of retinal degeneration. However it is evident that there is still much research to be done before gene therapy is routinely used in clinics. The recent investigations into the way in which gene therapy clinical trials are conducted has prompted a tightening of regulations, and protocols are now carefully scrutinised before they progress into the clinics.

One of the main criteria for progression into clinical trials is that therapeutic results must be shown in an eye of human size [235]. Many of the current studies are performed on rats or mice. Apart from being easier and cheaper to keep, the rate of the degeneration in these animals is much quicker, leading to a faster turnover of results. However, it is questionable whether a model like the *Prph2*$^{Rd2/Rd2}$ mouse is a good one in which to study retinal degeneration and treatment. The strengths of this model have already been discussed in Chapter 5 (section 5.1). The null mutation makes this an attractive model for early studies but similar mutations are not frequently found in the clinics. Only one family has been reported with a null mutation [236]. These patients are heterozygous for the mutation and demonstrate a phenotype that is more similar to

autosomal dominant retinitis punctata albescens than retinitis pigmentosa. This disease is clinically similar to RP in its attenuation of retinal vessels and abnormal ERGs. However, it is distinct in that the predominant early feature is the presence of sub-retinal white dots, while intra-retinal pigmentation is rare. The differences in disease progression in the mouse and human are significant and, in addition, the lower cone to rod ratio and the lack of a fovea in mice make them less suitable for studies of cone degeneration. Nevertheless the mouse has proved to be a good starting point in the study of transduction and expression of reporter genes, since these studies have translated well into larger models including the dog [192] and non-human primates [112]. A recent success in a dog model of Leber's congenital amaurosis (LCA), one of the most clinically severe forms of retinal degeneration, has shown that the approach can be further extended to the restoration of photoreceptor cell function in larger animals [237].

The production of suitable animal models in which to test protocols is a difficult problem. The techniques involved in producing transgenic mice and rats are now regarded as routine but they are time consuming, while the production of larger transgenic animals such as non-human primates has been hampered by the low efficiency of gene transfer protocols. A recent success is the production of a transgenic rhesus monkey carrying *gfp* [238], and this augurs well for the future production of transgenic models. These models should provide a more accurate representation of the human condition, with slower degeneration of PR cells and more obvious involvement of cones.

The production and use of large animal models, however, increases the cost of the assessment of gene therapy protocols, and it is meeting those costs that may perhaps present ocular gene therapy with its biggest hurdle. Although they can be met by public sector money more rapid advancement of experiments could be made if there were some input from the commercial sector. This first requires a clear demonstration that this type of gene therapy is economically viable. The problem is that RP is caused by such a heterogeneous array of mutations, with multiple different mutations even within the same genes. While it is theoretically preferable to be able to tailor treatment to each individual case of RP, this may not be possible when it is considered that the ultimate aim is to provide a treatment that is universally available. In this context non-specific

gene therapy strategies, such as those involving the delivery of neurotrophic factors and anti-apoptotic factors described in section 1.6.3, may provide a better, more practical alternative. Whether this approach will be of greater benefit to the patient is not known. In its support it is often said that those patients suffering from a loss of vision would still be able to maintain an almost normal lifestyle if they were to retain only the cone photoreceptor cells of the macula. This suggests that it may be better to concentrate on developing non-specific strategies that would achieve this, the most obvious being treatment with neurotrophic factors. It should, however, be noted that the presence of healthy rods has a significant impact on the survival of cones.

Overall it seems clear that there is a fundamental need to understand more fully the mechanisms through which genetic mutations lead to degeneration of the retina. This would provide a more accurate definition of exactly what is required of a treatment based on gene therapy. Experimental work on gene therapy strategies plays an integral part in this understanding and, with further development, may result in successful clinical application in the future.

Appendix I

Additional data for section 5.5. Measurements of the outer nuclear layer thickness in untreated control *Prph2*$^{Rd2/Rd2}$ mice.

Time Point	Retinal location							
	S3	S2	S1	Mean superior thickness	I3	I2	I1	Mean inferior thickness
10-day old *Prph2*$^{Rd2/Rd2}$ control mouse								
Eye 1	60.45	58.90	64.78	61.38	61.43	68.12	62.24	63.93
Eye 2	66.11	65.31	70.02	67.15	76.66	70.35	59.86	68.94
5 + 32-day old *Prph2*$^{Rd2/Rd2}$ control mouse								
Eye 1	37.86	38.87	40.74	39.16	44.90	43.89	41.53	43.44
Eye 2	38.80	41.2	44.51	41.50	44.16	42.13	41.08	42.45
Eye 3	36.54	39.06	40.36	38.65	42.19	42.91	39.04	41.38
Mean	37.73	39.7	41.87	39.77	43.75	42.98	40.55	42.42
SE	0.65	0.74	1.32	0.878	0.81	0.51	0.77	0.59
10 + 32-day old *Prph2*$^{Rd2/Rd2}$ control mouse								
Eye 1	35.46	35.52	41.22	37.40	43.57	40.88	36.45	40.30
Eye 2	33.95	36.26	38.32	36.18	43.99	39.82	37.71	40.51
Eye 3	32.61	34.30	37.59	34.83	41.23	39.22	37.28	39.24
Mean	34.01	35.36	39.04	36.14	42.93	39.97	37.15	40.02
SE	0.82	0.57	1.11	0.74	0.86	0.49	0.37	0.39
20 + 32-day old *Prph2*$^{Rd2/Rd2}$ control mouse								
Eye 1	30.99	36.01	33.22	33.41	39.95	39.17	34.94	38.02
Eye 2	34.49	36.52	35.75	35.59	38.56	38.61	36.92	38.03
Eye 3	25.01	24.22	30.23	26.49	33.77	30.95	30.91	31.87
Eye 4	23.62	25.58	27.75	25.65	31.23	30.75	30.76	30.91
Mean	28.53	30.58	31.74	30.28	35.88	34.87	33.38	34.71
SE	2.55	3.29	1.744	2.48	2.04	2.32	1.53	1.92
40 + 32-day old *Prph2*$^{Rd2/Rd2}$ control mouse								
Eye 1	28.53	29.51	31.44	29.83	34.09	32.20	30.42	32.24
Eye 2	26.22	30.34	33.11	29.89	30.98	30.58	31.07	30.87
Eye 3	27.72	31.49	31.22	30.14	34.74	30.04	27.30	30.69
Mean	27.49	30.45	31.92	29.95	33.27	30.94	29.60	31.27
SE	0.68	0.58	0.60	0.10	1.16	0.65	1.16	0.49

Additional data for section 5.5. Measurements of the outer nuclear layer thickness in treated *Prph2*$^{Rd2/Rd2}$ mice eyes.

Time Point	Retinal location							
	S3	S2	S1	Mean superior thickness	I3	I2	I1	Mean inferior thickness
***Prph2*$^{Rd2/Rd2}$ mouse injected P5 sacrificed 35 days later**								
Eye 1	42.33	38.79	42.43	41.18	46.46	42.06	42.65	43.72
Eye 2	30.81	39.47	42.17	37.48	41.64	43.18		42.41
Eye 3	38.35	38.08	42.76	39.73	41.31	40.23	39.36	40.30
Mean	37.16	38.78	42.45	39.47	43.14	41.82	41.00	42.14
SE	3.38	0.40	0.17	1.08	1.66	0.86	1.64	1.00
***Prph2*$^{Rd2/Rd2}$ mouse injected P10 sacrificed 35 days later**								
Eye 1	32.96	32.69	32.43	32.69	39.54	38.60	37.51	38.55
Eye 2	35.09	41.08	31.63	35.93	35.12	35.92	34.15	35.06
Eye 3	38.35	45.86	31.46	38.55	42.29	46.36	38.27	42.31
Eye 4	22.77	31.35	33.32	29.15	37.93	33.53	28.10	33.19
Mean	32.29	37.74	32.21	34.08	38.72	38.60	34.51	37.28
SE	3.36	3.46	0.43	2.04	1.50	2.79	2.31	2.01
***Prph2*$^{Rd2/Rd2}$ mouse injected P20 sacrificed 35 days later**								
Eye 1	20.89	27.80	36.59	28.42	36.79	33.97	35.43	35.40
Eye 2	23.94	32.34	30.15	28.81	35.40	35.04	36.06	35.50
Eye 3	34.47	32.32	33.05	33.28	37.87	34.96	32.79	35.20
Mean	26.43	30.82	33.26	30.17	36.69	34.66	34.76	35.37
SE	4.12	1.51	1.86	1.56	0.72	0.34	1.00	0.09
***Prph2*$^{Rd2/Rd2}$ mouse injected P40 sacrificed 35 days later**								
Eye 1	25.80	27.11	26.83	26.58	27.67	34.21	32.36	31.41
Eye 2	27.55	29.42	29.68	28.89	31.72	35.06	29.67	32.15

Appendix II

Additional data for section 6.2.2. The a-wave amplitudes and latencies and the b-wave amplitudes and implicit times are shown for the right and left eyes of seven mice at flash intensities of (**a**) 0.1 mcd/m^2, (**b**) 1 mcd/m^2 and (**c**) 10 mcd/m^2. Paired t-tests were performed to shown no significant variation between the left and right eyes.

a) 0.1 mcd/m^2

	a-Wave				b-Wave			
	Maximum amplitude (μV)		Latency (msec)		Maximum amplitude (μV)		Implicit time (msec)	
Mouse	**Right**	**Left**	**Right**	**Left**	**Right**	**Left**	**Right**	**Left**
1								
2	12.1	13.3	16.4	16.8	163.7	157.8	103.6	102.4
3	9.6	8.6	26.0	26.0	194.7	189.6	93.6	93.2
4	1.9	2.8	19.2	20.0	61.9	37.1	98.0	97.2
5	31.8	36.4	26.0	26.0	58.0	75.2	94.0	96.0
6	3.2	5.2	12.8	13.2	80.1	76.5	105.2	104.0
7	41.8	41.1	26.0	26.0	100.4	76.9	106.8	106.8
P value	**0.22**		**0.10**		**0.28**		**0.61**	

b) 1 mcd/m^2

	a-Wave				b-Wave			
	Maximum amplitude (μV)		Latency (msec)		Maximum amplitude (μV)		Implicit time (msec)	
Mouse	**Right**	**Left**	**Right**	**Left**	**Right**	**Left**	**Right**	**Left**
1	3.3	2.4	26.0	26.0	270.0	245.8	83.6	85.6
2	13.8	16.5	20.0	19.6	234.7	217.5	117.2	121.2
3	4.1	8.8	20.0	19.6	206.7	173.6	88.4	91.6
4	0.4	1.1	40.4	40.0	199.7	171.8	114.0	114.0
5	32.8	30.9	30.4	31.2	281.9	327.1	105.6	104.4
6	31.2	29.9	20.0	20.0	340.3	365.9	104.0	104.0
7	0.9	0.6	26.0	26.0	322.9	257.6	99.2	95.6
P value	**0.58**		**0.74**		**0.36**		**0.55**	

c) 10 mcd/m^2

	a-Wave				b-Wave			
	Maximum amplitude (μV)		Latency (msec)		Maximum amplitude (μV)		Implicit time (msec)	
Mouse	**Right**	**Left**	**Right**	**Left**	**Right**	**Left**	**Right**	**Left**
1	23.1	25.6	26.0	26.0	479.9	473.7	82.4	84.0
2	5.5	3.0	16.0	17.2	421.1	423.8	90.4	88.4
3	56.6	60.3	26.4	26.8	400.9	411.8	79.6	77.6
4	12.2	4.8	26.0	26.0	358.6	342.6	79.2	81.2
5	11.7	15.4	10.4	11.6	477.0	530.3	88.0	86.8
6	12.4	14.3	20.4	20.0	461.4	526.0	77.6	76.0
7	24.4	24.7	26.0	26.0	560.6	518.7	83.2	84.8
P value	**0.84**		**0.20**		**0.52**		**0.76**	

Appendix III

Additional data for section 6.2.3. The b-wave amplitude from the left eye of seven mice was recorded at four different recording sessions in responses to flash intensities of (**a**) 1 mcd/m^2 and (**b**) 10 mcd/m^2. Repeated measure ANOVA tests on these data set demonstrated that the variability between recording sessions was significantly more than the variability between mice within one recording session.

a) 1 mcd/m^2

Mouse	Maximum amplitude of b-wave from left eye (μV)			
	Week 1	Week 2	Week 3	Week 4
1	404.7	463.0	296.0	344.4
2	423.8	378.1	303.0	412.2
3	411.8	452.1	404.3	447.2
4	342.6	372.3	284.4	291.7
5	483.3	463.1	272.7	384.5
6	530.3	500.1	206.3	449.0
7	526.0	322.5	281.2	399.1

P = 0.0007 (repeated measures ANOVA)

b) 10 mcd/m^2

Mouse	Maximum amplitude of b-wave from left eye (μV)			
	Week 1	Week 2	Week 3	Week 4
1	271.8	327.4	148.5	176.9
2	217.5	311.4	93.3	184.3
3	173.6	261.1	191.4	255.3
4	171.8	144.6	167.6	169.8
5	275.0	181.9	155.1	201.1
6	327.1	275.0	141.3	327.4

P = 0.03 (repeated measures ANOVA)

References

1. Dryja, T.P., et al., *A point mutation of the rhodopsin gene in one form of retinitis pigmentosa.* Nature, 1990. **343**(6256): p. 364-6.
2. Bessant, D.A., R.R. Ali, and S.S. Bhattacharya, *Molecular genetics and prospects for therapy of the inherited retinal dystrophies.* Curr Opin Genet Dev, 2001. **11**(3): p. 307-16.
3. Curcio, C.A., et al., *Human photoreceptor topography.* J Comp Neurol, 1990. **292**(4): p. 497-523.
4. Nguyen-Legros, J. and D. Hicks, *Renewal of photoreceptor outer segments and their phagocytosis by the retinal pigment epithelium.* Int Rev Cytol, 2000. **196**: p. 245-313.
5. Bunker, C.H., et al., *Prevalence of retinitis pigmentosa in Maine.* Am J Ophthalmol, 1984. **97**(3): p. 357-65.
6. Haim, M., N.V. Holm, and T. Rosenberg, *Prevalence of retinitis pigmentosa and allied disorders in Denmark. I Main results.* Acta Ophthalmol (Copenh), 1992. **70**(2): p. 178-86.
7. Spalton, D.J., Hitchings, R.A., and Hunter, P.A., *Slide Atlas of Ophthalmology*, ed. D.J. Spalton, Hitchings, R.A., and Hunter, P.A. 1984: Gower Medical Publishing Ltd.
8. Chong, V., Downes, S. M., Freeman, G. M., S and K. Sehmi, Holder, G. E., and Bird, A. C., *Medical Retina CD-ROM.* x ed, ed. V. Chong, Downes, S. M., Freeman, G. M., S and K. Sehmi, Holder, G. E., and Bird, A. C. Vol. x. 1999, xx: Moorfields Eye Hospital, London, UK. x.
9. Wachtmeister, L. and J.E. Dowling, *The oscillatory potentials of the mudpuppy retina.* Invest Ophthalmol Vis Sci, 1978. **17**(12): p. 1176-88.
10. Gal, A., Apfelstedt-Sylla, E., Janecke, AR., Zrenner, E., *Rhodopsin mutations in inherited retinal dystrophies and dysfunctions.* Prog Retin Eye Res, 1997. **16**: p. 51-79.
11. Kumaramanickavel, G., et al., *Missense rhodopsin mutation in a family with recessive RP.* Nat Genet, 1994. **8**(1): p. 10-1.
12. Danciger, M., et al., *Mutations in the PDE6B gene in autosomal recessive retinitis pigmentosa.* Genomics, 1995. **30**(1): p. 1-7.
13. Huang, S.H., et al., *Autosomal recessive retinitis pigmentosa caused by mutations in the alpha subunit of rod cGMP phosphodiesterase.* Nat Genet, 1995. **11**(4): p. 468-71.
14. Kajiwara, K., et al., *Mutations in the human retinal degeneration slow gene in autosomal dominant retinitis pigmentosa.* Nature, 1991. **354**(6353): p. 480-3.
15. Kajiwara, K., E.L. Berson, and T.P. Dryja, *Digenic retinitis pigmentosa due to mutations at the unlinked peripherin/RDS and ROM1 loci.* Science, 1994. **264**(5165): p. 1604-8.
16. Maw, M.A., et al., *Mutation of the gene encoding cellular retinaldehyde-binding protein in autosomal recessive retinitis pigmentosa.* Nat Genet, 1997. **17**(2): p. 198-200.
17. Bessant, D.A., et al., *A mutation in NRL is associated with autosomal dominant retinitis pigmentosa.* Nat Genet, 1999. **21**(4): p. 355-6.

18. Sohocki, M.M., et al., *A range of clinical phenotypes associated with mutations in CRX, a photoreceptor transcription-factor gene.* Am J Hum Genet, 1998. **63**(5): p. 1307-15.
19. Wells, J., et al., *Mutations in the human retinal degeneration slow (RDS) gene can cause either retinitis pigmentosa or macular dystrophy.* Nat Genet, 1993. **3**(3): p. 213-8.
20. Weleber, R.G., et al., *Phenotypic variation including retinitis pigmentosa, pattern dystrophy, and fundus flavimaculatus in a single family with a deletion of codon 153 or 154 of the peripherin/RDS gene.* Arch Ophthalmol, 1993. **111**(11): p. 1531-42.
21. Bascom, R.A., et al., *Cloning of the cDNA for a novel photoreceptor membrane protein (rom-1) identifies a disk rim protein family implicated in human retinopathies.* Neuron, 1992. **8**(6): p. 1171-84.
22. Chang, G.Q., Y. Hao, and F. Wong, *Apoptosis: final common pathway of photoreceptor death in rd, rds, and rhodopsin mutant mice.* Neuron, 1993. **11**(4): p. 595-605.
23. Portera-Cailliau, C., et al., *Apoptotic photoreceptor cell death in mouse models of retinitis pigmentosa.* Proc Natl Acad Sci U S A, 1994. **91**(3): p. 974-8.
24. Milam, A.H., Z.Y. Li, and R.N. Fariss, *Histopathology of the human retina in retinitis pigmentosa.* Prog Retin Eye Res, 1998. **17**(2): p. 175-205.
25. Huang, P.C., et al., *Cellular interactions implicated in the mechanism of photoreceptor degeneration in transgenic mice expressing a mutant rhodopsin gene.* Proc Natl Acad Sci U S A, 1993. **90**(18): p. 8484-8.
26. Kedzierski, W., D. Bok, and G.H. Travis, *Non-cell-autonomous photoreceptor degeneration in rds mutant mice mosaic for expression of a rescue transgene.* J Neurosci, 1998. **18**(11): p. 4076-82.
27. Berson, E.L., *Nutrition and retinal degenerations.* Int Ophthalmol Clin, 2000. **40**(4): p. 93-111.
28. LaVail, M.M., et al., *Protection of mouse photoreceptors by survival factors in retinal degenerations.* Invest Ophthalmol Vis Sci, 1998. **39**(3): p. 592-602.
29. Kwan, A.S., S. Wang, and R.D. Lund, *Photoreceptor layer reconstruction in a rodent model of retinal degeneration.* Exp Neurol, 1999. **159**(1): p. 21-33.
30. Young, M.J., et al., *Neuronal differentiation and morphological integration of hippocampal progenitor cells transplanted to the retina of immature and mature dystrophic rats.* Mol Cell Neurosci, 2000. **16**(3): p. 197-205.
31. Tropepe, V., et al., *Retinal stem cells in the adult mammalian eye.* Science, 2000. **287**(5460): p. 2032-6.
32. Sauve, Y., et al., *Visual field loss in RCS rats and the effect of RPE cell transplantation.* Exp Neurol, 1998. **152**(2): p. 243-50.
33. Gal, A., et al., *Mutations in MERTK, the human orthologue of the RCS rat retinal dystrophy gene, cause retinitis pigmentosa.* Nat Genet, 2000. **26**(3): p. 270-1.
34. Blaese, R.M., et al., *T lymphocyte-directed gene therapy for ADA- SCID: initial trial results after 4 years.* Science, 1995. **270**(5235): p. 475-80.
35. Cavazzana-Calvo, M., et al., *Gene therapy of human severe combined immunodeficiency (SCID)-X1 disease.* Science, 2000. **288**(5466): p. 669-72.
36. Li, S. and L. Huang, *Nonviral gene therapy: promises and challenges.* Gene Ther, 2000. **7**(1): p. 31-4.
37. Ginsberg, H.S., et al., *Role of early region 3 (E3) in pathogenesis of adenovirus disease.* Proc Natl Acad Sci U S A, 1989. **86**(10): p. 3823-7.

38. Kay, M.A., J.C. Glorioso, and L. Naldini, *Viral vectors for gene therapy: the art of turning infectious agents into vehicles of therapeutics.* Nat Med, 2001. **7**(1): p. 33-40.
39. Lewis, P.F. and M. Emerman, *Passage through mitosis is required for oncoretroviruses but not for the human immunodeficiency virus.* J Virol, 1994. **68**(1): p. 510-6.
40. Bukrinsky, M.I., et al., *A nuclear localization signal within HIV-1 matrix protein that governs infection of non-dividing cells.* Nature, 1993. **365**(6447): p. 666-9.
41. Naldini, L., et al., *In vivo gene delivery and stable transduction of nondividing cells by a lentiviral vector.* Science, 1996. **272**(5259): p. 263-7.
42. Kafri, T., et al., *Sustained expression of genes delivered directly into liver and muscle by lentiviral vectors.* Nat Genet, 1997. **17**(3): p. 314-7.
43. Zufferey, R., et al., *Multiply attenuated lentiviral vector achieves efficient gene delivery in vivo.* Nat Biotechnol, 1997. **15**(9): p. 871-5.
44. Dull, T., et al., *A third-generation lentivirus vector with a conditional packaging system.* J Virol, 1998. **72**(11): p. 8463-71.
45. Miyoshi, H., et al., *Development of a self-inactivating lentivirus vector.* J Virol, 1998. **72**(10): p. 8150-7.
46. Blomer, U., et al., *Highly efficient and sustained gene transfer in adult neurons with a lentivirus vector.* J Virol, 1997. **71**(9): p. 6641-9.
47. Kordower, J.H., et al., *Neurodegeneration prevented by lentiviral vector delivery of GDNF in primate models of Parkinson's disease.* Science, 2000. **290**(5492): p. 767-73.
48. Miyoshi, H., et al., *Transduction of human CD34+ cells that mediate long-term engraftment of NOD/SCID mice by HIV vectors.* Science, 1999. **283**(5402): p. 682-6.
49. Park, F., et al., *Efficient lentiviral transduction of liver requires cell cycling in vivo.* Nat Genet, 2000. **24**(1): p. 49-52.
50. Kaplan, J.M., et al., *Humoral and cellular immune responses of nonhuman primates to long-term repeated lung exposure to Ad2/CFTR-2.* Gene Ther, 1996. **3**(2): p. 117-27.
51. Yang, Y., et al., *Cellular and humoral immune responses to viral antigens create barriers to lung-directed gene therapy with recombinant adenoviruses.* J Virol, 1995. **69**(4): p. 2004-15.
52. Morsy, M.A. and C.T. Caskey, *Expanded-capacity adenoviral vectors--the helper-dependent vectors.* Mol Med Today, 1999. **5**(1): p. 18-24.
53. Chen, H.H., et al., *Persistence in muscle of an adenoviral vector that lacks all viral genes.* Proc Natl Acad Sci U S A, 1997. **94**(5): p. 1645-50.
54. Schiedner, G., et al., *Genomic DNA transfer with a high-capacity adenovirus vector results in improved in vivo gene expression and decreased toxicity.* Nat Genet, 1998. **18**(2): p. 180-3.
55. Kafri, T., et al., *Cellular immune response to adenoviral vector infected cells does not require de novo viral gene expression: implications for gene therapy.* Proc Natl Acad Sci U S A, 1998. **95**(19): p. 11377-82.
56. Chirmule, N., et al., *Immune responses to adenovirus and adeno-associated virus in humans.* Gene Ther, 1999. **6**(9): p. 1574-83.
57. Harvey, B.G., et al., *Variability of human systemic humoral immune responses to adenovirus gene transfer vectors administered to different organs.* J Virol, 1999. **73**(8): p. 6729-42.

58. Stein, C.S., et al., *Effects of macrophage depletion and anti-CD40 ligand on transgene expression and redosing with recombinant adenovirus.* Gene Ther, 1998. **5**(4): p. 431-9.
59. Jooss, K., L.A. Turka, and J.M. Wilson, *Blunting of immune responses to adenoviral vectors in mouse liver and lung with CTLA4Ig.* Gene Ther, 1998. **5**(3): p. 309-19.
60. Benihoud, K., et al., *Efficient, repeated adenovirus-mediated gene transfer in mice lacking both tumor necrosis factor alpha and lymphotoxin alpha.* J Virol, 1998. **72**(12): p. 9514-25.
61. Dmitriev, I., et al., *An adenovirus vector with genetically modified fibers demonstrates expanded tropism via utilization of a coxsackievirus and adenovirus receptor-independent cell entry mechanism.* J Virol, 1998. **72**(12): p. 9706-13.
62. Vigne, E., et al., *RGD inclusion in the hexon monomer provides adenovirus type 5-based vectors with a fiber knob-independent pathway for infection.* J Virol, 1999. **73**(6): p. 5156-61.
63. Chao, H., et al., *Several log increase in therapeutic transgene delivery by distinct adeno-associated viral serotype vectors.* Mol Ther, 2000. **2**(6): p. 619-23.
64. Zabner, J., et al., *Adeno-associated virus type 5 (AAV5) but not AAV2 binds to the apical surfaces of airway epithelia and facilitates gene transfer.* J Virol, 2000. **74**(8): p. 3852-8.
65. Kotin, R.M., et al., *Site-specific integration by adeno-associated virus.* Proc Natl Acad Sci U S A, 1990. **87**(6): p. 2211-5.
66. Samulski, R.J., et al., *Cloning of adeno-associated virus into pBR322: rescue of intact virus from the recombinant plasmid in human cells.* Proc Natl Acad Sci U S A, 1982. **79**(6): p. 2077-81.
67. Xiao, X., J. Li, and R.J. Samulski, *Efficient long-term gene transfer into muscle tissue of immunocompetent mice by adeno-associated virus vector.* J Virol, 1996. **70**(11): p. 8098-108.
68. Kessler, P.D., et al., *Gene delivery to skeletal muscle results in sustained expression and systemic delivery of a therapeutic protein.* Proc Natl Acad Sci U S A, 1996. **93**(24): p. 14082-7.
69. Fisher, K.J., et al., *Recombinant adeno-associated virus for muscle directed gene therapy.* Nat Med, 1997. **3**(3): p. 306-12.
70. Kaplitt, M.G., et al., *Long-term gene expression and phenotypic correction using adeno- associated virus vectors in the mammalian brain.* Nat Genet, 1994. **8**(2): p. 148-54.
71. McLaughlin, S.K., et al., *Adeno-associated virus general transduction vectors: analysis of proviral structures.* J Virol, 1988. **62**(6): p. 1963-73.
72. Urcelay, E., et al., *Asymmetric replication in vitro from a human sequence element is dependent on adeno-associated virus Rep protein.* J Virol, 1995. **69**(4): p. 2038-46.
73. Young, S.M., Jr., et al., *Roles of adeno-associated virus Rep protein and human chromosome 19 in site-specific recombination.* J Virol, 2000. **74**(9): p. 3953-66.
74. Yang, C.C., et al., *Cellular recombination pathways and viral terminal repeat hairpin structures are sufficient for adeno-associated virus integration in vivo and in vitro.* J Virol, 1997. **71**(12): p. 9231-47.

75. Balague, C., M. Kalla, and W.W. Zhang, *Adeno-associated virus Rep78 protein and terminal repeats enhance integration of DNA sequences into the cellular genome.* J Virol, 1997. **71**(4): p. 3299-306.
76. Vincent-Lacaze, N., et al., *Structure of adeno-associated virus vector DNA following transduction of the skeletal muscle.* J Virol, 1999. **73**(3): p. 1949-55.
77. Miao, C.H., et al., *The kinetics of rAAV integration in the liver.* Nat Genet, 1998. **19**(1): p. 13-5.
78. Nakai, H., et al., *Isolation of recombinant adeno-associated virus vector-cellular DNA junctions from mouse liver.* J Virol, 1999. **73**(7): p. 5438-47.
79. Rinaudo, D., et al., *Conditional site-specific integration into human chromosome 19 by using a ligand-dependent chimeric adeno-associated virus/Rep protein.* J Virol, 2000. **74**(1): p. 281-94.
80. Monahan, P.E., et al., *Direct intramuscular injection with recombinant AAV vectors results in sustained expression in a dog model of hemophilia.* Gene Ther, 1998. **5**(1): p. 40-9.
81. Snyder, R.O., et al., *Persistent and therapeutic concentrations of human factor IX in mice after hepatic gene transfer of recombinant AAV vectors.* Nat Genet, 1997. **16**(3): p. 270-6.
82. Conrad, C.K., et al., *Safety of single-dose administration of an adeno-associated virus (AAV)- CFTR vector in the primate lung.* Gene Ther, 1996. **3**(8): p. 658-68.
83. Jooss, K., et al., *Transduction of dendritic cells by DNA viral vectors directs the immune response to transgene products in muscle fibers.* J Virol, 1998. **72**(5): p. 4212-23.
84. Brockstedt, D.G., et al., *Induction of immunity to antigens expressed by recombinant adeno- associated virus depends on the route of administration.* Clin Immunol, 1999. **92**(1): p. 67-75.
85. Russell, D.W. and M.A. Kay, *Adeno-associated virus vectors and hematology.* Blood, 1999. **94**(3): p. 864-74.
86. Nakai, H., T.A. Storm, and M.A. Kay, *Increasing the size of rAAV-mediated expression cassettes in vivo by intermolecular joining of two complementary vectors.* Nat Biotechnol, 2000. **18**(5): p. 527-32.
87. Duan, D., et al., *A new dual-vector approach to enhance recombinant adeno-associated virus-mediated gene expression through intermolecular cis activation.* Nat Med, 2000. **6**(5): p. 595-8.
88. Fisher, K.J., et al., *Transduction with recombinant adeno-associated virus for gene therapy is limited by leading-strand synthesis.* J Virol, 1996. **70**(1): p. 520-32.
89. Ferrari, F.K., et al., *Second-strand synthesis is a rate-limiting step for efficient transduction by recombinant adeno-associated virus vectors.* J Virol, 1996. **70**(5): p. 3227-34.
90. Streilein, J.W., *Immunologic privilege of the eye.* Springer Semin Immunopathol, 1999. **21**(2): p. 95-111.
91. van Nie, R., D. Ivanyi, and P. Demant, *A new H-2-linked mutation, rds, causing retinal degeneration in the mouse.* Tissue Antigens, 1978. **12**(2): p. 106-8.
92. Carter-Dawson, L.D., M.M. LaVail, and R.L. Sidman, *Differential effect of the rd mutation on rods and cones in the mouse retina.* Invest Ophthalmol Vis Sci, 1978. **17**(6): p. 489-98.

93. Suber, M.L., et al., *Irish setter dogs affected with rod/cone dysplasia contain a nonsense mutation in the rod cGMP phosphodiesterase beta-subunit gene.* Proc Natl Acad Sci U S A, 1993. **90**(9): p. 3968-72.
94. Olsson, J.E., et al., *Transgenic mice with a rhodopsin mutation (Pro23His): a mouse model of autosomal dominant retinitis pigmentosa.* Neuron, 1992. **9**(5): p. 815-30.
95. Lewin, A.S., et al., *Ribozyme rescue of photoreceptor cells in a transgenic rat model of autosomal dominant retinitis pigmentosa.* Nat Med, 1998. **4**(8): p. 967-71.
96. Li, Z.Y., et al., *Rhodopsin transgenic pigs as a model for human retinitis pigmentosa.* Invest Ophthalmol Vis Sci, 1998. **39**(5): p. 808-19.
97. Petters, R.M., et al., *Genetically engineered large animal model for studying cone photoreceptor survival and degeneration in retinitis pigmentosa.* Nat Biotechnol, 1997. **15**(10): p. 965-70.
98. Hagstrom, S.A., et al., *Retinal degeneration in tulp1-/- mice: vesicular accumulation in the interphotoreceptor matrix.* Invest Ophthalmol Vis Sci, 1999. **40**(12): p. 2795-802.
99. Hong, D.H., et al., *A retinitis pigmentosa GTPase regulator (RPGR)-deficient mouse model for X-linked retinitis pigmentosa (RP3).* Proc Natl Acad Sci U S A, 2000. **97**(7): p. 3649-54.
100. D'Cruz, P.M., et al., *Mutation of the receptor tyrosine kinase gene Mertk in the retinal dystrophic RCS rat.* Hum Mol Genet, 2000. **9**(4): p. 645-51.
101. Mullen, R.J. and M.M. LaVail, *Inherited retinal dystrophy: primary defect in pigment epithelium determined with experimental rat chimeras.* Science, 1976. **192**(4241): p. 799-801.
102. Davidson, B.L., et al., *A model system for in vivo gene transfer into the central nervous system using an adenoviral vector.* Nat Genet, 1993. **3**(3): p. 219-23.
103. Bennett, J., et al., *Adenovirus vector-mediated in vivo gene transfer into adult murine retina.* Invest Ophthalmol Vis Sci, 1994. **35**(5): p. 2535-42.
104. Li, T., et al., *In vivo transfer of a reporter gene to the retina mediated by an adenoviral vector.* Invest Ophthalmol Vis Sci, 1994. **35**(5): p. 2543-9.
105. Reichel, M.B., et al., *Immune responses limit adenovirally mediated gene expression in the adult mouse eye.* Gene Ther, 1998. **5**(8): p. 1038-46.
106. Ali, R.R., et al., *Co-injection of adenovirus expressing CTLA4-Ig prolongs adenovirally mediated lacZ reporter gene expression in the mouse retina.* Gene Ther, 1998. **5**(11): p. 1561-5.
107. Hoffman, L.M., A.M. Maguire, and J. Bennett, *Cell-mediated immune response and stability of intraocular transgene expression after adenovirus-mediated delivery.* Invest Ophthalmol Vis Sci, 1997. **38**(11): p. 2224-33.
108. Kumar-Singh, R. and D.B. Farber, *Encapsidated adenovirus mini-chromosome-mediated delivery of genes to the retina: application to the rescue of photoreceptor degeneration.* Hum Mol Genet, 1998. **7**(12): p. 1893-900.
109. Ali, R.R., et al., *Gene transfer into the mouse retina mediated by an adeno-associated viral vector.* Hum Mol Genet, 1996. **5**(5): p. 591-4.
110. Bennett, J., et al., *Real-time, noninvasive in vivo assessment of adeno-associated virus- mediated retinal transduction.* Invest Ophthalmol Vis Sci, 1997. **38**(13): p. 2857-63.
111. Anand, V., et al., *Additional transduction events after subretinal readministration of recombinant adeno-associated virus.* Hum Gene Ther, 2000. **11**(3): p. 449-57.

112. Bennett, J., et al., *Stable transgene expression in rod photoreceptors after recombinant adeno-associated virus-mediated gene transfer to monkey retina.* Proc Natl Acad Sci U S A, 1999. **96**(17): p. 9920-5.
113. Miyoshi, H., et al., *Stable and efficient gene transfer into the retina using an HIV-based lentiviral vector.* Proc Natl Acad Sci U S A, 1997. **94**(19): p. 10319-23.
114. McLaughlin, M.E., et al., *Recessive mutations in the gene encoding the beta-subunit of rod phosphodiesterase in patients with retinitis pigmentosa.* Nat Genet, 1993. **4**(2): p. 130-4.
115. Pittler, S.J. and W. Baehr, *Identification of a nonsense mutation in the rod photoreceptor cGMP phosphodiesterase beta-subunit gene of the rd mouse.* Proc Natl Acad Sci U S A, 1991. **88**(19): p. 8322-6.
116. Lem, J., et al., *Retinal degeneration is rescued in transgenic rd mice by expression of the cGMP phosphodiesterase beta subunit.* Proc Natl Acad Sci U S A, 1992. **89**(10): p. 4422-6.
117. Jomary, C., et al., *Rescue of photoreceptor function by AAV-mediated gene transfer in a mouse model of inherited retinal degeneration.* Gene Ther, 1997. **4**(7): p. 683-90.
118. Bennett, J., et al., *Photoreceptor cell rescue in retinal degeneration (rd) mice by in vivo gene therapy.* Nat Med, 1996. **2**(6): p. 649-54.
119. Takahashi, M., et al., *Rescue from photoreceptor degeneration in the rd mouse by human immunodeficiency virus vector-mediated gene transfer.* J Virol, 1999. **73**(9): p. 7812-6.
120. Travis, G.H., et al., *Identification of a photoreceptor-specific mRNA encoded by the gene responsible for retinal degeneration slow (rds).* Nature, 1989. **338**(6210): p. 70-3.
121. Travis, G.H., et al., *Complete rescue of photoreceptor dysplasia and degeneration in transgenic retinal degeneration slow (rds) mice.* Neuron, 1992. **9**(1): p. 113-9.
122. Guerrier-Takada, C. and S. Altman, *Catalytic activity of an RNA molecule prepared by transcription in vitro.* Science, 1984. **223**(4633): p. 285-6.
123. Cech, T.R., A.J. Zaug, and P.J. Grabowski, *In vitro splicing of the ribosomal RNA precursor of Tetrahymena: involvement of a guanosine nucleotide in the excision of the intervening sequence.* Cell, 1981. **27**(3 Pt 2): p. 487-96.
124. Steiberg, R.H., Flannery, J. G., Naash, M. I., et al., *Transgenic rat models of inherited retinal degeneration caused by mutatnt opsin genes. [ARVO abstract].* Invest Ophthalmol Vis Sci, 1996. **37**(Supplement): p. S698. Abstract number 3190.
125. Sung, C.H., et al., *Rhodopsin mutations in autosomal dominant retinitis pigmentosa.* Proc Natl Acad Sci U S A, 1991. **88**(15): p. 6481-5.
126. Berson, E.L., et al., *Ocular findings in patients with autosomal dominant retinitis pigmentosa and a rhodopsin gene defect (Pro-23-His).* Arch Ophthalmol, 1991. **109**(1): p. 92-101.
127. Drenser, K.A., et al., *Ribozyme-targeted destruction of RNA associated with autosomal-dominant retinitis pigmentosa.* Invest Ophthalmol Vis Sci, 1998. **39**(5): p. 681-9.
128. Flannery, J.G., et al., *Efficient photoreceptor-targeted gene expression in vivo by recombinant adeno-associated virus.* Proc Natl Acad Sci U S A, 1997. **94**(13): p. 6916-21.

129. LaVail, M.M., et al., *Ribozyme rescue of photoreceptor cells in P23H transgenic rats: long- term survival and late-stage therapy.* Proc Natl Acad Sci U S A, 2000. **97**(21): p. 11488-93.
130. O'Neill, B., et al., *Ribozyme-based therapeutic approaches for autosomal dominant retinitis pigmentosa.* Invest Ophthalmol Vis Sci, 2000. **41**(10): p. 2863-9.
131. L'Huillier, P.J., et al., *Efficient and specific ribozyme-mediated reduction of bovine alpha- lactalbumin expression in double transgenic mice.* Proc Natl Acad Sci U S A, 1996. **93**(13): p. 6698-703.
132. Levin, L.A., et al., *Identification of the bcl-2 family of genes in the rat retina.* Invest Ophthalmol Vis Sci, 1997. **38**(12): p. 2545-53.
133. Chen, J., et al., *bcl-2 overexpression reduces apoptotic photoreceptor cell death in three different retinal degenerations.* Proc Natl Acad Sci U S A, 1996. **93**(14): p. 7042-7.
134. Joseph, R.M. and T. Li, *Overexpression of Bcl-2 or Bcl-XL transgenes and photoreceptor degeneration.* Invest Ophthalmol Vis Sci, 1996. **37**(12): p. 2434-46.
135. Bennett, J., et al., *Adenovirus-mediated delivery of rhodopsin-promoted bcl-2 results in a delay in photoreceptor cell death in the rd/rd mouse.* Gene Ther, 1998. **5**(9): p. 1156-64.
136. Nir, I., et al., *Expression of Bcl-2 protects against photoreceptor degeneration in retinal degeneration slow (rds) mice.* J Neurosci, 2000. **20**(6): p. 2150-4.
137. Liu, C., et al., *Activation of caspase-3 in the retina of transgenic rats with the rhodopsin mutation s334ter during photoreceptor degeneration.* J Neurosci, 1999. **19**(12): p. 4778-85.
138. Faktorovich, E.G., et al., *Photoreceptor degeneration in inherited retinal dystrophy delayed by basic fibroblast growth factor.* Nature, 1990. **347**(6288): p. 83-6.
139. Cayouette, M. and C. Gravel, *Adenovirus-mediated gene transfer of ciliary neurotrophic factor can prevent photoreceptor degeneration in the retinal degeneration (rd) mouse.* Hum Gene Ther, 1997. **8**(4): p. 423-30.
140. Cayouette, M., et al., *Intraocular gene transfer of ciliary neurotrophic factor prevents death and increases responsiveness of rod photoreceptors in the retinal degeneration slow mouse.* J Neurosci, 1998. **18**(22): p. 9282-93.
141. Kirsch, M., et al., *Evidence for multiple, local functions of ciliary neurotrophic factor (CNTF) in retinal development: expression of CNTF and its receptors and in vitro effects on target cells.* J Neurochem, 1997. **68**(3): p. 979-90.
142. Harada, T., et al., *Modification of glial-neuronal cell interactions prevents photoreceptor apoptosis during light-induced retinal degeneration.* Neuron, 2000. **26**(2): p. 533-41.
143. Liang, F.Q., et al., *AAV-mediated delivery of ciliary neurotrophic factor prolongs photoreceptor survival in the rhodopsin knockout mouse.* Mol Ther, 2001. **3**(2): p. 241-8.
144. Reichel, M.B., et al., *An immune response after intraocular administration of an adenoviral vector containing a beta galactosidase reporter gene slows retinal degeneration in the rd mouse.* Br J Ophthalmol, 2001. **85**(3): p. 341-4.
145. Green, E.S., et al., *Two animal models of retinal degeneration are rescued by recombinant adeno-associated virus-mediated production of fgf-5 and fgf-18.* Mol Ther, 2001. **3**(4): p. 507-15.

146. Lau, D., et al., *Retinal degeneration is slowed in transgenic rats by AAV-mediated delivery of FGF-2.* Invest Ophthalmol Vis Sci, 2000. **41**(11): p. 3622-33.
147. Buller, R.M., et al., *Herpes simplex virus types 1 and 2 completely help adenovirus- associated virus replication.* J Virol, 1981. **40**(1): p. 241-7.
148. Im, D.S. and N. Muzyczka, *The AAV origin binding protein Rep68 is an ATP-dependent site-specific endonuclease with DNA helicase activity.* Cell, 1990. **61**(3): p. 447-57.
149. Im, D.S. and N. Muzyczka, *Partial purification of adeno-associated virus Rep78, Rep52, and Rep40 and their biochemical characterization.* J Virol, 1992. **66**(2): p. 1119-28.
150. Chejanovsky, N. and B.J. Carter, *Mutagenesis of an AUG codon in the adeno-associated virus rep gene: effects on viral DNA replication.* Virology, 1989. **173**(1): p. 120-8.
151. Lusby, E., K.H. Fife, and K.I. Berns, *Nucleotide sequence of the inverted terminal repetition in adeno- associated virus DNA.* J Virol, 1980. **34**(2): p. 402-9.
152. Wang, X.S., S. Ponnazhagan, and A. Srivastava, *Rescue and replication signals of the adeno-associated virus 2 genome.* J Mol Biol, 1995. **250**(5): p. 573-80.
153. Samulski, R.J., L.S. Chang, and T. Shenk, *A recombinant plasmid from which an infectious adeno-associated virus genome can be excised in vitro and its use to study viral replication.* J Virol, 1987. **61**(10): p. 3096-101.
154. de la Maza, L.M. and B.J. Carter, *Heavy and light particles of adeno-associated virus.* J Virol, 1980. **33**(3): p. 1129-37.
155. Samulski, R.J., L.S. Chang, and T. Shenk, *Helper-free stocks of recombinant adeno-associated viruses: normal integration does not require viral gene expression.* J Virol, 1989. **63**(9): p. 3822-8.
156. Ferrari, F.K., et al., *New developments in the generation of Ad-free, high-titer rAAV gene therapy vectors.* Nat Med, 1997. **3**(11): p. 1295-7.
157. Xiao, X., J. Li, and R.J. Samulski, *Production of high-titer recombinant adeno-associated virus vectors in the absence of helper adenovirus.* J Virol, 1998. **72**(3): p. 2224-32.
158. Matsushita, T., et al., *Adeno-associated virus vectors can be efficiently produced without helper virus.* Gene Ther, 1998. **5**(7): p. 938-45.
159. Clark, K.R., et al., *Cell lines for the production of recombinant adeno-associated virus.* Hum Gene Ther, 1995. **6**(10): p. 1329-41.
160. Rose, J.A. and F. Koczot, *Adenovirus-associated virus multiplication. VII. Helper requirement for viral deoxyribonucleic acid and ribonucleic acid synthesis.* J Virol, 1972. **10**(1): p. 1-8.
161. Ali, M., N.R. Lemoine, and C.J. Ring, *The use of DNA viruses as vectors for gene therapy.* Gene Ther, 1994. **1**(6): p. 367-84.
162. Fan, P.D. and J.Y. Dong, *Replication of rep-cap genes is essential for the high-efficiency production of recombinant AAV.* Hum Gene Ther, 1997. **8**(1): p. 87-98.
163. Li, J., R.J. Samulski, and X. Xiao, *Role for highly regulated rep gene expression in adeno-associated virus vector production.* J Virol, 1997. **71**(7): p. 5236-43.
164. Vincent, K.A., S.T. Piraino, and S.C. Wadsworth, *Analysis of recombinant adeno-associated virus packaging and requirements for rep and cap gene products.* J Virol, 1997. **71**(3): p. 1897-905.

165. Holscher, C., et al., *Cell lines inducibly expressing the adeno-associated virus (AAV) rep gene: requirements for productive replication of rep-negative AAV mutants.* J Virol, 1994. **68**(11): p. 7169-77.
166. Yang, Q., F. Chen, and J.P. Trempe, *Characterization of cell lines that inducibly express the adeno- associated virus Rep proteins.* J Virol, 1994. **68**(8): p. 4847-56.
167. Conway, J.E., et al., *Recombinant adeno-associated virus type 2 replication and packaging is entirely supported by a herpes simplex virus type 1 amplicon expressing Rep and Cap.* J Virol, 1997. **71**(11): p. 8780-9.
168. Johnston, K.M., et al., *HSV/AAV hybrid amplicon vectors extend transgene expression in human glioma cells.* Hum Gene Ther, 1997. **8**(3): p. 359-70.
169. Zolotukhin, S., et al., *A "humanized" green fluorescent protein cDNA adapted for high-level expression in mammalian cells.* J Virol, 1996. **70**(7): p. 4646-54.
170. Kozak, M., *Compilation and analysis of sequences upstream from the translational start site in eukaryotic mRNAs.* Nucleic Acids Res, 1984. **12**(2): p. 857-72.
171. Heim, R. and R.Y. Tsien, *Engineering green fluorescent protein for improved brightness, longer wavelengths and fluorescence resonance energy transfer.* Curr Biol, 1996. **6**(2): p. 178-82.
172. Ryan, J.H., S. Zolotukhin, and N. Muzyczka, *Sequence requirements for binding of Rep68 to the adeno-associated virus terminal repeats.* J Virol, 1996. **70**(3): p. 1542-53.
173. Ma, J., et al., *Retinal degeneration slow (rds) in mouse results from simple insertion of a t haplotype-specific element into protein-coding exon II.* Genomics, 1995. **28**(2): p. 212-9.
174. Cheng, T., M.R. al Ubaidi, and M.I. Naash, *Structural and developmental analysis of the mouse peripherin/rds gene.* Somat Cell Mol Genet, 1997. **23**(3): p. 165-83.
175. Dominguez, O. and C. Lopez-Larrea, *Gene walking by unpredictably primed PCR.* Nucleic Acids Res, 1994. **22**(15): p. 3247-8.
176. Bennett, K.L., et al., *Most highly repeated dispersed DNA families in the mouse genome.* Mol Cell Biol, 1984. **4**(8): p. 1561-71.
177. Zack, D.J., et al., *Unusual topography of bovine rhodopsin promoter-lacZ fusion gene expression in transgenic mouse retinas.* Neuron, 1991. **6**(2): p. 187-99.
178. Wang, X.S., S. Ponnazhagan, and A. Srivastava, *Rescue and replication of adeno-associated virus type 2 as well as vector DNA sequences from recombinant plasmids containing deletions in the viral inverted terminal repeats: selective encapsidation of viral genomes in progeny virions.* J Virol, 1996. **70**(3): p. 1668-77.
179. Wang, X.S., et al., *Adeno-associated virus type 2 DNA replication in vivo: mutation analyses of the D sequence in viral inverted terminal repeats.* J Virol, 1997. **71**(4): p. 3077-82.
180. Wang, X.S., et al., *Characterization of wild-type adeno-associated virus type 2-like particles generated during recombinant viral vector production and strategies for their elimination.* J Virol, 1998. **72**(7): p. 5472-80.
181. Cormack, B.P., R.H. Valdivia, and S. Falkow, *FACS-optimized mutants of the green fluorescent protein (GFP).* Gene, 1996. **173**(1): p. 33-8.
182. Forrester, A., et al., *Construction and properties of a mutant of herpes simplex virus type 1 with glycoprotein H coding sequences deleted.* J Virol, 1992. **66**(1): p. 341-8.

183. Zhang, X., et al., *High-titer recombinant adeno-associated virus production from replicating amplicons and herpes vectors deleted for glycoprotein H.* Hum Gene Ther, 1999. **10**(15): p. 2527-37.
184. Zhang, X., et al., *An efficient selection system for packaging herpes simplex virus amplicons.* J Gen Virol, 1998. **79**(Pt 1): p. 125-31.
185. Hart, S.L., et al., *Lipid-mediated enhancement of transfection by a nonviral integrin- targeting vector.* Hum Gene Ther, 1998. **9**(4): p. 575-85.
186. Zolotukhin, S., et al., *Recombinant adeno-associated virus purification using novel methods improves infectious titer and yield.* Gene Ther, 1999. **6**(6): p. 973-85.
187. Samulski, R.J., et al., *Rescue of adeno-associated virus from recombinant plasmids: gene correction within the terminal repeats of AAV.* Cell, 1983. **33**(1): p. 135-43.
188. Inoue, N. and D.W. Russell, *Packaging cells based on inducible gene amplification for the production of adeno-associated virus vectors.* J Virol, 1998. **72**(9): p. 7024-31.
189. Gossen, M., et al., *Transcriptional activation by tetracyclines in mammalian cells.* Science, 1995. **268**(5218): p. 1766-9.
190. Grant, C.A., et al., *Evaluation of recombinant adeno-associated virus as a gene transfer vector for the retina.* Curr Eye Res, 1997. **16**(9): p. 949-56.
191. Baskar, J.F., et al., *The enhancer domain of the human cytomegalovirus major immediate-early promoter determines cell type-specific expression in transgenic mice.* J Virol, 1996. **70**(5): p. 3207-14.
192. Dudus, L., et al., *Persistent transgene product in retina, optic nerve and brain after intraocular injection of rAAV.* Vision Res, 1999. **39**(15): p. 2545-53.
193. Rolling, F., et al., *Evaluation of adeno-associated virus-mediated gene transfer into the rat retina by clinical fluorescence photography.* Hum Gene Ther, 1999. **10**(4): p. 641-8.
194. Carter-Dawson, L.D. and M.M. LaVail, *Rods and cones in the mouse retina. I. Structural analysis using light and electron microscopy.* J Comp Neurol, 1979. **188**(2): p. 245-62.
195. Jeon, C.J., E. Strettoi, and R.H. Masland, *The major cell populations of the mouse retina.* J Neurosci, 1998. **18**(21): p. 8936-46.
196. Ali, R.R., et al., *Adeno-associated virus gene transfer to mouse retina.* Hum Gene Ther, 1998. **9**(1): p. 81-6.
197. Klein, R.L., et al., *Neuron-specific transduction in the rat septohippocampal or nigrostriatal pathway by recombinant adeno-associated virus vectors.* Exp Neurol, 1998. **150**(2): p. 183-94.
198. Paterna, J.C., et al., *Influence of promoter and WHV post-transcriptional regulatory element on AAV-mediated transgene expression in the rat brain.* Gene Ther, 2000. **7**(15): p. 1304-11.
199. Nir, I., N. Agarwal, and D.S. Papermaster, *Opsin gene expression during early and late phases of retinal degeneration in rds mice.* Exp Eye Res, 1990. **51**(3): p. 257-67.
200. Lois, N., et al., *Quantitative evaluation of fundus autofluorescence imaged "in vivo" in eyes with retinal disease.* Br J Ophthalmol, 2000. **84**(7): p. 741-5.
201. Hawes, N.L., et al., *Mouse fundus photography and angiography: a catalogue of normal and mutant phenotypes.* Mol Vis, 1999. **5**: p. 22.

202. Blanks, J.C. and L.V. Johnson, *Specific binding of peanut lectin to a class of retinal photoreceptor cells. A species comparison.* Invest Ophthalmol Vis Sci, 1984. **25**(5): p. 546-57.
203. LaVail, M.M., et al., *Variability in rate of cone degeneration in the retinal degeneration (rd/rd) mouse.* Exp Eye Res, 1997. **65**(1): p. 45-50.
204. Bennett, J., et al., *Cross-species comparison of in vivo reporter gene expression after recombinant adeno-associated virus-mediated retinal transduction.* Methods Enzymol, 2000. **316**: p. 777-89.
205. Rolling, F., et al., *Long-term real-time monitoring of adeno-associated virus-mediated gene expression in the rat retina.* Clin Experiment Ophthalmol, 2000. **28**(5): p. 382-6.
206. Summerford, C. and R.J. Samulski, *Membrane-associated heparan sulfate proteoglycan is a receptor for adeno-associated virus type 2 virions.* J Virol, 1998. **72**(2): p. 1438-45.
207. Summerford, C., J.S. Bartlett, and R.J. Samulski, *AlphaVbeta5 integrin: a co-receptor for adeno-associated virus type 2 infection.* Nat Med, 1999. **5**(1): p. 78-82.
208. Duan, D., et al., *Dynamin is required for recombinant adeno-associated virus type 2 infection.* J Virol, 1999. **73**(12): p. 10371-6.
209. Arikawa, K., et al., *Localization of peripherin/rds in the disk membranes of cone and rod photoreceptors: relationship to disk membrane morphogenesis and retinal degeneration.* J Cell Biol, 1992. **116**(3): p. 659-67.
210. Travis, G.H., et al., *The human retinal degeneration slow (RDS) gene: chromosome assignment and structure of the mRNA.* Genomics, 1991. **10**(3): p. 733-9.
211. Gregory-Evans, K. and S.S. Bhattacharya, *Genetic blindness: current concepts in the pathogenesis of human outer retinal dystrophies.* Trends Genet, 1998. **14**(3): p. 103-8.
212. Sanyal, S. and H.G. Jansen, *Absence of receptor outer segments in the retina of rds mutant mice.* Neurosci Lett, 1981. **21**(1): p. 23-6.
213. Jansen, H.G. and S. Sanyal, *Development and degeneration of retina in rds mutant mice: electron microscopy.* J Comp Neurol, 1984. **224**(1): p. 71-84.
214. Hawkins, R.K., H.G. Jansen, and S. Sanyal, *Development and degeneration of retina in rds mutant mice: photoreceptor abnormalities in the heterozygotes.* Exp Eye Res, 1985. **41**(6): p. 701-20.
215. Travis, G.H., *Mechanisms of cell death in the inherited retinal degenerations.* Am J Hum Genet, 1998. **62**(3): p. 503-8.
216. Mattson, M.P., *Apoptosis in neurodegenerative disorders.* Nat Rev Mol Cell Biol, 2000. **1**(2): p. 120-9.
217. Clarke, G., et al., *A one-hit model of cell death in inherited neuronal degenerations.* Nature, 2000. **406**(6792): p. 195-9.
218. Cheng, T., et al., *The effect of peripherin/rds haploinsufficiency on rod and cone photoreceptors.* J Neurosci, 1997. **17**(21): p. 8118-28.
219. Frade, J.M. and Y.A. Barde, *Microglia-derived nerve growth factor causes cell death in the developing retina.* Neuron, 1998. **20**(1): p. 35-41.
220. Thanos, S., *Sick photoreceptors attract activated microglia from the ganglion cell layer: a model to study the inflammatory cascades in rats with inherited retinal dystrophy.* Brain Res, 1992. **588**(1): p. 21-8.
221. Reuter, J.H. and S. Sanyal, *Development and degeneration of retina in rds mutant mice: the electroretinogram.* Neurosci Lett, 1984. **48**(2): p. 231-7.

222. Peachey, N.S., K.R. Alexander, and G.A. Fishman, *Rod and cone system contributions to oscillatory potentials: an explanation for the conditioning flash effect.* Vision Res, 1987. **27**(6): p. 859-66.
223. Lachapelle, P., et al., *The oscillatory potentials in response to stimuli of photopic intensities delivered in dark-adaptation: an explanation for the conditioning flash effect.* Vision Res, 1990. **30**(4): p. 503-13.
224. Faktorovich, E.G., et al., *Basic fibroblast growth factor and local injury protect photoreceptors from light damage in the rat.* J Neurosci, 1992. **12**(9): p. 3554-67.
225. Nusinowitz, S., W.H. Ridder, 3rd, and J.R. Heckenlively, *Rod multifocal electroretinograms in mice.* Invest Ophthalmol Vis Sci, 1999. **40**(12): p. 2848-58.
226. Wang, L., et al., *Sustained expression of therapeutic level of factor IX in hemophilia B dogs by AAV-mediated gene therapy in liver.* Mol Ther, 2000. **1**(2): p. 154-8.
227. Herzog, R.W., et al., *Long-term correction of canine hemophilia B by gene transfer of blood coagulation factor IX mediated by adeno-associated viral vector.* Nat Med, 1999. **5**(1): p. 56-63.
228. Kay, M.A., et al., *Evidence for gene transfer and expression of factor IX in haemophilia B patients treated with an AAV vector.* Nat Genet, 2000. **24**(3): p. 257-61.
229. Wu, P., et al., *Mutational analysis of the adeno-associated virus type 2 (AAV2) capsid gene and construction of AAV2 vectors with altered tropism.* J Virol, 2000. **74**(18): p. 8635-47.
230. Girod, A., et al., *Genetic capsid modifications allow efficient re-targeting of adeno- associated virus type 2.* Nat Med, 1999. **5**(9): p. 1052-6.
231. Bartlett, J.S., et al., *Targeted adeno-associated virus vector transduction of nonpermissive cells mediated by a bispecific F(ab'gamma)2 antibody.* Nat Biotechnol, 1999. **17**(2): p. 181-6.
232. Fisher, K.J., et al., *A novel adenovirus-adeno-associated virus hybrid vector that displays efficient rescue and delivery of the AAV genome.* Hum Gene Ther, 1996. **7**(17): p. 2079-87.
233. Recchia, A., et al., *Site-specific integration mediated by a hybrid adenovirus/adeno- associated virus vector.* Proc Natl Acad Sci U S A, 1999. **96**(6): p. 2615-20.
234. McGee Sanftner, L.H., et al., *Recombinant aav-mediated delivery of a tet-inducible reporter gene to the rat retina.* Mol Ther, 2001. **3**(5 Pt 1): p. 688-96.
235. Hauswirth, W.W. and L. Beaufrere, *Ocular gene therapy: quo vadis?* Invest Ophthalmol Vis Sci, 2000. **41**(10): p. 2821-6.
236. Kajiwara, K., et al., *A null mutation in the human peripherin/RDS gene in a family with autosomal dominant retinitis punctata albescens.* Nat Genet, 1993. **3**(3): p. 208-12.
237. Acland, G.M., et al., *Gene therapy restores vision in a canine model of childhood blindness.* Nat Genet, 2001. **28**(1): p. 92-5.
238. Chan, A.W., et al., *Transgenic monkeys produced by retroviral gene transfer into mature oocytes.* Science, 2001. **291**(5502): p. 309-12.
239. Carr, R.E. and Heckenlively, J.R., *Hereditary pigmentary degenerations of the retina.* In: Tasman, W., Jaeger, E.A. editors. Clinical Ophthalmology, Vol 3. Philadelphia. Lippencott, Williams, and Wilkins; 1986: p. 1-28.
240. Heckenlively, J.R., *Retinitis pigmentosa.* Philadelphia: Lippencott; 1988.

241. Heckenlively, J.R., *RP syndromes.* See Ref. 240. p. 221-52.
242. Ogden, T.E., *Clinical Electrophysiology.* In: Ryan, S.J. editor. Retina 2nd edition. St Louis: Mosby; 1994: p. 321-32.
243. Noguchi, M., et al., *Interleukin-2 receptor gamma chain mutation results in X-linked severe combined immunodeficiency in humans.* Cell, 1993. **73**(1): p. 147-57.
244. Fung, B., Hurley, J. and Stryer, L., *Flow of information in the light triggered cyclic nucleotide cascade of vision.* Proc Natl Acad Sci U S A, 1981. **78**(1): p. 152-6.
245. Cook, N.J., Hanke, W. and Kaupp, U.B., *Identification, purification and functional reconstitution of the cyclic GMP-dependent channel from rod photoreceptor cells.* Proc Natl Acad Sci U S A, 1987. **84**(2): p. 585-9.
246. Atwell, D: The Sharpey-Schafer Lecture: *Ion channels and signal processing in the outer retina.* Q J Exp Physiol, 1986. **71**: p. 497-536.
247. Wald, G., *Molecular basis of visual excitation.* Science, 1968. **162**(850): p. 230-9.
248. Donders, F.C., *Torpeur de la rétine congénital e héréditarie,* Ann Occul (Paris), 1855. **34**: 270-3.
249. Doehmer, J. et al., *Introduction of rat growth hormone gene into mouse fibroblasts via a retroviral DNA vector: expression and regulation.* Proc Natl Acad Sci U S A, 1982. **79**(7): p. 2268-72.
250. Cone, R.D. and Mulligan, R.C., *High efficiency gene transferinto mammalian cells: generation of helper-free recombinant retrovirus with broad mammalian host range.* Proc Natl Acad Sci U S A, 1984. **81**(20): p. 6349-53.